

**ASSESSMENT OF LAND USE URBANIZATION IMPACTS ON
SURFACE TEMPERATURE AND HYDROLOGY**

by

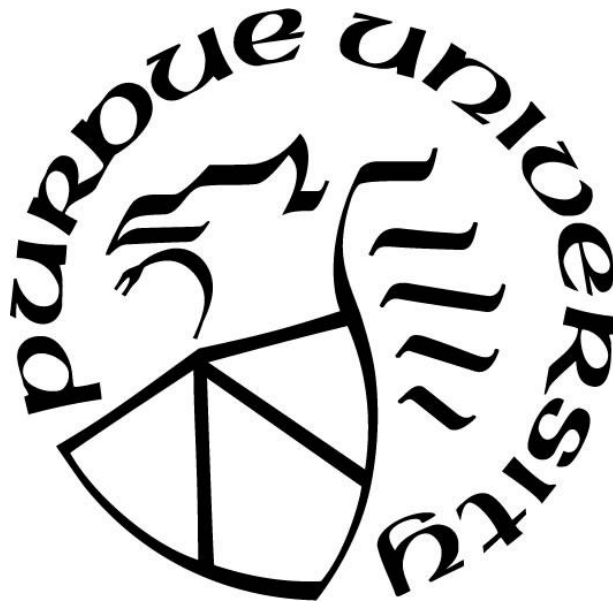
Mohamed Aboelnour

A Dissertation

Submitted to the Faculty of Purdue University

In Partial Fulfillment of the Requirements for the degree of

Doctor of Philosophy



Department of Agricultural and Biological Engineering

West Lafayette, Indiana

May 2020

**THE PURDUE UNIVERSITY GRADUATE SCHOOL
STATEMENT OF COMMITTEE APPROVAL**

Dr. Bernard A. Engel, Chair

School of Agricultural and Biological Engineering

Dr. Dennis Flanagan

School of Agricultural and Biological Engineering

Dr. Margaret Gitau

School of Agricultural and Biological Engineering

Dr. Marty Frisbee

Department of Earth, Atmospheric and Planetary Sciences

Approved by:

Dr. Nathan S. Mosier

I would like to dedicate my work to my parents, brothers and sister for their prayers, love and constant support.

I further dedicate this dissertation to my wife, Erin Sorlien Aboelnour, whose unyielding love, encouragements and support have enriched my soul and inspired me to pursue and complete this work.

ACKNOWLEDGMENTS

I sincerely thank my friends, colleagues and my teammates, without whom this journey would have been far less rewarding. To Farid, Josept and Johann, I cannot thank you enough for the laughs, the help, the support, and the friendship throughout these years. To my soccer teammate, Alejandro Rodriguez, you have been both friend and teammate, and I sincerely look forward to our future adventures together! To the lovely friends who have made hanging outs, sports, meals and our shows an incredibly fun addition to my time here! To all the members of the Los Gordos and soccer community I have had the privilege to play with, and to my IM teams across sports, thank you all for the t-shirts and great memories.

I acknowledge the very helpful guidance of my thesis committee: Dr. Margaret Gitau, Dr. Marty Frisbee, Prof. Dennis Flanagan, and my adviser Prof. Bernie Engel. Thank you to each of you for the contributions you have made to this work, and to helping me grow into a thoughtful scientist. You have provided me with your tremendous and commendable scientific support right from the concept development and throughout the study. I would like to extend a special thank you to Prof. Engel, for allowing me to conduct this research under his supervision and for all his support and encouragement during my study. Thank you for showing me the different perspectives and approaches for doing great research and also for instilling in me many soft skills that will help me immensely in my future career. In addition, I appreciate the administrative support that I received from Becky, Barb, Nikki and all ABE staff.

To my lab mates and ABE graduate students, both past and present, your help and companionship will never be forgotten. I would also like to acknowledge support provided by my fellow graduate students. Especially, Sushant Mehan and Celena Alford for providing assistance with SWAT model development and proof readings. Next, I gratefully acknowledge the financial support provided by the Egyptian Government General Scholarship Programme administrated by the Egyptian Cultural and Education Bureau, Washington, DC, USA. To my advisors in Geology Department, Suez Canal University. I deeply appreciate their belief in me. I really appreciate constant help and moral support provided. I am also thankful to the ABE Department, for proving funding in the form of Research Assistantship in times when I needed it.

I owe my deepest gratitude to my family back in Egypt who have always believed in me and encouraged me throughout my life. None of this would have been possible without their love and

patience. Numerous thanks to my parents-in-law. It was not long before I became your son-in-law and I could not have felt more loved if I was your actual son.

Finally and most importantly, my heartfelt gratitude goes to my wife, Erin Aboelnour, I would especially like to thank you for unwavering support during my PhD studies. You have been extremely supportive of me throughout this entire process and have made countless sacrifices to help me get to this point.

All praise is to Allah, the Almighty, who helped me and guided me to complete my Ph.D. dissertation.

TABLE OF CONTENTS

LIST OF TABLES	10
LIST OF FIGURES	13
LIST OF ABBREVIATIONS.....	17
ABSTRACT.....	21
CHAPTER 1. INTRODUCTION: EFFECTS OF LAND USE CONVERSION ON ENVIRONMENTAL AND ECOLOGICAL ISSUES	23
1.1 Introduction.....	23
1.2 Objectives	27
1.3 Dissertation Organization	28
CHAPTER 2. APPLICATION OF REMOTE SENSING AND GEOGRAPHIC INFORMATION SYSTEMS TO ANALYZE LAND SURFACE TEMPERATURE IN RESPONSE TO LAND USE/LAND COVER CHANGE IN THE GREATER CAIRO REGION, EGYPT	30
2.1 Introduction.....	30
2.2 Study area.....	34
2.3 Dataset description.....	36
2.3.1 Satellite data.....	36
2.3.2 Auxiliary data	37
2.4 Methodology.....	38
2.4.1 Image preprocessing	39
2.4.2 Optimum Index Factor (OIF) Calculation	40
2.4.3 Land Use/Land Cover Classification.....	41
2.4.3.1 Unsupervised Classification	42
2.4.3.2 Supervised Classification	42
2.4.4 Post classification smoothing	43
2.4.4.1 Accuracy assessment and validation	43
2.4.4.2 Land Use/Land Cover Change detection.....	44
2.4.5 Derivation of land surface indices (NDVI and NDBI).....	44
2.4.6 Land surface temperature retrieval from Landsat 5 TM data	45

2.4.7	Land surface temperature retrieval from Landsat 8 OLI.....	47
2.5	Results and Discussion	49
2.5.1	Spatial distribution and accuracy assessment of LULC	49
2.5.2	Land Use/Land Cover change detection.....	51
2.5.3	Land Surface Temperature (LST) change and the relationship with Land Use/Land Cover (LULC) change	57
2.5.4	Analysis of land indices and relationship with LST	60
2.5.5	Pearson’s correlation coefficient between LST, NDVI and NDBI by different LULC types	65
2.6	Summary and conclusions	67
CHAPTER 3. HYDROLOGIC RESPONSE IN AN URBAN WATERSHED AS AFFECTED BY CLIMATE AND LAND-USE CHANGE.....		70
3.1	Introduction.....	70
3.2	Materials and Methods.....	75
3.2.1	Study area	75
3.2.2	Datasets Description	76
3.2.2.1	Hydro-Meteorological Data.....	76
3.2.2.2	Topography and Soil Type	76
3.2.2.3	Land-Use Data.....	77
3.2.2.4	Hydrological SWAT Model	77
3.2.3	Methods	78
3.2.3.1	Land-Use Change Detection.....	78
3.2.3.2	Temporal Trend Analysis Method.....	78
3.2.3.3	Baseflow Separation Using Web-Based Bflow.....	79
3.2.3.4	Scenario Analysis: Modeling Hydrological Response to Climate Variability and Land-Use Dynamic	79
3.3	Results and Discussion	81
3.3.1	Land Use Changes from 1992 to 2011	81
3.3.2	Changes in Temperatures and Precipitation	83
3.3.3	Changes in Hydrological Variables.....	85
3.3.4	The SUFI-2 Calibration and Uncertainty Analysis Algorithm.....	86

3.3.5	Parameter Sensitivity Analysis	90
3.3.6	Selection of SWAT Model Structure.....	91
3.3.7	Calibration and Validation of SWAT Model.....	92
3.3.8	Changes in Total Water Yield and Baseflow within Various Simulation Scenario ..	95
3.4	Summary and Conclusions	100
CHAPTER 4. A COMPARISON OF STREAMFLOW AND BASEFLOW RESPONSES TO LAND-USE CHANGE AND THE VARIATION IN CLIMATE PARAMETERS USING SWAT		102
4.1	Introduction.....	102
4.2	Study Areas.....	106
4.2.1	Upper West Branch DuPage River Watershed	106
4.2.2	Walzem Creek	107
4.3	Materials and Methods.....	109
4.3.1	Data Development	109
4.3.1.1	Spatial Data.....	109
4.3.1.2	Hydro-Meteorological Data.....	110
4.3.2	Methodology.....	110
4.3.2.1	Baseflow Separation	110
4.3.2.2	Soil and Water Assessment Tool (SWAT) Model Calibration and Validation..	111
4.3.2.3	Model Sensitivity Analysis.....	113
4.3.2.4	Statistical Criteria and Model Evaluation Performance	114
4.3.2.5	Scenarios Separating the Impact of Land Use Change and Climate Change	114
4.4	Results and Discussions.....	115
4.4.1	Trends in Hydrologic Components.....	115
4.4.2	Trends in Climatic Components	117
4.4.3	Changes in Land Use Characteristics	121
4.4.4	SWAT Model Calibration and Validation Results	124
4.4.5	Impacts of Land use Change.....	130
4.4.6	Impacts of climate variation	136
4.4.7	Combined Impacts of Both Land Use Change and Climate Variations	138
4.5	Summary and Conclusions	141

CHAPTER 5. IMPACTS OF WATERSHED PHYSICAL PROPERTIES AND LAND-USE ON BASEFLOW IN TEXAS, USA	144
5.1 Introduction.....	145
5.2 Materials and Methods.....	152
5.2.1 Study area description.....	152
5.2.2 Watershed selection	156
5.2.3 Baseflow Index Evaluation.....	157
5.2.4 Dataset Development.....	158
5.2.4.1 Topographical Variables.....	159
5.2.4.2 Hydro-Meteorological and land use data.....	159
5.2.4.3 Soil Types and Lithology	160
5.2.4.4 Hydrogeological variables	160
5.2.5 Model development	163
5.3 Results and Discussions.....	171
5.3.1 BFI estimation	171
5.3.2 Regression models.....	174
5.3.2.1 Category 1.....	174
5.3.2.2 Category 2.....	180
5.3.2.3 Category 3.....	187
5.3.2.4 Category 4.....	193
5.3.2.5 Category 5.....	200
5.3.3 Limitations of our Approach	207
5.4 Summary and Conclusions	209
CHAPTER 6. CONCLUSIONS AND FUTURE WORK	213
6.1 Conclusions.....	213
6.2 Recommendations and Future Work	218
REFERENCES	220
VITA.....	242

LIST OF TABLES

Table 2.1. Specification of Landsat satellite images used in the study (*TIR=120×30, data is acquired at 100 m and resampled to 30 m).....	37
Table 2.2. Classification schema of LULC in the study area.	42
Table 2.3. Landsat thermal band calibration constants.....	46
Table 2.4. Accuracy assessment of different supervised classification algorithms used for LULC maps in GCR.....	50
Table 2.5. Accuracy assessment of the LULC classification results for GCR.....	50
Table 2.6. ‘From-to’ LULC change detection statistics for 1990-2003 for GCR in hectare.....	53
Table 2.7. ‘From-to’ LULC change detection statistics for 2003-2016 for GCR in hectare.....	53
Table 2.8. Areas of LULC classes in the three time periods 1990, 2003 and 2016 in the study area.....	55
Table 2.9. Cross validation of the estimated LST from Landsat data with meteorological data for GCR.....	58
Table 2.10. Average LST distribution (°C) over different LULC classes in GCR for 1990, 2003 and 2016.....	59
Table 2.11. Average LST change in different LULC change types from 1990 to 2016 in GCR.	60
Table 2.12. Mean values of NDVI and NDBI for the years 1990, 2003 and 2016 for GCR.....	61
Table 2.13. Correlation coefficient matrix from the indices and LST for the years 1990, 2003 and 2016 for GCR.....	61
Table 2.14. Pearson’s correlation between LST and two indices at 0.05 significance level.....	62
Table 2.15. Pearson’s correlation between LST and NDVI by LULC type at 0.05 significance level.....	65
Table 2.16. Pearson’s correlation between LST and NDBI by LULC type at 0.05 significance level.....	66
Table 3.1. Land use change transition matrix in LEC from 1992 to 2011 (km ²).	83
Table 3.2. Temporal trends in annual precipitation and temperature in the LEC watershed.	84
Table 3.3. Trend analysis and significance test for monthly precipitation and temperature in the LEC Watershed.....	85
Table 3.4. Temporal trends in annual streamflow and baseflow in the LEC watershed.	85
Table 3.5. SWAT input parameters used for the LEC calibration of streamflow and baseflow. .	88

Table 3.6. SWAT performance evaluation criteria according to Lee et al. (2018), Moriasi et al. (2013), and Thirel et al. (2015).....	90
Table 3.7. List of top 10 ranking sensitive parameters for SWAT in the LEC watershed and their calibrated values.....	91
Table 3.8. Values of statistical indicators in the calibration and validation periods for streamflow and baseflow in the LEC watershed.....	95
Table 3.9. Average annual change in water yield and baseflow in the LEC watershed.	96
Table 4.1. SWAT input parameters used for the UWBDR and Walzem Creek watersheds calibration of streamflow and baseflow (Aboelnour et al., 2020).	112
Table 4.2. Top 10 optimized SWAT sensitive parameter values in the UWBDR watershed and Walzem Creek watershed.	114
Table 4.3. Temporal trends in annual streamflow and baseflow in the study areas.	116
Table 4.4. Temporal trends in annual streamflow and baseflow in the study areas.	119
Table 4.5. Summary of significance test and trend analysis for monthly precipitation and temperature in the UWBDR and Walzem Creek watersheds.	120
Table 4.6. Transition matrix (in percentages) of land use change in UWBDR from 1992 to 2011.	122
Table 4.7. Transition matrix (in percentages) of land use change in the Walzem Creek watershed from 1992 to 2011.....	124
Table 4.8. Statistical indicators for calibration and validation periods for streamflow and baseflow in the UWBDR watershed and Walzem Creek watershed.....	126
Table 4.9. Average annual change in water balance components in the UWBDR watershed. ..	131
Table 4.10. Average annual change in water balance components in the Walzem Creek watershed.	131
Table 5.1. Review of some research evaluating the relationship between watershed properties and baseflow.	151
Table 5.2. Variables representing watershed properties for developing regression model.	162
Table 5.3. Baseflow prediction models developed for the Category 1 area.	175
Table 5.4. Values of statistical indicators in model development and validation for BFI prediction in the Category 1 region.....	178
Table 5.5. Baseflow prediction models developed for the Category 2 area.	182
Table 5.6. Values of statistical indicators in model development and validation for BFI prediction in the Category 2 region.....	185
Table 5.7. Baseflow prediction models developed for the Category 3 area.	189

Table 5.8. Values of statistical indicators in model development and validation for BFI prediction in the Category 3 region.....	190
Table 5.9. Baseflow prediction models developed for the Category 4 area.	195
Table 5.10. Values of statistical indicators in model development and validation for BFI prediction in the Category 4 region.....	196
Table 5.11. Baseflow prediction models developed for the Category 5 area.	202
Table 5.12. Values of statistical indicators in model development and validation for BFI prediction in the Category 5 region.....	204
Table 5.13. Values of statewide statistical indicators in model development for BFI prediction.	207

LIST OF FIGURES

Figure 2.1. Greater Cairo Region (GCR), Egypt: (a) Location map, (b) the study area (Source: (a) ESRI online, (b) Landsat 8 Pan-Sharpended with Digital Elevation Model (DEM) from Shuttle Radar Topography Mission (SRTM) (U.S.Geological Survey, n.d.)).....	35
Figure 2.2. Growth of GCR urban population during 1990-2016 according to Central Agency of Public Mobilization and Statistics (CAPMAS, 2017)	36
Figure 2.3. Data processing flow chart depicting procedures applied for preparation of LULC maps and LST evaluation from Landsat datasets	39
Figure 2.4. RGB band combination according to the highest OIF values of (a) TM 1990, (b) TM 2003, and (c) OLI 2016.....	41
Figure 2.5. LULC map produced by classification processes for the years 1990, 2003 and 2016 showing the change for types of classes within the study area.....	51
Figure 2.6. LULC change in GCR during 1990-2016	52
Figure 2.7. Land cover conversion in GCR from 1990 to 2016	54
Figure 2.8. Percentage of land cover types in GCR for the three time periods	55
Figure 2.9. Contribution to the net change in the urban land cover in GCR (Area percentage %)	56
Figure 2.10. Spatial distribution of GCR LST for the years (a) 1990, (b) 2003 and (c) 2016.....	57
Figure 2.11. Spatial distribution of NDVI for the years (a) 1990, (b) 2003 and (c) 2016.....	62
Figure 2.12. Spatial distribution of NDBI for the years (a) 1990, (b) 2003 and (c) 2016	62
Figure 2.13. Correlation between NDVI and LST for the years (a) 1990, (b) 2003 and (c) 2016 for GCR	64
Figure 2.14. Correlation between NDBI and LST for the years (a) 1990, (b) 2003 and (c) 2016 for GCR	64
Figure 2.15. Correlation among LST, NDVI and NDBI from a West/East profile in 2016 imagery	65
Figure 3.1. Index map showing location of the Little Eagle Creek (LEC) watershed in Indiana.	75
Figure 3.2. Flow chart depicting procedure for SWAT model setup, calibration and validation of both streamflow and baseflow in the LEC watershed.	81
Figure 3.3. Land use types in LEC watershed in (A) 1992; (B) 2011 and (C) the transition between 1992 and 2011.....	82
Figure 3.4. Annual precipitation (a) and temperature (b) in the LEC watershed.	84
Figure 3.5. Average daily streamflow (a) and baseflow (b) over time in the LEC watershed.	86

Figure 3.6. Observed and simulated streamflow of LEC watershed for calibration and validation period.	93
Figure 3.7. Observed and simulated baseflow of LEC watershed for calibration and validation period.	93
Figure 3.8. Average monthly water yield for the LEC watershed under different scenarios.	98
Figure 3.9. Average monthly baseflow for the LEC watershed under different scenarios.	98
Figure 3.10. Relative change in average monthly streamflow in the LEC watershed.	99
Figure 3.11. Relative change in average monthly baseflow in the LEC watershed.	99
Figure 4.1. Index map showing location of the study watersheds: (a) Upper West Branch DuPage River in Illinois; and (b) Walzem Creek in Texas.	108
Figure 4.2. Flow chart showing the methodology used in this study	109
Figure 4.3. Average daily streamflow (a) and baseflow (b) in the UWBDR watershed; and average daily streamflow (c) and baseflow (d) in the Walzem Creek watershed.	117
Figure 4.4. Annual precipitation (a) and temperature (b) in the UWBDR watershed; and annual precipitation (c) and temperature (d) in the Walzem Creek watershed.	119
Figure 4.5. Land use types in the UWBDR watershed in: (A) 1992; (B) 2011; and (C) the transition between 1992 and 2011.	122
Figure 4.6. Land use types in the Walzem Creek watershed in: (A) 1992; (B) 2011; and (C) the transition between 1992 and 2011.	123
Figure 4.7. Observed and simulated time series streamflow for the UWBDR watershed during calibration and validation periods.	126
Figure 4.8. Observed and simulated time series baseflow for the UWBDR watershed during calibration and validation periods.	127
Figure 4.9. Observed and simulated time series streamflow for the Walzem Creek watershed during calibration and validation periods.	129
Figure 4.10. Observed and simulated time series baseflow for the Walzem Creek watershed during calibration and validation periods.	129
Figure 4.11. Monthly water yield change for the UWBDR watershed under different scenarios.	132
Figure 4.12. Monthly baseflow change for the UWBDR watershed under different scenarios.	132
Figure 4.13. Monthly water yield change for the Walzem Creek watershed under different scenarios.	134
Figure 4.14. Monthly baseflow change for the Walzem Creek watershed under different scenarios.	134

Figure 4.15. Absolute change in mean monthly streamflow for the UWBDR watershed under different scenarios.....	136
Figure 4.16. Absolute change in mean monthly streamflow for the Walzem Creek watershed under different scenarios.....	141
Figure 5.1. Geologic regions of Texas (Texas Water Development Board, 2012).	152
Figure 5.2. Average annual precipitation in Texas (ESRI, 2020).....	153
Figure 5.3. Average annual evapotranspiration in Texas (ESRI, 2020).	153
Figure 5.4. Average annual runoff in Texas in thousands of gallons from a typical 2000 ft ² area (Texas Water Development Board, 2012).	154
Figure 5.5. Watersheds used for model development and validation in Texas.	156
Figure 5.6. Climate zones of Texas and categories used in this study.....	164
Figure 5.7. Correlation matrix of watershed variables used for BFI prediction in this study. (a) variables representing topography, stream properties, metrology and land use; (b) variables representing geomorphology, soil, lithology and hydrogeology.....	167
Figure 5.8. Flow charts showing the procedures to develop models examining the relationship between baseflow and watershed properties.....	170
Figure 5.9. Map of major aquifers in Texas (Texas Water Development Board, 2012).	171
Figure 5.10. BFI at gauged station locations of each selected watershed in this study.	174
Figure 5.11. Boxplots of RE for BFI prediction model development and validation for the Category 1 region.	177
Figure 5.12. Boxplots of ARE for BFI prediction model development and validation for the Category 1 region.....	177
Figure 5.13. Observed (filtered) and predicted BFI measured within the three scenarios in the Category 1 region.....	179
Figure 5.14. Observed (filtered) and predicted BFI for the validation dataset within the three scenarios in the Category 1 region.....	180
Figure 5.15. Boxplots of RE for BFI prediction model development and validation for the Category 2 region.	184
Figure 5.16. Boxplots of ARE for BFI prediction model development and validation for the Category 2 region.....	184
Figure 5.17. Observed (filtered) and predicted BFI measured within the three scenarios in the Category 2 region.....	186
Figure 5.18. Observed (filtered) and predicted BFI for the validation dataset within the three scenarios in the Category 2 region.....	187

Figure 5.19. Boxplots of RE for BFI prediction model development and validation for the Category 3 region.	191
Figure 5.20. Boxplots of ARE for BFI prediction model development and validation for the Category 3 region.....	191
Figure 5.21. Observed (filtered) and predicted BFI measured within the three scenarios in the Category 3 region.....	192
Figure 5.22. Observed (filtered) and predicted BFI for the validation dataset within the three scenarios in the Category 3 region.....	193
Figure 5.23. Boxplots of RE for BFI prediction model development and validation for the Category 4 region.	197
Figure 5.24. Boxplots of ARE for BFI prediction model development and validation for the Category 4 region.....	197
Figure 5.25. Observed (filtered) and predicted BFI measured within the three scenarios in the Category 4 region.....	199
Figure 5.26. Observed (filtered) and predicted BFI for the validation dataset within the three scenarios in the Category 4 region.....	200
Figure 5.27. Boxplots of RE for BFI prediction model development and validation for the Category 5 region.	203
Figure 5.28. Boxplots of ARE for BFI prediction model development and validation for the Category 5 region.....	203
Figure 5.29. Observed (filtered) and predicted BFI measured within the three scenarios in the Category 5 region.....	205
Figure 5.30. Observed (filtered) and predicted BFI for the validation dataset within the three scenarios in the Category 4 region.....	206

LIST OF ABBREVIATIONS

ACF	Auto Correlation Function
AIC	Akaike Information Criteria
All	Alluvial sediments
ARE	Absolute relative error
ASTER	Advanced Spaceborne Thermal Emission and Reflection Radiometer
AVHRR	Advanced Very High Resolution Radiometer
AWS	Available water storage at depth 0-1.5 m
BEG	Bureau of Economic Geology
BFI	Baseflow Index
Brn	Barren lands
CCF	Cloud Cover Fraction
Clt	Cultivated areas
Cstl	Coastal zone sediments
Coll	Colluvial sediments
DA	Basin drainage areas for each stream gauge
DEM	Digital Elevation Model
DN	Digital number
Dvlp	Developed areas
Elev	Average watershed elevation
ENS	Nash–Sutcliffe model efficiency
ENVI	Environment for Visualizing Images
Eol	Eolian sediments
ERDAS	Earth Resources Data Analysis Systems
ETM+	Enhanced Thematic Mapper
FAO	Food and Agriculture Organization
FDC	Flow Duration Curve
Frst	Forests
GCP	Ground Control Points

GCR	Greater Cairo Region
GDG	Geospatial Data Gateway
GIS	Geographic Information Systems
GOES-8	Geostationary Operational Environmental Satellite
GPS	Global Positioning System
Hrb	Herbaceous cover
HRUs	Hydrologic Response units
HUC	Hydrologic units codes
Hydx	Hydrologic soil group
K	Hydrologic conductivity
ILWIS	Integrated Land and Water Information System
L1T	Level-one terrain
LCCS	Land Cover Classification System
LEC	Little Eagle Creek
LST	Land Surface Temperature
LULC	Land use/land cover
MODIS	Moderate Resolution Imaging Spectroradiometer
MMS	Multi-spectral Scanner
NCDC	National Climate Data Center
NDBI	Normalized Different Built-up Index
NDVI	Normalized Different Vegetation Index
NHD	National Hydrography Dataset
NLCD	National Land Cover Database
NMV	National Map Viewer
NWIS	National Water Information System
OLI	Operational Land Imager
PBIAS	Percentage of biasness
PCA	Principle Component Analysis
PRCP	Annual precipitation
R2	Correlation Coefficient
Relv	Average watershed relief

Res	Residual deposits
RGB	Red, green, blue
ROI	Region of Interest
RS	Remote Sensing
SAS	Statistical Analysis System
SCS	Soil Conservation Service
SPI	Stream Power Index
Srb	Shrubland
SRTM	Shuttle Radar Topography Mission
STI	Sediment transport Index
StrD	Stream Density
SVM	Support Vector Machine
SWAT	Soil and Water Assessment Tool
TAVG	Average temperature
TI	Topographic index
TIR	Thermal Infrared
TM	Thematic Mapper
TMAX	Maximum temperature
TMIN	Minimum temperature
TOA	Top of Atmospheric
Tr	Transmissivity
TStrL	Total Stream Length
TWDB	Texas Water Development Board
UTM	Universal Transverse Mercator
UWBDR	Upper West Branch DuPage River
VIF	Variance inflation factor
WGS-84	World Geodetic System 1984
WSA	Watershed areas
WSlp	Average watershed slope
WTD	Depth to water
Wtl	Wetland areas

Wtr Water cover

ABSTRACT

Land use alteration and climate change are major contributors to the hydrological cycle within watersheds. They can influence the quantity and quality of water resources, the ecosystem and environmental sustainability. Urban areas have expanded in recent decades, accompanied by a noticeable increase in energy and water use. Such changes in land use have many implications for humans to meet the increasing share of the planet's resources and water issues. Hence, distinguishing the effects of land use change from concurrent climate variability is a particular challenge for studies on operational management processes. In this work, some shortcomings related to climate variability and land use change have been addressed, as applied to land surface temperature (LST) and groundwater resources. Thus, the main goal of this study is to evaluate the impacts of land use change on surface temperature and the impact of urbanization and climate variation on hydrology. The research methodology included modeling approaches that were used to estimate the land surface temperature and the responses of hydrology to climate change and urbanization.

Land use maps derived from Landsat datasets were analyzed using several classification techniques to evaluate the intensity and pattern of urbanization and land surface temperature in the Greater Cairo Region (GCR), Egypt. Accuracy of Landsat derived land use data were relatively high and up to 96.5%. Findings indicated that the GCR land use alteration was dynamic and that vegetation loss was the main contributor to urban expansion in the GCR. Consequently, this led to increased LST and modified urban microclimate. The results showed that vegetation cover decreased by 7.73% within a 26-year timespan (1990-2016).

Land use alteration impacted not only land surface temperature, but also, combined with variation in climate, affected watershed hydrology, specifically streamflow and baseflow. Changes in streamflow and filtered baseflow in three watersheds: Little Eagle Creek (LEC), Upper West Branch DuPage River (UWBDR) and Walzem Creek watershed, from 1980 to 2017, caused by climate alteration and land use change were separated and assessed using the SWAT (Soil and Water Assessment Tool) model. Results showed that SWAT performed well in capturing the streamflow and baseflow in urban catchments. SWAT model calibration and validation was within acceptable levels for streamflow and baseflow. About 30%, 30% and 12% of the LEC, UWBDR and Walzem Creek watershed areas changed from agricultural to urban areas. Findings for the

LEC watershed indicated that the variability in the baseflow and streamflow appeared to be heavily driven by the response to climate change in comparison to the variability due to altered land use. The contribution of both land use alteration and climate variability on the flow variation was higher in the UWBDR watershed. In Walzem Creek, the alteration in streamflow and baseflow appeared to be driven by the effect of climate variability more than that of urbanization.

Finally, the impacts of basin lithology and physical properties on baseflow were examined using multiple regression models. Results suggest that the baseflow index (BFI) can be predicted using the basin's physical and geological characteristics. This included different land uses and climate variables with high accuracy and low relative errors. BFI was found to be highly driven by precipitation and fractional areas of different lithologies in the basins in various regions. These could be estimated with a high accuracy, as opposed to evapotranspiration that caused lower model accuracy.

Information gleaned from these outputs can help in understanding the dynamics of land use change and climate variation, in order to help policy-makers predict and plan for future expansion in developing countries and across the globe, in achieving long-term sustainability of soil and water resources and their impact on climate change. Increasing efforts to prevent further urbanization and vegetation loss should be regarded as a practical management strategy and are of vital significance to many communities. In addition, the regression models developed in this study can be easily exploited in other areas with poor hydrological data quality and ungauged sites in order to estimate the amount of groundwater discharge.

CHAPTER 1. INTRODUCTION

EFFECTS OF LAND USE CONVERSION ON ENVIRONMENTAL AND ECOLOGICAL ISSUES

1.1 Introduction

Land use conversion has generally been considered a local environmental and ecological issue, but it is becoming a force of global importance. Population growth and associated urban expansion are one of the main factors that impact climate, soil, water quality and quantity. Land surface impacts that occur during the process of urbanization include, but are not limited to, soil compaction, waterways, vegetation reduction and change from permeable to impervious surfaces as buildings, parking lots and roads are constructed. However, several decades of studies have uncovered the broader environmental effects of land use change throughout the globe, ranging from changes in atmospheric composition to the extensive alteration of Earth's ecosystems. A seeming lack of planning of land use has been a problem at local to regional scales, making it a major issue in the study of worldwide ecological change (Adger et al., 2005; Omran, 2012).

Urban areas have expanded in recent decades, accompanied by a noticeable increase in energy and water use. Such changes in land use have many implications for humans to appropriate an increasing share of the planet's resources (Foley et al., 2005), environmental resilience, and water issues, such as the alteration of runoff, infiltration and groundwater discharge (Chen et al., 2017). Distinguishing the effects of land use change from concurrent climate variability and understanding the water balance is a particular challenge for studies on operational management processes. This problem can be solved by understanding the interaction between the Earth's surface, atmosphere, hydrological components and the dynamics of land use change at various scales that drive them.

In light of the above discussion, three main issues or gaps in this work related to the interaction between land use change, surface properties and hydrology, have been identified for making a contribution to the scientific community.

First, land use dynamics can alter local and regional climates through their impacts on net radiation, the division of energy into sensible and latent heat, and partitioning of rainfall into soil water, evapotranspiration and runoff (Foley et al., 2005). Urban heat islands are an extreme case of how land use alters regional climate. The increases in land surface temperature over the past

several decades are considered a major issue in urban regions, due to the conversion of vegetation cover to impervious cover (Pal & Ziaul, 2016), which in turn has a negative impact on people (Tran et al., 2017), affects many environmental processes and modifies the degree of solar radiation absorption, evaporation rates, desertification, air pollution, albedo, heat storage, wind turbulence and many aspects of the water balance (Javed Mallick et al., 2008).

Here, two significant facts were identified: 1) Studies revealed that settlements in developing countries grow five times as fast as those in developed ones (Bhagyanagar et al., 2012). Modeling research suggested that land use conversion in arid region impacts climate through the change in water balance, but the modification in temperate and boreal vegetation affects climate primarily through changes in surface radiation balance. Cities located in semi-arid and arid regions require more attention to be better evaluated and understood. In Egypt, the reduction of vegetation cover, increase of impervious cover, and the morphology of buildings in big cities combines to store heat, lower evaporative cooling and warm the surface air. The reduction of vegetation cover and agricultural area, especially for urbanization purposes, illustrates the poor planning of farmland protection laws and the ignoring of environmental and ecological legislation implemented in the urban master plan. In addition, there are limited regional figures on land expense for monitoring urban expansion. 2) In recent decades, accurate mapping of land surface temperature and urban heat islands have become more significant in providing information about surface physical properties. Even though land surface temperature and land use alteration can be monitored by traditional surveys in developed countries, the use of satellite images has become the predominant way to monitor surface radiant temperature on local and regional scales (Li et al., 2014; Kimuku & Ngigi, 2017). Satellite datasets are considered a time and cost-effective technique that can provide more information with respect to geographical distribution of land use (Abdulaziz et al., 2009). As a result, they have been widely used to evaluate land use change with useful outputs and different scales. Nevertheless, acquiring observed meteorological data is quite challenging in Egypt, due to the limited resources of data acquisition. Therefore, in this sense, the concept of using remote sensing data in conjunction with Geographic Information Systems (GIS) can provide effective ways for mapping urban areas, modeling urban growth and monitoring the dynamic changes of land use.

Second, the diversities of water-related challenges are large and expected to increase in the future. Hydrological modeling is essential to help understand these ongoing issues including water

quality and quantity, soil moisture and erosion, climate change, and land use change impacts at different scales (Anache et al., 2017; Martinez-Martinez et al., 2014). Land use conversion plays an important role in the distribution of surface water balance and the partitioning of precipitation into evapotranspiration, runoff, and groundwater discharge. Nonetheless, water demands associated with land use practices, e.g. irrigation, directly affect freshwater supplies through water diversion and withdrawal (Foley et al., 2005).

Groundwater is considered the primary source of water for over 1.5 billion people worldwide, and is a critical component of the global environment (Alley et al., 2002). In the United States, approximately one-half of the population depends on groundwater for its supply of potable water. Despite the widespread use of groundwater as potable drinking water in the United States and globally, groundwater is a poorly understood resource by most people (Solly et al., 1998), and it has been increasingly threatened, directly and indirectly, by the action of human activities and land use alteration. Therefore, studies to evaluate the spatial and temporal distribution of water resources, and accurate analysis of water flow (streamflow and baseflow) is critical for sustainable groundwater management, which is required for sound ecosystems and quality of human life.

This problem can be solved by the combination of hydrologic models and the study of land use dynamics. Compared to groundwater sampling and monitoring, groundwater modeling is less complex and costly, and allows evaluation of broad areas (Jang et al., 2018). In this sense, three main points must also be considered: 1) The impacts of land use change and climate variability on watershed hydrology are theoretically interlinked and, therefore, cannot be separated. This coupling effect, together with water withdrawal and retention, contributes to the uncertainties in identifying the specific impact of each factor on watershed hydrology. It makes inferring causation difficult to accomplish at a sufficient scale, and, therefore, it remains unclear which of these factors dominantly contributes to watershed hydrology (Omer et al., 2017). In this sense, distinguishing the effects of land use change from concurrent climate variability and understanding the water balance and water flow are considered a particular challenge for studies on operational management of reservoirs and river basins. 2) Impacts of climate and land use change on watershed hydrology vary from place to place and need to be investigated on a local scale (Khoi & Thom, 2015). Therefore, there is a need to use comprehensive and physical tools to evaluate as much information as possible from limited existing data. Hence, hydrological models, rather than paired catchment and statistical approaches, are considered the most appealing approach to carry out

impact assessments studies. They provide a conceptualized framework and are suitable to be used as part of scenario studies on the relationship between climate variability, land use change and hydrological components. Among these models is the Soil and Water Assessment Tool (SWAT). SWAT is a conceptual mathematical semi-physical, semi-distributed based model (Luo et al., 2012) that can simulate surface flow and shallow groundwater dynamics based on hydrologic response units (HRUs). 3) Streamflow and baseflow in the US Midwest region reported upward trends with both land use change and climate variability in urbanized watersheds (Ahiablame et al., 2013a; Ahiablame et al., 2013b; Kumar et al., 2009). While previous streamflow and baseflow trend investigations included urbanized watersheds in the Midwest region, they lacked integration analysis, which exclusively focuses on the interactive effects of both land use change and climate variability on urbanized catchments. In this context, it is critical to focus on this issue, considering both the individual and coupled effects of both human and natural impacts.

Third, baseflow is that part of streamflow that is derived from groundwater and other delayed sources such as snowmelt into the stream, and considered to be one of the most important low-flow components in the hydrological cycle of a watershed in different climatic conditions. Baseflow displays spatial and temporal variability. Here, it is believed that, not only land use variation and climate conditions play a role in controlling baseflow, but also other watershed properties, for instance topography, geology, geomorphology, vegetation, frequency and amount of discharge, and soil types. Many of these factors may be altered due to human activities on the landscape, and therefore, it is critical to understand the relationship between catchment physical properties and baseflow.

Two main facts related to this point can be identified: 1) Previous studies indicated that the effects of watershed physical properties on baseflow can be evaluated through relationships between catchment properties and baseflow but not in the context of regional scale that has different climatic pattern and geologic features. In addition, when it comes to which geologic unit and which climate category to consider in quantifying the impacts on baseflow, nothing is definitely known. Even though there is an assumption that the underlying geology influences baseflow, previous studies that estimate average annual baseflow typically simplify the effect of watershed geology to physical parameters that represent the fractional area of aquifer in a catchment (Bloomfield et al., 2009). To date the relationship between catchment geology and baseflow index (BFI) has not been quantified in a systematic manner. 2) Baseflow is generally

derived from available stream flow data using hydrograph separation methods. However, most of these methods are limited to estimating baseflow in gauged sites. With the development of geographic information systems and continuously increasing availability of digital data, it is much more feasible today to derive variables representing soil, geology, climate, and geomorphological characteristics of a basin than a decade ago. In this sense, it is now possible to explore relationships between more basin variables and groundwater recharge in ungauged watersheds, with possibilities of finding more accurate and meaningful models. Therefore, the last objective in this project is to test the impact of geological bedrock on baseflow along with other catchment properties.

1.2 Objectives

The overall goals of this dissertation are to 1) Analyze land use alteration by utilizing multi-spectral Landsat data of Greater Cairo Region (GCR), Egypt, for 1990, 2003 and 2016 through the integration of remote sensing and GIS. In addition, the use of these Landsat data to estimate land surface temperature (LST) in GCR; 2) assess the response of watershed streamflow and baseflow to climate variability and land use change in urban watersheds in the Midwest region of the United States, and compare it with an urban catchment in a semi-arid region; and 3) develop statewide numerical regression models in Texas to evaluate the effects of bedrock geology and other catchment properties on baseflow and to estimate average annual baseflow in watershed tributaries. In this research, various modeling approaches were used to estimate the land surface temperature and the responses of hydrology to climate change and urbanization. Data were acquired from different sources. The specific objectives in this study are as follows:

1. Evaluate the land use and land surface temperature changes through classifications and post-classification change detection techniques by utilizing multi-spectral Landsat Thematic Mapper (TM) and Operational Land Imager (OLI) data of GCR for 1990, 2003 and 2016. 1) quantitatively delineate different LULC classes and evaluate the pattern of LULC change from 1990 to 2016 in GCR; 2) provide tools to reliably investigate the variation of LST values in relation to land use change through time; and 3) examine the potential and the accuracy of RS and GIS utilization in monitoring the spatial distribution of LULC changes. Two of the most important underlying premises of the objectives tested in the investigation are the opportunity

of obtaining land use and LST maps from synoptic view of Landsat images over large spatial areas and improvement of thermal studies in Egypt that will be used to justify subsidies in legislation seeking to reduce impacts of thermal comfort in existing urban areas.

2. Evaluate the response of watershed streamflow and baseflow to climate variability and land-use change in urban watersheds, based on simulation following a comprehensive calibration. 1) analyze long-term trends of historical streamflow, land use and rainfall in an urban watershed; and identify changes in land use from 1992 to 2011; 2) calibrate and validate the SWAT model, using different land-use patterns for different periods; and 3) investigate hydrological streamflow and baseflow sensitivity to land-use change and climate variability and simulate the joint effects of both climate and land-use change on hydrology in these watersheds. For this goal, plausible scenarios of land-use change and climate variation were developed based on trends and information exploited from different watersheds.
3. Investigate the impact of geological bedrock on baseflow and BFI along with other catchment properties. 1) Estimation of average annual baseflow in watershed tributaries in Texas from gauged sites using hydrograph separation models (recursive digital filter method); 2) Develop different geology-soil groups in the entire state of Texas to examine the physical relationship between average BFI and lithology/geological control in addition to other descriptive catchment properties, for instance climate, soil and topography; and 3) Make a statewide numerical regression model calibrated to the hydrograph separation results to estimate baseflow for ungauged areas and validate with regional relationships. This study hypothesizes that some catchment properties are more useful than others, and the more watershed variables included in the study, the more accurate the BFI prediction.

1.3 Dissertation Organization

This dissertation contains six chapters. Chapter 1: Introduction explaining the impacts of urbanization on ecological and environmental issues. It will focus of the research problems, gaps and the specific objectives of this study. Chapters 2 to 4 are standalone papers for each of the

proposed objectives in Chapter 1. Chapters 2 to 4 are reformatted from articles which are published in journals.

Chapter 2 covers the first objective that evaluates the effect of urbanization on land surface temperature in the Greater Cairo Region (GCR). Chapter 3 and 4 cover the second objective of analyzing the single and combined effects of land use alteration and climate variation on hydrology in different urbanized watersheds using the SWAT model. Chapter 5 covers the third objective to evaluate the relationship between baseflow index and geology along with other watershed characteristics. Finally, Chapter 6 is designed as an overall summary and conclusion of this research, in addition to pointing out significant outputs, uncertainties, and recommendations for conducting further studies in the future.

CHAPTER 2. APPLICATION OF REMOTE SENSING AND GEOGRAPHIC INFORMATION SYSTEMS TO ANALYZE LAND SURFACE TEMPERATURE IN RESPONSE TO LAND USE/LAND COVER CHANGE IN THE GREATER CAIRO REGION, EGYPT

Abstract

The Greater Cairo Region (GCR), Egypt, has experienced rapid urban expansion and broad development over the past several decades, and faces many environmental consequences. In order to mitigate these consequences, it is essential to examine the historical change in the urban sprawl of GCR, and its effect on land surface temperature (LST). This study fulfills this goal by generating land use/land cover (LULC) maps derived from Landsat 5 Thematic Mapper (TM) for 1990 and 2003 and Landsat 8 Operational Land Imager (OLI) for 2016, using several classification techniques. A spectral radiance model and a web-based atmospheric correction model were used to successfully evaluate LST from thermal bands of Landsat data. Overall accuracy of Landsat derived land use data were 90.3%, 96.5% and 94.9% for 1990, 2003 and 2016, respectively. The LULC change analysis revealed vegetation loss to urban land of 7.73% and from barren lands to urban uses of 8.70% within a 26-year timespan (1990-2016). This rapid urban growth significantly decreases vegetation areas, consequently increasing the LST and modifying the urban microclimate. Results from this study can help policymakers characterize the evolution of urban construction for future developments.

2.1 Introduction

Cities are dynamic due to unavoidable changes that can be assigned to many factors. One of the main factors behind these changes is urban growth and population expansion (Kafi et al., 2014). As the population of a given area increases, the interest for new settlements continues increasing at the expense of other land cover classes, for instance, vegetation and barren lands. Land surface impacts that occur during the process of urbanization include, but are not limited to, soil compaction, vegetation reduction and change from permeable to impervious surfaces as buildings, parking lots and roads are constructed. A seeming lack of planning of land use/land cover (LULC) has been a problem at local and regional scales, making it a major issue in the study of worldwide ecological change (Adger et al., 2005; Foley et al., 2005; Omran, 2012). Such changes have many

implications for human society, environmental resilience, and water issues, such as the alteration of runoff, infiltration and groundwater discharge (Chen et al., 2017). In addition, poor water quality occurs due to a lack of planning with comprehensive arrangements or any consideration regarding their effects on nature. Nevertheless, an increase in land surface temperatures (LST) is one of the key effects of LULC changes (Abdulaziz et al., 2009; Huyen et al., 2016; Li et al., 2014; Ogashawara & Bastos, 2012; Sahana et al., 2016; Sheikhi et al., 2015). Increases in LST over the past several decades are considered a major issue in urban regions, due to the conversion of vegetation cover to impervious cover (Pal & Ziaul, 2016), which in turn has a negative impact on people (Tran et al., 2017), affects many environmental processes and modifies the degree of solar radiation's absorption, evaporation rates, desertification, air pollution, albedo, heat storage, wind turbulence and many aspects of the water balance (Javed Mallick et al., 2008). Therefore, the impact on environmental processes cannot be well-understood and mitigated without understanding the impacts of climate change, the interaction between the earth and the atmosphere and knowledge of land use/land cover change at various scales that drive them (Omran, 2012).

Using remote sensing data in conjunction with Geographic Information Systems (GIS) have proved effective for mapping urban areas, modeling urban growth and monitoring the dynamic changes of LULC (Bhagyanagar et al., 2012; Kimuku & Ngigi, 2017). Remote sensing (RS) provides medium and high spatial, spectral and temporal resolution data with consistent and repetitive coverage of the earth's surface (Owen et al., 1998), and a high capability to extract change information from satellite data (Pal & Ziaul, 2016). However, LULC change and LST can be monitored by traditional surveys and land based observation stations, as well as satellite data, because it is a time and cost-effective technique that can provide more information with respect to land use's geographical distribution (Abdulaziz et al., 2009). Satellite RS techniques, therefore, have become prevalent in monitoring change detection in both rural and urban regions (Bauer et al., 1994; Wilson et al., 2002; Yang, 2002; Yuan et al., 2005). As a result, they have been widely used to evaluate LULC change with useful outputs and at different scales (Esam et al., 2012; Gilmore et al., 2008).

Landsat imagery, in particular, is among the most widely used satellite system. These datasets are available since 1972 from seven satellites in the Landsat series and they have been a major component of NASA's Earth observation program with four primary sensors: Multi-spectral Scanner (MSS), Thematic Mapper (TM), Enhanced Thematic Mapper (ETM+) and Operational

Land Imager (OLI). Landsat datasets have provided high resolution visible and infrared data, with thermal data and a panchromatic image. In addition, Landsat supplies an extraordinary level of information on the classification of several earth components at large scale (Butt et al., 2015; Ozesmi & Bauer, 2002) using a variety of automated change detection techniques and commonly applied classification algorithms (i.e. principle component analysis (PCA), unsupervised clustering, Hybrid, Fuzzy, Bayes and supervised classification). These change detection and classification techniques require personal experience and additional ancillary data with respect to study areas, i.e. very high resolution aerial images and ground data, which can be used to construct a trustworthy dataset for different classification algorithms that can be used further in training samples and accuracy assessments (Abdulaziz et al., 2009). Although ground data are considered to be the most reliable reference data, they are often either not accessible or very costly. Therefore, a pre-defined statistical characterizations file for the image is created to store a per-pixel signature of a certain land cover class. This uses the stored information and the raw digital number (DN) of each individual pixel in the scene and converts them to radiance values. Several researchers have applied similar techniques to achieve satisfactory results. For example, Landsat satellite images themselves were used to evaluate the performance of classification algorithms used to map forest clear cuts in the Pacific Northwest (Cohen et al., 1998). In addition, supervised classification maximum likelihood algorithms were applied to detect land cover change in a watershed in Pakistan and India with 95% and 92% overall accuracy, respectively (Butt et al., 2015; Rawat & Kumar, 2015). Although a high accuracy was obtained from these results, the presence of other reference data are essential to evaluate the overall accuracy and performance of the created geospatial maps (Abdulaziz et al., 2009).

Accurate mapping of LST is becoming more significant in providing information about surface physical properties (Javed Mallick et al., 2008), and the use of satellite images has become the predominant way to monitor LST on local and regional scales (Kimuku & Ngigi, 2017; Li et al., 2014). The use of thermal remote sensing data were first demonstrated by Rao in 1972 for monitoring urban areas in the mid-Atlantic coast of the USA (Rao, 1972). The contributions of RS and GIS have since been used to evaluate and model LST in many regions with several climatic conditions by various scholars using a diversity of thermal infrared (TIR) sensors. For instance, LST and Normalized Difference Vegetation Index (NDVI) were evaluated to compare the spatial occurrence of droughts over the geo-botanical zone of Mongolia using the NOAA-Advanced Very

High Resolution Radiometer (AVHRR) (Bayarjargal et al., 2006). Sun and Kafatos (2007) calculated the mean target brightness temperature and cloud cover fraction (CCF) derived from the Geostationary Operational Environmental Satellite (GOES-8) to find the correlation between LST and NDVI over North America. In addition, different algorithms were applied to retrieve LST from different satellite data, for instance, Landsat TM, Advanced Spaceborne Thermal Emission and Reflection Radiometer (ASTER) and Moderate Resolution Imaging Spectroradiometer (MODIS), in different regional scales (Liu & Zhang, 2011; Omran, 2012; Youneszadeh et al., 2015). Also, the patterns of LULC change were identified in some studies, followed by an investigation for the impact of these changes on LST (Ahmed et al., 2013; Sahana et al., 2016).

Cities located in semi-arid and arid regions require more attention to be better evaluated and understood (Rasul et al., 2017). In many developing countries of the world, including Egypt, there are limited regional figures on land expense for monitoring urban expansion. Settlements in developing countries grow five times as fast as those in developed ones (Bhagyanagar et al., 2012). The present study focuses mainly on change detection evaluation of LULC and LST in the Greater Cairo Region (GCR) of Egypt for the past two decades, from 1990 to 2016. The GCR contains the largest portion of facilities and services, enabling the foundation of dwelling places for qualified work forces that are generally found close to and within the city (Zaki et al., 2011). Moreover, due to the suitable topographic and geologic setting, the areas surrounding GCR showed the highest proportion of urban expansion. This has contributed to the high rate of population growth, city expansion and extravagant development.

The main thrust of this objective is to analyze LULC change through classifications and post-classification change detection techniques by utilizing multi-spectral Landsat TM and OLI data of GCR for 1990, 2003 and 2016 through the integration of remote sensing and GIS. In addition, the use of these Landsat data to estimate LST in GCR will be evaluated through different models and algorithms, as described in detail in the methodology section. The current study aims to: 1) quantitatively delineate different LULC classes and evaluate the pattern of LULC change from 1990 to 2016 in GCR; 2) provide tools to reliably investigate the variation of LST values in relation to LULC change through time; 3) further evaluate the effect of vegetation on LST as derived from different algorithms for satellite imagery through an examination of the NDVI-LST and NDBI-LST (Normalized Difference Built-up Index) correlation based on statistical analysis methods and the texture of LULC changes, to determine the main causes of these environmental

changes; and 4) examine the potential and the accuracy of RS and GIS utilization in monitoring the spatial distribution of LULC changes. The information gleaned from the validated change detection outputs can help in understanding the dynamics of LULC change in order to help policy-makers predict and plan for future developments in GCR, achieve long-term sustainability of soil and water resources, address impacts of climate change, and therefore characterize the evolution of new hot spots for urban construction lands and infrastructure development.

Two of the most important underlying premises of the objectives tested in the investigation are the opportunity to obtain a LULC and LST maps from synoptic view of Landsat images over large spatial areas, and improved thermal studies in Egypt that will be used to justify subsidies in legislation seeking to reduce impacts on thermal comfort in existing urban areas.

2.2 Study area

The selected study area for this research is the Greater Cairo Region (GCR), Egypt, which includes three sectors. The main sector is the metropolitan Cairo city on the eastern bank of the Nile River, parts of Giza City on the western bank of the Nile, and Qalyoubia, north of Cairo. The study area is located at 30°00'N and 31°20'E, in the middle and southern part, i.e. apex, of the Nile Delta Region, covering an area of 845,137 hectares (Figure 2.1). The Nile forms the administrative division between Cairo and Giza sectors, running through the study area in a floodplain 9 to 35 km wide. This is constricted by hills on both the eastern and western sides, with desert areas extending in the eastern and western direction (Shahin, 1990), characterizing it as a subtropical climatic region with high temperatures and solar radiation, dry and rainless summers, and cold, moist and rainy winters (Khoder, 2009).

The GCR was selected because of its unique location and climatic conditions, with a diversity of historical heritages, making it one of the most dynamic urban regions in Egypt. It now represents about 23 % of the total population of Egypt and 43 % of the urban population. While the population expansion has grown tenfold in the whole country, the GCR has grown more than thirty fold in the last century and a half (El-batran & Arandel, 1998). Half of this expansion has taken place on vegetated and rich agricultural land, while the other half has been on the agglomeration fringes located at the borders of GCR. Little sporadic growth in the form of new communities has been created on what was desert land on the eastern district. Based on Central

Agency for Public Mobilization and Statistics (CAPMAS) estimation, it appears that GCR has a population of about 20 million as of 2016 (CAPMAS, 2017) (Figure 2.2).

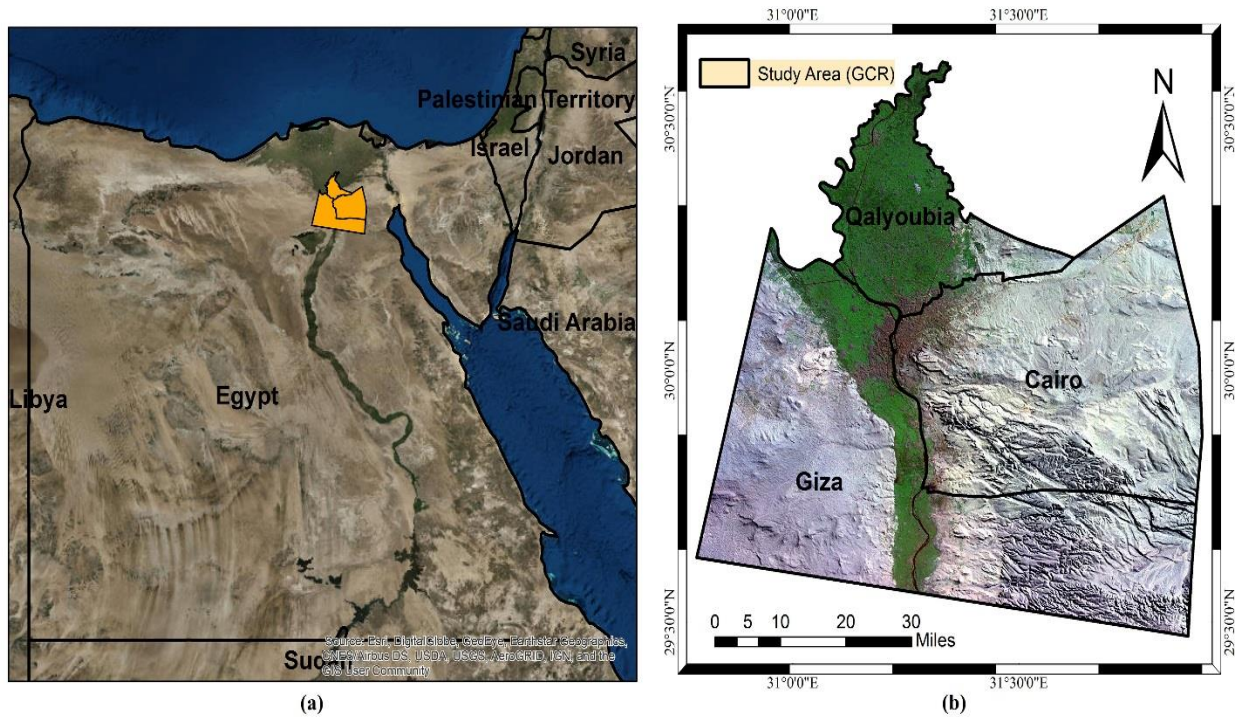


Figure 2.1. Greater Cairo Region (GCR), Egypt: (a) Location map, (b) the study area (Source: (a) ESRI online, (b) Landsat 8 Pan-Sharpned with Digital Elevation Model (DEM) from Shuttle Radar Topography Mission (SRTM) (U.S.Geological Survey, n.d.))

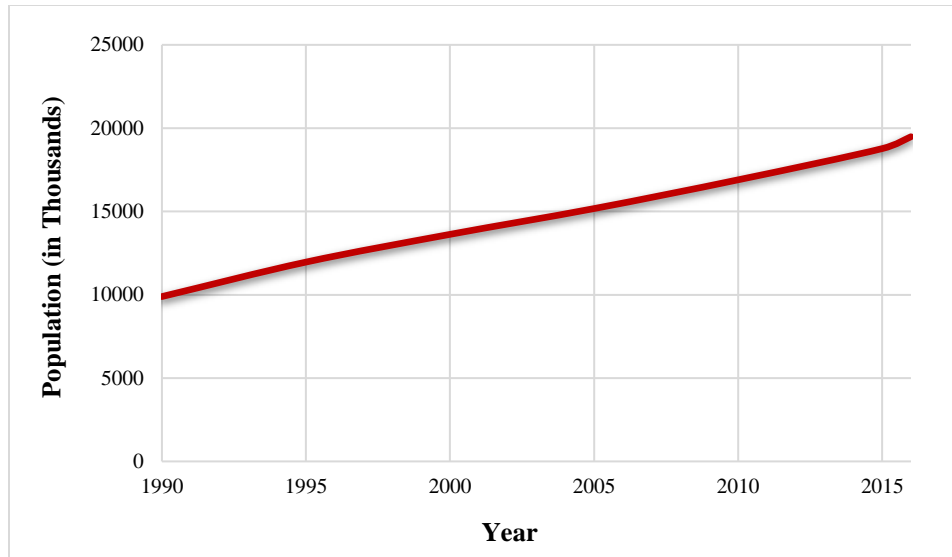


Figure 2.2. Growth of GCR urban population during 1990-2016 according to Central Agency of Public Mobilization and Statistics (CAPMAS, 2017)

2.3 Dataset description

2.3.1 Satellite data

Landsat 5 TM for 1990 and 2003 and Landsat 8 OLI 2016 were selected due to their high spatial resolution for both multispectral and thermal bands, which benefits an accurate location of different land uses and monitoring LST. Due to their availability, three cloud-free Landsat images were selected to detect changes in the study area: August 4, 1990; August 8, 2003; and August 11, 2016 with scenes along the same path. The details of the Landsat data used in the current study are furnished in Table 2.1. All the satellite images were acquired during the summer season, intermediate to the agricultural growth season, in which most agricultural fields are green and active, which maximizes the spectral difference between these agricultural fields, urban areas and barren lands (Abdulaziz et al., 2009). High-quality Landsat data acquisition is available from private and public sources.

Table 2.1. Specification of Landsat satellite images used in the study (*TIR=120×30, data is acquired at 100 m and resampled to 30 m)

Satellite	Sensor	Acquisition Date	Path/Row	Number of bands	Radiometric Resolution	Spatial Resolution (m)
Landsat 5	TM	Aug. 4 th 1990	176/39	7	8 bit	30 *TIR= 120×30
Landsat 5	TM	Aug. 8 th 2003	176/39	7	8 bit	30 TIR= 120×30
Landsat 8	OLI/TIRS	Aug. 11 th 2016	176/39	11	16 bit	30 TIR= 100×30

2.3.2 Auxiliary data

Reference data were compiled for each of the three years and then randomly divided for use in either classifier training or for accuracy assessment. These data were used to collect sufficient information for image preprocessing, evaluate the ground truth of a certain type of land use with its imaging characteristics (Omran, 2012), and to determine the major types of land cover in the study area. The generated reference data include Egyptian topographic maps with a large scale (1:50,000) prepared by the Egyptian Military Survey, geologic maps, Digital Elevation Model (DEM) (U.S. Geological Survey, n.d.) and road networks (OpenStreetMap, n.d.). Different spectral classes was done on the basis of land-cover types obtained from Food and Agriculture Organization FAO-Land Cover Classification System (LCCS) of 2004, knowledge-based approaches and incorporated information from organizations and institutions of the Egyptian Government. The ground truth data were in the form of reference data points used for assessing accuracy of the classification, selected using high resolution GeoEye and QuickBird imagery (DigitalGlobe, n.d.) in addition to points collected during a field survey using Global Positioning System (GPS) receivers.

Image processing, such as image extraction, rectification, atmospheric correction for Landsat data, restoration and classification, and GIS analysis and interpretation were performed using a set of software to assure higher accuracy: Earth Resources Data Analysis Systems (ERDAS) Imagine 2014, the Environment for Visualizing Images (ENVI 5.3), the Integrated Land and Water

Information System (ILWIS), ArcGIS 10.4 (ESRI) software, Python and Statistical Analysis System (SAS) software.

2.4 Methodology

The analysis included image preprocessing, image classification, land cover indices (NDVI and NDBI) derivation and the evaluation of LST using thermal bands in the Landsat dataset. A flowchart of the research process is described and summarized in Figure 2.3.

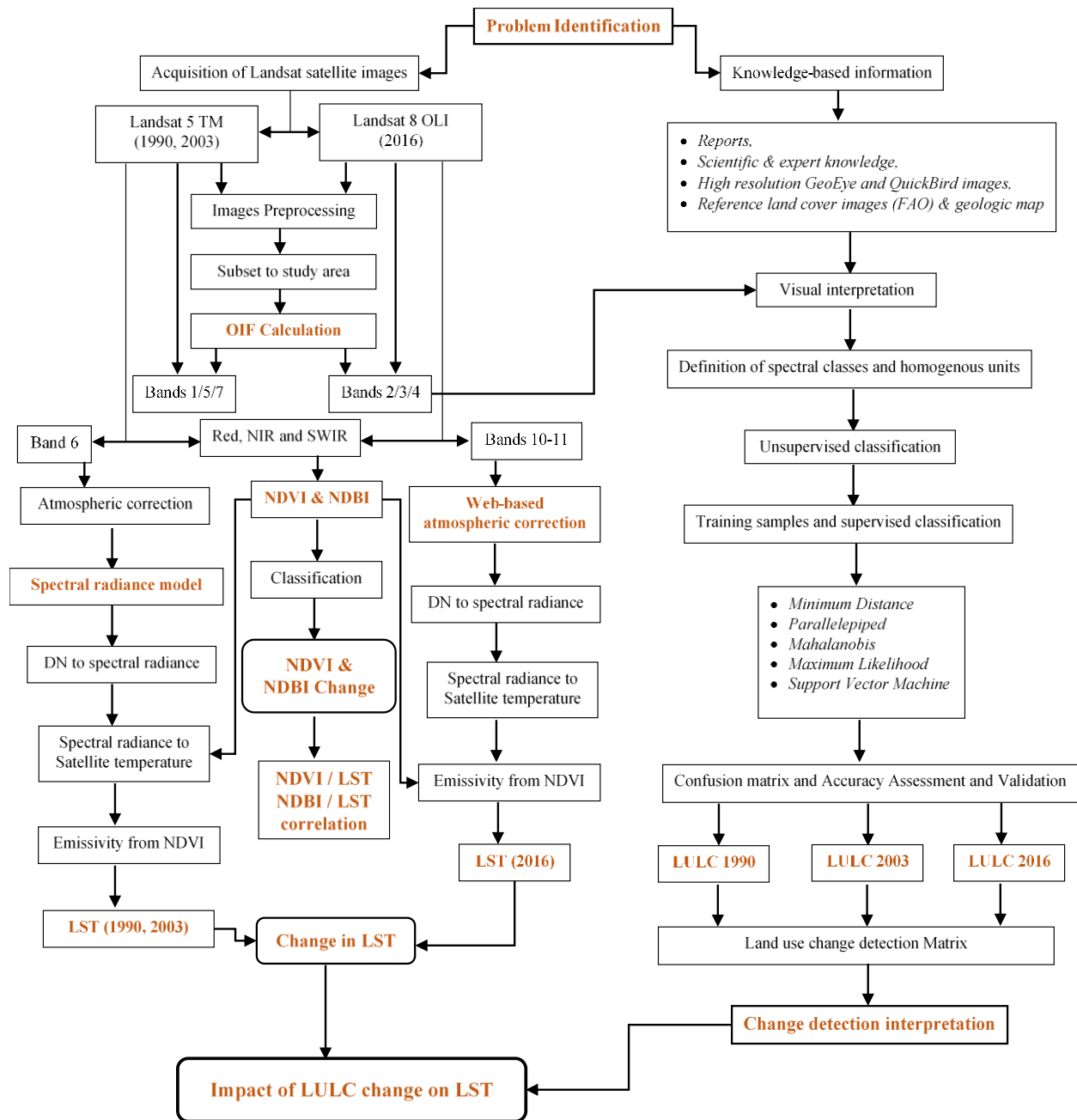


Figure 2.3. Data processing flow chart depicting procedures applied for preparation of LULC maps and LST evaluation from Landsat datasets

2.4.1 Image preprocessing

Both Landsat TM and OLI data are composed of independent single-band images. Therefore, it was necessary to combine these single-band images to a multi-band image of TM and OLI using a layer stacking tool. Landsat images were processed to a level-one terrain (L1T) corrected product,

which provided radiometrically calibrated and orthorectified images using ground control points (GCPs) and DEM to attain absolute geodetic accuracy (Ahmed et al., 2013). Therefore, the end result is a geometrically rectified image, free from any distortion related to the sensor, satellite and Earth's surface (Zanter, 2016). The input Landsat data were georeferenced using the World Geodetic System 1984 datum (WGS-84) and the Universal Transverse Mercator (UTM) projection within zone 36 North, as the study area lay in this region.

Although the data acquisition dates had clear atmospheric conditions for the study area, the three images were captured in different periods of time resulting in different atmospheric conditions. Hence, atmospheric corrections were conducted using the FLAASH module (VIS, 2009), which was implemented in ENVI software. These atmospherically corrected images were clipped to occupy the study area using an image subset tool. Other radiometric and spatial enhancement techniques, like histogram equalization, principle component analysis (PCA), edge enhancement and spatial filtering, were carried out on each image to improve their visual interpretability.

2.4.2 Optimum Index Factor (OIF) Calculation

This study used the analytical method of the Optimum Index Factor (OIF) to determine the best RGB band combination emerging from all bands of the Landsat images (Chavez et al., 1982), without the thermal band. The OIF is a statistical approach to rank all possible red, green, blue (RGB) color combinations of multispectral remote sensing data according to total variance within bands and inter-band correlation coefficients. Its role is to provide spectral information of the object, i.e. the highest OIF has the highest variance and lowest duplication for the scene, and therefore, contains the highest amount of spectral information about the scene. The algorithm used to compute the OIF was (Qaid & Basavarajappa, 2008):

$$OIF = Max \left[\frac{\sum_{i=1}^n \sigma(i)}{\sum_{j=1}^n |r(j)|} \right] \quad (2.1)$$

where $\sigma()$ is the standard deviation of band i , and $r(j)$ is the absolute value of correlation coefficient of any two arbitrary bands. For the Landsat 5 TM data (1990 and 2003), the top ranked RGB band combinations were band1/band5/band7 (157) with OIF values of 60.784 and 56.431

for 1990 and 2003, respectively. The OIF calculation indicated that the band2/band3/band4 (234) RGB band combination had the highest spectral information with OIF value of 8155.43 for Landsat 8 OLI 2016 (Figure 2.4). Overall classification accuracy was high when these bands were utilized in the classification process instead of using all bands (Omran, 2012).

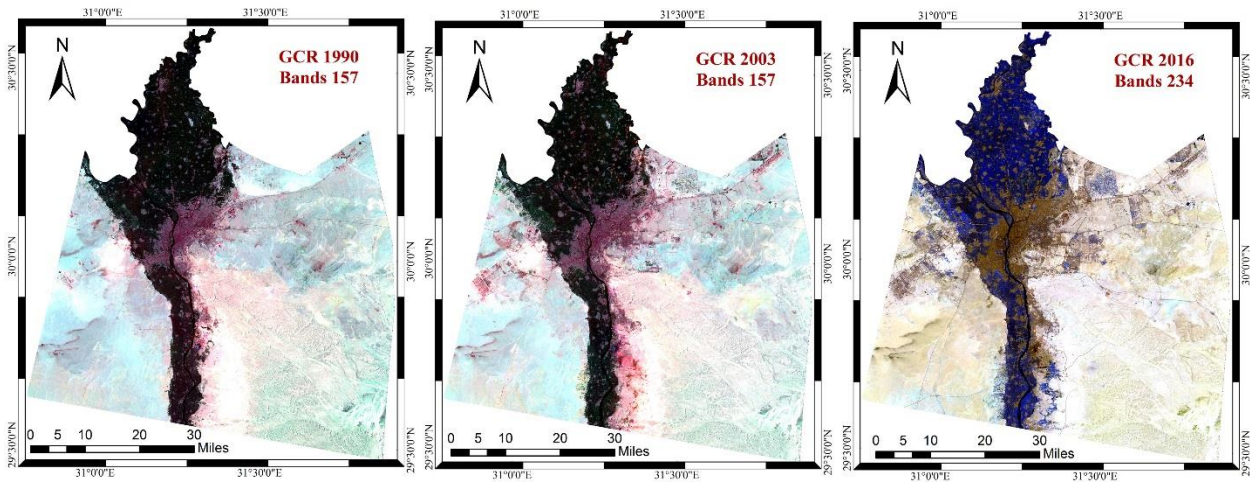


Figure 2.4. RGB band combination according to the highest OIF values of (a) TM 1990, (b) TM 2003, and (c) OLI 2016

2.4.3 Land Use/Land Cover Classification

A classification scheme had to be established before image classification. By computing average spectra of each class, a spectral characteristic of each land use class in each of the acquired data had been recognized, resulting in a classification schema comprised of four LULC level classes described in Table 2.2. As highlighted below, a number of classification approaches were evaluated for their effectiveness in large area classification (Bauer et al., 1994).

Table 2.2. Classification schema of LULC in the study area.

LULC classes	Description
Barren land	Open spaces, bare lands and soils, sands, dunes and excavation sites
Water	Channels, rivers, waterlogged areas, estuaries and open water sources
Vegetation	Crop fields, agricultural lands, forests, trees, parks, playground and grassland
Urban	All infrastructure including commercial, residential, industrial areas, villages, settlements and roads

2.4.3.1 Unsupervised Classification

A combination of unsupervised classification methods were used to classify the study area. Images were first classified using the Unsupervised Interactive Self-organizing Data Analysis (ISODATA) algorithm to identify spectral cluster information from image data and convert image data to thematic data. This information contains average spectra for each of the identified LULC stored in a signature file, which in turn makes use of analyst with the help of the ground truth points and first-hand knowledge of the study area to recognize and assign spectrally uniform training data for a subsequent application of different supervised classification algorithms (Abdulaziz et al., 2009). This clustering process was repeated several times through many iterations until a threshold was reached and there was no significant change in the cluster statistics or the maximum number of iterations was reached (Rahman, 2016). Clustering processes are highly automated with no direction from the users, so are ideal for large study area application.

2.4.3.2 Supervised Classification

The data were processed further using different supervised classification algorithms after they were classified using an unsupervised ISODATA algorithm. Training samples were first digitized from different representative classes to identify pixels of a single class. Grouping different spectral and spatial classes was done on the basis of LULC classes by utilizing reference data obtained from GCPs; auxiliary information and knowledge-based approaches collected from various resources, as mentioned before, were used to evaluate the statistical signature files of each LULC class (Ahmed, 2011) and ensure that there was minimal confusion of the land use to be mapped (Gao & Liu, 2010). Different supervised classification algorithms were then applied to the

Landsat images; Parallelepiped, Minimum distance, Mahalanobis distance, Maximum Likelihood and Support Vector Machine. Several algorithms were applied to identify the best for the study area location.

In order to increase classification accuracy and reduce classification error caused by confusion in spectral response of specific classes, the generalized images were spatially reclassified and refined for classification validation. Spectral confusion occurred due to the fact that several LULC have similar spectral response with respect to sensor characteristics especially in urban areas (Yang, 2002). Therefore, data reclassification has to be applied to consolidate different LULC types using the image spatial and contextual properties. Reclassification was carried out based on auxiliary data and several GIS functions, for instance: digitizing, overlaying and region of interest (ROI) functionality to produce the last version of LULC maps for different years.

2.4.4 Post classification smoothing

2.4.4.1 Accuracy assessment and validation

Quantitative statements about accuracy assessment for the classification processes were an essential approach to validate how well the classification represented the real world and ensure the reliability of the information derived from LULC maps. Confusion matrices were computed to evaluate the relationship between the reference data used and the resulting classified LULC maps. Confusion matrices are one of the most popular ways to evaluate the overall classification accuracy providing information about a producer's accuracy or errors of omission (percentage of a specific LULC class on the ground which is correctly classified) and user's accuracy or error of commission (percentage of a certain pixel class on the produced map corresponding to the actual class on the ground) (Lillesand et al., 2004; Tran et al., 2017). Percentage of the overall accuracy was computed using the following formula (Pal & Ziaul, 2016):

$$\text{Overall accuracy (\%)} = \frac{\text{total number of correct samples}}{\text{total number of samples}} \times 100 \quad (2.2)$$

Congalton (1991) was the first to point out that 250 reference pixels ($\pm 5\%$) are needed to construct the confusion matrix and to estimate the actual mean of accuracy assessment (Congalton, 1991). Therefore, 300 randomly selected reference pixels, placed on the classified images, for each time period were generated, representing a specific coordinate of the image. These points, distributed using the stratified random method, were then listed in two classes, one representing the class or reference values, while the other represented the actual LULC type. The percentage of the actual agreement of the automated classifier over a purely random assignment to classes was determined using a non-parametric Kappa coefficient (Ahmed, 2011) to remove the contribution of correct classification due to chance (Bauer et al., 1994). The Kappa coefficient for the different classification algorithms was evaluated by the following simplified equation (Gwet, 2002; Viera & Garrett, 2005):

$$Kappa = \frac{P(A) - P(E)}{1 - P(E)} \quad (2.3)$$

where $P(A)$ is the observed accuracy and $P(E)$ is the chance agreement.

2.4.4.2 Land Use/Land Cover Change detection

A multi-date post-classification comparison change detection method was employed to quantify the temporal change in LULC in the area of interest (Ridd & Liu, 1998). Three change detection statistics were obtained over time from the independent classified images for this research by conducting cross-tabulation analysis on a pixel-by-pixel basis, i.e. thematic overlay of the classified images (Al-Bakri et al., 2013). The possibilities were (1990-2003), (2003-2016) and (1990-2016) to evaluate the matrix table of “from-to” change information that revealed the main gains and losses in each category of the study site.

2.4.5 Derivation of land surface indices (NDVI and NDBI)

NDVI and NDBI were utilized to characterize the LULC classes and evaluate the relationship between these classes and LST. NDVI is the most commonly used index to express information about the density of vegetation, predict crop production, monitor drought, map desert

encroachment (Xiong et al., 2012), and measure surface radiant temperature (Omran, 2012). NDBI was first developed to investigate the extent of imperviousness and built-up areas and map these areas, as it can highlight the urban distribution with a typically higher reflectance in the short-wave infrared region band than that of the near-infrared one (Alhawiti & Mitsova, 2016; Zha et al., 2003). NDVI and NDBI were computed using the following formulas from different wavelength regions of the Landsat data:

$$NDVI = \frac{NIR-Red}{NIR+Red} \quad (2.4)$$

$$NDBI = \frac{SWIR-NIR}{SWIR+NIR} \quad (2.5)$$

where NIR, Red and SWIR are the reflectance in the Near-Infrared band (0.76-0.9 μm), Red band (0.63-0.69 μm) and Short-wave Infrared band (1.55-1.75 μm), respectively, for Landsat 5 TM. However, for Landsat 8 OLI these differed slightly: Near-Infrared band (0.85-0.88 μm), Red band (0.64-0.67 μm) and Short-wave Infrared band (1.57-1.65 μm).

2.4.6 Land surface temperature retrieval from Landsat 5 TM data

Atmospheric correction was first required to eliminate the atmospheric effect from thermal bands, as the satellite imagery measures the radiance of surface features modified by the atmosphere (Li et al., 2014). Therefore, the Top of Atmospheric (TOA) radiance correction model was applied on Landsat 5 TM imageries for both 1990 and 2003. TOA radiance is a simple model based on the scene calibration data available from the imagery header file. Based on Chander & Markham (2003), the brightness temperature from Landsat 5 can be obtained first by the conversion of the digital number of band 6 to the Top of Atmospheric (TOA) radiance using the following equation:

$$L_{\lambda} = \left(\frac{L_{\lambda MAX} - L_{\lambda MIN}}{Q_{Cal MAX}} \right) Q_{Cal} + L_{\lambda MIN} \quad (2.6)$$

where L_λ is TOA radiance, $L_{\lambda MAX}$ is highest radiance corresponding to Q_{CalMAX} (DN=255), $L_{\lambda MIN}$ is lowest radiance corresponding to Q_{CalMIN} (DN=0), and Q_{Cal} is the quantized calibrated pixel value of band 6 in DNs.

The thermal band can then be converted from TOA radiance to effective at-sensor brightness temperature under the assumption that the Earth's surface is a blackbody with a uniform emissivity and includes atmospheric effects using the following expression:

$$T_{sensor} = \frac{K_2}{\ln\left(\frac{K_1}{L_\lambda} + 1\right)} \quad (2.7)$$

where T_{sensor} is at-satellite temperature in Kelvin, K_1 is a calibration constant 1 (W/m^2 sr μm), and K_2 is a calibration constant 2 in Kelvin (Table 2.3).

Table 2.3. Landsat thermal band calibration constants

Satellite	Band Number	K_1 ($W/m^2 \times sr \times \mu m$)	K_2 (Kelvin)	$L_{\lambda MAX}$ ($W/m^2 \times sr \times \mu m$)	$L_{\lambda MIN}$ ($W/m^2 \times sr \times \mu m$)
Landsat 5	6	607.76	1260.56	1.2378	15.303
Landsat 8	10	774.8853	1321.0789		
Landsat 8	11	480.8883	1201.1442		

Thereafter, the TOA radiance (L_λ) was converted to reflectance measures, as L_λ does not consider atmospheric effects. Assuming that urban areas behave as a Planck surface, the expression to convert the TOA radiance to surface reflectance, correcting for solar irradiance, solar zenith and atmospheric effects is (Li et al., 2014):

$$\rho_\lambda = \frac{\pi \times L_\lambda \times d^2}{ESUN_\lambda \times \cos\theta_s} \quad (2.8)$$

The correct evaluation of LST was constrained to an accurate estimation of surface emissivity. In this work, we considered NDVI to calculate emissivity using the following formula (Giannini et al., 2015):

$$\varepsilon = a + b \times \ln(NDVI) \quad (2.9)$$

where a and b are obtained by regression analysis based on a large dataset (Faridatul, 2017), $a = 1.0094$ and $b = 0.047$.

Finally, the LST corrected, in Celsius, for spectral emissivity is computed using the following expression (Faridatul, 2017):

$$LST(^{\circ}C) = \left(\frac{T_{sensor}}{1 + \left(\frac{\lambda \times T_{sensor}}{\rho} \right) \times \ln(\varepsilon)} \right) - 273.15 \quad (2.10)$$

where λ is the wavelength of emitted radiance (the average wavelengths = 11.45 μ m) (Markham & Barker, 1985), $\rho = h \times c / \sigma$ (1.438 $\times 10^{-2}$ m \times K) with: σ is Boltzman constant (1.38 $\times 10^{-23}$ J/K), h is Planck's constant (6.626 $\times 10^{-34}$ J \times s), and c is the velocity of light (2.998 $\times 10^8$ m/s).

2.4.7 Land surface temperature retrieval from Landsat 8 OLI

In the case of Landsat 8, TOA spectral radiance was computed using the radiance rescaling factors corresponding to each band provided in the metadata file using the following equation (Zanter, 2016):

$$L_{\lambda} = M_L \times Q_{Cal} + A_L \quad (2.11)$$

where M_L is the radiance multiplier, Q_{Cal} is the pixel value in DN and A_L is the radiance additive scaling factor for the bands obtained from the metadata.

A web-based atmospheric correction model was used to evaluate surface temperature by first converting the previously calculated TOA radiance to surface-leaving radiance, taking into account the atmospheric correction of thermal regions of Landsat 8 OLI (Barsi et al., 2005):

$$L_T = \frac{L_\lambda - L_{up}}{\tau \times \varepsilon} - \frac{1 - \varepsilon}{\varepsilon} \times L_d \quad (2.12)$$

where L_T is atmospherically corrected radiance, L_{up} and L_d are upwelling and downwelling radiance, respectively ($\text{W}/\text{m}^2 \times \text{sr} \times \mu\text{m}$), and τ and ε are transmissivity and emissivity, respectively. These parameters can be assessed using the Atmospheric Correction Parameter Calculator online tool (<https://atmcorr.gsfc.nasa.gov/>). This uses the MODTRAN radiative transfer code that integrates algorithms to estimate atmospheric global profiles and parameters for a certain date, time, and location as the input (Barsi et al., 2003). Land surface emissivity was computed according to Equation (2.9). Even though the emissivity was calculated via NDVI in both Landsat 5 TM and Landsat 8 OLI, it was also preferable to use the same emissivity model for both Landsat datasets, hence avoiding uncertainty in the change in LST. Additional emissivity models introduced by (Jiménez-Muñoz & Sobrino, 2004) were also applied; however, results obtained corresponding to Equation (9) were considered the most reliable and the closest to the real life after validation, with only small differences found between the models.

Thermal Infrared bands of Landsat 8 OLI were converted from spectral radiance to effective at-sensor brightness temperature by converting the radiance using the inverse Landsat Plank's law (Chander & Markham, 2003):

$$BT = \frac{K_2}{\ln\left(\frac{K_1}{L_T} + 1\right)} - 273.15 \quad (2.13)$$

where K_1 is the band specific-thermal conversation constant 1 ($\text{W}/\text{m}^2 \text{ sr } \mu\text{m}$), and K_2 is a calibration constant 2 in Kelvin (Table 2.3). Lastly, the emissivity-corrected LST, in Celsius, was retrieved using Equation (2.10) with the replacement of BT instead of T_{Sensor} .

2.5 Results and Discussion

2.5.1 Spatial distribution and accuracy assessment of LULC

The Support Vector Machine (SVM) and maximum likelihood algorithms provided higher overall accuracy and kappa coefficients than other supervised classification algorithms (Table 2.4). Utilizing this observation, image processing and spectral characteristics, the final product combining the unsupervised and supervised classifications in which the spatial distribution and patterns of the LULC changes and persistence for the years 1990, 2003 and 2016, are shown in Figure 2.5. Spatial distribution patterns reveal that the area was dominated by deserts and barren lands, vegetation in the northern region and urban cover in the middle. Due to the heterogenic and dense vegetation cover in the north central part of the study region, we could not obtain higher overall accuracies than the ones presented, even after repeated classification with different algorithms.

The overall classification accuracies achieved for the images were found to be 90.3%, 96.5% and 94.9% with kappa coefficients of 0.85, 0.94 and 0.86 for 1990, 2003 and 2016, respectively. Note that in all classification algorithms, the vegetation class was responsible for producer errors; however, the urban class was the main reason for user errors (Table 2.5). On the other hand, classes of barren land and water were classified relatively accurately, approximately 98% or higher. The overall classifications in 2003 and 2016 are higher because of the availability of more detailed and higher resolution aerial reference images. Meanwhile, the use of OIF and enhancement techniques prior to classification increased the overall accuracy by 15 to 20%.

Table 2.4. Accuracy assessment of different supervised classification algorithms used for LULC maps in GCR

Classification Algorithms	Overall accuracy (%)			Kappa Coefficient		
	1990	2003	2016	1990	2003	2016
Minimum Distance	86.7	90.6	86.6	0.78	0.84	0.79
Parallelepiped	80.8	86.1	78.9	0.71	0.78	0.70
Mahalanobis	87.1	92.7	89.0	0.80	0.88	0.83
Maximum Likelihood	88.3	95.9	88.4	0.82	0.93	0.81
Support Vector Machine	90.3	96.5	94.9	0.85	0.94	0.86

Table 2.5. Accuracy assessment of the LULC classification results for GCR

LULC classes	1990 Classification		2003 Classification		2016 Classification	
	Accuracy (%)		Accuracy (%)		Accuracy (%)	
	Producer	User	Producer	User	Producer	User
Barren lands	98.8	94.4	99.9	96.8	98.7	95.1
Water	99.5	99.8	97.8	99.9	98.2	99.8
Vegetation	82.1	98.9	85.2	99.3	81.5	91.6
Urban	97.5	75.3	98.2	92.7	82.0	70.1
<i>Overall Accuracy %</i>	90.3 %		96.5 %		94.9 %	
<i>Kappa coefficient</i>	0.85		0.94		0.86	

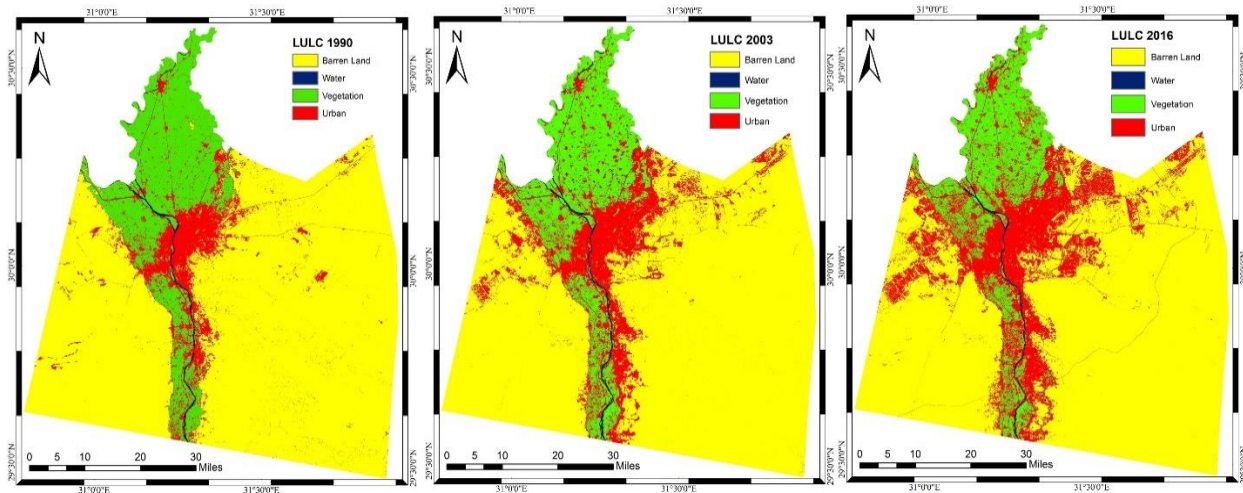


Figure 2.5. LULC map produced by classification processes for the years 1990, 2003 and 2016 showing the change for types of classes within the study area

2.5.2 Land Use/Land Cover change detection

Change detection statistics were computed from each consecutive pair of LULC maps (1990-2003 and 2003-2016), and the results of these changes are furnished in Tables 2.6 and 2.7. This shows the nature of change with respect to each class obtained from a matrix algorithm. Change detection analysis results show a sharp growth of 128% in the urban class during the 26-year period (1990-2016) (Figure 2.6). Significant differences appear to be related to barren land and vegetation land cover classes. Vegetation cover was reduced by 17,665 ha (14.3%) during 2003-2016 as compared to 14,432 ha (10.5%) during 1990-2003. Meanwhile, the barren land had a major decline of 30,669 ha (4.8%) and 24,822 ha (4.1%) during the two periods of 1990-2003 and 2003-2016, respectively, with a total amount of 55,491 ha during the entire period. These massive changes are related to desert-urbanization activities and construction of new housing developments, initiated by the Egyptian government in the early 1980s and that have since been accelerated (Abdulaziz et al., 2009). This increasing trend in urbanization enhances the effect of human interference and reinforces that socio-economic forces are the main stimulus on these anthropogenic land changes, specifically around streams coming out from the Nile River. However, the reduction of vegetation cover and agricultural area, especially for urbanization purposes, illustrates the poor planning of farmland protection laws and ignoring of environmental and ecological legislation implemented in the urban master plan. Water bodies, on the other hand, increased in area during 1990-2003, and then decreased again, due to the use of surrounding land for agriculture. Results obtained from this

study were similar to those evaluated by Megahed et al. (2015). They used three satellite images (1984, 2003 and 2014) to produce three LULC maps in GCR using the SVM algorithm. Results indicated that 13% of the vegetation was lost to urban areas between the period of 1984 to 2003, and 12% was lost between 2003 and 2014. However, only 3% of desert became urban areas in the first period, jumping to 5% between 2003 and 2014.

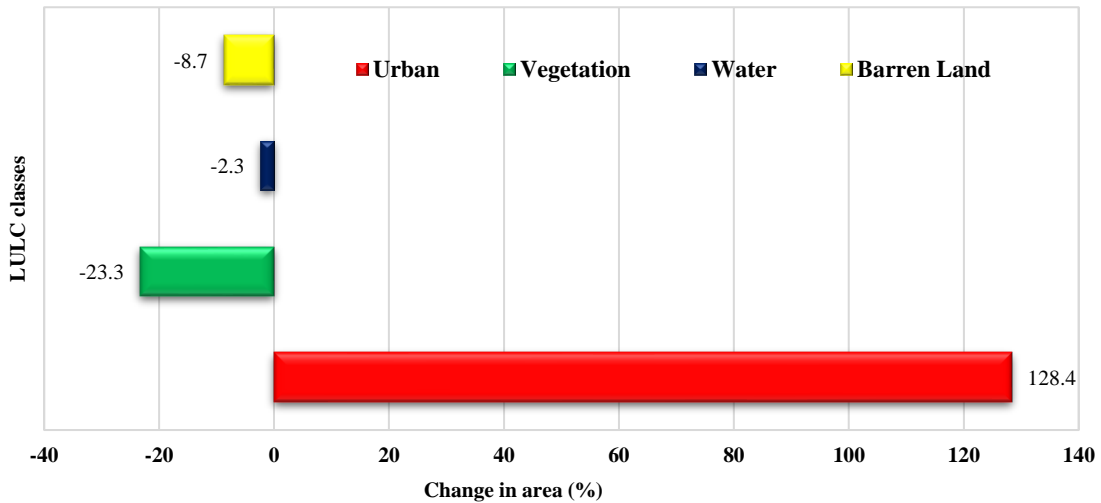


Figure 2.6. LULC change in GCR during 1990-2016

Table 2.6. 'From-to' LULC change detection statistics for 1990-2003 for GCR in hectare

Classes Area (Ha)	2003				LULC 2013	Difference 1990-2003	
	<i>Barren Land</i>	<i>Water</i>	<i>Vegetation</i>	<i>Urban</i>			
1990	<i>Barren Land</i>	598519	2	134	5428	604083	-30669
	<i>Water</i>	25	4231	945	987	6188	+1710
	<i>Vegetation</i>	829	95	115167	7069	123160	-14432
	<i>Urban</i>	35379	149	21346	54832	111706	+43387
LULC 1990	634752	4478	137592	68316	845137	0	
Class Change	36233	247	22426	13484	0	0	

Table 2.7. 'From-to' LULC change detection statistics for 2003-2016 for GCR in hectare

Classes Area (Ha)	2016				LULC 2016	Difference 2003-2016	
	<i>Barren Land</i>	<i>Water</i>	<i>Vegetation</i>	<i>Urban</i>			
2003	<i>Barren Land</i>	570451	3	210	8597	579260	-24822
	<i>Water</i>	51	4120	62	140	4373	-1815
	<i>Vegetation</i>	361	662	95118	9354	105496	-17665
	<i>Urban</i>	33220	1403	27770	93615	156008	+44302
LULC 2003	604083	6188	123160	111706	845137	0	
Class Change	33632	2068	28042	18091	0	0	

In order to better understand these 'From-to' relationships, further GIS and statistical analyses were conducted. A post-classification comparison was conducted through cross-tabulation GIS modules to overlay the two LULC maps (1990 and 2016) to produce a LULC change detection map pointing out the spatial pattern of change for the 26-year timespan (Figure 2.7). Figure 2.8 and Table 2.8 show the areas and the percentage of different land covers in the GCR for the three time periods considered in this study. Results highlighted from these analyses showed two clearly recognizable trends; (a) barren land and vegetation cover declined gradually

and (b) urban area increased drastically and rapidly (at the rate of 128% as mentioned before). The conversion patterns between different land cover classes to urban land cover are illustrated in Figure 2.9. This reveals that barren land was the main contributor in shaping urban area by an amount of 8.70% followed by vegetation land cover by a rate of 7.73% within the 26-year timespan (1990-2016). This emphasizes the importance of RS in conjunction with GIS in the study of LULC change detection providing essential information about the dynamic nature and patterns of spatial change of land cover.

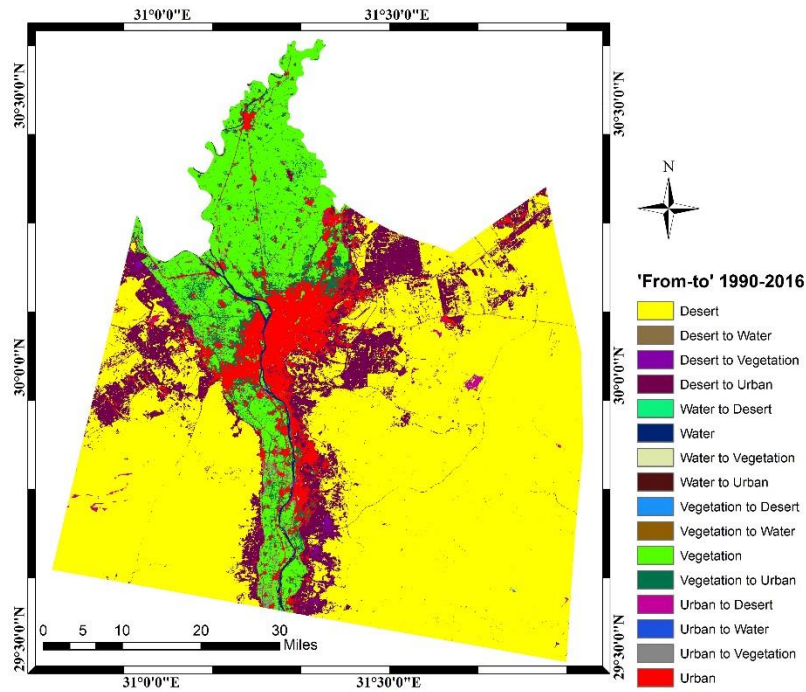


Figure 2.7. Land cover conversion in GCR from 1990 to 2016

Table 2.8. Areas of LULC classes in the three time periods 1990, 2003 and 2016 in the study area

LULC Area	1990	2003	2016
	Hectares	Hectares	Hectares
<i>Barren Land</i>	634752	604083	579260
<i>Water</i>	4478	6188	4373
<i>Vegetation</i>	137592	123160	105496
<i>Urban</i>	68315	111706	156008

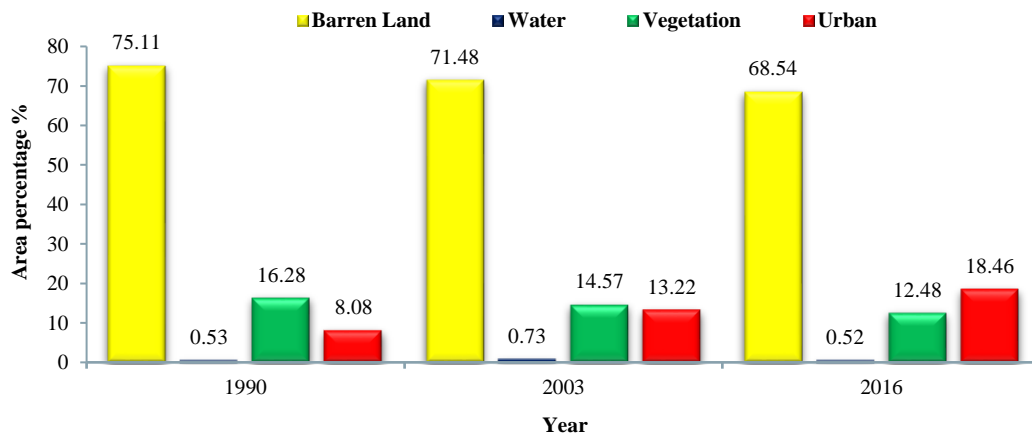


Figure 2.8. Percentage of land cover types in GCR for the three time periods

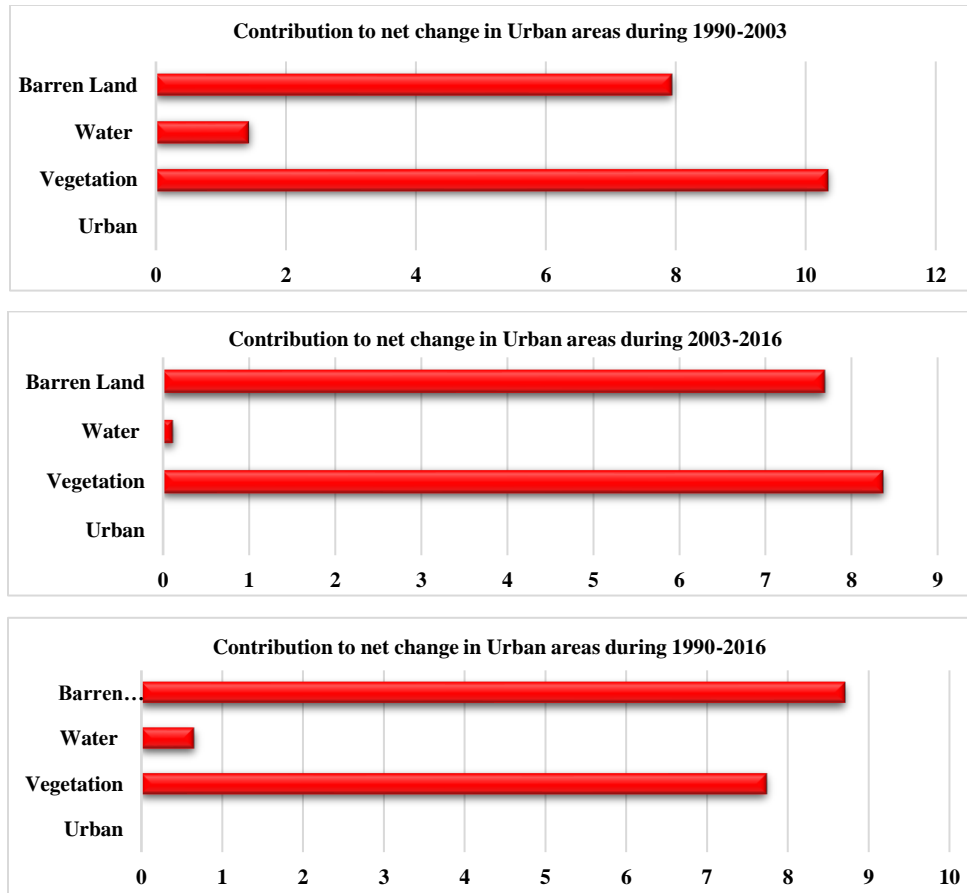


Figure 2.9. Contribution to the net change in the urban land cover in GCR (Area percentage %)

Areas classified as urban in the northern part of the study area, particularly in Qalyoubia Governorate, are mainly disseminated as urban encroachments within areas classified as vegetation land cover (Figure 2.5). However, the change in the central part of the study area, in the political capital of the Cairo Governorate, indicates a rough spherical sprawling tendency with large regions containing concentrations of many areas of localized change with a dense and granulated texture, especially during the period of 2003-2016. These are related to the establishment and implementation of new settlements, industries and communities at the expense of desert land that relies on surface water from the Nile River, for instance, El-Obour city and Tenth of Ramadan cities to the east of Cairo, and Six of October City in the western part. In general, these intense expansions occurred to accommodate the increasing population which caused the need for creating new jobs and maintaining food security, and is confirmed by Census data discussed in section 2.2 (Figure 2.2).

2.5.3 Land Surface Temperature (LST) change and the relationship with Land Use/Land Cover (LULC) change

Figure 2.10 shows the spatial distribution and the pattern of change in LST throughout the different time periods of the study (1990, 2003, and 2016). The enormous increase of LST for all LULC types is highly evident, in addition to the wide range of LST values over the period from 1990 to 2016. Due to the dominance of desert and barren land in the study area, LST ranged from 28.78 °C to 47.11 °C, with a mean of 38.4 °C in 1990, 27.02 °C to 53.84 °C, with a mean of 40.6 °C in 2003, and 29.35 °C to 52.71 °C, with a mean of 42.1 °C in 2016. The estimated LST from different Landsat data were cross validated with near-surface air temperatures obtained from two meteorological stations on the same day of the obtained satellite data in the study area (Table 2.9). The higher estimates of LST from satellite data over the three time periods were due to the effect of surface roughness on the surface temperature (Omran, 2012). Landsat data can be used to calibrate the distribution of LST in such dense places as GCR. Different algorithms for LST evaluation from Landsat were applied in this study to obtain accurate results. The calibration of LST should be refined with more data and in situ measurements of LST in future studies, as suggested by (Liu & Zhang, 2011).

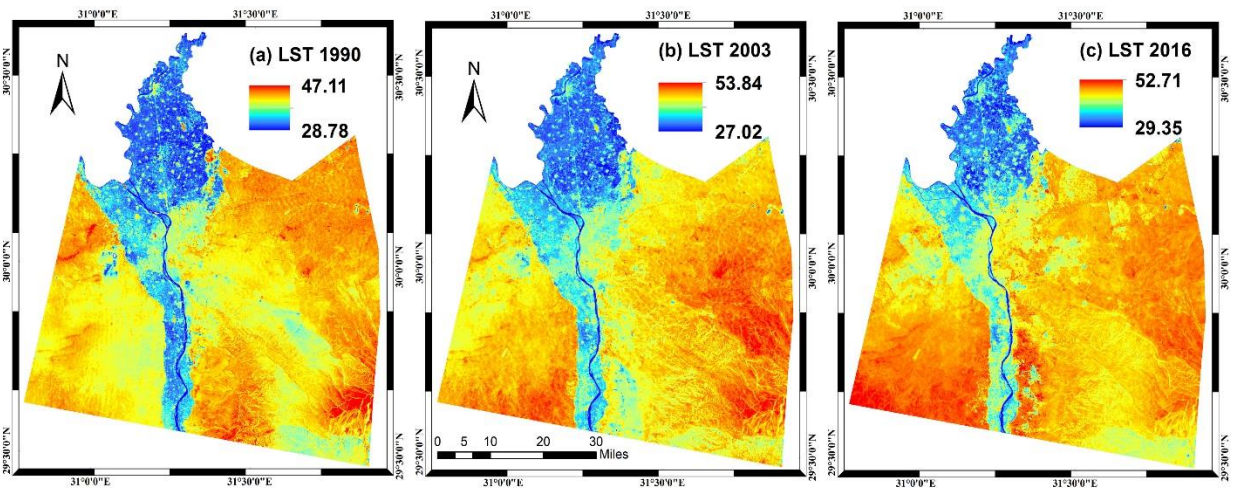


Figure 2.10. Spatial distribution of GCR LST for the years (a) 1990, (b) 2003 and (c) 2016

Table 2.9. Cross validation of the estimated LST from Landsat data with meteorological data for GCR

Acquisition date	Satellite LST estimation	Meteorological stations	Difference
Aug. 4 th 1990	38.4	38	0.4
Aug. 8 th 2003	40.6	36	4.6
Aug. 11 th 2016	42.1	39	3.1

GIS analysis coupled with image interpretation can help us to evaluate the relationship between the thermal signature and LULC types and highlight the impact of land cover changes on LST. We expressed the results of average LST in degree Celsius (°C) by LULC classes over three time frames in Table 2.10. LST distribution of 2016 demonstrated that these new high LST were related to non-evaporating impervious surfaces, like the industrial and residential areas that had been converted from other land cover types (Li et al., 2014). Results revealed that the highest maximum and mean LST were associated with barren land (mean value of 39.81 °C to 43.69 °C) and high density urban areas (mean value of 36.83 °C to 41.47 °C), followed by vegetation (mean value of 33.05 °C to 36 °C) and, lastly, water cover (mean value of 30.59 °C to 32.89 °C), in all three periods. Due to the urban-warming effect and rapid urban growth in GCR, urban areas, such as industrial districts and commercial centers in the eastern and western side of Cairo, experienced an increase in LST by 4.91 °C over the entire period. This implies that these noticeable increases were due to high emissions of pollutants and multiple artificial heat sources, and the replacement of native vegetation areas that reduce the amount of heat stored through transpiration with other non-transpiring and non-evaporating surfaces such as concrete, metals and stones. These high density building surfaces experience high radiance temperatures, confirming the phenomena of the urban-warming effect in which man-made materials in dense urban areas alter the superficial temperature and strongly link the urban category to higher LST in GCR.

Table 2.10. Average LST distribution (°C) over different LULC classes in GCR for 1990, 2003 and 2016

LULC Classes	1990		2003		2016		Average Change in LST (1990-2016)	Range
	Mean LST	St. Dev	Mean LST	St. Dev	Mean LST	St. Dev		
Barren Land	39.81	1.48	42.49	1.85	43.69	1.43	3.88	0.15
Water	30.59	2.28	31.33	2.17	32.89	2.50	2.30	0.09
Vegetation	33.05	2.29	34.00	2.32	36.00	2.82	2.95	0.11
Urban	36.83	2.11	38.14	2.24	41.74	2.48	4.91	0.19

Vegetation cover showed the highest standard deviation values, reflecting the heterogeneous and complex nature of the vegetation cover with a wide range of surface radiant temperatures. On the other hand, barren lands exhibited the lowest standard deviation due to the dry nature of these surfaces and a lack of wide variation in surface radiant temperatures.

Table 2.11 shows how the newly formed lands reacted with regard to LST after transformation, excluding water cover that accounts for less than 1% of the study area. The newly developed barren lands and urban areas had measured greater temperatures when transformed from vegetation cover with rates of 2.60 °C and 2.06 °C, respectively. On the other hand, vegetation cover tended to decrease the radiant LST in the conversion from either urban areas (1.90 °C) or barren lands (0.43 °C). Note that the transformation between barren lands and urban areas (and vice versa) had minimal effect on LST. In general, different land covers had different influences on the thermal distribution with a different magnitude, and LST acted as an important function of the change in LULC. Therefore, it is vital to increase green area to strengthen the study area protection.

Table 2.11. Average LST change in different LULC change types from 1990 to 2016 in GCR

Newly created land	LST (°C) in 1990	LST (°C) in 2016	Average change (°C)
Barren Land to Urban	39.11	39.02	-0.09
Barren Land to Vegetation	37.27	36.84	-0.43
Vegetation to Urban	32.91	34.97	2.06
Vegetation to Barren Land	33.53	36.13	2.60
Urban to Barren Land	39.91	40.01	0.10
Urban to Vegetation	36.09	34.19	-1.90

2.5.4 Analysis of land indices and relationship with LST

Two indices, NDVI and NDBI, as mentioned in section 2.4.5, were derived to quantify the relationship between LST and land indices. The visual depiction of the spatial pattern of both NDVI and NDBI are shown in Figures 2.11 and 2.12, respectively. Greater NDVI values correspond to dense vegetation areas in the central north of GCR, while lower values were observed in urban areas and barren land (Table 2.12). NDVI values are in the range of -0.525 to 0.79 in 1990, have a mean value of 0.04 and standard deviation of 0.15. These values dropped to -0.444 and 0.681 with a mean of 0.026 and a 0.14 standard deviation in 2003, and gradually decreased to be between -0.528 and 0.681, with a mean of -0.02 and a 0.08 standard deviation in 2016. As documented in the literature (Sun & Kafatos, 2007), higher levels of NDVI were associated with lower values of LST. On the other hand, NDBI values were found to increase over the study period. For 1990, 2003 and 2016, the average NDBI was -0.043, -0.039 and 0.021, respectively. In general, decreasing surface transpiration through the reduction of green canopy cover and increasing impervious surfaces modified thermal behavior and were essential for the reduced value of NDVI and increased NDBI. This pattern can be clearly seen in Tables 2.13 and 2.14, showing the statistical analysis and the Pearson's correlation coefficient between the indices and LST at a 0.05 significance level. The results revealed that NDVI was negatively correlated with LST, indicating the impact of green cover on LST is negative, in which the more green areas, the weaker LST will be (Figure 2.13). In comparison, NDBI presents a high positive correlation coefficient with LST over the three time periods of the study. Therefore, urban areas can strengthen

urban heat effects and increase LST (Liu & Zhang, 2011) (Figure 2.14). It was interesting to note that the high negative correlation between NDVI and NDBI in the three years could be explained by the action of establishing urban settlements in favor of green cover.

Table 2.12. Mean values of NDVI and NDBI for the years 1990, 2003 and 2016 for GCR

LULC classes	1990		2003		2016	
	NDVI	NDBI	NDVI	NDBI	NDVI	NDBI
<i>Barren lands</i>	-0.029	0.050	-0.040	0.049	-0.061	0.077
<i>Water</i>	-0.147	-0.429	-0.042	-0.047	0.071	-0.235
<i>Vegetation</i>	0.467	-0.444	0.357	-0.043	0.255	-0.226
<i>Urban</i>	0.033	-0.075	0.025	-0.054	0.008	-0.015

Table 2.13. Correlation coefficient matrix from the indices and LST for the years 1990, 2003 and 2016 for GCR

	1990			2003			2016		
	LST	NDVI	NDBI	LST	NDVI	NDBI	LST	NDVI	NDBI
LST	1.00	-0.87	0.91	1.00	-0.86	0.90	1.00	-0.88	0.89
NDVI	-0.87	1.00	-0.96	-0.86	1.00	-0.96	-0.88	1.00	-0.98
NDBI	0.91	-0.96	1.00	0.90	-0.96	1.00	-0.98	0.89	1.00

Table 2.14. Pearson's correlation between LST and two indices at 0.05 significance level

	1990			2003			2016		
	R ²	Root MSE	P-value	R ²	Root MSE	P-value	R ²	Root MSE	P-value
LST Vs. NDVI	0.7566	1.825	<.0001	0.7419	2.323	<.0001	0.7821	1.902	<.0001
LST Vs. NDBI	0.8310	1.520	<.0001	0.8033	2.028	<.0001	0.7980	1.832	<.0001

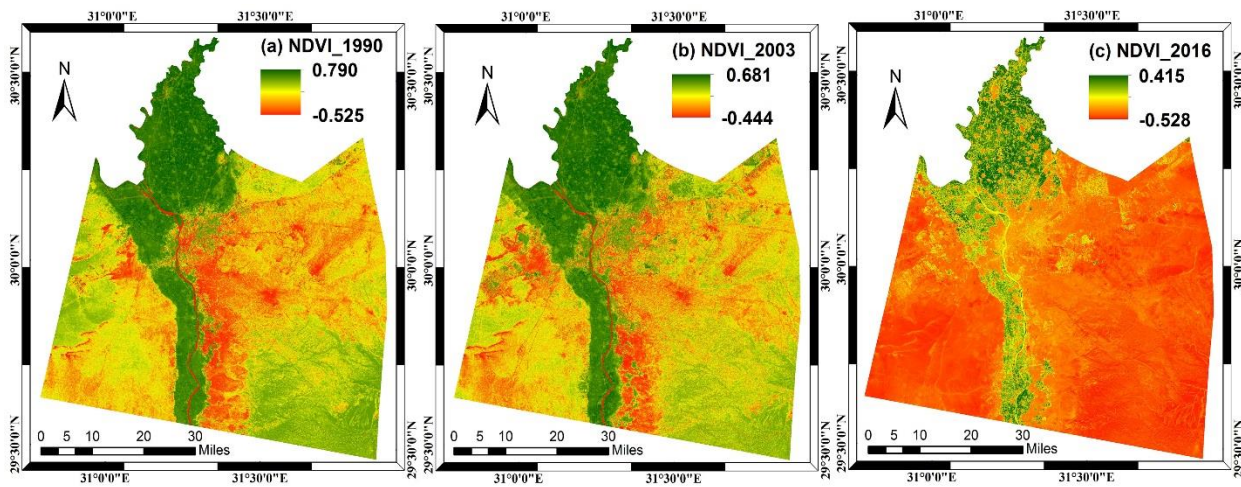


Figure 2.11. Spatial distribution of NDVI for the years (a) 1990, (b) 2003 and (c) 2016

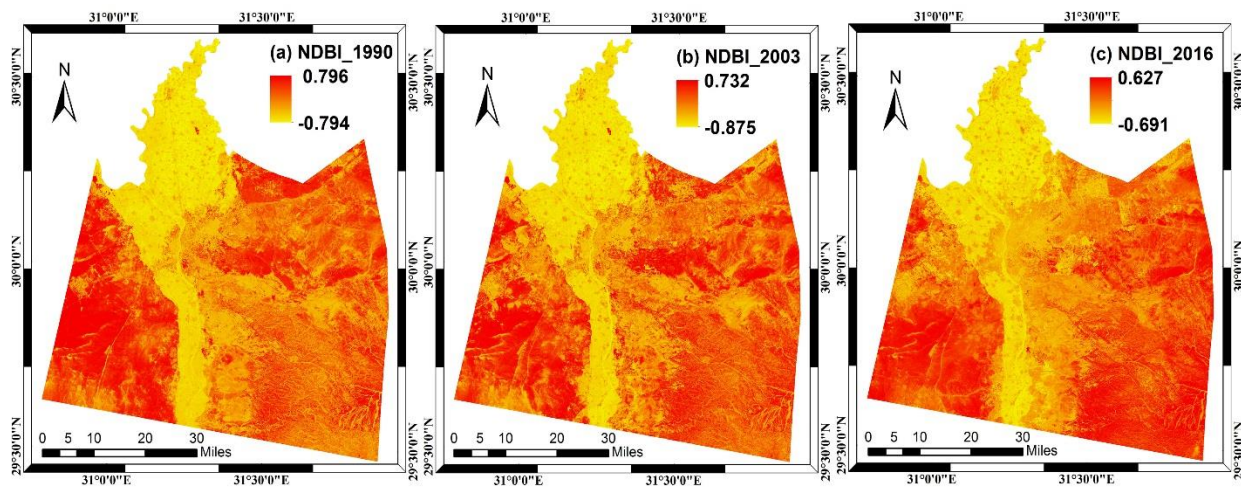


Figure 2.12. Spatial distribution of NDBI for the years (a) 1990, (b) 2003 and (c) 2016

In order to disclose the variance among LST and land surface indices, we took the 2016 image as an example to quantify the relationship among LST, NDVI and NDBI. Figure 2.15 shows the derived pixel values of LST and the two other indices based on West/East profile from the 2016 image, showing that lower LST are usually found in areas of lower NDVI; however, the peak values of LST are consistent with higher values of NDBI along the profile. A multivariate linear regression analysis between LST and the indices was performed, leading to a relationship among the variables as shown in Equation (14), with a correlation coefficient of $R^2 = 0.80$, $p < 0.001$, and $Root\ MSE = 1.82$ at a 0.05 significance level.

$$ST = -6.79 \times NDVI + 21.60 \times NDBI + 41.26 \quad (2.14)$$

The finding of Equation (2.14) showed a higher correlation coefficient in the multivariate linear regression than those of simple linear ones for the same year ($R^2 = 0.78$ for LST-NDVI and $R^2 = 0.79$ for LST-NDBI).

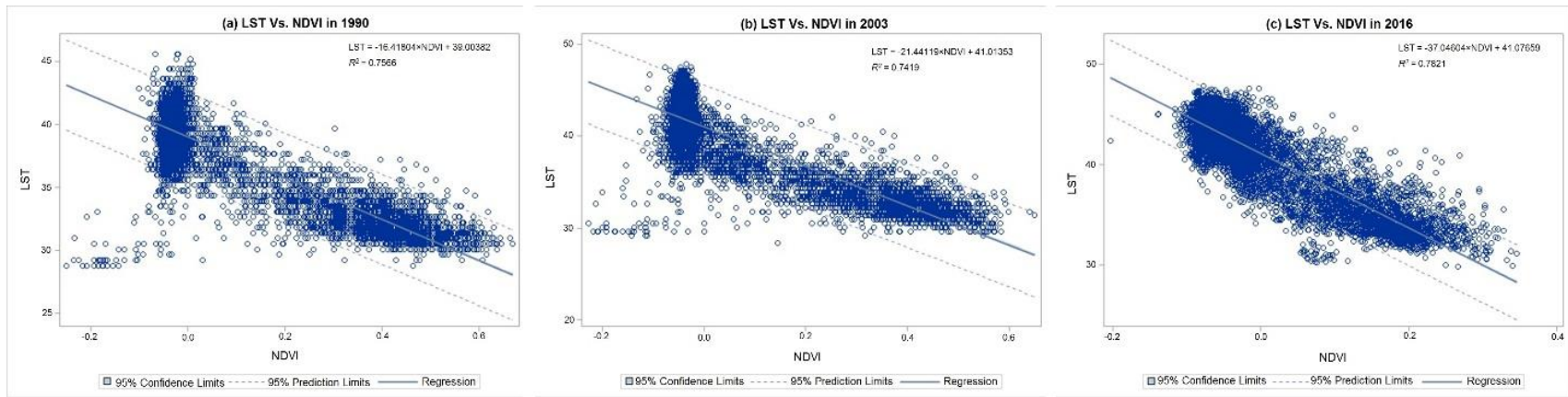


Figure 2.13. Correlation between NDVI and LST for the years (a) 1990, (b) 2003 and (c) 2016 for GCR

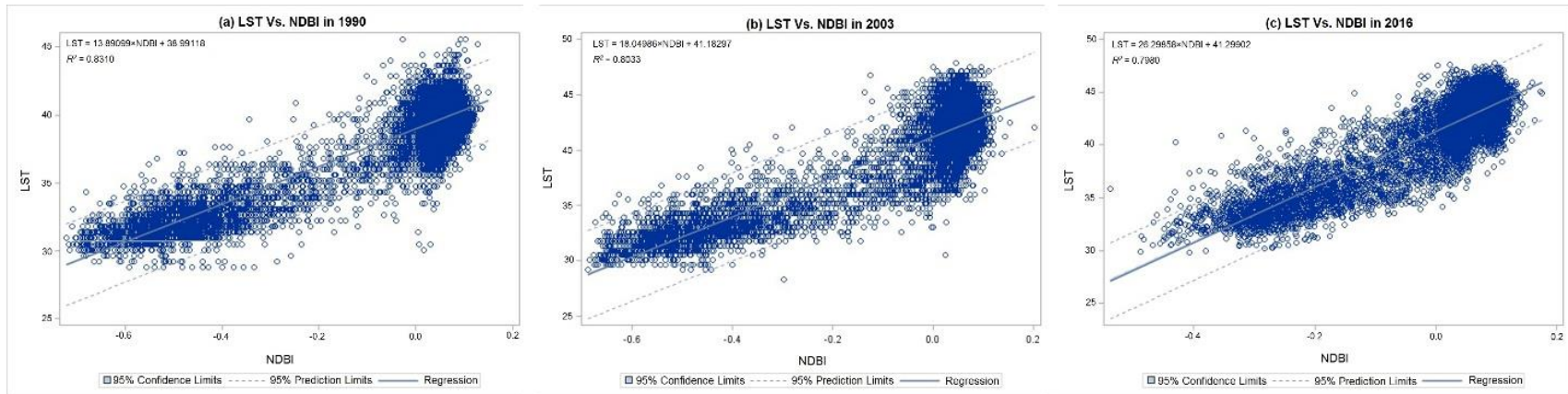


Figure 2.14. Correlation between NDBI and LST for the years (a) 1990, (b) 2003 and (c) 2016 for GCR

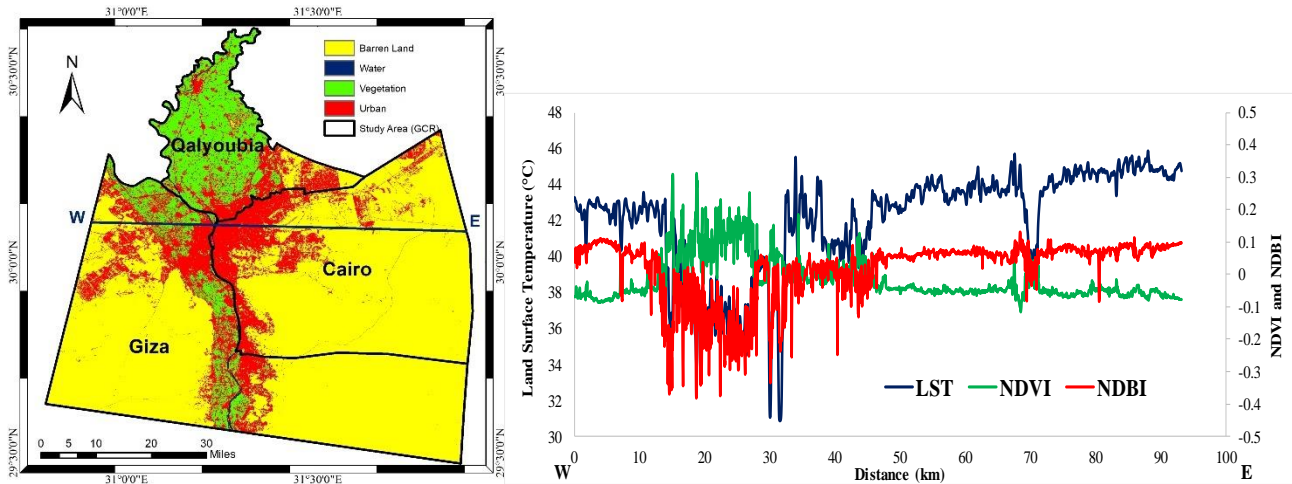


Figure 2.15. Correlation among LST, NDVI and NDBI from a West/East profile in 2016 imagery

2.5.5 Pearson's correlation coefficient between LST, NDVI and NDBI by different LULC types

In order to analyze the influence of specific LULC on LST accurately, Pearson's correlation was evaluated between mean LST/NDVI (Table 2.15) and mean LST/NDBI (Table 2.16) for LULC, pixel-by-pixel, in 1990 and 2016.

Table 2.15. Pearson's correlation between LST and NDVI by LULC type at 0.05 significance level

LULC classes	LST/NDVI (1990)				LST/NDVI (2016)			
	R ²	Regression functions	Correlation	RMSE	R ²	Regression functions	Correlation	RMSE
Barren lands	0.008	LST = -6.58 × NDVI + 39.8	-0.090	0.93	0.105	LST = -34.45 × NDVI + 41.9	-0.325	1.54
Water	0.081	LST = 4.67 × NDVI + 30.5	0.284	1.16	0.108	LST = -28.92 × NDVI + 34.0	-0.329	1.36
Vegetation	0.385	LST = -9.69 × NDVI + 36.4	-0.620	1.34	0.349	LST = -20.15 × NDVI + 38.5	-0.590	1.79
Urban	0.355	LST = -7.19 × NDVI + 37.7	-0.596	2.14	0.392	LST = -30.64 × NDVI + 40.30	-0.626	2.02

Table 2.16. Pearson's correlation between LST and NDBI by LULC type at 0.05 significance level

LULC classes	LST/NDBI (1990)				LST/NDBI (2016)			
	R ²	Regression functions	Correlation	RMSE	R ²	Regression functions	Correlation	RMSE
Barren lands	0.009	LST = -3.04 × NDBI + 40.2	-0.097	0.93	0.107	LST = 27.55 × NDBI + 41.9	0.327	1.54
Water	0.013	LST = 1.68 × NDBI + 30.5	0.114	1.20	0.280	LST = 14.16 × NDBI + 35.2	0.529	1.24
Vegetation	0.483	LST = 9.12 × NDBI + 36.9	0.695	1.23	0.381	LST = 14.67 × NDBI + 38.7	0.618	1.75
Urban	0.435	LST = 13.58 × NDBI + 38.2	0.660	2.01	0.423	LST = 20.60 × NDVI + 40.31	0.652	1.96

Results showed that the correlation between LST and NDVI were all negative in both 1990 and 2016 except for water coverage in 1990, likely due to lower amounts of pollutants in the 1990 water. However, the lowest negative correlation was found on barren lands in 1990 due to the high area coverage in the study region. On the other hand, the highest negative coefficient of the regression function was found to be in vegetation covers (-0.620) and dropped slightly for urban cover (-0.596). In 2016, barren area still showed the lowest negative correlation, however urban cover experienced the highest correlation coefficient (0.652), slightly higher than that of the vegetation one. Results of this analysis are consistent with other studies discussing the relationship between LST and NDVI (Weng et al., 2004; Wilson et al., 2003). This indicates that by increasing NDVI, the LST of both vegetation and urban areas decreases more quickly than that of barren land cover.

However, the NDBI index showed a positive correlation with all LULC types except for barren lands in 1990 which had negative or almost no correlation with LST. Similar to NDVI, the highest coefficient was related to vegetation in 1990 and urban cover in 2016. In general, the correlation coefficient between LST and land surface indices for the whole study area showed a higher correlation than in the case of using indices as indicators for LST according to each LULC type. However, the moderate relationship obtained for each LULC by surface indices and LST can provide important information for preliminary studies; for example, they can be simply used as proxies for temperature and for better planning by policy makers in large areas.

2.6 Summary and conclusions

In this study, multi-temporal Landsat satellite data were used to accurately monitor the spatial and temporal change of LULC and to study the impact of rapid urbanization on land surface temperature in the GCR in Egypt. Three Landsat dates, TM 1990, TM 2003 and OLI 2016, were acquired at the same time of the season (summer) due to the availability of reference data and to keep the weather factor as constant as possible. The study showed the effectiveness of the remote sensing techniques in conjunction with GIS to enable us to delineate the urban expansion due to the establishment of new settlements and to produce an accurate landscape change map in the study area. Different image enhancements, atmospheric correction, information extraction techniques, and unsupervised and supervised classification algorithms were performed on each Landsat image to ensure accurate image classification and LULC mapping. This revealed that SVM and maximum likelihood gave higher accuracies with rates of 90.3%, 96.5% and 94.9% for the years 1990, 2003 and 2016, respectively. The post-classification comparison change detection method was employed to quantify the spatial change of land cover units. In addition, statistical 'from-to' information was applied to quantify the magnitude of change through the entire 26 year timespan. Results demonstrated that the most distinct change was related to vegetation cover that drastically decreased by an amount of 32,097 ha (23.3%) from 1990 to 2016. In the same time period, significant reduction in barren land by 55,491 ha (8.70%) occurred. On the other hand, urban areas, due to the construction of new industrial and commercial settlements, showed a considerable increase by 87,689 ha (128.3%), particularly in the central and northern parts of the study area around water resources. These two land covers, barren lands and vegetation, were the main contributors to form new urban areas.

LST evaluation through Landsat satellite images is easily recognizable. Different algorithms were applied to the thermal infrared data of different Landsat images to accurately calculate LST of different land covers. A very minor shift was found from different emissivity models, however results obtained in this study were considered the most reliable based on cross validation. Results showed that mean LST values were higher in barren lands and urban areas than in the surroundings over the entire period. These anomalies were associated with settlements and industrial and commercial areas that experienced dense populations. Moreover, the most typical impact of rapid urbanization on LST was investigated within a single LULC. The change in LULC modified the radiant temperature of the surface. It was believed that the change in LST and climatic response

was strongly related to the removal of vegetation cover and its replacement with non-evaporative surfaces. This can be concluded from the increase in the magnitude of LST by a rate of 2.06 °C in the areas that were transformed from vegetation cover to urban and 2.60 °C due to the transformation of barren lands from green areas in the entire period of study from 1990 to 2016. In general, rapid urbanization was considered the major contributor to urban climatic warming that creates the major spatiotemporal variation in LST, particularly due to the vegetation reduction and pollution expansion that can be attributed to settlement expansion that results in a large amount of waste heat which in turn affects the surface energy budget.

Results from remote sensing studies show that LST and land surface indices, NDVI and NDBI together can identify the pattern of temporal variation and spatial distribution in urban thermal environments. The highest NDVI was found in vegetated areas while the highest NDBI was found in barren lands and urban areas. Statistical analysis showed a strong inverse relationship between LST and NDVI in contrast to a high positive one between LST and NDBI along different profiles in the study areas. These relationships dropped in the case of quantitative analysis among LST, LULC pattern and land surface indices. By way of conclusion, the study area reveals comparatively higher LST and NDBI, and lower NDVI over the period of study. These findings recommend the establishment of measures that can mitigate the strong effect of increasing LST on sustainable developments, population density control that is not limited to horizontal growth only, green coverage improvements like parks and gardens, and roof top area cultivation with horticultural plants that can alleviate the effect of LST. More multi-date images from the same season are also recommended to be investigated and evaluated, in a manner of providing more evidence of the thermal behavior on urban areas for better understanding of the impact of urbanization on LST. Moreover, RS satellite images are likely to be affected by cloud cover and other atmospheric effects, in addition to surface roughness, that in turn affect the DN values and therefore, it is highly recommended for future work that the integration of RS imageries from different sources with more land surface meteorological data be explored, and more attention on surface roughness be considered for more accurate results (Li et al., 2014).

In general, results indicate the potential of multi-temporal Landsat images that can accurately quantify the change pattern in LULC and LST in GCR in Egypt. In addition, the integration of RS and GIS can provide a valuable opportunity for surveying, environmental monitoring and the nature of land cover change. Hence, the information gleaned from the change detection outputs

can help in understanding the dynamics of LULC change in order to help policy-makers predict and plan for future developments in GCR, achieve long-term sustainability of soil and water resources and its impacts on climate change, and therefore characterize the evolution of urban construction lands.

CHAPTER 3. HYDROLOGIC RESPONSE IN AN URBAN WATERSHED AS AFFECTED BY CLIMATE AND LAND-USE CHANGE

Abstract

The change in both streamflow and baseflow in urban catchments has received significant attention in recent decades as a result of their drastic variability. In this research, effects of climate variation and dynamics of land use were measured separately and in combination with streamflow and baseflow in the Little Eagle Creek (LEC) watershed (Indianapolis, Indiana). These effects were examined using land-use maps, statistical tests, and hydrological modeling. Transition matrix analysis was used to investigate the change in land use between 1992 and 2011. Temporal trends and changes in meteorological data were evaluated from 1980–2017 using the Mann–Kendall test. Changes in streamflow and baseflow were assessed using the Soil and Water Assessment Tool (SWAT) hydrological model using multiple scenarios that varied in land use and climate change. Evaluation of the model outputs showed streamflow and baseflow in LEC were well represented using SWAT. During 1992–2011, roughly 30% of the watershed experienced change, typically cultivated agricultural areas became urbanized. Baseflow was significantly affected by the observed urbanization; however, the combination of land and climate variability had a larger effect on the baseflow in LEC. Generally, the variability in the baseflow and streamflow appears to be heavily driven by the response to climate change in comparison to variability due to altered land use. The results reported herein expand the current understanding of variation in hydrological components, and provide useful information for management planning regarding water resources, as well as water and soil conservation in urban watersheds in Indiana and beyond.

3.1 Introduction

Water is an indispensable natural resource for life and an increasingly limiting factor to socioeconomic developments (Abdi & Yasi, 2015). Water resources issues are widely discussed throughout the world. Addressing these issues requires information about the factors that drive hydrological changes and their related effects on local water resources. Evaluating water resources becomes a complex task that needs to consider many facets. Studies that detail the spatial and temporal distribution of water resources are of vital significance to inform management strategies.

Both climate variation and human actions act as stressors that contribute to putting water resources under severe pressure (Wang et al., 2018). Intensive human activities apart from climate change, such as land use change, urbanization, economic development and population growth, have posed unprecedented impacts on watershed hydrological conditions. For example, these stressors can alter surface runoff, evapotranspiration, baseflow, the frequency of floods, annual mean discharge, flow routing time, peak flows and volume (Kibria et al., 2016). Moreover, the pressures of these human activities are associated with climate variation which in turn will affect water sustainability for socioeconomic developments (Duan et al., 2019a).

The impacts of individual factors on watershed hydrology theoretically cannot be separated (Zhang et al., 2015). This coupling effect, together with water withdrawal and retention, contributes to the uncertainties in identifying the specific impact of each factor on watershed hydrology (Guo et al., 2014). This creates difficulty in inferring causation on a sufficient scale, and therefore, it remains unclear which of these factors dominantly contributes to watershed hydrology (Duan et al., 2019; Zhang et al., 2015). Indeed, several reports show conflicting conclusions when the combined hydrological responses are measured (Guo et al., 2014; Omer et al., 2017; Park et al., 2011; Zheng et al., 2009). Climate variation exerts a control on dominant agricultural and land use practices including their spatial properties (Shi et al., 2013; Tao et al., 2015; Tong et al., 2012). The joint impact on hydrology of climate variation and land use change has been shown to be similar to that of a single climate change factor (Kim et al., 2013; Zhang et al., 2015). Hence, identifying the distinct impacts of changing land use from climate variability and understanding the water balance is considered a particular challenge for studies on operational management of reservoirs and river basins.

In recent years, several investigators have studied the effect of climate variation and land use change on watershed hydrology (Duan et al., 2016; Xu et al., 2013; Zhang et al., 2013). Zhang et al. (2013) studied these effects on streamflow in the China Fenhe River Basin, and found a stronger influence of land use on streamflow than climate change. Xu et al. (2013) similarly showed that land use affected streamflow variation twice as much across more than 50 watersheds throughout the Midwestern United States.

Although an increase in high streamflow and decrease in low streamflow is often associated with urbanization (Tu, 2009), the impact of land use change often varies with climate (Kim et al., 2013). On the other hand, the changes in watershed hydrology and annual water balance can also

be attributed to climate variability, especially in large scale watersheds, likely caused by compensatory effects in a complex watershed (Fohrer et al., 2001). Novotny and Stefan (2007) reported a correlation between the mean annual streamflow trend and rainfall in five major Minnesota River watersheds, while in Indiana rainfall has shown a strong relationship with low flow (Kumar et al., 2009). In addition, Frans et al. (2013) concluded that wet climates, rather than land use change, had the most impact on streamflow in the Upper Mississippi River Basin. Comparable research conducted in the Johor River Basin in Malaysia indicated that climate change was the main driving force that impacted watershed hydrology (Tan et al., 2015). In the Yellow River Basin in China, climate fluctuation accounted for a 10 mm per year reduction in mean annual streamflow (Wang et al., 2013). River discharge significantly increased in the upper Syr Darya river basin due to temperature increase from 1930 to 2006 (Zou et al., 2019). Duan et al. (2017) evaluated the effects of projected climate change scenarios on watershed streamflow in the Upper Ishikari river basin in Japan, finding annual mean streamflow will likely increase for future climate scenarios. Thus, it is important to distinguish between effects related to land use changes and those due to climate variability for accurate estimation of surface and groundwater responses.

Impacts of these factors on watershed hydrology is different across watersheds. Therefore, sites must be evaluated on a local scale (Khoi & Thom, 2015). Due to limited available data, it is essential to use both comprehensive and physical tools to extract as much information about hydrologic responses as possible (Li et al., 2009). Hydrological models are considered an appealing approach to carry out impact assessment studies, as they provide a conceptualized framework to be used in scenario studies on the relationship between hydrological components, land use change and climate variability (Jothityangkoon et al., 2001). Model parameters can have physical meaning as related to measurable landscape properties and meteorological conditions (Legesse et al., 2003), and explicitly represent spatial variability (Lu et al., 2015). Initial model parameters describing vegetation, land use and soil types are called physically based parameter values; they can be adjusted to improve streamflow simulation through subsequent model calibration processes (Beven, 2006).

Recently, water resource managers and modelers have counted on hydrological models to identify alternative strategies for water resource allocation and to obtain more information about watershed systems, hydrological processes, and their responses to both anthropogenic and natural factors (Rusli et al., 2017), including insight regarding the impacts of future climate projections

(Duan et al., 2019b). Some of these models incorporate the watershed's heterogeneity and the spatial distribution of land use, topography, soil type, and meteorological conditions (Setegn et al., 2008). Among these models is the Soil and Water Assessment Tool (SWAT) model. SWAT is a conceptual mathematical semi-physical, semi-distributed based model (Arnold et al., 1998). SWAT employs parameters with time steps at a daily scale (Arnold et al., 2012). The model is designed with basic components, for example, climate, sediments, nutrients, and hydrology (Huang et al., 2016). This allows for interconnections of different physical processes that occur in the environment, allowing the model to evaluate how the hydrological components are impacted by land management methods in complex catchments with different land covers, and climate scenarios in extreme events such as droughts and floods (Abbaspour et al., 2015).

Streamflow and baseflow in watersheds in the US Midwest region reported upward trends with both urbanization and climate change (Beven, 2006; Zhang et al., 2013). While previous streamflow and baseflow trend investigations included urbanized watersheds in the Midwest region (Ahiablame et al., 2013b), they lacked integration analysis, which exclusively focuses on the interactive impacts of land and climate variability on urbanized catchments. In addition, multiple factors, nonlinear relationships, and poor understanding of mechanisms limits the ability to attribute causation (McIntyre et al., 2014). Therefore, the current study focuses on this issue through a systematic investigation, taking into account the effects of both individual and coupled impacts of human and natural impacts.

The study area, Little Eagle Creek (LEC) in central Indiana is an ideal candidate site for this type of study because it has been previously examined for many water-related issues and has substantial data available for this study. Previously, the LEC was investigated to evaluate impacts of urbanization on water issues. Bhaduri et al. (2000) utilized the Long-Term Hydrologic Impact Assessment (L-THIA) model with different land use patterns to evaluate nonpoint source (NPS) pollution and to assess impacts on annual average runoff from the watershed. The study concluded that the 18% increase in urban areas, from 1973 to 1991, resulted in an estimated 80% and 50% increase in annual average runoff and pollutant loads, respectively. Grove et al. (2001) conducted a similar study; results were consistent with Bhaduri et al. (2000), though they reported an increase of 60% in average annual runoff depth from 1973 to 1991 due to urbanization. Doyle et al. (2000) reported that stream incision occurring in the LEC was a response to urbanization though the measures of channel stability were not directly related to levels of urbanization. Choi et al. (2003)

estimated an increase in direct runoff from 49% to 63% during a 12-year time-span (1973 to 1984), suggesting that urbanization impacted direct runoff more than total runoff. In addition, they also pointed out that substantial baseflow is essential to maintain sound stream ecosystems in the LEC watershed. In their attempt to minimize the runoff impact of urbanization in the LEC, Tang et al. (2005) were able to reduce runoff increase by as much as 4.9% from 1973 to 1997.

More recently, Lim et al. (2006) estimated the effect of initial abstraction and urban growth on estimated runoff using modified curve number values in the L-THIA model. Results showed improvements in the prediction of direct runoff over the long term, resulting from using modified curve numbers and hydrologic soil groups for urbanized areas. They reported that improved input parameters could improve L-THIA model performance (Lim et al., 2006).

The overall aim of this research was to evaluate the response of watershed streamflow and baseflow to climate variability and land use change in an urban watershed in Indiana, based on simulation following a comprehensive calibration. The specific objectives were: 1) to evaluate long-term trends of historical streamflow, land use and rainfall in an urban watershed; 2) identify changes in land use from 1992 and 2011 through transition matrix analysis; 3) calibrate and validate SWAT model performance, using different land use patterns for different periods; 4) investigate hydrological streamflow and baseflow sensitivity to land use change and climate variability; and 5) simulate the joint effects of both climate and land use change on hydrology in this watershed. For this goal, plausible scenarios of land use change and climate variation were developed based on trends and information exploited from the LEC watershed. The results obtained provide useful information towards the improvement of the current understanding of hydrological component variation. Additionally, the results are informative to planning and management strategies for water resources that seek to minimize the undesirable effects of land use change and climate variation as well as water and soil preservation in urban watersheds in the Midwestern USA and potentially beyond.

3.2 Materials and Methods

3.2.1 Study area

Little Eagle Creek Watershed is located in northwest Indianapolis, Marion County in central Indiana (Figure 3.1). The watershed covers approximately 74.5 km² (USGS Gauge 03353600), with annual precipitation ranging from 795 to 1443 mm from 1980 to 2017. The minimum, maximum and mean elevation in the area were 208, 275 and 242 meters above sea level, respectively. This watershed has undergone significant urbanization in the past several decades due to its proximity to the capitol city, creating a possible threat to the watershed's water resources. Current land use includes 95.8% typical urban residential and commercial categories that are the majority of land use, 3.2 % non-urban natural grass and forest, and only 0.5 % agricultural and cultivated areas (Lim et al., 2006). Regionally, thunderstorms occur throughout the year and particularly in the spring and summer seasons (Doyle et al., 2000).

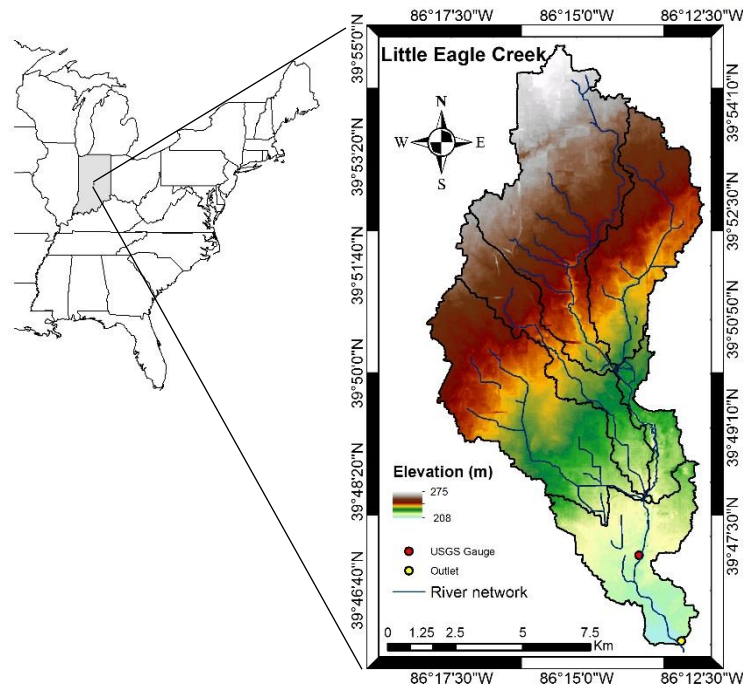


Figure 3.1. Index map showing location of the Little Eagle Creek (LEC) watershed in Indiana.

3.2.2 Datasets Description

The explicit datasets used to build and calibrate the SWAT model can be classified into statistical, geographical or spatial data for hydrologic simulation. The statistical data includes hydro-meteorological data, while the spatial data include Digital Elevation Model (DEM), land use and soil maps.

3.2.2.1 Hydro-Meteorological Data

The sets of data used included long-term daily meteorological data from 1980–2017, (precipitation, minimum/maximum air temperature, wind speed, solar radiation and humidity), obtained from the National Climatic Data Center (NCDC). The weather station was approximately 4 kilometers from the LEC watershed. Hydrological streamflow data were based on observations from 1980 to 2017 at a gauged station within the watershed. The streamflow data were used for the calibration and validation of the SWAT model and to separate the baseflow from the direct discharge. Streamflow data were complete with no missing records.

3.2.2.2 Topography and Soil Type

The results reported herein used elevation, flow direction, accumulation, stream network, channel properties, slope and aspect to describe the topography of the study areas. The DEM topographical data had a resolution of 10 m by 10 m and was obtained from the Geospatial Data Gateway (GDG). DEM data were first used to delineate watersheds into sub-basins and the drainage patterns and identify flow direction of the land surface terrain. Soil type, slope and land use was then used to classify these sub-basins into small Hydrologic Response Units (HRUs) (Mehan et al., 2017). HRUs represent the smallest hydrologic unit of the watershed. Soil type data were obtained from Soil Survey Geographic Data (SSURGO) with a resolution ranging from 1:12,000 to 1:63,630. The SWAT model requires these soil parameters, as the soil's chemical and physical properties play an important role in evaluating water movement within the HRU (Welde & Gebremariam, 2017).

3.2.2.3 Land-Use Data

This study used digital land-use data acquired from the National Map Viewer (NMV). To examine the consequence of land-use change on the hydrology of the watershed, raster land-use maps of 1992 and 2011 were used in this research.

3.2.2.4 Hydrological SWAT Model

The SWAT model, developed by the USDA Agricultural Research Service, is designed to model hydrology at the scale of a watershed (Arnold et al., 1998). SWAT is structured on fundamental components, including climate, hydrology, sediment, nutrients and management (Almeida et al., 2018; Neitsch et al., 2005; Wallace et al., 2018) and can be used to predict the variation in these components by change in land use and climate. SWAT follows a defined operating sequence; (1) data preparation, (2) discretization of sub-basins and definition of HRUs, (3) sensitivity analysis, (4) parameter calibration and (5) validation. The computational simulations in this study were performed with the SWAT 2012 extension, using the ArcSWAT interface of ArcGIS 10.4.1 (Arnold et al., 2012).

The hydrologic routine within SWAT includes the vadose zone processes (plant uptake, evaporation, infiltration, lateral flows, and percolation), groundwater flows and snow fall and melt. The hydrologic cycle in the SWAT model is based on water balance and is expressed as follows (Neitsch et al., 2002):

$$SW_t = SW_0 + \sum_{i=1}^t (R_{day} - Q_{surf} - E_a - W_{seep} - Q_{gw}) \quad (3.1)$$

where SW_t is the final soil water content (mm); SW_0 is the previous soil water (mm); t is the time step (day); R_{day} , Q_{surf} , and E_a are the precipitation, surface runoff, and evaporation measurements on day i (mm), respectively; W_{seep} is the amount of water entering the vadose zone from the soil profile on day i (mm), and Q_{gw} is the amount of return flow on day i (mm).

For each HRU, SWAT simulates surface water and shallow groundwater. Then, these values are calculated for the sub-basins by a weighted value using the combined HRUs. Using daily rainfall amounts and a modified version of the Soil Conservation Service (SCS) curve number method, surface runoff is computed. Estimation of baseflow and groundwater flow is based on the

hydraulic conductivity of the shallow aquifer, water table height and the distance between the sub-basin and main channel.

The SWAT framework serves to conceptualize the relationship between climate variation, land-use change and human activities and their synchronous impacts on watershed hydrology (Omer et al., 2017). For further information on the SWAT model, refer to the online resource at <https://swat.tamu.edu/> and (Arnold et al., 2012).

3.2.3 Methods

3.2.3.1 Land-Use Change Detection

Post-classification change detection analysis was applied to determine the temporal change in land use of the watershed. Statistics for change detection from the land-use maps have been obtained over time (1992 and 2011) for this research through the thematic overlay of the classified land-use maps using pixel-by-pixel cross-tabulation analysis. This was used to evaluate the “from-to” change detection matrix table that shows the major gains and losses in each category (Aboelnour & Engel, 2018; Gitau & Bailey, 2012; Gitau & Chaubey, 2010).

3.2.3.2 Temporal Trend Analysis Method

The modified Mann–Kendall (M-K) test was applied in this study to analyze the change in annual precipitation and temperature in the LEC watershed (Hamed & Rao, 1998). The M-K test is a widely-used, non-parametric, rank-based test (Kendall, 1975), that has found considerable use in hydrology and climatology given its robustness and ability to avoid the effects of extreme values (Tesemma et al., 2010). The modified M-K was chosen for this research due to the presence of negative and positive serial correlations recognized in meteorological data, that can result in overestimation or underestimation of the trends (Kibria et al., 2016). The M-K test can identify the magnitude of the slope of individual variables, whereby a positive slope magnitude indicates an upward trend and vice versa (Hirsch et al., 1982; Sen, 1968). The M-K test statistic is calculated by:

$$S = \sum_{i=1}^{n-1} \sum_{j=i+1}^n \text{sgn}(x_j - x_i) \quad (3.2)$$

and

$$gn(x_j - x_k) = \begin{cases} +1, & \text{if } (x_j - x_i) > 0 \\ 0, & \text{if } (x_j - x_i) = 0 \\ -1, & \text{if } (x_j - x_i) < 0 \end{cases} \quad (3.3)$$

where S is the M-K test statistic, x_j and x_i are the sequential data values; and n is the dataset size (Hirsch et al., 1982).

3.2.3.3 Baseflow Separation Using Web-Based Bflow

Baseflow separation methods were used for streamflow separation into direct runoff and baseflow since the measurement of baseflow is considered more difficult as compared to streamflow measurement. Baseflow measurements were calculated from USGS daily streamflow data using the ‘BFlow’ digital filter program. The BFlow program calculates baseflow by filtering streamflow data three times (1-Pass, 2-Pass and 3-Pass) through the filter in Equation (3.4), allowing the user to select the required number of passes for baseflow evaluation (Jung et al., 2016; Lee et al., 2018):

$$BF_t = \alpha \times BF_{t-1} + \frac{1-\alpha}{2} \times (Q_t + Q_{t-1}) \quad (3.4)$$

where BF is the baseflow, α is the filter parameter (0.925), Q is the total streamflow, and t is the time step. Equation (3.4) is applied only when $BF \leq Qt$ (Eckhardt, 2008).

3.2.3.4 Scenario Analysis: Modeling Hydrological Response to Climate Variability and Land-Use Dynamic

Land-use data and HRU outputs for the LEC watershed showed a dramatic change in impervious cover after 1992. However, little change was detected in impervious cover between 2001 and 2011, as the watershed area was mostly urbanized by 2001. Therefore, at this stage, only land-use data for 1992 and 2011 were considered in the calibration and validation processes for the two climate periods. Land-use data from the National Land Cover Database (NLCD) for 2001 and 2006 were not used in further analysis.

To evaluate the separate and combined influences of land-use dynamics and climate alteration on hydrological components, the “fix-changing” approach was used, in which one factor at a time was changed while holding others constant. Based on the change detection analysis of temporal trends of precipitation and temperature and land-use change, the meteorological data from 1980–2017 were divided into two periods, with each period including one land use map. The period of 1980–1998 was called CP1, representing the 1980s and 1990s and was considered the baseline period, and the impacted period of 1999–2017 was called CP2 and represented the 2000s and 2010s. The 1992 land-use map for 1992 represented the patterns in CP1, while the 2011 land-use map for 2011 was used to show the patterns in CP2, assuming that minimal change existed in the watershed land use after 1992 to 1998, similarly after 2011. The calibrated baseline SWAT model of Scenario 1 (or S1) was applied for each of the other three scenarios of the two meteorological time periods to give four scenarios overall to evaluate the influences of land use and climate change. For SWAT simulation, these four scenarios were developed:

Scenario 1 (S1: Baseline): 1992 land use and CP1 climate data (1980–1998).

Scenario 2 (S2: Land-use change): 2011 land use and CP1 climate data (1980–1998).

Scenario 3 (S3: Climate change): 1992 land use and CP2 climate data (1999–2017).

Scenario 4 (S4: Climate and land-use change): 2011 land use and CP2 climate data (1999–2017).

In order to evaluate the separate and combined impacts of climate and land use dynamics on streamflow and baseflow, the four modeling experiments were used to run the well-calibrated and validated SWAT model. The simulated output values were compared to the corresponding values for the baseline period under a no-change scenario. In these four scenarios, S1 and S4 represent actual circumstances, and the difference between S2 and S1 outputs indicates the individual impacts of land use on flows, while the difference between S3 and S1 simulations describes the impacts of climate variation on flows. Finally, comparison between S1 and S4 attempted to depict the combined effects of climate change and land use change on flows in the watershed.

A flow chart of the model set up, sensitivity analysis, calibration and validation process of the streamflow and baseflow for the LEC watershed is described and summarized in Figure 3.2.

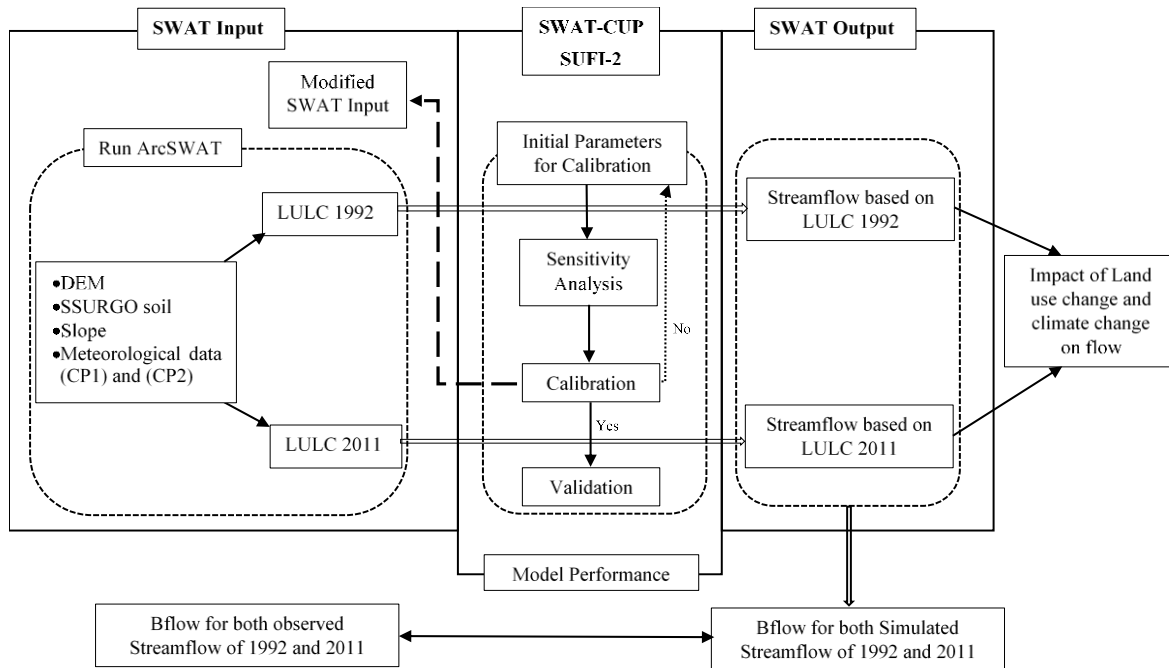


Figure 3.2. Flow chart depicting procedure for SWAT model setup, calibration and validation of both streamflow and baseflow in the LEC watershed.

3.3 Results and Discussion

3.3.1 Land Use Changes from 1992 to 2011

The 1992 and 2011 land use maps for the LEC watershed are shown in Figure 3.3a,b, and the change in land use types is shown in Figure 3.3c. The most commonly distributed land use types in LEC are developed and cultivated areas. Results highlighted from the land use change detection showed two clearly recognizable trends; (a) the decline of cultivated areas; and (b) rapid increase in developed areas. Developed areas showed an increase of 30.75 km² or 75.8%. On the other hand, cultivated surface experienced a reduction of 30.16 km² or 99.1% from 1992 to 2011.

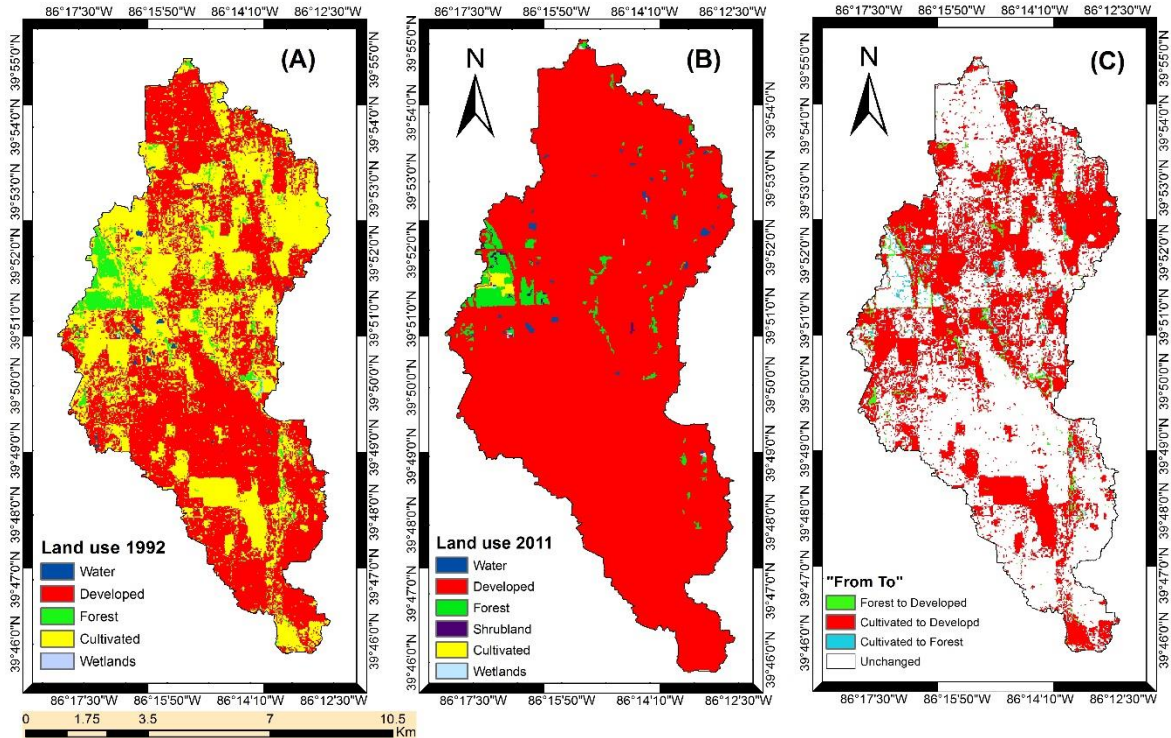


Figure 3.3. Land use types in LEC watershed in (A) 1992; (B) 2011 and (C) the transition between 1992 and 2011.

Table 3.1 explains the variation in the LEC from 1992 to 2011 by analyzing the transition matrix of land use. 40.4 km² of urban area remained unchanged, whereas the most notable transition is the conversion of 29.3 km² of cultivated areas and 1.50 km² of forests to urban uses from 1992 to 2011. The transition between other land uses was very small and has been omitted from analysis and the map. For instance, the change from water to developed and planted to water are only 0.14 and 0.16 km², respectively. This might be attributed to the different classification algorithms used in NLCD data of 1992 and 2011.

Table 3.1. Land use change transition matrix in LEC from 1992 to 2011 (km²).

1992	2011						
	Water	Developed	Forest	Shrubland	Cultivated	Wetlands	Total
Water	0.10	0.14	0	0	0	0	0.25
Developed	0.05	40.38	0.15	0.01	0	0.02	40.62
Forest	0.01	1.50	1.59	0.07	0.03	0.01	3.21
Cultivated	0.16	29.34	0.62	0	0.24	0.02	30.38
Wetlands	0	0.04	0	0	0	0	0.05
Total	0.33	71.41	2.36	0.08	0.27	0.05	

3.3.2 Changes in Temperatures and Precipitation

Both annual precipitation and temperature experienced a significant increase during the past 38 years. In order to quantify the magnitude of the increase in the meteorological data, the non-parametric M-K test was applied. The analysis showed that the meteorological time series data were not stationary, and there was one change point in the time series that occurred in 1998. This change is likely associated with regional environmental change such as urbanization and climate variability.

The trend Z-test statistics and the slope of precipitation and temperature were all positive and are displayed in Table 3.2. The results show that the monotonic trends of annual precipitation and temperature were different. For the overall period from 1980 to 2017, the annual precipitation increased at significance levels greater than 0.1, while air temperature passed the 0.001 significance level. These findings mean that the long-term monotonic trend of annual temperature exhibited a significant increase during the study period, whereas the long-term monotonic trend of annual precipitation is statistically insignificant and weak over time. Of note, statistical significance, or lacking of significance with respect to climate can be misleading. Although increase in annual temperature and precipitation were obtained, changes in seasonal precipitation and temperature might impact the increase in precipitation and temperature during the study period. For instance, Sekaluvu et al. (2018) reported an overall insignificant decrease in precipitation by 0.4 mm/year during the period 2005–2015; however, winter and fall precipitation decreased by

approximately 7.8 mm/year and 5.4 mm/year, respectively, and that reduction was significant. While spring precipitation increased significantly by 20 mm/year, and summer precipitation decreased insignificantly by about 4.0 mm/year (Sekaluvu et al., 2018).

Table 3.2. Temporal trends in annual precipitation and temperature in the LEC watershed.

	Precipitation	Temperature
Z-Stat	1.521	2.930
Slope	4.219	0.032
α	>0.1	0.001

Figure 3.4 shows the average values of annual precipitation and temperature before (red dashed line) and after (green dashed line) the change point. Compared to CP1, the results show that the average annual precipitation increased by 6.8% (73.7 mm, from 1080 mm to 1154 mm), while air temperature increased by 0.6 °C (from 11.6 °C to 12.2 °C) in the LEC.

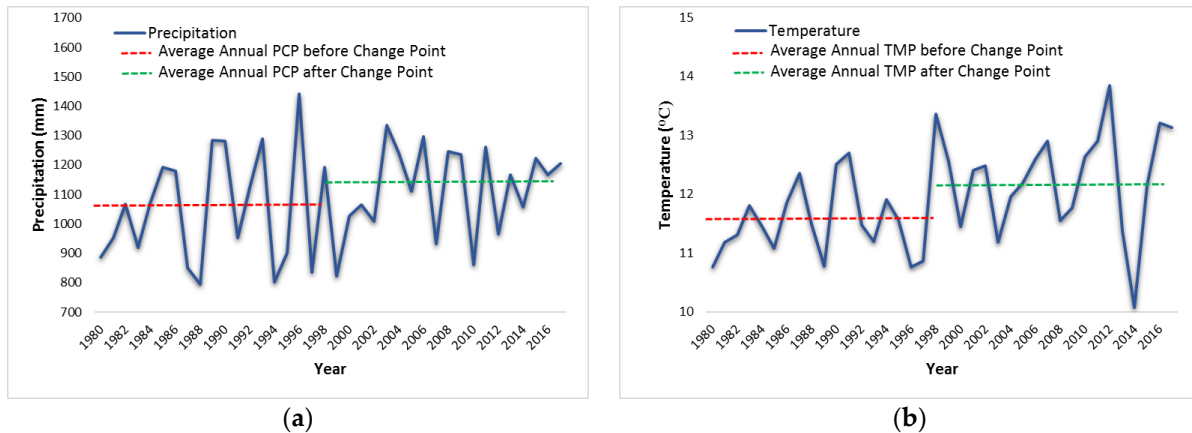


Figure 3.4. Annual precipitation (a) and temperature (b) in the LEC watershed.

In some cases, annual temperature and precipitation might not provide a true picture for the change in trends given the change in seasonality. Therefore, taking $\alpha = 0.05$ as the significance level, the Mann–Kendall test was conducted at a monthly scale for the monthly precipitation and temperature data series. The outcomes showed a significant, positive, monotonic trend in the

monthly precipitation in January and June in the LEC, while the monthly temperature exhibited a significant increase in April and September (Table 3.3).

Table 3.3. Trend analysis and significance test for monthly precipitation and temperature in the LEC Watershed.

	Jan	Feb	Mar	Apr	May	Jun	Jul	Aug	Sep	Oct	Nov	Dec
Precipitation												
Z-Stat	2.238	-0.352	0.402	1.308	-0.214	2.226	-0.063	-0.038	-0.013	0.780	-0.478	0.339
Slope	1.167	-0.037	0.206	1.216	-0.116	2.055	0.243	-0.321	0.194	0.290	-0.834	0.153
Sig	¹ S	NS	NS	NS	NS	S	NS	NS	NS	NS	NS	NS
p-value	0.006	0.181	0.172	0.048	0.208	0.006	0.237	0.242	0.247	0.109	0.158	0.184
Temperature												
Z-Stat	0.83	0.201	1.031	2.552	1.144	1.396	-0.717	1.195	1.974	1.107	0.779	0.05
Slope	0.33	0.004	0.05	0.066	0.028	0.029	-0.005	0.027	0.048	0.035	0.02	0.044
Sig	NS	NS	NS	S	NS	NS	NS	NS	S	NS	NS	NS
p-value	0.102	0.210	0.076	0.002	0.063	0.041	0.118	0.058	0.012	0.067	0.109	0.240

¹ S: Significant. NS: Not significant. Significant level (α) = 0.05.

3.3.3 Changes in Hydrological Variables

The monotonic trends of streamflow and baseflow in the LEC watershed were quantified using the Mann–Kendall test. The Z-statistics and the slope of annual streamflow and baseflow were positive (Table 3.4). Both long-term annual streamflow and baseflow in LEC were positively trending and significant at a level of 0.001; this implies that both showed significant increasing trends over the 1980–2017 period (Figure 3.5).

Table 3.4. Temporal trends in annual streamflow and baseflow in the LEC watershed.

	Streamflow	Baseflow
Z-Stat	3.319	3.395
Slope	5.078	2.062
α	0.001	0.001

The increases in streamflow have a relationship with the increased rainfall. The increasing trend in annual baseflow might seem contradictory at first, as urbanization and imperviousness is increasing, the surface runoff is expected to increase instead of baseflow and infiltration. However, with a conducive hydrologic and geologic setting, evapotranspiration reductions, meeting water supply needs in urban areas and import of water into watersheds, sewage leakage, water distribution lines, retention and detention basins can all contribute to the baseflow to be increased in urban watersheds (Ahiablame et al., 2013). Detention basins have vital roles in increasing baseflow in urban watersheds, as water retained at the surface due to an increasing portion of surface runoff, and then slowly released into the stream as a form of baseflow. Therefore, increasing measures to maintain storm water over time may be a main reason for the increase of groundwater and baseflow in urban watersheds (Meyer, 2005).

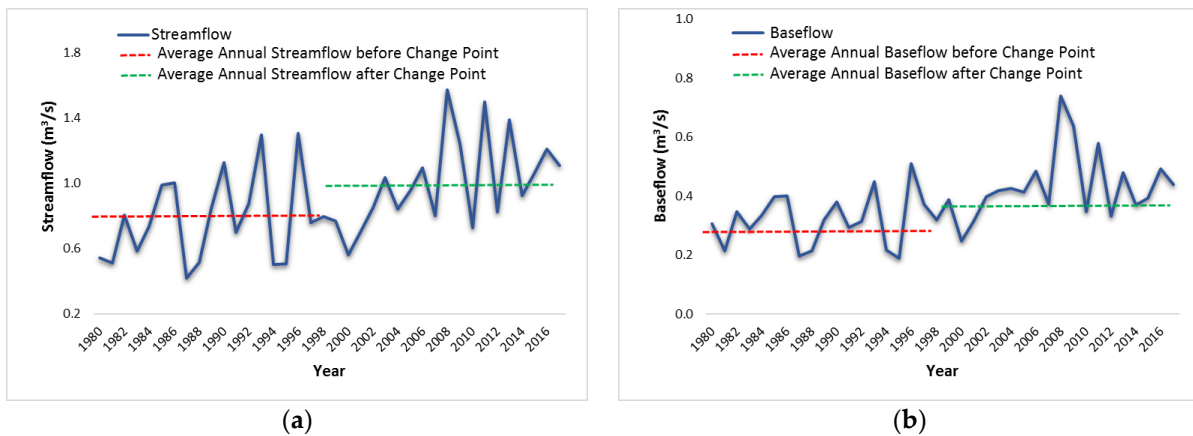


Figure 3.5. Average daily streamflow (a) and baseflow (b) over time in the LEC watershed.

3.3.4 The SUFI-2 Calibration and Uncertainty Analysis Algorithm

The Sequential Uncertainty Fitting program algorithm (SUFI-2) approach within the SWAT-CUP interface was applied for optimization, calibration, validation and uncertainty analysis of parameters in the model (Abbaspour, 2015). In this algorithm, several sources of uncertainties, such as conceptual model, measured data (e.g., observed flow, sediments), driving variables (e.g., precipitation) and parameters, were quantified by the 95 Percent Prediction Uncertainty (95PPU), that calculate the cumulative distribution of an output variable at the 2.5% and 97.5% levels achieved through Latin Hypercube Sampling (LHS).

Based on previous studies, 20 hydrologic parameters were considered (Table 3.5). These parameters were described according to their existence among the main flow rate variable calibration parameters (Almeida et al., 2018). SUFI-2 begins with wide ranges of meaningful parameters that capture most of the observed data within the 95PPU and then iteratively decreases the uncertainty of the parameters (Neitsch et al., 2011). Newer and narrower parameter ranges of uncertainties are computed after each iteration, in which larger uncertainty reductions are more related to the sensitive parameters (Zuo et al., 2016). Finally, the best fitted parameters obtained from SUFI-2 were incorporated into SWAT for streamflow and baseflow simulations at a daily time step but summarized monthly (Mehan et al., 2017).

Performance assessment of the default model showed discrepancies between observed and simulated values; therefore, both automatic and manual calibration were done. Due to the large number of parameters within the SWAT model, a sensitivity analysis was first conducted, in order to decrease the number of parameters to be optimized. The calibration process included only sensitive parameters, and parameters were optimized based on monthly values (Welde & Gebremariam, 2017).

Table 3.5. SWAT input parameters used for the LEC calibration of streamflow and baseflow.

Parameter	¹ Ext.	Description	Adjustment	¹ IV	¹ LB	¹ UB	¹ FV
Parameters controlling water balance							
ESCO	hru	Soil evaporation compensation factor	R	0.95	0.01	1	0.08
EPCO	hru	Plant uptake compensation factor	R	1	0.01	1	0.48
CANMX	hru	Max canopy storage	R	0	0	25	23.5
SFTMP	bsn	Snowfall temp	R	1	-5	5	-3.4
SMTMP	bsn	Snowmelt base temp	R	0.5	-5	5	3.8
TIMP	bsn	Snow back temp lag factor	R	1	0.01	1	0.59
SMFMX	bsn	Melt factor for snow on 21 June	R	4.5	0.01	10	1.38
SMFMN	bsn	Melt factor for snow on 21 December	R	4.5	0.01	10	4.09
Parameters controlling surface water response							
CN2	mgt	Initial SCS Curve number	V	--	-0.25	0.25	0.22
SURLAG	bsn	Surface runoff lag coefficient	R	4	0.1	10	3.28
Parameters controlling subsurface water response							
ALPHA_BF	gw	Baseflow alpha factor	R	0.048	0.01	1	0.75
GWQMN	gw	Depth of water for return flow	R	1000	0.01	5000	1273
GW_DELA Y	gw	Groundwater delay time	R	31	0.1	50	19.4
REVAPMN	gw	Depth of water for evaporation	R	750	0.01	250	124
GW_REVAP	gw	Groundwater evaporation coefficient	R	0.02	0.02	0.2	0.15
RCHRG_DP	gw	Deep aquifer percolation fraction	R	0.05	0.01	1	0.59
Parameters controlling soil's physical properties							
SOL_AWC	sol	Available water capacity of the soil water	V	--	-0.25	0.25	0.10
SOL_K	sol	Saturated hydraulic conductivity	V	--	-0.15	0.15	0.03
Parameters controlling channel's physical properties							
CH_K2	rte	Effective hydraulic conductivity	R	0	5	300	32.6
CH_N2	rte	Main channel manning	R	0.014	0.01	0.15	0.08

¹Ext: Extension, R: Replace by value, V: Multiply by value, IV: Initial values, LB: Lower bound, UB: Upper bound, FV: Final value.

The SUFI-2 global sensitivity analysis, in concurrence with the calibration procedure, was used to test 20 recommended parameters. Global sensitivity is important in identifying the relative significance of each parameter and the objective function sensitivity using the *t*-test. As a statistical measurement, the *t*-stat and *p*-value were used. A *t*-stat provides a sensitivity measure, in which greater absolute values are more sensitive, while the *p*-value determines the importance of the sensitivity (Zuo et al., 2016).

Following Moriasi et al. (2007), graphical comparison and statistical indices can assess the performance of the calibrated parameters. The coefficient of determination (R^2), Nash–Sutcliffe model efficiency (ENS), PBIAS and modified Kling–Gupta Efficiency (KGE) were used to evaluate the model performance for the simulated streamflow and baseflow. The formulas for R^2 and ENS, PBIAS and KGE can be acquired as previously outlined by Gupta et al. (2009) and Nie et al. (2011), respectively, and can be calculated as follow:

$$R^2 = \left[\frac{\sum_i [(Y^{obs} - \mu^{obs})(Y^{sim} - \mu^{sim})]^2}{\sqrt{\sum_i (Y^{obs} - \mu^{obs})^2 \sum_i (Y^{sim} - \mu^{sim})^2}} \right]^2 \quad (3.5)$$

$$ENS = 1 - \left[\frac{\sum_i (Y^{obs} - Y^{sim})^2}{\sum_i (Y^{obs} - \mu^{obs})^2} \right] \quad (3.6)$$

$$PBIAS = \frac{\sum (Y^{obs} - Y^{sim})}{\sum Y^{obs}} \times 100 \quad (3.7)$$

$$KGE = 1 - \sqrt{(r - 1)^2 + (\beta - 1)^2 + (\gamma - 1)^2} \quad (3.8)$$

where

$$\beta = \frac{\mu^{sim}}{\mu^{obs}} \quad (3.9)$$

and

$$\gamma = \frac{CV^{sim}}{CV^{obs}} = \frac{\sigma^{sim} / \mu^{sim}}{\sigma^{obs} / \mu^{obs}} \quad (3.10)$$

Y^{obs} is the observed data, Y^{sim} is the simulated output, μ^{obs} and μ^{sim} are the mean of the observed and simulated flow, respectively, r is the correlation between the measured and simulated values, β is the ratio between the simulated mean (μ^{sim}) and the observed mean (μ^{obs}) flow, and γ is the variation coefficient ration between the simulated (CV^{sim}) and the observed (CV^{obs}) flow,

in which σ^{sim} and σ^{obs} represent the standard deviations of both simulated and measured data, respectively. Calibration and validation results were utilized to evaluate model success. Table 3.6 reports a model performance rating of “Very good, good, satisfactory and unsatisfactory” for each parameter.

Table 3.6. SWAT performance evaluation criteria according to Lee et al. (2018), Moriasi et al. (2013), and Thirel et al. (2015).

Measure	Output	Evaluation Criteria of the Model [†]			
		<i>Very Good</i>	<i>Good</i>	<i>Satisfactory</i>	<i>Unsatisfactory</i>
R ²	Flow	>0.85	0.75 < R ² < 0.85	0.60 < R ² < 0.75	R ² ≤ 0.60
ENS	Flow	>0.80	0.70 < ENS < 0.80	0.50 < ENS < 0.70	ENS ≤ 0.50
PBIAS	Flow	<±10	±10 ≤ PBIAS ≤ ±15	±15 ≤ PBIAS ≤ ±30	PBIAS ≥ ±30
KGE	Flow	>0.80	0.70 < KGE < 0.80	0.50 < KGE < 0.70	KGE ≤ 0.50

[†] Sources: (Lee et al., 2018; Moriasi et al., 2013; Thirel et al., 2015)

3.3.5 Parameter Sensitivity Analysis

In this research, Little Eagle Creek data at the Speedway gauging station were used to calibrate the model. The threshold for defining HRUs was set as zero percent for soil, land and slope. The overlay of soil and land use maps, in addition to the slope percentage resulted in 516 HRUs, distributed over seven sub-basins. The sensitive parameters were optimized using the extension of auto-calibration in SWAT2012 to calibrate the hydrological model, and were recognized on the basis of global sensitivity analysis. Most of the parameters were modified on a trial and error basis within reasonable limits after consideration of the physical properties of the watershed. The global sensitivity analysis showed that parameters representing surface runoff, soil properties, and groundwater return flow were sensitive. Hence, it was important to accurately estimate these parameters for streamflow simulation. The 10 most sensitive input parameters are shown in Table 3.7, while the remaining parameters had less significant effect on streamflow simulation. Different ranks have been commonly detected in the same parameter for different watersheds and with a different number of simulations, which indicates the stochastic nature of SWAT-CUP (Mehan et al., 2017).

Table 3.7. List of top 10 ranking sensitive parameters for SWAT in the LEC watershed and their calibrated values.

Rank	Parameter	Calibrated Value	<i>t</i>-Stat	<i>p</i>-Value
1	ALPHA_BF	0.81	44.71	0
2	CN2	0.02	18.47	0
3	CH_K2	28.39	-13.34	0
4	CH_N2	0.08	-4.72	0
5	SOL_AWC	-0.17	-4.13	0
6	RCHRG_DP	0.01	-3.16	0
7	EPCO	0.16	-2.99	0
8	SMTMP	-1.51	2.48	0.01
9	SFTMP	4.90	-2.24	0.03
10	CANMX	23.27	1.95	0.05

For the LEC watershed, SUFI-2 outlined the most sensitive parameters to input changes, and these were ALPHA_BF, CN2, CH_K2, CH_N2, SOL_AWC, RCHRG_DP, EPCO, SMTMP, SFTMP, and CANMX. They each have a *p*-value close to zero. The ALPHA_BF and CN2, ranked first and second in sensitivity, respectively, and higher than the others which appeared to have made the most contribution in improving the ENS. In general, CN2, ALPHA_BF, SOL_AWC, and RCHRG_DP were important parameters for both baseflow and streamflow simulation, as the water traveling from the root zone in SWAT to deep aquifers was not redistributed into the main channel, soil, or shallow aquifers, but considered lost from the system boundary (Jang et al., 2018). The high ALPHA_BF constant in the LEC watershed indicated a rapid response to groundwater recharge.

3.3.6 Selection of SWAT Model Structure

After incorporating all the data inputs, and in accordance with the detection of temporal trends in temperature and precipitation results, the period of 1980–2017 was divided into two time-

spans, 1980–1998 and 1999–2017. The model was run for 1980–1998 with the first 4 years (1980–1983) used as a warm up period for the model. On the basis of the 1992 land use map, the period of 1980–1998 was recognized as the baseline condition for the SWAT model. The 1980–1993 period was assigned for model calibration, while the years from 1994–1998 were used for model validation. Careful consideration was taken so that both calibration and validation periods had similar water balance (Arnold et al., 2012). The monthly statistical streamflow and baseflow outputs for the baseline model were used to evaluate the model performance.

3.3.7 Calibration and Validation of SWAT Model

The proportion of baseflow (ratio of baseflow over total streamflow) of the measured and simulated streamflow were 36.5% and 39.1%, respectively. The good match indicated that partitioning between baseflow and surface runoff could be represented by the calibrated model in the LEC watershed (Nie et al., 2011).

Figures 3.6 and 3.7 show the simulated and measured monthly streamflow and baseflow for LEC during the calibration period (1984–1993) and validation period (1994–1998), with the first four years assigned as a warm up period (1980–1983). Model assessment statistics for monthly simulated streamflow and baseflow are summarized in Table 3.8. The ENS and R^2 were 0.84 and 0.87, respectively, within the calibration period of streamflow, and 0.74 and 0.83 over the course of the validation period. These statistical outputs indicated that the simulated streamflow in calibration and validation were in ‘Very Good’ agreement, according to the Moriasi et al. (2007) criteria.

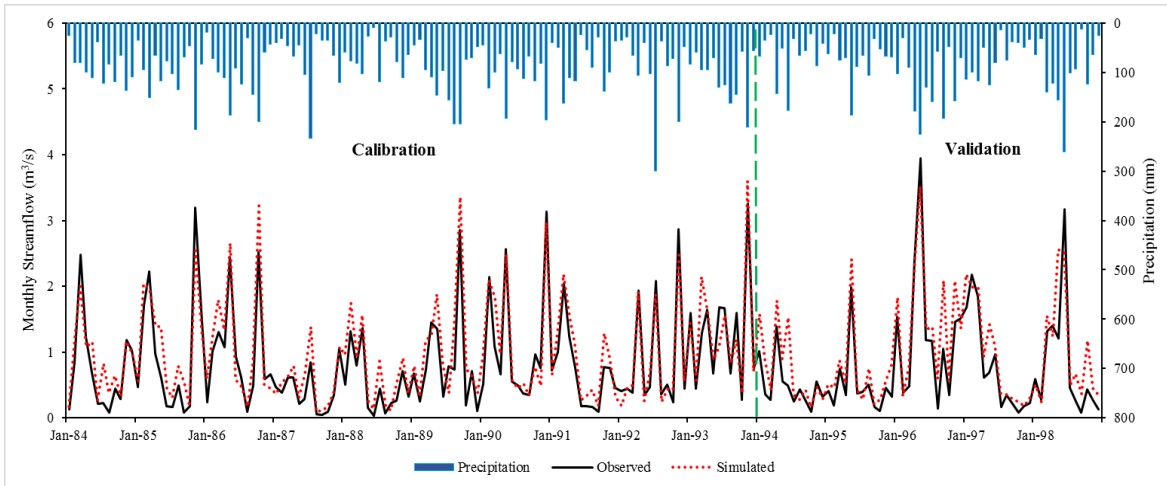


Figure 3.6. Observed and simulated streamflow of LEC watershed for calibration and validation period.

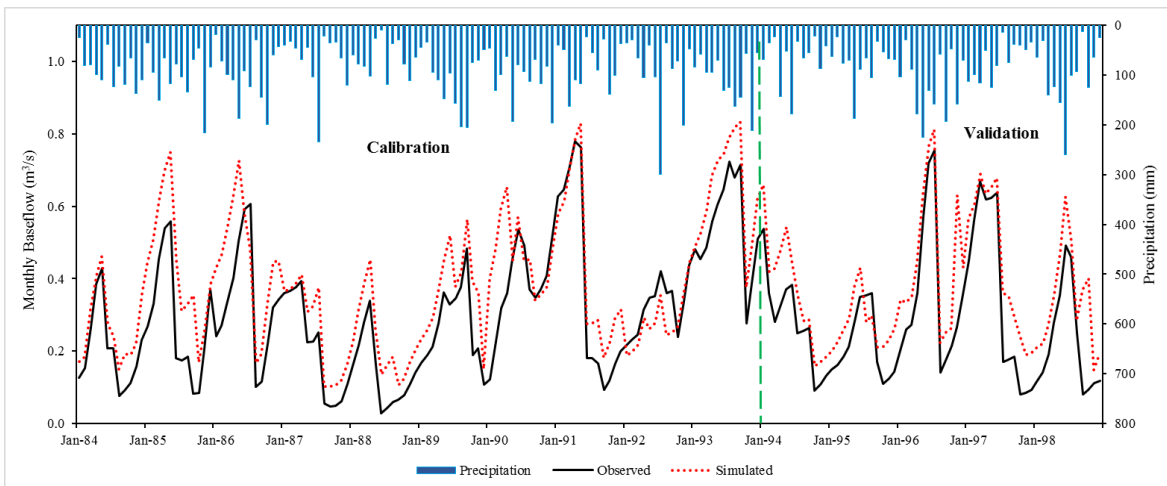


Figure 3.7. Observed and simulated baseflow of LEC watershed for calibration and validation period.

As shown in Figure 3.6, observed and simulated streamflow outputs had a similar trend; in addition, the simulated streamflow showed a reasonable match with the observed records. Therefore, most of the measured and simulated streamflow values were bracketed by the 95 PPU, therefore, indicating comparatively little uncertainty for the streamflow simulation (Zuo et al., 2016). However, the relatively low agreements at the end of winter of some years could be explained by the model deficiency in capturing certain hydrological processes such as soil

freezing-thawing and snowmelt during this period. In addition, some differences were observed in the peaks of observed and simulated values. These might have been due to the precipitation pattern or due to the limitations of the curve number (CN) method, as the CN method used in SWAT does not consider the duration and intensity of precipitation (Nie et al., 2011). Results showed that the CN method overestimated streamflow for some large rainfall events. Overall, the observed and simulated average annual streamflow during the baseline model period were 0.83 m³/s and 0.98 m³/s, respectively.

The agreement between the measured and simulated streamflow during the calibration and validation period, to some extent, involves a good groundwater discharge simulation. The computed baseflow agreed well with the observed results for the LEC (Figure 3.7). During the calibration period, the R², PBIAS, ENS and KGE were 0.80, -24.97, 0.60 and 0.67, respectively, while they were 0.84, -31.40, 0.58 and 0.58 for model validation (Table 3.8). The performance of the SUFI-2 model for baseflow simulation was considered 'Good' for calibration and 'Satisfactory' for validation, according to Moriasi et al. (2007) and Moriasi et al. (2015). However, the peak baseflow was not well matched, as the SWAT simulation tended to overestimate baseflow, likely because of the spatial distribution of precipitation data was unevenly represented. In addition, peak baseflow may be attributed to the change in land use that influences hydrological phenomena and is related to direct runoff as well. An alternative possibility for the differences might be the presence of practices like surface detention and retention basins, in addition to the effect of soil freezing/thawing on infiltration and recharge during initial snowmelt. Overall, the average annual baseflow during the period from 1984 to 1998 for both measured and simulated data was 0.30 m³/s and 0.38 m³/s, respectively. These results ensure that the model can be further applied to assess hydrologic response analysis to various land use and climate change scenarios. Of note, despite the good agreements between the observed and simulated results, some uncertainty is associated with any hydrologic model (Duan et al., 2017). Uncertainties in hydrologic models can arise from many different sources, including the structure of the conceptual model itself, initial conditions, parameters, observed input data, and interaction processes. However, the study area covers only 74.5 km², and the amount of intense urbanization in which the watershed undergone may create some uncertainties, such as the surface water model not fully accounting for the complicated infrastructure in urbanized watersheds. Moreover, only 20 parameters were used to calibrate the model. Duan et al. (2017) suggest that these may not be sufficient to represent. In addition,

hydraulic conductivity can affect groundwater response time; however, most of the parameters in the SWAT model are surface-related such as hydraulic conductivity, saturated soil zones and channels (Duan et al., 2017). These parameters were used in the calibrated baseline model to obtain an estimate of baseflow, but this assumed that the recharge of groundwater came only from shallow aquifers to allow quicker contribution to baseflow. Additionally, SWAT divides underground storage into shallow and deep aquifers. The shallow aquifer receives recharge from unsaturated soil percolation. However, surface water models like SWAT hypothesize that water entering deep aquifers is considered lost from the system and therefore is not considered in future water budgets.

Table 3.8. Values of statistical indicators in the calibration and validation periods for streamflow and baseflow in the LEC watershed.

Period	Streamflow (m ³ /s)				Baseflow (m ³ /s)			
	R ²	ENS	PBIAS	KGE	R ²	ENS	PBIAS	KGE
Calibration (1984–1993)	0.87	0.84	-14.4	0.81	0.80	0.60	-24.9	0.67
Validation (1994–1998)	0.83	0.74	-26.9	0.72	0.84	0.58	-31.4	0.58

3.3.8 Changes in Total Water Yield and Baseflow within Various Simulation Scenario

Table 3.9 demonstrates the simulated SWAT annual average water yield and baseflow under different land use climate changes scenarios, as discussed in Section 3.2.3.4, in the LEC watershed. Results indicated that the difference in average annual water yield between S2 and S1, that simulated the impacts of land use change, showed an increase of 30.5 mm (6.7%). Meanwhile, the average annual water yield increased by 88.1 mm (17.9%) in S3 as compared to S1, which indicated the impacts of climate variability. Water yield increased by 91.9 mm (20.3%) due to the combined effects of land use change and climate variation; i.e., the contrast between S1 and S4. These findings indicated that the average annual water yield increased in the LEC during CP1 and CP2 due to the effects of both land use dynamics and climate variation, with the influences of climate change greater than that of the land use alteration. Meanwhile, the contribution of the combined impacts was greater than that of land use change and climate change separately. Therefore, the results emphasized that when climate variation played a dominant role, the impact of land use dynamics on water yield was not obvious. However, urban expansion also had a

considerable impact on annual water yield by increasing impervious area, therefore, increasing surface runoff and decreasing water infiltration (Zhao et al., 2015).

On the other hand, simulation suggested the reduction of the average annual baseflow due to the effect of land use change and the combined impacts of land use and climate change by an amount of 42.2 mm (28.8%) and 33.7 mm (23.0%), respectively, while the average annual baseflow increased by an amount of 22.3 mm (15.2%) due to the separate effects of climate change. Therefore, both land use change and the combined effects of land use and climate change had a greater negative impact on average annual baseflow, which illustrates the greater effect of land use change on baseflow in the LEC watershed. Climate variation has reduced the negative impact of land use change by 5.8%, as it increased from -28.8% to -23.0% from S2 to S4. The reduction of average annual baseflow in S2 and S4 may be because of several activities, for instance, over-exploitation, industrial uses, water withdrawal and groundwater pumping that are primarily used in the LEC watershed for production, manufacturing and daily human consumption. In addition, the decreasing trend seen in average annual baseflow could be due to the increase in surface runoff and lower soil infiltration, due to urbanization and increasing imperviousness that resulted in less water reaching unsaturated soils.

Table 3.9. Average annual change in water yield and baseflow in the LEC watershed.

Scenario	Land Use	Climate	Water Yield (mm)			Baseflow (mm)			Surface Runoff (mm)		
			Av.	Ch. Δ	(%)	Av.	Ch. Δ	(%)	Av.	Ch. Δ	(%)
S1	NLCD 1992	CP1	452.7	-	-	146.5	-	-	294.1	-	-
S2	NLCD 2011	CP1	483.2	30.5	6.7	104.3	-42.2	-28.8	374.7	80.6	27.4
S3	NLCD 1992	CP2	533.8	81.1	17.9	168.8	22.3	15.2	360.9	66.8	22.7
S4	NLDC 2011	CP2	544.6	91.9	20.3	112.8	-33.7	-23.0	428.5	134.3	45.7

Figures 3.8 and 3.9 show the results of the LEC watershed average monthly water yield and baseflow in different simulated scenarios. Most of the water yield was concentrated from March to July in all scenarios, i.e., within the rainy season. However, water yields accounted for 50% in both S1 and S2, while increasing to 55% in S3 and S4 during the rainy season. After evaluating the change in monthly precipitation between CP1 and CP2 (Figure 3.8), it might be concluded that

the rainfall increase between CP1 and CP2 and the change in the pattern of average annual rainfall resulted in increased flood peaks between the two periods. The combined effects of climate variability and land use change caused an increase in monthly water yield in all months except November, which experienced a higher rainfall pattern in the first time period (CP1) as compared to CP2. Meanwhile, the average monthly baseflow response showed a similar behavior to the water yield response; however, the effect of climate change on baseflow was greater than the impact on water yield in the rainy season (Figure 3.9). Overall, both climate change and land use change had a greater impact on baseflow than water yield. Furthermore, average monthly baseflow showed an increase under the effect of solely climate change impacts of S3 in all months for the LEC watershed except for July and October, which showed a very minor reduction in baseflow (Figure 3.9). The highest average monthly increase occurred in the coldest months of the year with respect to S3 with the lowest amount of rainfall. This might be attributed to the process of freeze-thaw that can change the runoff process, soil infiltration and subsurface water storage. Therefore, baseflow from shallow aquifers was considered the main contributor to total streamflow with the reduction of average monthly precipitation.

Figure 3.10 shows the average monthly streamflow changes relative to the baseline scenario (S1). Under the S2 scenario, the streamflow showed a reduction in January, February and June by 0.8% to 3.7%, while it increased in other months by 1.6 to 16.5%. Under the S3 scenario, however, streamflow showed an increase in all months, especially in summer, by an amount of 3.4% to 30.3%. Furthermore, the S4 scenario showed a similar trend in streamflow increase in all months by an amount ranging from 7.6% to 34.2%, with the only reduction recorded in May of 2.1%. On the other hand, Figure 3.11 shows the average monthly absolute changes in baseflow relative to the S1 (baseline) scenario. At the monthly timescale, baseflow showed a reduction in all months with respect to the S2 scenario (land use change) from 8.9% in March to the greatest reduction in August of 58.7%. A significant increase of baseflow occurred in all months ranging from 6.6% to 81.9% under the climate variation scenario (S3), while baseflow decreased with respect to the baseline scenario in the wet season by 2.9% to 15.5%. Finally, the S4 scenario showed reductions in baseflow for nearly the whole year ranging from 1.3% to 61.8%, while the only increase was found in January by 23.1%. Generally, the impact of the combined effects of land use and climate variation were reduced when land use and climate variation caused changes in opposite directions. This can be clearly seen in all months of the year with respect to baseflow variation (Figure 3.9).

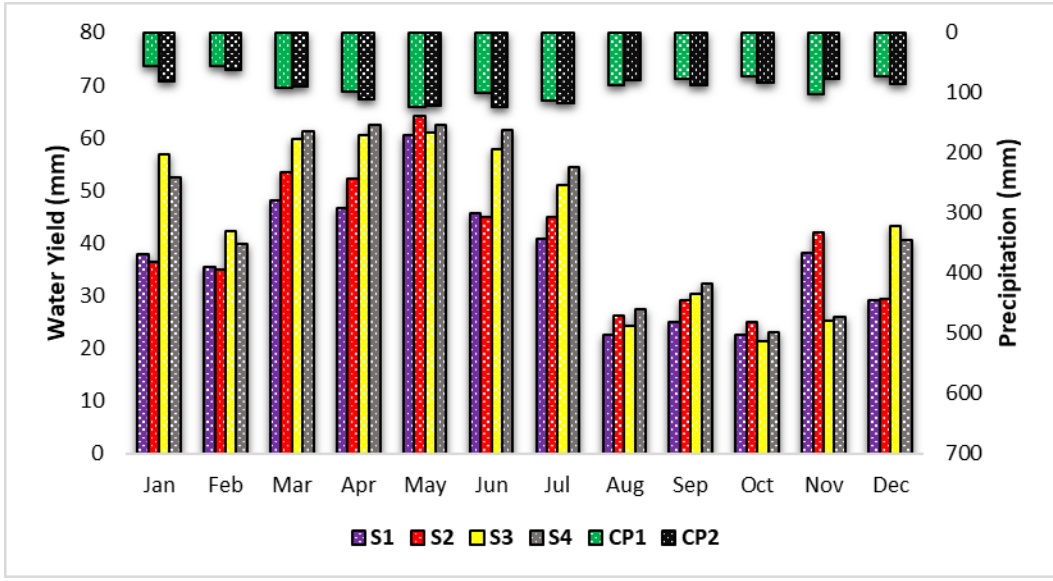


Figure 3.8. Average monthly water yield for the LEC watershed under different scenarios.

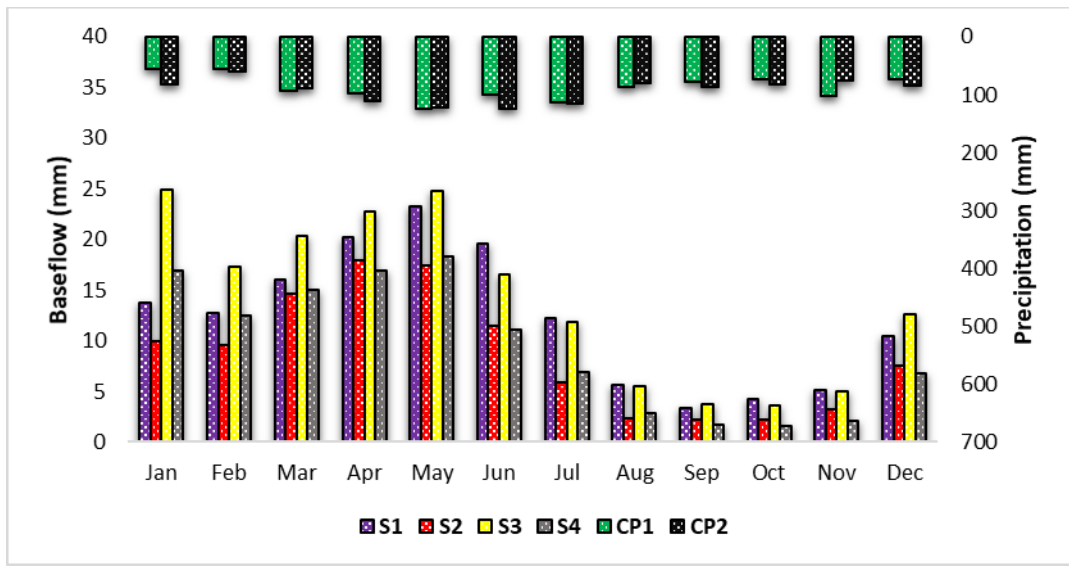


Figure 3.9. Average monthly baseflow for the LEC watershed under different scenarios.

These changes in streamflow and baseflow were intimately bound up with the variation of precipitation between the two time periods. As can be seen in Figures 3.8 and 3.9, the variation in precipitation generally reflects the variation in water yield in most months. However, the exception in other months may be attributed to the impacts of temperature fluctuation. For example, baseflow declined in October under the S3 scenario even with the increase in rainfall. That was possibly in

connection with temperature rise in CP2 compared to CP1 (Zhang et al., 2015), which could lead to an increase in evapotranspiration. In addition, compensatory contributors to baseflow, for example lawn irrigation, may contribute to this fundamental change in baseflow; therefore, a reduction in lawn irrigation might lead to the decline in the amount of water discharged to the shallow aquifer that contributed to baseflow.

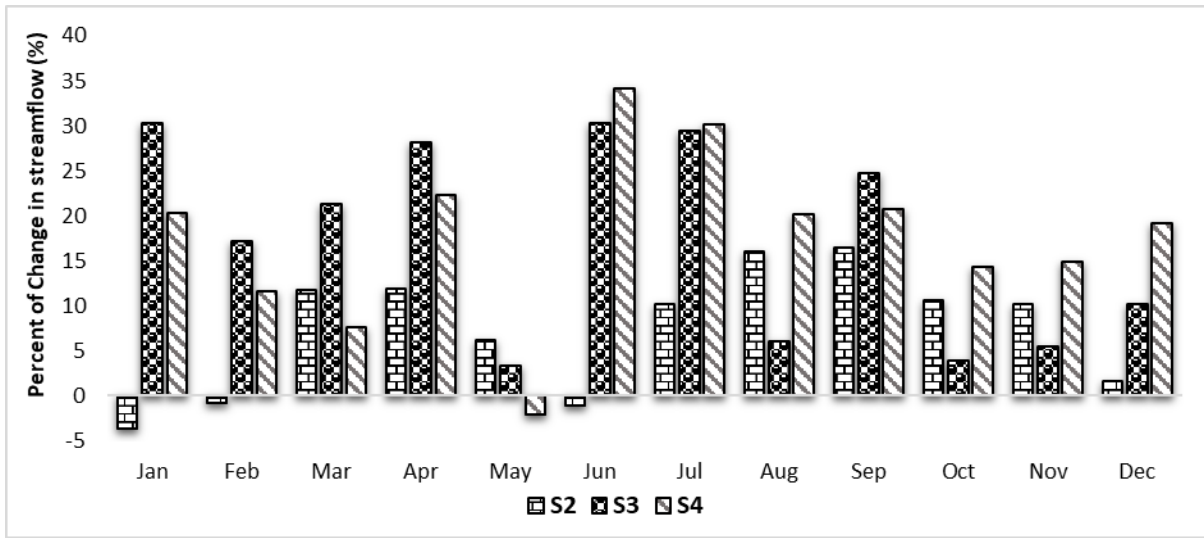


Figure 3.10. Relative change in average monthly streamflow in the LEC watershed.

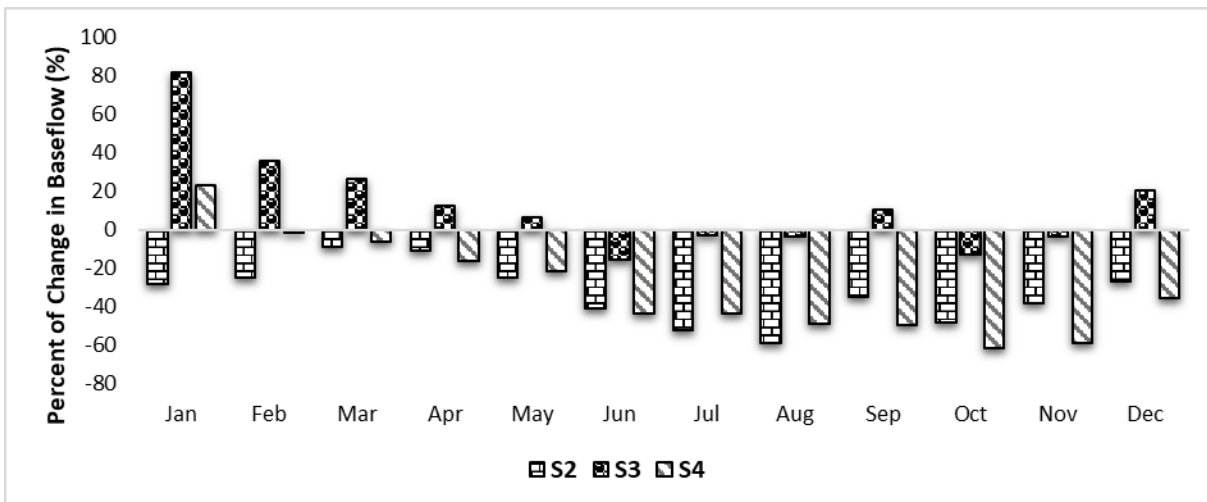


Figure 3.11. Relative change in average monthly baseflow in the LEC watershed.

3.4 Summary and Conclusions

Recognizing the impacts of land use alteration and climate variability on hydrologic systems is the basis for pragmatic watershed sustainability and ecological restoration efforts. In this study, the impacts of climate variability and land use change from 1980 to 2017 on water streamflow and baseflow in the Little Eagle Creek watershed were evaluated using the non-parametric Mann–Kendall statistical test, land use maps and hydrologic modeling. The novelty lies in that not only were the effects of climate variation on hydrological response investigated, but the combined impact of land use dynamics and climate variation was also evaluated in an urbanized watershed in the US Midwest.

The long-term streamflow and baseflow response to land use change and climate variability were evaluated using the calibrated SWAT model. The model contained four scenarios in two periods, and applied two land use datasets (1992 and 2011) for the two climate periods (CP1 and CP2). By simulating the historical, continuous variation in streamflow, the SWAT model was calibrated and validated over the period 1980 to 1998 throughout the SUFI-2 approach within the SWAT-CUP interface. The SUFI-2 algorithm played an important role in minimizing the differences between measured and simulated streamflow in the LEC watershed. Discrepancies observed between the outputs of the model simulation and the observed data may in part occur due to the lack of meteorological input data from more than a single station. The SWAT model produced ‘very good’ and ‘good’ results for calibrating and validating observed streamflow and baseflow data. Hence, the calibrated parameters in this study can be used to carry out further future environmental and hydrological studies in similar watersheds. The hydrological balance assessment has shown that baseflow is a key component of the total discharge as it accounted for 36.5% of total flow within the LEC watershed. In general, SWAT proved versatile in modeling the effects of environmental changes in urban watersheds.

The model was used to explore likely impacts of urbanization and climate variation in an urban watershed. Much of the original cultivated and forest areas had already been converted to developed areas or urbanization. During the period of 1992–2011, about 30% of the LEC watershed area changed from cultivated to urban areas, while the climate became warmer and wetter. Overall, climate variability had the dominant impact on streamflow, while urban expansion influenced baseflow more significantly than climate change. Urbanization can be considered a major environmental stressor controlling hydrological components, including surface runoff,

baseflow, and water yield in a catchment. Understanding the variation in streamflow and baseflow due to the separate and coupled effects of climate variation and land use dynamics is essential for sustainable management of water resources. The results gleaned from this study can be useful in providing information for management and planning of water resources, in addition to assessing the prospective impacts of adaptation measures to cope with climate variation, particularly in areas that are sensitive to climate variability and experiencing high urbanization.

The results obtained in this study must be interpreted carefully, with the caveat that the meteorological station records reflect data that are the result of the combined impacts of land use alteration and climate variability. Since these effects cannot be separated in this data, the predicted impact of climate variability alone on streamflow and baseflow may not be simulated accurately. Studies that focus on quantifying the effect of each land use category change on streamflow and baseflow are likely to yield useful additional insights on how climate variability and land use impact hydrological response separately. Furthermore, additional studies using catchments that exhibit different urbanization and climate regions could provide beneficial comparative results to determine the impacts of these variables on hydrological components.

CHAPTER 4. A COMPARISON OF STREAMFLOW AND BASEFLOW RESPONSES TO LAND-USE CHANGE AND THE VARIATION IN CLIMATE PARAMETERS USING SWAT

Abstract

Alteration of land use and climate change are among the main variables affecting watershed hydrology. Characterizing the impacts of climate variation and land use alteration on water resources is essential in managing watersheds. Thus, in this research, streamflow and baseflow responses to climate and land use variation were modeled in two watersheds, the Upper West Branch DuPage River (UWBDR) watershed in Illinois and Walzem Creek watershed in Texas. The variations in streamflow and baseflow were evaluated using the Soil and Water Assessment Tool (SWAT) hydrological model. The alteration in land use between 1992 and 2011 was evaluated using transition matrix analysis. The non-parametric Mann–Kendall test was adopted to investigate changes in meteorological data for 1980–2017. Our results indicate that the baseflow accounted for almost 55.3% and 33.3% of the annual streamflow in the UWBDR and Walzem Creek watersheds, respectively. The contribution of both land use alteration and climate variability on the flow variation was greater in the UWBDR watershed. In Walzem Creek, the alteration in streamflow and baseflow appeared to be driven by the effect of climate variability more than that of urbanization. The results reported herein were compared with results reported in chapter three in order to provide necessary information for water resources management planning, as well as soil and water conservation, and to broaden the current understanding of hydrological components variation in different climate regions.

4.1 Introduction

Ecosystems and humans are fundamentally dependent on different water resources. Thus, for the general development of any country, the quality and the quantity of these water resources flowing through rivers are of vital importance to socio-economic development (Ficklin et al., 2016). Issues related to changes in water resources are commonly evaluated around the globe (Duan et al., 2016; Tong et al., 2012; Zhang et al., 2013b). In the United States, evaluation of streamflow and baseflow has been documented (Aboelnour & Engel, 2018b; Kumar et al., 2009; Zhang &

Schilling, 2006). However, the quantitative change in streamflow and baseflow has yet to be evaluated across different climatic conditions.

Climate alterations and human actions both act as stressors to place severe pressure on water resources (Aboelnour et al., 2019). The variations in climate and land use directly impact total streamflow, interflow, surface runoff, and baseflow, causing events of droughts and floods that impact the sustainability of these resources and the social ecosystem (Jin et al., 2016). Several studies have examined alterations in streamflow due to changes in temperature and precipitation (Duan et al., 2017; Frans et al., 2013; Novotny & Stefan, 2007), urbanization (Chen et al., 2017b), and land use change (Xu et al., 2013; Zhang et al., 2013b). Baseflow is the portion of streamflow sustained in a river by delayed pathways. Baseflow is often assumed to be equal to groundwater recharge (Gebert et al., 2007). It provides a relatively high water quality with a high clarity and stable temperature, and is considered indicative of sustained streamflow during dry periods of the season, which is important to stream biota and helps recreation-based industries (Neff et al., 2005). These low-flow data are essential in understanding the current and future changes to watershed hydrology. Several reports have indicated that the change in baseflow over time is due to variations in agricultural management (Charles, 2007), climate change (Aboelnour et al., 2020), urbanization (King et al., 2016), and land use alteration (Price et al., 2011). Therefore, to develop scenarios for water resources evaluation, land use change and climate variation are usually chosen as the main influencing factors. The impacts of climate variation and urbanization on streamflow and baseflow were reviewed by different scholars (Aboelnour et al., 2019; Price, 2011).

Different methods have been used to evaluate the response of watershed streamflow and baseflow to human activities and climate change. These techniques include hydrologic similarities within the watersheds, paired catchments, statistical methods, and hydrological modeling (Dey & Mishra, 2017). Since climate and land use change need to be investigated on a local scale and can vary from place to place (Khoi & Thom, 2015), there is a need to use comprehensive and physical tools to evaluate as much information as possible from the limited existing data (Li et al., 2009). Hence, hydrological models are considered the most appealing approach to carry out impact assessment studies. They provide a conceptualized framework and are suitable for use as part of scenario studies on the relationship among hydrological components, climate variability, and land use change (Gitau & Chaubey, 2010; Jothityangkoon et al., 2001). Among these models is the Soil and Water Assessment Tool (SWAT) model.

The SWAT model, developed by the United States Department of Agriculture (USDA) Agricultural Research Service, is designed to model hydrology at the scale of a watershed (J. G. Arnold et al., 1998). SWAT is widely used around the world to evaluate the influences of ecological and environmental alterations and for hydrological processes at different catchment scales, even with limited data (Liu et al., 2018). In addition, it offers several software tools, and was therefore selected for this research. Each watershed was divided into smaller sub-basins in the SWAT model. These sub-basins were then divided into smaller Hydrologic Response Units (HRUs), which were fundamentally based on land use, soil type, and slope (Arnold et al., 2012). Within each HRU, the Soil Conservation Service (SCS) curve number and Green–Ampt infiltration were adapted to compute surface runoff using daily precipitation. In addition, SWAT subdivides the groundwater system into deep confined aquifers, which contribute to flow outside of the catchment, and shallow unconfined ones, in which the groundwater and baseflow return to the stream (Neitsch et al., 2009). The SWAT model has proven to perform well in streamflow and baseflow simulations around the world and in complex catchments with extreme events (Abbaspour et al., 2015), since it allows the interconnections of different physical processes (Luo et al., 2012; Yan et al., 2018; Zhang et al., 2011). Therefore, in this research, the SWAT model was adopted to assess the impacts of land use and climate change.

Streamflow and baseflow responses to human activities, urbanization, and climate variation are different in various basins with respect to climate regions, geographical variances, scale, and urbanization levels (Mwakalila et al., 2002; Price, 2011). However, the need to fully understand the streamflow and baseflow responses to external stimuli is of vital importance. Many studies in the last few years have been carried out to investigate the hydrological response to urbanization and climate change (Zhang et al., 2016). Outputs of these studies can help in understanding the cause of shifts in water resources. However, these studies mainly focus on the single impact of either land use change or climate variation, but neglect the combined effects of climate alteration and human activities and their contributions to the change. Thus, the combined effects are still not fully understood over different climatic conditions and geographical regions. For this reason, the responses of streamflow and baseflow to urbanization and climate variation will be evaluated for varying climate conditions with different urbanization levels. Two watersheds, the Upper West Branch DuPage River (UWBDR) watershed, Illinois, and Walzem Creek watershed, Taxes, were

used as examples to quantify the changes in streamflow and baseflow as a response to climate and land use change.

As evidenced by the USA Census population data, the Upper West Branch DuPage River (UWBDR) watershed, Illinois, has undergone intense urbanization in the last four decades. In addition to this dramatic urbanization, the watershed has experienced major flood events, such as the floods of 1996 and 2008 (Burke et al., 2006). Other incidences in the watershed have been identified as impactful on the development of the UWBDR. One of the main contributors is floodplain management that addressed overbank flooding of the main stream and its tributaries (Burke et al., 2006). Hejazi and Markus (2009) investigated the impacts of urbanization and climate variability on annual flooding in 12 urban watersheds in Cook County, northeastern Illinois. They found that urbanization had a greater impact than climate on the increase in flood discharge, and, due to increasing urbanization, discharge volume may become even higher in the future. In addition to floodplain management, wetland protection, bank stabilization, stream restoration, water quality, and groundwater recharge are also concerns within the catchments (Hejazi & Markus, 2009). Some sections of the stream are supplied with a substantial amount of their baseflow from local groundwater discharge, while other sections release baseflow to groundwater due to the presence of a large outwash plain at the base of the West Chicago Moraine that creates conditions that promote rapid flooding and groundwater movement from the border of the moraine through the outwash (Burke et al., 2006).

The second watershed is the Walzem Creek, San Antonio, Texas. The city of San Antonio, Bexar County and other partners initiated a watershed protection plan in 2006 for the Upper San Antonio basin, including the Walzem Creek watershed, to track efforts that enhance urban outreach, and to bring the basin back into compliance with water resource and water quality recreation standards. In 2015, the Environmental Protection Agency (EPA) approved this protection plan, making the state eligible for project funding within the watershed to address nonpoint source runoff. The report can be viewed at <https://www.brwm-tx.org/>. A combination of rocky and clay soils contributes to larger runoff than groundwater flow in this watershed. Rock, clay, and slopes create nearly impervious conditions in the northern portion of the watershed and thus reduce the effect of development and its associated impervious cover on storm water flow (Clean River Program San Antonio River Basin, 2017).

The main target of this study was to evaluate the impact of separate and combined impacts of land use changes and climate alteration on streamflow and baseflow in two watersheds under different land use and climatic conditions. The specific goals of this research were: (1) identify the long term trend and the abrupt changes in hydrological and meteorological data; (2) determine the change in land use maps from 1992 to 2011; (3) use the new calibrated and validated SWAT model to assess the individual and combined impacts of land use change and climate variation on streamflow and baseflow; and (4) compare the outputs of this study with the findings of Aboelnour et al. (2019). Information gleaned from this study can be used to understand the variations in hydrological flow components, and are necessary for water resources management and planning, as well as water and soil conservation in geographically different watersheds.

4.2 Study Areas

4.2.1 Upper West Branch DuPage River Watershed

The Upper West Branch DuPage River watershed (UWBDR) is located in northeast Illinois, within the six-county Chicago metropolitan region. The watershed is located approximately in the western one third of DuPage County (Figure 4.1a). The headwaters originate in the northwestern part of Cook County where the water flows generally to the south into and through DuPage County. The UWBDR is part of the West Branch DuPage River (WBDR) watershed that divides into upper, middle, and lower branches within the DuPage catchment and belongs to the Des Plaines River basin. The UWBDR covers approximately 91.7 km² (USGS Gauge 05539900) with mean annual precipitation ranging from 612 to 1293 mm from 1980 to 2017, and average annual temperatures ranging from 8.4 to 12.5 °C. The minimum, maximum, and mean elevations in the area are 217, 298 and 240 m above sea level, respectively. Developed and residential areas were the dominant land use type in the UWBDR at the end of the last century (44.1%), followed by cultivated and forest land cover at 39.0% and 8.8%, respectively. Current land use varies from residential (84.2%) to forest (4.4%), vacant (4.5%), and cultivated (2.7%). The river network in the watershed receives treated effluent and wastewater from the city of West Chicago, Illinois (Drury et al., 2013).

4.2.2 Walzem Creek

Walzem Creek is located in Bexar County in the state of Texas and in the San Antonio East USGS quad (Figure 4.1b). Currently, except for the lower most portion of the watershed, the majority of Walzem Creek is characterized by dense, urban development. The lower portion of the watershed is characterized by a mix of vegetation and forests and normally dry except during rain events. The Walzem Creek is a part of the Upper San Antonio Watershed and covers approximately 109 km² (USGS Gauge 08178800), with a mean annual precipitation ranging from 320 to 1200 mm and average annual temperatures ranging from 19.3 to 22.3 °C. Mean elevation in the area is 204 m, with a minimum and maximum of 152 and 266 m above sea level, respectively. Similar to the UWBDP watershed, recently, most of Walzem Creek is covered with developed areas (84.5%); however, other land uses include wetlands (7.2%), shrublands (4.2%), and forests (2.5%). However, it was characterized by only 64.4% of residential areas, 17.5% of planted cover, and 8.7% and 7.0% of forest and shrublands covers, respectively, at the beginning of the 1990s. This area is a large portion of the Upper San Antonio Watershed; hence, it contributes a large amount of total streamflow. According to the main Koppen–Geiger climate classes for US counties, the San Antonio, Bexar County area lies at the border between the warm, humid, equatorial zone and fully hot arid and steppe zone (Kottek et al., 2006). Therefore, this watershed is representative of semi-arid regions.

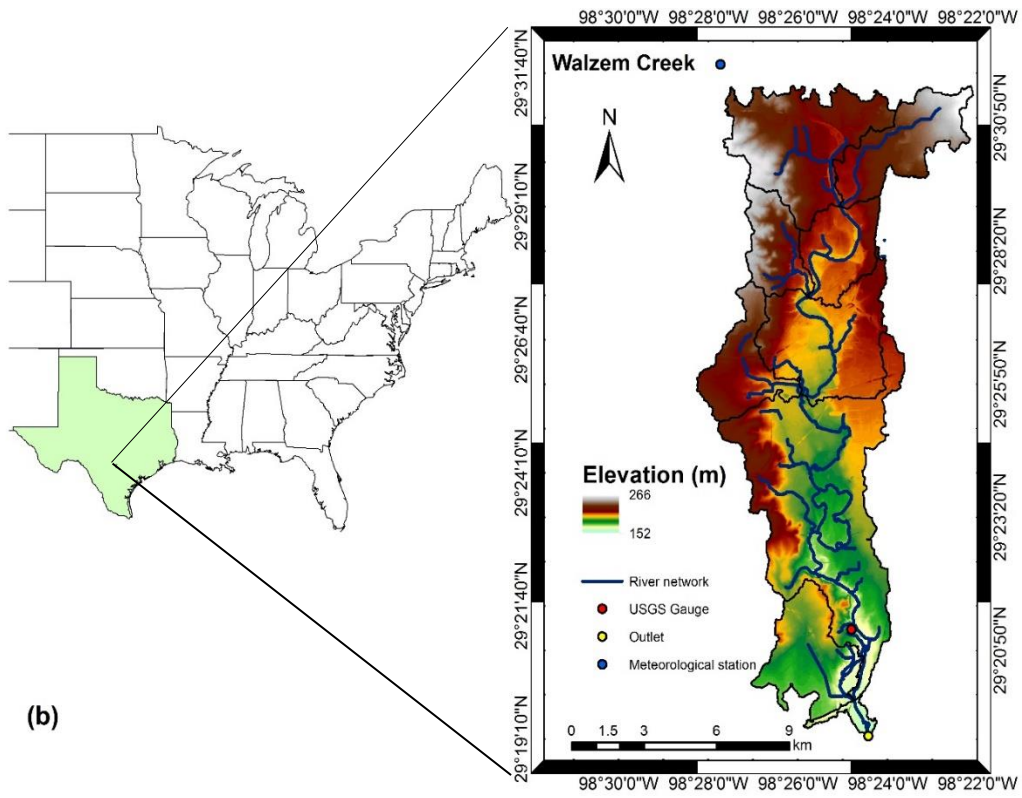
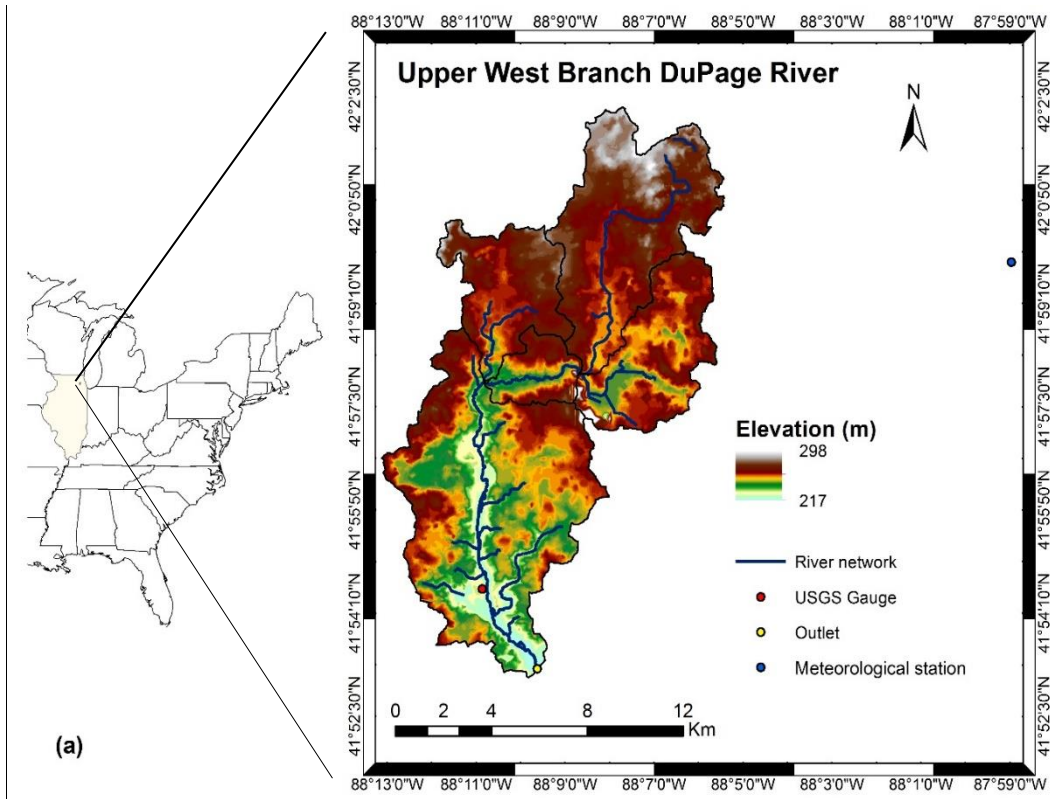


Figure 4.1. Index map showing location of the study watersheds: (a) Upper West Branch DuPage River in Illinois; and (b) Walzem Creek in Texas.

4.3 Materials and Methods

The data described herein include spatial topography, Digital Elevation Model (DEM), land use and soil data, and hydro-meteorological data. Data analysis procedures and methods used are detailed extensively in the work presented in Chapter 3. A flow chart depicting procedures used in this study is shown in Figure 4.2.

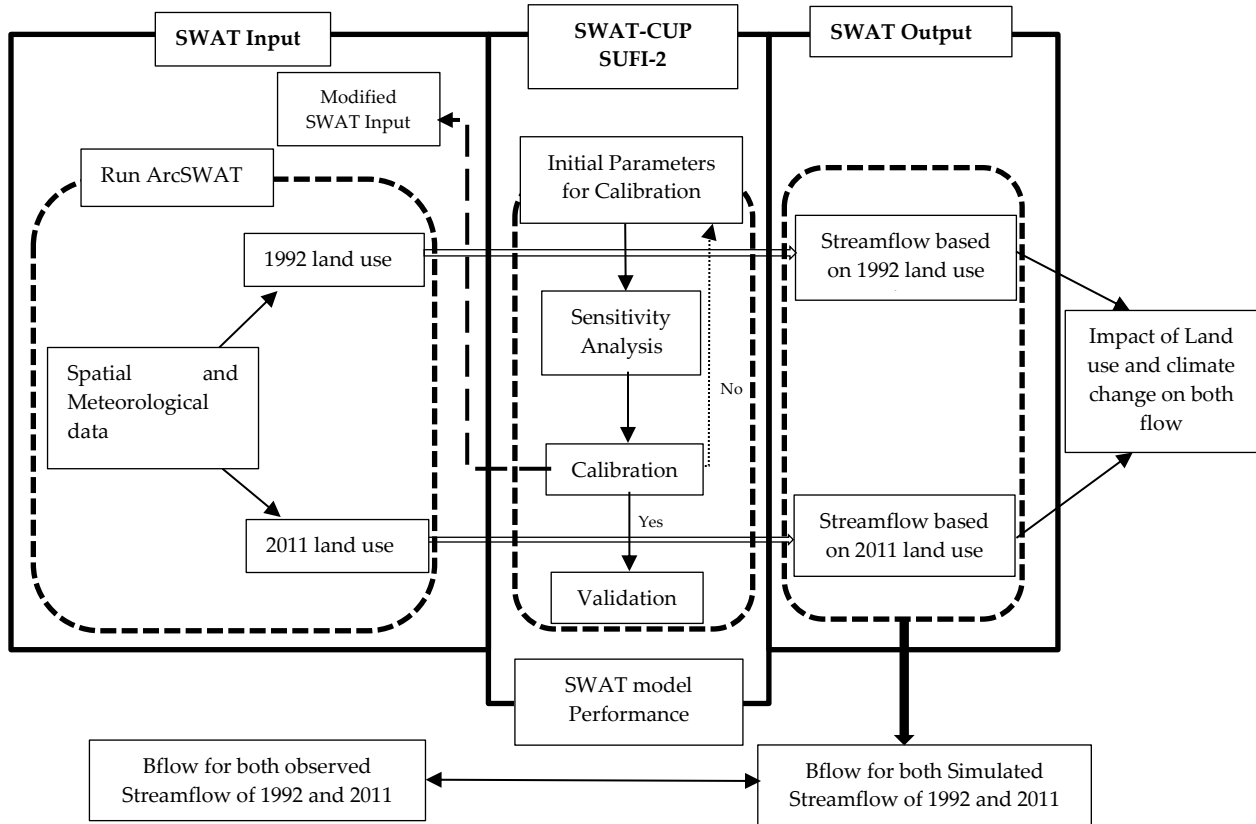


Figure 4.2. Flow chart showing the methodology used in this study

4.3.1 Data Development

4.3.1.1 Spatial Data

Two raster land use maps for the years 1992 and 2011 were obtained from the National Map Viewer (NMV). Digital Elevation Model (DEM) data were acquired from the Geospatial Data Gateway (GDG) with a resolution of 10 m. Soil Survey Geographic Data (SSURGO) data were used in this research with a resolution ranging from 1:12,000 to 1:63,630. Land use, soil type, and

slope were then used to divide the delineated sub-basins into a small series of uniform HRUs that represent the smallest representative units within the watershed (Mehan et al., 2017).

4.3.1.2 Hydro-Meteorological Data

The required datasets used include daily observed streamflow data at gauged USGS stations for the period 1980 to 2017. The streamflow data were used to separate baseflow from surface runoff, and for the SWAT model calibration and validation. In addition, long-term daily meteorological datasets for the same period (1980–2017) were collected from the National Climatic Data Center (NCDC). The meteorological weather stations were 12 km and 0.8 km away from the borders of the UWBDR and Walzem Creek watersheds, respectively.

4.3.2 Methodology

4.3.2.1 Baseflow Separation

Baseflow measurements were separated from daily streamflow data acquired from USGS gauged stations using the automatic baseflow digital filter method (BFlow). The BFlow filter separates streamflow data into baseflow and surface runoff by passing the observed streamflow through the filtering equation three times (Jung et al., 2016; Lee et al., 2018):

$$BF_t = \alpha \times BF_{t-1} + \frac{1 - \alpha}{2} \times (Q_t + Q_{t-1}) \quad (4.1)$$

where BF is the baseflow, α is the filter parameter (0.925), Q is the total streamflow, and t is the time step. Equation (1) is applied only when $BF \leq Q_t$ (Eckhardt, 2008). BFlow is a conservative filter that enables the user to filter streamflow data to calculate the baseflow, and also to generate a tabular dataset or graphical hydrograph interface from USGS gaging stations. Herein, BFlow filtered streamflow data three times (Equation 4.1), and it is commonly observed that the 1-pass baseflow is consistent with manually estimated baseflow and thus was subsequently used in this study (Eckhardt, 2008).

4.3.2.2 Soil and Water Assessment Tool (SWAT) Model Calibration and Validation

The monotonic trends in the historical meteorological data were evaluated using the modified Mann–Kendall (MK) test developed by Hamed and Rao (1998). Based on the abrupt change in the trends in precipitation and temperature using the MK test, the study period from 1980 to 2017 was split into two time spans, 1980–1998 and 1999–2017, with a breakpoint in 1998. The period 1980–1998 was assigned as a baseline for model calibration and validation. The model simulation time was segmented into a warm up period (1980–1983), calibration period (1984–1993), and validation period (1994–1998). The SWAT model calibration and validation were performed using the land use map of 1992 and streamflow data from 1980 to 1998 for each of the selected watersheds. Model optimization, sensitivity analysis, calibration, validation, and uncertainty analysis of parameters were carried out using the Sequential Uncertainty Fitting program algorithm (SUFI-2) approach within the SWAT-CUP interface (Abbaspour et al., 2015). Based on methodology reported in Chapter 3, the twenty hydrologic parameters listed in Table 4.1 were used in this study for the UWBDR and Walzem Creek watersheds calibration of streamflow and baseflow. However, sensitivity analysis using the SUFI-2 global sensitivity analysis was carried out in the first stage due to the presence of many parameters within the SWAT model [44]. Only parameters sensitive for the watersheds were then used in the calibration process and optimized based on monthly values (Welde & Gebremariam, 2017). Both automatic and manual calibration were carried out to allow qualitative and quantitative comparisons of the values, to fine tune the values of the auto-calibrated parameters, and to decrease the differences between the observed and simulated outputs (Ghazal et al., 2019).

Table 4.1. SWAT input parameters used for the UWBDR and Walzem Creek watersheds calibration of streamflow and baseflow (Aboelnour et al., 2020).

Parameter	¹ Ext.	Description	Adjustment	¹ IV	¹ LB	¹ UB
Parameters Controlling Water Balance						
ESCO	hru	Soil evaporation compensation factor	R	0.95	0.01	1
EPCO	hru	Plant uptake compensation factor	R	1	0.01	1
CANMX	hru	Max canopy storage	R	0	0	25
SFTMP	bsn	Snowfall temp	R	1	-5	5
SMTMP	bsn	Snowmelt base temp	R	0.5	-5	5
TIMP	bsn	Snow back temp lag factor	R	1	0.01	1
SMFMX	bsn	Melt factor for snow on 21 June	R	4.5	0.01	10
SMFMN	bsn	Melt factor for snow on 21 December	R	4.5	0.01	10
Parameters Controlling Surface Water Response						
CN2	mgt	Initial SCS Curve number	V	—	-0.25	0.25
SURLAG	bsn	Surface runoff lag coefficient	R	4	0.1	10
Parameters Controlling Sub-Surface Water Response						
ALPHA_BF	gw	Baseflow alpha factor	R	0.048	0.01	1
GWQMN	gw	Depth of water for return flow	R	1000	0.01	5000
GW_DELAY	gw	Groundwater delay time	R	31	0.1	50
REVAPMN	gw	Depth of water for evaporation	R	750	0.01	250
GW_REVAP	gw	Groundwater evaporation coefficient	R	0.02	0.02	0.2
RCHRG_DP	gw	Deep aquifer percolation fraction	R	0.05	0.01	1
Parameters Controlling Soil's Physical Properties						
SOL_AWC	sol	Available water capacity of the soil water	V	--	-0.25	0.25
SOL_K	sol	Saturated hydraulic conductivity	V	--	-0.15	0.15
Parameters Controlling Channel's Physical Properties						
CH_K2	rte	Effective hydraulic conductivity	R	0	5	300
CH_N2	rte	Main channel Manning's "n"	R	0.014	0.01	0.15

¹ **Ext**, Extension; **R**, Replace by value; **V**, Multiply by value; **IV**, Initial values; **LB**, Lower bound; **UB**, Upper bound

4.3.2.3 *Model Sensitivity Analysis*

The global sensitivity analysis procedures showed that the sensitive parameters obtained from the LEC in Chapter 3 were critical in the case of the UWBDP watershed, but with a different rank order. It was also found that these rankings were impacted by the selected objective function in the model. For example, curve number (CN2), soil evaporation compensation factor (ESCO), snowfall temperature (SFTMP), melt factor for snow (SMFMN), baseflow recession constant (ALPHA_BF), and deep aquifer percolation fraction (RCHRG_DP) were the most critical parameters in UWBDP when the Kling–Gupta Efficiency (KGE) was selected to be the objective function incorporated into the model (Table 4.2). These parameters characterize surface runoff, soil properties, and groundwater.

In the case of Walzem Creek, the parameters in Table 4.2 were consistent with other SWAT parameter sensitivity analyses completed for semi-arid regions. The SWAT model is highly sensitive to surface runoff and basin parameters when the watershed is characterized by inconsistent rainfall events (Veith et al., 2010; Yuan et al., 2015). ALPHA_BF followed by CN2 were the most sensitive parameters in Walzem Creek. In contrast to the other watersheds, snowfall and snow melt parameters were not sensitive in Walzem Creek since there was no persistent snowpack. The high ALPHA_BF constant in Walzem Creek indicated a rapid response to groundwater recharge. However, the lower baseflow recession constant in the UWBDP indicated large storage discharge and slow drainage in the shallow aquifer, which might be attributed to the complex geological structure of the watershed such as the presence of folds and faults (Zhang et al., 2016). The high deep aquifer percolation parameter (RCHRG_DP) in Walzem Creek indicated the increase of water movement to the deep aquifer. SOL_AWC represented the soil moisture content and hence played a role in surface runoff and was considered to be directly proportional to the soil's ability to hold water, affecting streamflow.

Table 4.2. Top 10 optimized SWAT sensitive parameter values in the UWBDR watershed and Walzem Creek watershed.

UWBDR Watershed					Walzem Creek Watershed				
Rank	Parameter	Fitted	<i>t</i> -Stat	<i>p</i> Value	Rank	Parameter	Fitted	<i>t</i> -Stat	<i>p</i> Value
1	ALPHA_BF	0.81	44.71	0	1	CN2	-0.10	-24.87	0.00
2	CN2	0.02	18.47	0	2	ESCO	0.99	5.78	0.00
3	CH_K2	28.39	-13.34	0	3	SFTMP	0.31	-3.12	0.00
4	CH_N2	0.08	-4.72	0	4	SMFMN	0.86	-2.79	0.01
5	SOL_AWC	-0.17	-4.13	0	5	ALPHA_BF	0.23	-2.51	0.01
6	RCHRG_DP	0.01	-3.16	0	6	RCHRG_DP	0.01	2.47	0.01
7	EPCO	0.16	-2.99	0	7	SOL_AWC	0.03	-2.07	0.04
8	SMTMP	-1.51	2.48	0.01	8	GW_DELAY	32.14	-0.78	0.44
9	SFTMP	4.90	-2.24	0.03	9	SURLAG	0.92	0.75	0.45
10	CANMX	23.27	1.95	0.05	10	CANMX	0.31	-0.74	0.46

4.3.2.4 Statistical Criteria and Model Evaluation Performance

The performance of the SWAT model can be computed using statistical indices and graphical comparisons (Moriasi et al., 2007). For the simulated streamflow and baseflow, the coefficient of determination (R^2), Nash–Sutcliffe model efficiency (ENS), PBIAS, and modified KGE were adopted to evaluate the model performance (Gupta et al., 2009; Nie et al., 2011). The monthly statistical streamflow and baseflow values for the calibrated models were adopted to evaluate the model performance. The performance of the SWAT model is considered good on a monthly basis when $R^2 > 0.75$; *ENS* and *KGE* > 0.7 ; and *PBIAS* ≤ 15 according to Moriasi et al. (2013) and Thirel et al. (2015).

4.3.2.5 Scenarios Separating the Impact of Land Use Change and Climate Change

In this research, the “change-fix” approach used in Chapter 3 was applied to evaluate the streamflow and baseflow as a response to separate and combined impacts of urbanization and

climate alteration. Land use maps of 1992 and 2011 were used to represent the two time periods. The land use map of 1992 was adopted to represent the patterns in the first period (1980–1998), herein called TS1. On the other hand, the 2011 land use map was used to represent the second time span (1999–2017), herein called TS2.

A combination of four simulations were developed to evaluate the natural and human impacts on hydrology: (1) 1992 land use and TS1 climate data of 1980–1998 (X1); (2) 2011 land use and TS1 climate data of 1980–1998 (X2); (3) 1992 land use and TS2 climate data of 1999–2017 (X3); and (4) 2011 land use and TS2 climate data of 1999–2017 (X4). The well-calibrated SWAT model, using the land use data of 1992 and first climate period, was used to run the other four scenarios (X1–X4). The simulated output values obtained from these scenarios were compared to the corresponding baseline model. X1 represents the baseline scenario with the corresponding circumstances, while the difference between X4 and X1 simulation describes the combined effects of land use change and climate variation. The comparison between X1 and X2 attempts to depict the separate impact of land use change. Finally, the differences between X3 and X1 outputs emphasize the individual impact of climate alteration.

4.4 Results and Discussions

4.4.1 Trends in Hydrologic Components

Statistical analyses were performed on climatological variables using the modified non-parametric Mann–Kendall (MK) test, to evaluate possible transition points, trends, and their significance in the time series from 1980 to 2017. The modified MK test statistic, τ , is standardized and can be used in comparing variables that experience differences in their magnitude (Sen, 1968). A positive slope magnitude indicates an upward trend and vice versa (Hirsch et al., 1982). As shown in Table 4.3, the slope and the τ -statistics for annual streamflow and baseflow were all positive, except for the baseflow trend in Walzem Creek, which showed a significant decrease in monotonic trend. However, the null hypothesis was accepted in the case of annual streamflow, as it showed an insignificant increasing trend (Figure 4.3). Results also showed that the annual baseflow increased at a significance level greater than 0.1 for the UWBDR watershed, which indicates a slightly increasing trend. However, a significant increasing trend in streamflow during 1980–2017 was detected for the UWBDR watershed (Figure 4.3).

Table 4.3. Temporal trends in annual streamflow and baseflow in the study areas.

		Streamflow	Baseflow
UWBDR watershed	τ -Stat	2.238	1.848
	Slope	3.195	1.301
	α	0.001	>0.1
Walzem Creek	τ -Stat	0.277	-1.961
	Slope	2.043	-3.335
	α	>0.1	0.001

The increase in average precipitation played an important role in the increasing trend of streamflow for the UWBDR watershed, while the slight increase in streamflow at Walzem Creek was accompanied by decreased precipitation and an increase in temperature as well. Moreover, human activity, such as construction of urban areas on agricultural areas, played a vital role in the amount of streamflow and baseflow. A combination of temperature increase and either a reduction or increase in rainfall are likely the main reasons for climate variation affecting the global water balance. In other words, the magnitude and the directions of these changes will affect any particular change in streamflow and baseflow (Price et al., 2011).

The relationship between baseflow and human impacts and climate change varied. The reduction of annual baseflow in the Walzem Creek watershed may be attributed to the reduction of cultivated area and implementation of imperviousness, which in turn has a negative impact on the infiltration rate by increasing the surface runoff, specifically during the wet season of the year (Ghazal et al., 2019). On the other hand, the increasing trend in the annual baseflow in the UWBDR was similar to the trend of the Little Eagle Creek (LEC) watershed mentioned in Chapter 3. This increase is likely caused by several factors, including the influx of water from outside the watershed during the process of urban development and infrastructure and leakage from water supply pipes. Lerner (2002) reported that urbanized catchments are usually associated with leakage rates of 20–50% in sewer systems and septic tanks, causing large amounts of groundwater discharge. Wastewater from the West Chicago Moraine may also provide a significant amount of water, which likely originates outside the catchment. In addition, detention basins play essential roles in increasing baseflow in urban catchments, as water is retained at the surface due to an increasing amount of surface runoff, and then slowly released into the stream as a form of baseflow (Aboelnour et al., 2019). Lastly, physiological features may also contribute to this observed trend, including features such as the topography, geology and soil types that result from glacial melting

with high porous media, which can play a significant role in increasing infiltration (Bhaskar et al., 2016).

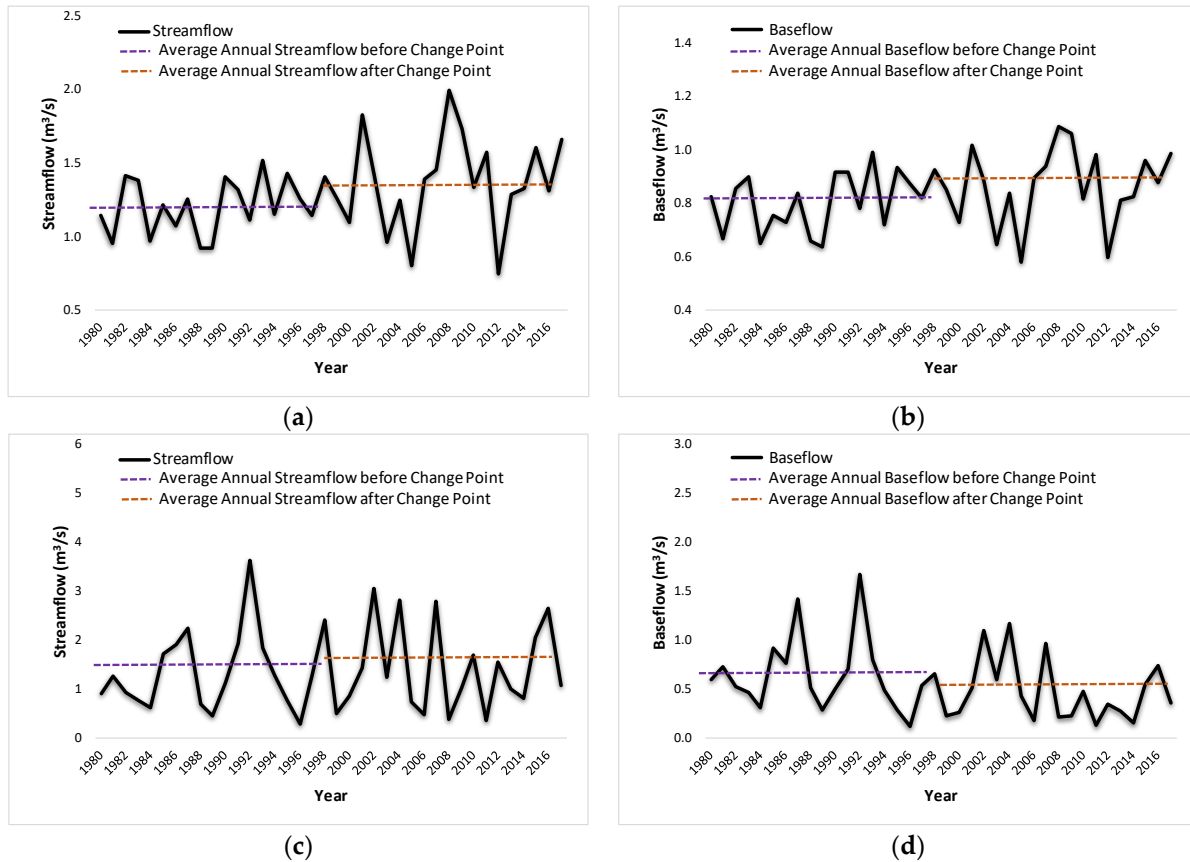


Figure 4.3. Average daily streamflow (a) and baseflow (b) in the UWBDR watershed; and average daily streamflow (c) and baseflow (d) in the Walzem Creek watershed.

4.4.2 Trends in Climatic Components

The MK test was furthermore employed to quantify the monotonic trends of precipitation and temperature in the selected watersheds. Compared to the first climate period (1980–1998), statistical results indicated that the mean air temperature increased by 0.7 °C (from 9.7 to 10.4 °C) and 0.6 °C (from 20.7 to 21.3 °C) during TS2 at the UWBDR and Walzem Creek watersheds, respectively. Average annual precipitation increased by 9.1% (82 mm, from 890 to 972 mm) during TS2 in the UWBDR, while decreasing by 6.5% (56 mm, from 858 to 802 mm) in Walzem Creek (Figure 4.4).

In the case of UWBDR, the trend of τ -test statistics and the slope of precipitation and temperature were positive and are provided in Table 4.4. The results show a difference in the

monotonic trends of annual temperature and precipitation. For the time series from 1980 to 2017, the annual air temperature increased at a significance level greater than 0.001, which indicates that the long-term trend of temperature was statistically significant. The annual precipitation increased only at a significance level greater than 0.1, indicating a minor increase of precipitation over time and that the trend is statistically insignificant at the 95% confidence level. On the other hand, the average annual precipitation after the change point in Walzem Creek exhibited a slight decrease from the average before the change point. However, the temperature at Walzem Creek showed an increasing trend at the 0.001 significance level, which indicates that the climate at Walzem Creek became warmer and drier during the study period. While the average annual precipitation and temperatures shifted over time, these trends may not reflect the true picture as the change displayed in both may have been seasonally influenced (Sekaluvu et al., 2018). Therefore, the MK test was further performed at a monthly scale for time series data from 1980 to 2017 (Table 4.5). The results show that the monotonic trends of the monthly meteorological data for the study were different. For the UWBDR watershed, the results indicate that the monthly temperature showed increasing trends in slope in every month of the year. The monotonic increasing trends of monthly temperature were only statistically significant at a confidence level of $p = 0.05$ in June, September, and October. Monthly precipitation trend for November decreased significantly, while it showed an insignificant reduction in August, September, and December. The remaining months showed an insignificant increase in monthly precipitation, with the highest increment recorded in June (1.36 mm/month). On the other hand, monthly precipitation in Walzem Creek Watershed showed decreasing trends in February, May, June, October, November, and December, while increasing trends in the other months with the highest increment recorded in September (1.52 mm/month) and maximum reduction recorded in June (1.68 mm/month). Change in monthly precipitation in the Walzem Creek Watershed was insignificant. Similar to the UWBDR watershed, increases in monthly temperature trends were recorded in every month, with only February showing a significant increase in the monotonic trend at a confidence level of $p = 0.05$.

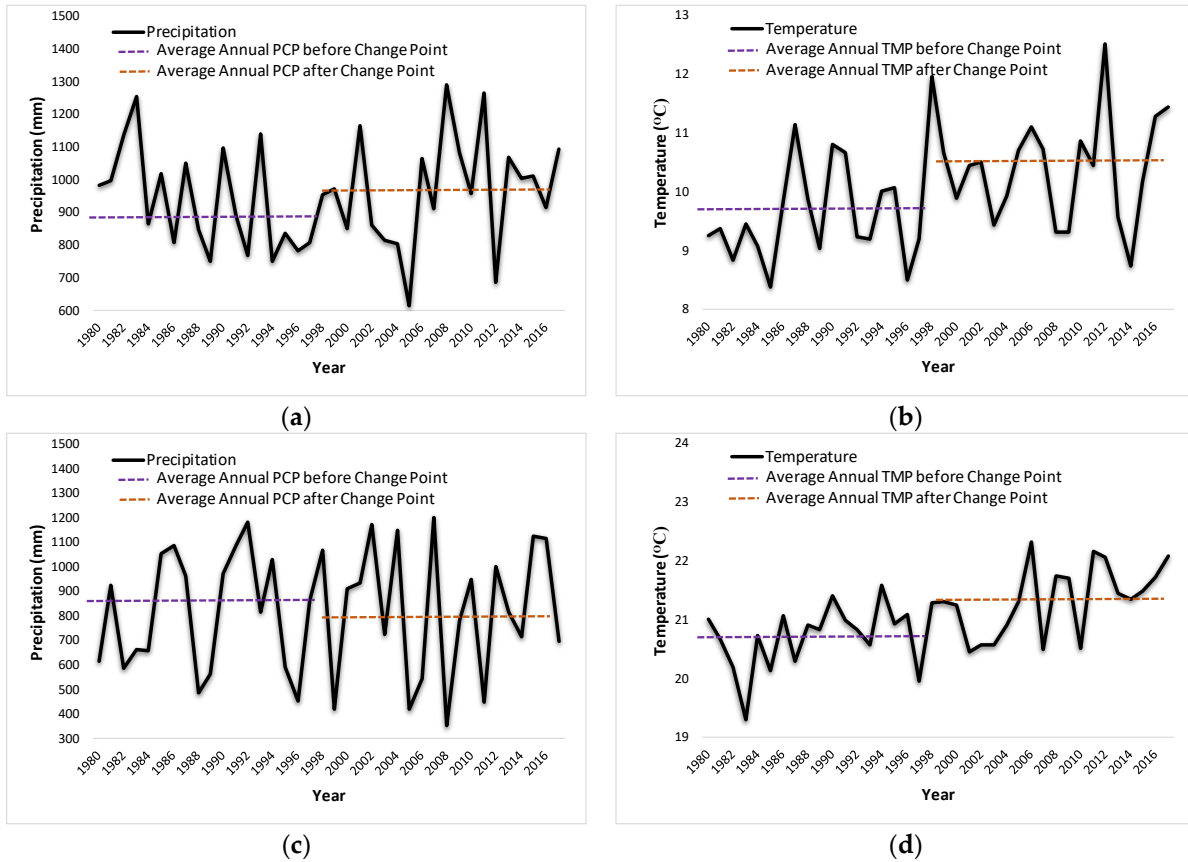


Figure 4.4. Annual precipitation (a) and temperature (b) in the UWBDR watershed; and annual precipitation (c) and temperature (d) in the Walzem Creek watershed.

Table 4.4. Temporal trends in annual streamflow and baseflow in the study areas.

		Precipitation	Temperature
UWBDR	τ -Stat	0.503	2.709
	Slope	0.821	0.037
	α	>0.1	0.001
Walzem	τ -Stat	0.327	3.640
	Slope	1.179	0.036
	α	>0.1	0.001

Table 4.5. Summary of significance test and trend analysis for monthly precipitation and temperature in the UWBDR and Walzem Creek watersheds.

		UWBDR				Walzem Creek			
		τ -Stat	Slope	¹ Sig	<i>p</i> -Value	τ -Stat	Slope	¹ Sig	<i>p</i> -Value
January	PRCP	1.245	0.551	NS	0.106	0.704	0.564	NS	0.240
	TEMP	0.805	0.045	NS	0.210	1.722	0.051	NS	0.042
February	PRCP	0.905	0.409	NS	0.183	-0.905	-0.142	NS	0.183
	TEMP	0.339	0.005	NS	0.367	2.351	0.071	S	0.009
March	PRCP	0.126	0.035	NS	0.450	0.855	0.248	NS	0.196
	TEMP	0.729	0.043	NS	0.233	1.685	0.048	NS	0.046
April	PRCP	0.805	0.425	NS	0.211	0.629	0.992	NS	0.265
	TEMP	1.383	0.036	NS	0.083	1.722	0.038	NS	0.043
May	PRCP	1.584	0.988	NS	0.057	-0.704	-0.268	NS	0.241
	TEMP	0.981	0.024	NS	0.163	0.893	0.017	NS	0.186
June	PRCP	1.534	1.364	NS	0.061	-1.282	-1.678	NS	0.100
	TEMP	2.012	0.051	S	0.022	1.798	0.03	NS	0.036
July	PRCP	-0.427	0.581	NS	0.335	0.729	0.741	NS	0.233
	TEMP	0.465	0.014	NS	0.321	1.031	0.013	NS	0.151
August	PRCP	-0.805	-1.349	NS	0.210	-0.641	0.493	NS	0.261
	TEMP	1.358	0.021	NS	0.087	1.585	0.025	NS	0.056
September	PRCP	-0.855	-0.442	NS	0.196	1.383	1.52	NS	0.083
	TEMP	2.364	0.054	S	0.009	1.245	0.019	NS	0.107
October	PRCP	0.151	0.25	NS	0.440	-0.930	-0.547	NS	0.176
	TEMP	2.087	0.058	S	0.018	1.207	0.031	NS	0.114
November	PRCP	-2.024	-1.669	S	0.021	-1.471	-0.504	NS	0.071
	TEMP	1.320	0.043	NS	0.093	1.886	0.042	NS	0.030
December	PRCP	-0.226	-0.324	NS	0.411	0.176	-0.238	NS	0.430
	TEMP	0.566	0.051	NS	0.286	1.119	0.04	NS	0.132

¹ Significance level (α) = 0.05. **S**, Significant; **NS**, Not significant.

4.4.3 Changes in Land Use Characteristics

Cross tabulation analysis and post classification comparison were applied to evaluate the quantity of temporal conversions and nature of changes from one land cover category to another in land use maps of 1992 and 2011 (Aboelnour & Engel, 2018a; Gitau & Bailey, 2012). In the UWBDR, a comparison of land use maps for the years 1992 and 2011 indicated that the most significant changes occurred in three classes: developed urban, planted, and forest (Figure 4.5). In 1992, the main land use types were planted and developed areas, which occupied 76.1% of the total watershed area. However, owing to urban expansion, the proportional extent of developed areas increased from 44% to 77% from 1992 to 2011. Conversely, the proportional extent of planted and forest decreased from 35.8% to 2.7% and from 8.1% to 4.4%, respectively. The transition matrix of UWBDR land use in Table 4.6 explains these changes in detail. Overall, 43.6% or 39.9 km² of the developed area in 1992 remained unchanged, whereas 27.7 km² (30.2%) and 5.38 km² (5.9%) of the planted and forest areas, respectively, were primarily converted to developed urban areas from 1992 to 2011. In hydrological modeling, uncertainties in land use data are determined by the sensitivity of the model output to different land use data inputs. Some uncertainties might be associated with different classification algorithms used in both the 1992 and 2011 NLCD land use data. Therefore, the presence of low percentages of land use changes between 1992 and 2011 is omitted. Uncertainties and accuracies in NLCD data are also dependent on the interpretation of the person(s) collecting the information and therefore may be assessed differently depending on how it was analyzed. Some uncertainties, therefore, might be applicable to the intended application, while others may have no effects (Castilla & Hay, 2007).

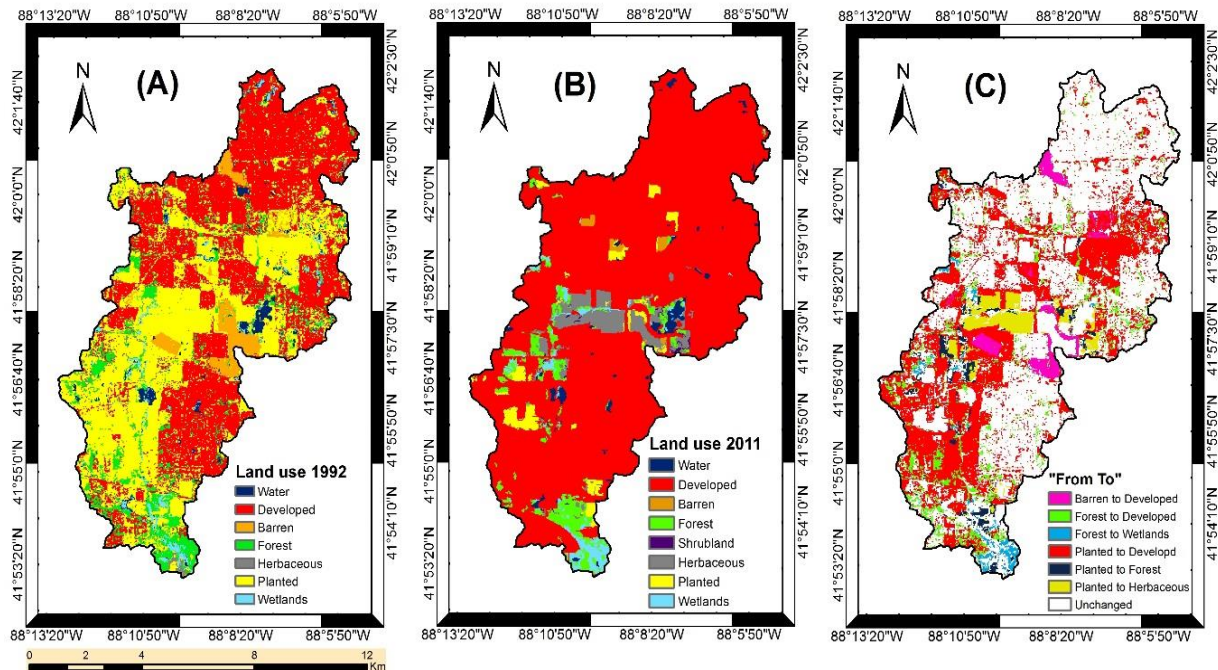


Figure 4.5. Land use types in the UWBDR watershed in: (A) 1992; (B) 2011; and (C) the transition between 1992 and 2011.

Table 4.6. Transition matrix (in percentages) of land use change in UWBDR from 1992 to 2011.

1992	2011								
	Water	Developed	Barren	Forest	Shrubland	Herbs	Planted	Wetlands	Total
Water	0.77	0.82	0.01	0.08	0.00	0.07	0.14	0.11	2.00
Developed	0.04	43.56	0.00	0.22	0.00	0.08	0.14	0.01	44.06
Barren	0.01	2.59	0.07	0.03	0.01	0.65	0.21	0.02	3.59
Forest	0.07	5.87	0.00	1.52	0.01	0.11	0.16	1.09	8.82
Herbs	0.01	0.39	0.00	0.16	0.00	0.02	0.00	0.10	0.69
Planted	0.20	30.25	0.47	2.03	0.23	3.52	1.96	0.35	39.01
Wetlands	0.24	0.76	0.01	0.36	0.01	0.07	0.03	0.36	1.84
Total	1.34	84.24	0.56	4.40	0.26	4.52	2.65	2.04	

The Walzem Creek watershed also underwent some land use changes over the past few decades (Figure 4.6). During the 20-year period, developed and planted areas were the two largest land use types, and they accounted for approximately 64% and 17% of the total area, respectively. The planted areas shrunk from 1992 to 2011 by 18.3 km². Developed and wetland areas had the greatest increase from 64% to 92% and from approximately 0% to 7.8%, respectively. These increases were due to a large scale, continuous decrease in planted areas (17.5% to 0.8% of the watershed area) and a gradual decrease in forests (9.5% to 2.5%). The increase in wetland areas mostly occurred after 2006 (from 0.06 to 7.82 km²) due to the ecological restoration program for watershed protection that enhanced the urban reaches, bringing the basin back into compliance with water resources and water quality recreation standards. On the other hand, developed areas increased to the detriment of planted and cultivated areas due to the rapid urban development and expansion in the city of San Antonio (Table 4.7).

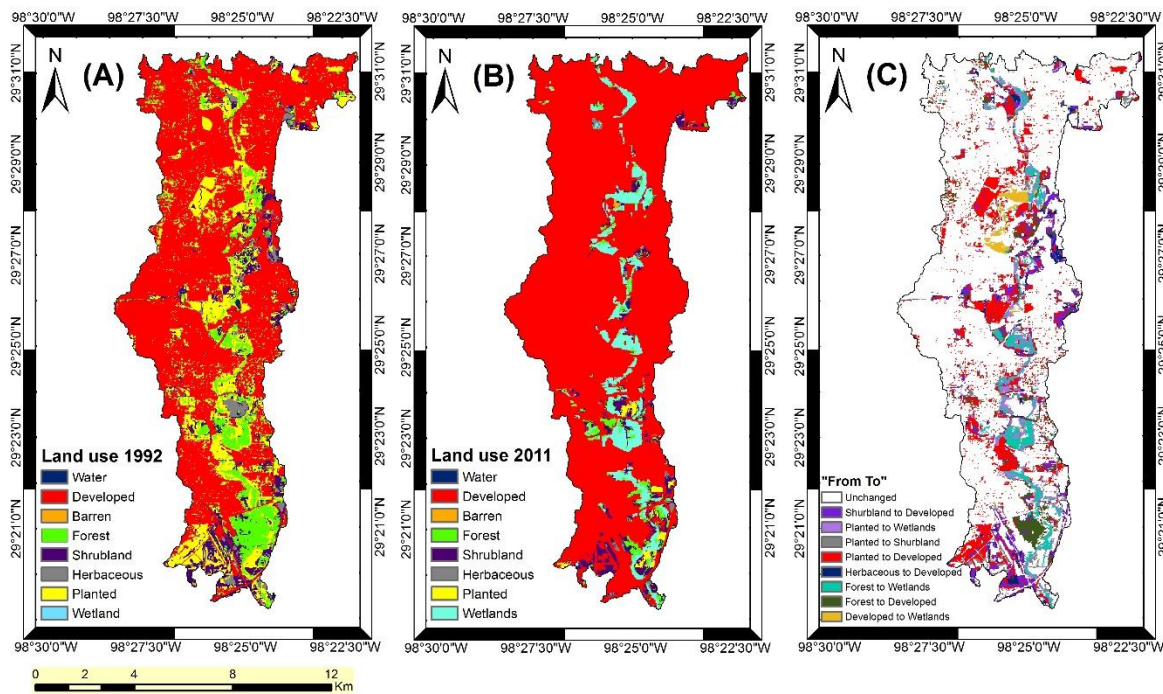


Figure 4.6. Land use types in the Walzem Creek watershed in: (A) 1992; (B) 2011; and (C) the transition between 1992 and 2011.

Table 4.7. Transition matrix (in percentages) of land use change in the Walzem Creek watershed from 1992 to 2011.

1992	2011								
	Water	Developed	Barren	Forest	Shrubland	Herbs	Planted	Wetlands	Total
Water	0.09	0.09	0.00	0.00	0.00	0.00	0.00	0.00	0.18
Developed	0.00	62.63	0.05	0.26	0.38	0.05	0.09	0.95	64.40
Barren	0.00	0.09	0.00	0.00	0.00	0.00	0.00	0.00	0.09
Forest	0.00	3.42	0.00	1.15	0.61	0.05	0.11	3.32	8.66
Herbs	0.00	1.32	0.00	0.05	0.43	0.12	0.21	0.00	2.13
Shrubland	0.00	4.79	0.00	0.23	1.47	0.09	0.12	0.26	6.95
Planted	0.00	12.15	0.00	0.87	1.26	0.29	0.29	2.64	17.50
Wetlands	0.00	0.09	0.00	0.00	0.00	0.00	0.00	0.00	0.09
Total	0.09	84.57	0.05	2.55	4.16	0.59	0.82	7.17	

4.4.4 SWAT Model Calibration and Validation Results

At the UWBDR, the total observed and simulated streamflow during the calibration period were 7.52 and 7.60 m³/s, respectively. The resulting hydrograph from SWAT streamflow in the UWBDR also showed agreement in trends between the two (Figure 4.7). The best calibration achieved was an R² of 0.69, PBIAS of 4.86, ENS of 0.67, and KGE of 0.82. Note that KGE was used as an objective function type in the SUFI-2 calibration and validation because it could be decomposed into three terms that represented the correlation, bias, and relative variability between the measured and simulated values (Lazzari Franco & Bonumá, 2017). Hence, it allowed the simultaneous use of baseflow and streamflow in calibration and enabled comparison between different strategies. The summed observed and simulated streamflow during the validation period were 9.03 and 8.27 m³/s, respectively. Streamflow validation showed a higher performance than the calibration with an R² of 0.84, PBIAS of 23.1, ENS of 0.68, and KGE of 0.67 (Table 4.8).

On the other hand, the total annual baseflow during the calibration and validation periods for both measured and simulated data were 8.02 and 7.82 m³/s, respectively. Goodness-of-fit measures were evaluated to test the performance of baseflow predictions. The R² for the calibration

period was 0.67, with a PBIAS of -1.08 , ENS of 0.60, and KGE of 0.80 (Table 4.8). Figure 4.8 shows the results of model calibration and validation of baseflow at the UWBDR. Overall, there was reasonably good agreement between computed and simulated baseflow. Further, the model performance was validated using data for the subsequent time period. It was observed that the computed baseflow from the USGS streamflow values were reasonably close to the simulated ones. The evaluation indices R^2 , PBIAS, ENS, and KGE were 0.79, 8.43, 0.58, and 0.79 for the baseflow of the validation period, respectively.

In general, the results suggested that the SWAT model performed satisfactorily in the UWBDR watershed according to the criteria set by Moriasi et al. (2007). However, the model underestimated the simulated streamflow for the validation period at a monthly time step during low streamflow, which indicates that there may be uncertainty in the results of SWAT simulations for urban watersheds. The lower performance of the SWAT model in the UWBDR may be attributed to the fact that the climate data obtained from the main weather station were located outside the basin, and the distribution of the climate stations with a complete record was sparse. In addition, the overestimation of some peaks in baseflow could be related to the existence of the West Chicago Moraine outwash plain, creating circumstances that promote fast groundwater movement from the moraine through the outwash. Ratios of baseflow to the total annual streamflow were 55.3% and 60.8% for both measured and simulated streamflow, respectively. This discrepancy is acceptable because all of the separation methods of baseflow using different filters are subject to uncertainties (Zhang et al., 2016).

Table 4.8. Statistical indicators for calibration and validation periods for streamflow and baseflow in the UWBDR watershed and Walzem Creek watershed.

Period			Streamflow (m ³ /s)				Baseflow (m ³ /s)			
			<i>R</i> ²	<i>ENS</i>	<i>PBIAS</i>	<i>KGE</i>	<i>R</i> ²	<i>ENS</i>	<i>PBIAS</i>	<i>KGE</i>
UWBDR	Calibration	(1984–1993)	0.69	0.67	4.9	0.82	0.67	0.60	-1.1	0.80
	Validation	(1994–1998)	0.84	0.68	23.1	0.67	0.79	0.58	8.4	0.79
Walzem	Calibration	(1984–1993)	0.87	0.87	-4.3	0.91	0.85	0.76	21.6	0.70
	Validation	(1994–1998)	0.83	0.70	-3.8	0.54	0.70	0.68	-5.12	0.79

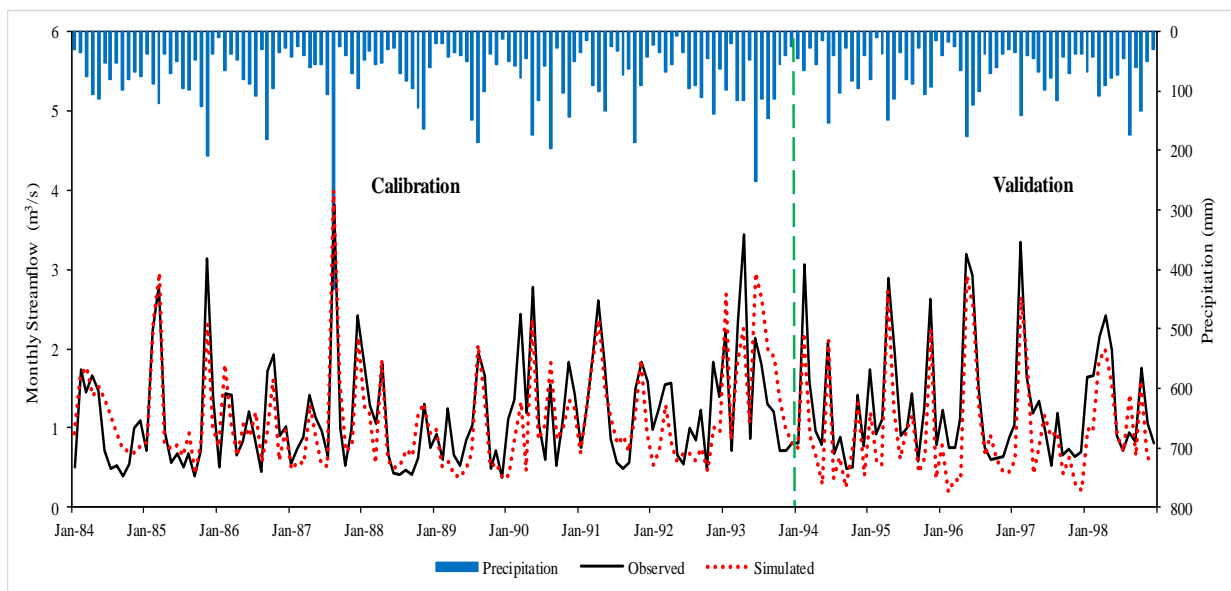


Figure 4.7. Observed and simulated time series streamflow for the UWBDR watershed during calibration and validation periods.

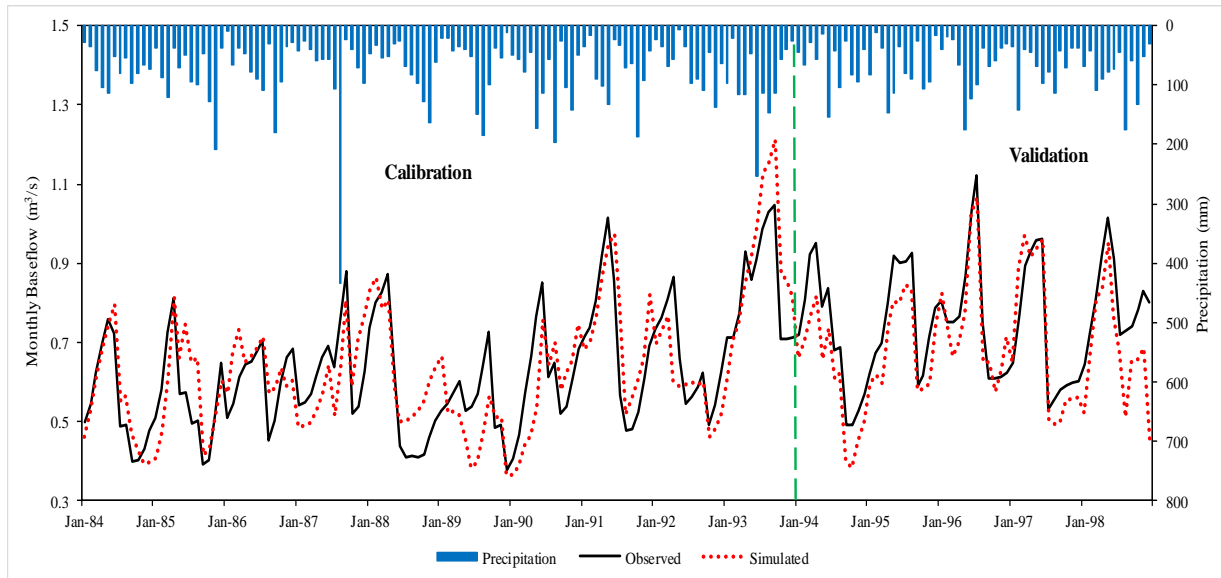


Figure 4.8. Observed and simulated time series baseflow for the UWBDP watershed during calibration and validation periods.

Unlike the UWBDP and the LEC watersheds results reported in Chapter 3, the baseflow proportion of the observed and simulated streamflow at the Walzem Creek watershed were 33.3% and 26.8%, respectively, which indicated that surface runoff was a major supply component for the stream. Figure 4.9 shows the comparison between the simulated and observed monthly streamflow for the calibration and validation periods. USGS records show that the total monthly streamflow for Walzem Creek was $18.7 \text{ m}^3/\text{s}$, while the simulated one was $19.5 \text{ m}^3/\text{s}$. However, streamflow was overestimated for most of the light rainfall events (dry climate periods) and showed very good agreement with the large rainfall events (wet periods). Previous studies have shown that SWAT performed better under more humid climatic conditions (Lazzari Franco & Bonumá, 2017; Van Liew et al., 2005). In addition, SWAT has some problems with precisely accounting for water loss through infiltration and evapotranspiration, especially during dry climate seasons, and evaluating the soil moisture storage (Feyereisen et al., 2007; Tobin & Bennett, 2009; Van Liew et al., 2007).

During the streamflow calibration period, the R^2 , ENS, PBIAS, and KGE were 0.87, 0.87, -4.31 , and 0.91, respectively, while they were 0.83, 0.70, -3.83 , and 0.54 during the validation period (Table 4.8). The SWAT performance for the monthly streamflow during both the calibration and validation periods was very good (Moriassi et al., 2007). Moreover, the high values of R^2 and ENS in the calibration and validation periods indicated that, with calibrated parameters, the SWAT

model was useful to simulate streamflow in this semi-arid region and to further quantify the hydrological impacts of climate variation and land use change over water balance components. Although the SWAT performance for the streamflow validation period was not as good as the calibration period, the results show that its performance was still good, implying that SWAT is applicable to Walzem Creek. The reason that SWAT validation performance was less than the calibration performance was most likely due to the occurrence of an extreme flooding event in October 1998, in which a strong flood killed at least 25 people and caused hundreds of millions of dollars in damages across counties in the southern and eastern regions of San Antonio. The SWAT model poorly matched the peak flow of this large event.

The results also indicate that the simulated values of baseflow were slightly lower than those of the computed ones from observed USGS records. The computed monthly baseflow from USGS records and the simulated one were 6.23 and 5.22 m³/s, respectively, during the whole calibration and validation periods. Figure 4.10 shows the comparison between the simulated and the computed monthly baseflow values at the Walzem Creek watershed in the calibration and validation periods. In the calibration period, the baseflow of the computed and simulated results had a similar trend. Meanwhile, the values of R², ENS, PBIAS, and KGE were 0.85, 0.76, 21.65, and 0.70, respectively, with a P-factor of 0.70 and R-factor of 0.62. In the validation period, these measures were 0.70, 0.68, -5.12, and 0.79, respectively. The statistical measure results indicate a “very good” to “good” match between the simulated baseflow in the calibration and validation periods and the computed records (Moriassi et al., 2007). However, SWAT overestimated the computed baseflow during the validation period, which was exemplified in the negative values of PBIAS. The statistical indicator and the similar trend between the computed and simulated results showed that the SWAT model was adequate in the semi-arid region of Walzem Creek, and confirmed that the optimized and calibrated model can be applied to evaluate the responses of the basin’s hydrology to land use and climate change.

However, considering the study area was in a semi-arid region and only one meteorological station within the catchment was used, it was difficult to detect whether the climatic conditions in the entire watershed were precisely captured. In addition, the design of the SWAT model may not fully capture the groundwater flow characteristics. However, the outputs are expected to be accurate and reliable since the model was calibrated and validated using observed streamflow.

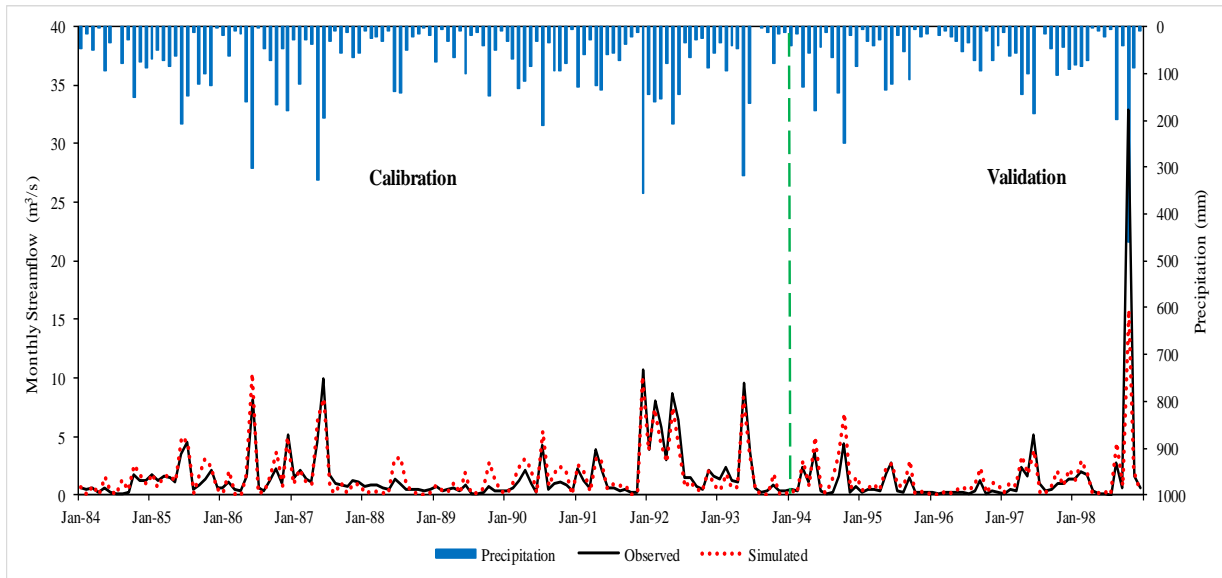


Figure 4.9. Observed and simulated time series streamflow for the Walzem Creek watershed during calibration and validation periods.

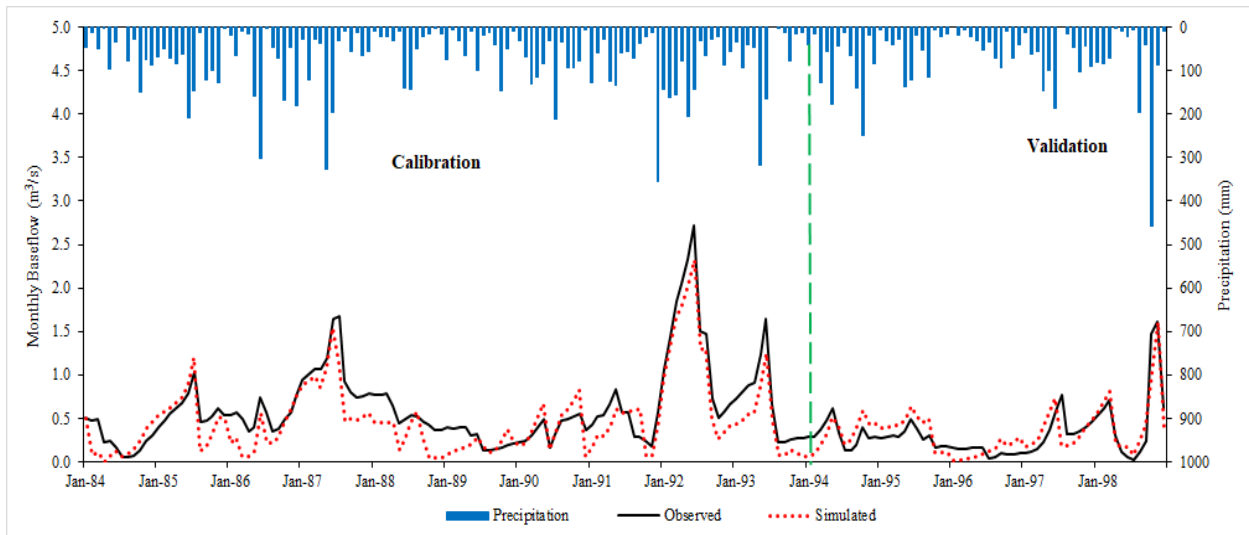


Figure 4.10. Observed and simulated time series baseflow for the Walzem Creek watershed during calibration and validation periods.

4.4.5 Impacts of Land use Change

One of the vital parameters assessed for sustainable management of water resources is water yield. Total water yield is the aggregate amount of water entering the main channel after leaving the HRUs during a time step and can be computed using the following equation (Arnold et al., 2012).

$$W_{YLD} = SUR_Q + LAT_Q + GW_Q - T_{LOSS} \quad (4.2)$$

where W_{YLD} is the total water yield (mm); SUR_Q is the surface runoff (mm); LAT_Q and GW_Q are the contributions of lateral flow and groundwater to streamflow (mm), respectively; and T_{LOSS} is the transmission loss through the bed from the tributary channels in the HRU (mm).

The SWAT simulation suggested that the conversion of the existing planted land cover to urban areas in the UWBDR watershed caused a minor increase in the annual mean water yield by 0.5% (Table 4.9). The variation could be explained by the reduction in the extent of forests and planted areas and implementation of imperviousness, leading to the reduction of evapotranspiration and infiltration, and increase in surface runoff. However, the reduction of evapotranspiration and the increase in surface runoff were considered not significant in the UWBDR watershed. This could explain the minor increase in the annual mean water yield at the area. Other than the total water yield, the SWAT simulation also suggested a considerable change in baseflow due to the effect of urbanization. Baseflow increased by 2 mm (accounting for 3.0%) when only the effect of land use dynamics between the two different periods was considered.

Figures 4.11 and 4.12 show the distribution of the monthly average water yield and baseflow simulated by SWAT, respectively, for the four scenarios for the UWBDR. Average monthly water yield was concentrated in the late fall/spring seasons and accounted for 29% in the land use change scenario (X2). The change in water yield tended to be positive under the X2 scenario except for the winter season. On the other hand, land use change had minimal effect on baseflow, with no obvious change between X1 and X2. Baseflow variation showed increasing trends in warm months from May to September, and then decreased from October to April. Such increase may be attributed to leakage from an outwash plain at the base of West Chicago Moraine and the increased precipitation during the wet season.

Table 4.9. Average annual change in water balance components in the UWBDR watershed.

Scenario	Land Use	Climate	Precipitation (mm)			Water Yield (mm)			Baseflow (mm)			Surface Runoff (mm)			Evapotranspiration (mm)		
			Av.	Ch. Δ	(%)	Av.	Ch. Δ	(%)	Av.	Ch. Δ	(%)	Av.	Ch. Δ	(%)	Av.	Ch. Δ	(%)
X1	1992	TS1	890.8	-	-	312.6	-	-	65.9	-	-	238.3	-	-	568.6	-	-
X2	2011	TS1	890.8	0	0	314.1	1.5	0.5	67.9	2.0	3.0	240.9	2.59	1.1	567.8	-0.8	-0.1
X3	1992	TS2	972.2	81.4	9.1	343.4	30.8	9.9	119.7	53.8	81.6	216.7	-21.57	-9.1	608.6	40	7.0
X4	2011	TS2	972.2	81.4	9.1	347.1	34.6	11.1	73.0	7.1	10.8	268.4	30.11	12.6	605.2	36.6	6.4

Table 4.10. Average annual change in water balance components in the Walzem Creek watershed.

Scenario	Land Use	Climate	Precipitation (mm)			Water Yield (mm)			Baseflow (mm)			Surface Runoff (mm)			Evapotranspiration (mm)		
			Av.	Ch. Δ	(%)	Av.	Ch. Δ	(%)	Av.	Ch. Δ	(%)	Av.	Ch. Δ	(%)	Av.	Ch. Δ	(%)
X1	1992	TS1	857.7	-	-	326.1	-	-	95.2	-	-	223.3	-	-	528.3	-	-
X2	2011	TS1	857.7	0	0	334.1	8.0	2.7	87.3	-7.9	-26.0	239.5	16.1	6.4	520.0	-8.3	-1.5
X3	1992	TS2	802	-55.7	-6.5	291.8	-34.3	-11.9	82.2	-13.0	-42.9	202.6	-20.8	-8.2	514.9	-13.4	-2.5
X4	2011	TS2	802	-55.7	-6.5	300.5	-25.7	-8.9	74.6	-20.7	-67.9	219.1	-4.2	-1.7	505.1	-23.2	-4.3

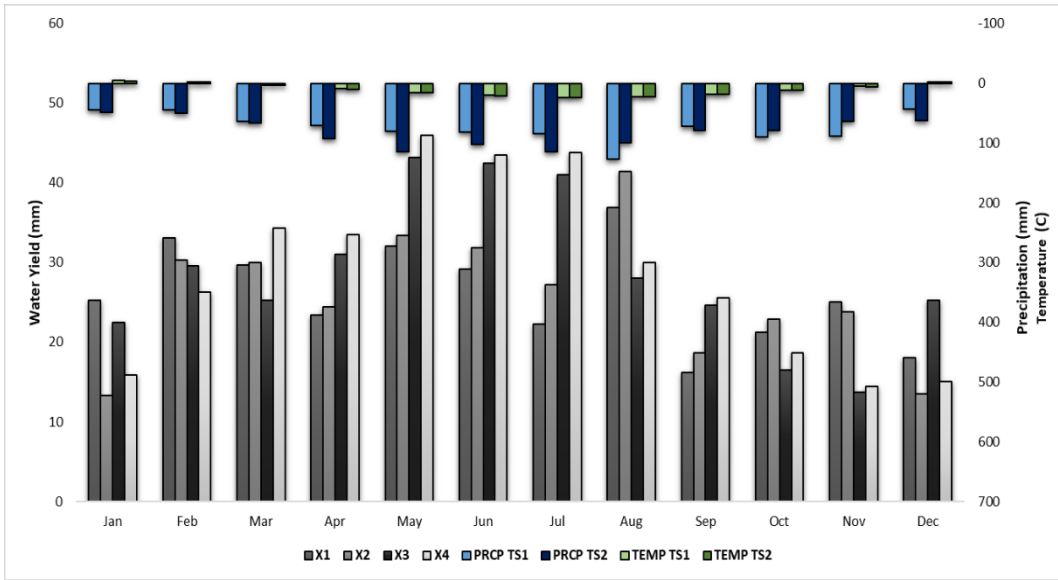


Figure 4.11. Monthly water yield change for the UWBDR watershed under different scenarios.

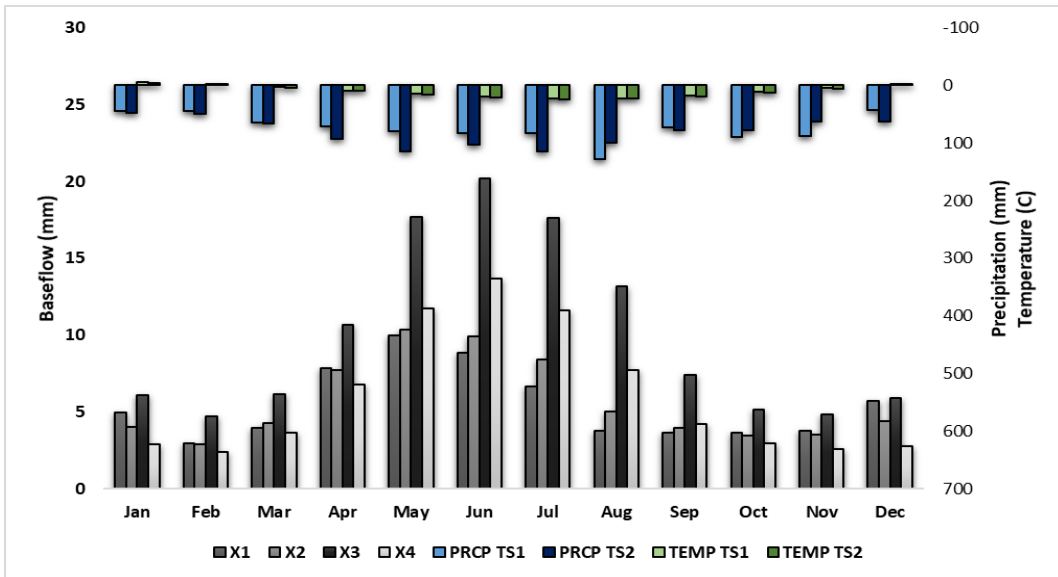


Figure 4.12. Monthly baseflow change for the UWBDR watershed under different scenarios.

The results in Table 4.10 show that the average annual water yield increased by 8.0% due to the urbanization effect in Walzem Creek (X2-X1). Meanwhile, urbanization caused the baseflow

to experience a reduction of 26.0%. Based on the proposed approach, the average annual evapotranspiration and surface runoff variability during the three scenarios were further analyzed to provide deeper insight into how climate and land use dynamics interacted with hydrologic systems in Walzem Creek watershed. In semi-arid regions, hydrologic systems could be very sensitive to climate variability. Evapotranspiration was an important component of the hydrologic process, often nearly equaling precipitation in the catchment water balance, and, under given climate conditions, it was mainly affected by vegetation cover (Zhang et al., 2017). Under the same precipitation conditions, decreased evapotranspiration brought an increase in baseflow and streamflow, while increased evapotranspiration led to the reduction in both (Schilling et al., 2008). This is illustrated in our findings shown in Table 4.10, in which evapotranspiration experienced a minor reduction of 1.5% due to the land use alteration. However, the reduction of groundwater discharge reported at the Walzem Creek Watershed was mainly due to urbanization, agriculture loss, and deforestation. Of note, the evapotranspiration rate was greater in the UWBDR Watershed than in the Walzem Creek Watershed, despite having a higher potential evapotranspiration (PET), as a result of several key differences. The PET recorded in the Walzem Creek Watershed was greater than that of the UWBDR Watershed for all scenarios. The PET ranged from 1016 to 1091 mm for the UWBDR Watershed, but was between 1800 and 2084 mm for the Walzem Creek Watershed. However, the amount of precipitation in the Walzem Creek Watershed was lower than that of the UWBDR Watershed, resulting in dryer soils that limit ET. Moreover, the areas of vegetation and forest cover in the UWBDR Watershed was greater for both 1992 and 2011 (Tables 4.6 and 4.7). In addition, the UWBDR watershed experienced a greater increase in temperature in TS2 compared to TS1 (0.7 °C). Finally, the UWBDR Watershed average daily wind speed was 4.5 and 4.3 ms⁻¹ in TS1 and TS2, respectively. In comparison, the average wind speed for the Walzem Creek watershed was 3.9 and 3.8 ms⁻¹ in TS1 and TS2, respectively.

Figure 4.13 illustrates the monthly impacts of land use change, climate, and their joint effect on Walzem Creek's water yield. Land use change had a more pronounced effect for all months in conjunction with a higher monthly average of rainfall in the first period of time (TS1). For example, the monthly average precipitation in June was 120.2 mm in TS1, and decreased to 75.0 mm in TS2. The contributions of land use impacts on monthly water yield were the highest in May, June, October, and December. Conversely, deforestation and urban expansion resulted in a reduction in

monthly baseflow in all months from with the greatest reduction recorded in the summer season from May to July with a total of 33.9% (Figure 4.14).

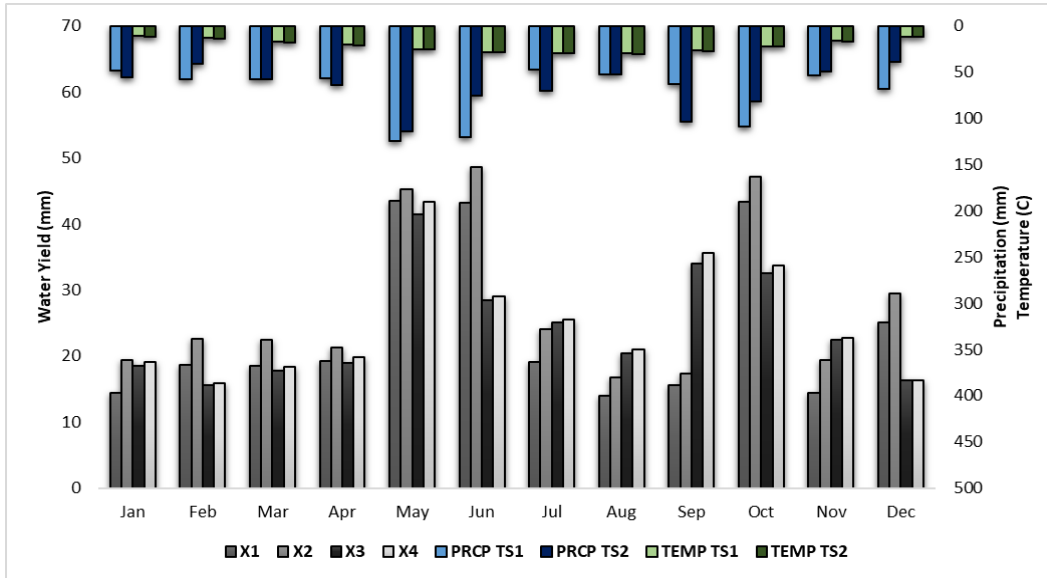


Figure 4.13. Monthly water yield change for the Walzem Creek watershed under different scenarios.

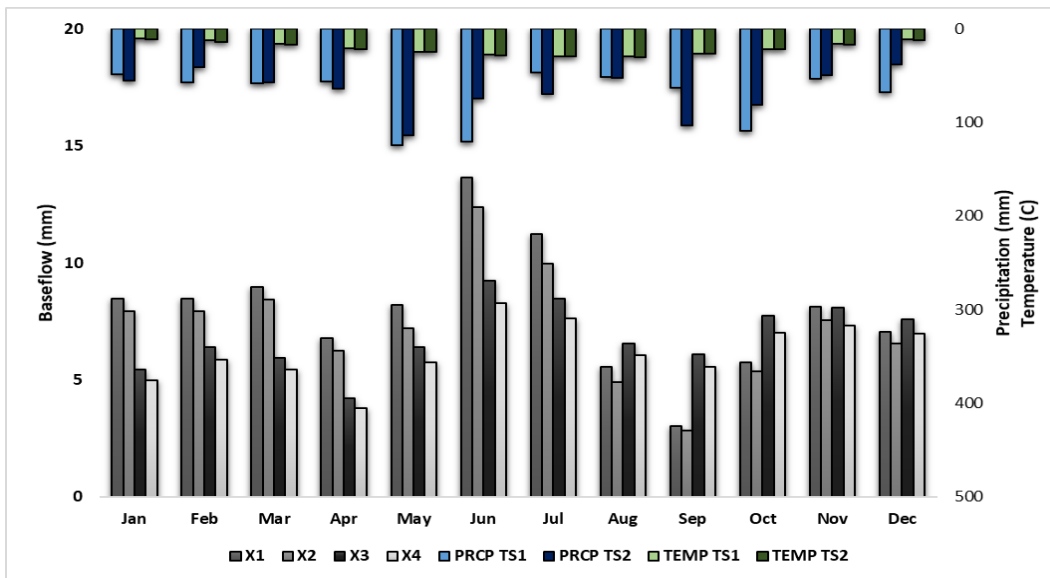


Figure 4.14. Monthly baseflow change for the Walzem Creek watershed under different scenarios.

The streamflow changes in the UWBDR watershed appeared to occur in the same manner as changes for the LEC watershed discussed in Chapter 3, with some minor differences (Figure 4.15). For instance, under X2, streamflow was reduced in the winter months by 5.4% to 35.8%. In addition, the average annual water year experienced an increase of 6.7% in the LEC watershed, while it was simulated to be only 0.5% and 8.0% in the UWBDR watershed and Walzem Creek watershed, respectively. In contrast to the LEC watershed, which showed a reduction in average annual baseflow as a result of reducing infiltration rate due to urbanization by 28.8%, the UWBDR watershed experienced an average increase in baseflow regardless of the urbanization trend. The reduction in baseflow in the LEC watershed could be caused by over-exploitation and excessive pumping of groundwater used in industry and production (Aboelnour & Engel, 2018b), while the minor increase in average annual baseflow in the UWBDR might be attributed to flooding of underground structure and the leakage of the groundwater into wastewater systems. The significant decrease in average annual baseflow at Walzem Creek might be due to clearing vegetation, deforestation, and increasing imperviousness, which in turn led to the reduction of evapotranspiration and groundwater discharge while increasing surface runoff. Urbanization is usually associated with measures that play a vital role in accelerating the removal of water from the catchment and stream system, especially during heavy rainfall events. Compacted soil, channelization, and imperviousness allow water to flow rapidly as a result of lower hydraulic resistance of channels and land surfaces of urbanized catchments, which might be an explanation for decreasing baseflow in the Walzem Creek Watershed.

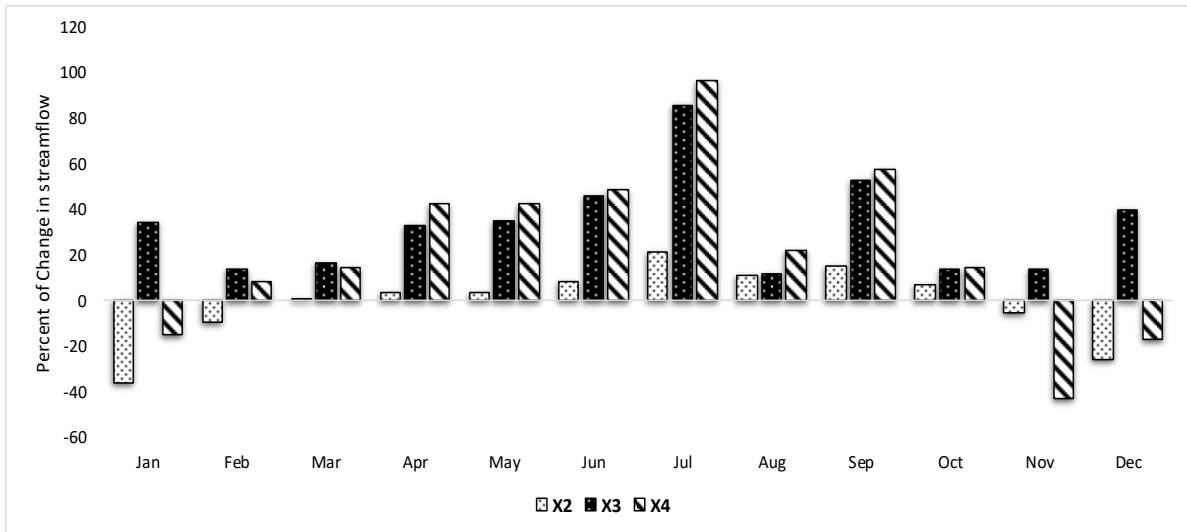


Figure 4.15. Absolute change in mean monthly streamflow for the UWBDR watershed under different scenarios.

4.4.6 Impacts of climate variation

In comparison to the land use change scenario, the climate variation scenario caused the average annual water yield to increase by 9.9% as a result of a prominent increase in precipitation at the UWBDR watershed. Baseflow also showed an increase when only climate variation was considered (X3); however, this was much more pronounced than the change in water yield, with an increase of 53.8 mm (81.6%) (Table 4.9). These results indicate that both land use change and climate variability played a role in increasing baseflow. However, climate change played a more pronounced role than land use change in impacting the hydrologic regime of the UWBDR during the recent past, due mainly to the increase in precipitation. This can also be seen in Table 4.9, in which the surface runoff decreased by 9.1% and evapotranspiration increased by 7.0%. Together, these results indicate that the climate alteration contributes more substantially to the effects observed on hydrological components compared to urbanization.

Similar to the land use change scenario, the average monthly water yield was predominantly observed in late fall/spring at the UWBDR watershed. Of note, the highest change in monthly water yield was observed in July (39%) due to the X3 (climate change) scenario. The change in water yield tended to be positive in months that experienced a significant increase in precipitation in the second period (TS2) compared to the first one (TS1) (Figure 4.11). On the other hand, the results show an increase in average monthly baseflow under the effect of climate change only,

impacts of X3 in all months, although the highest growth was detected in the warmest months of the year (May to September) (Figure 4.12).

The climate change scenario had the maximum impact on the average annual water yield, causing it to decrease by 11.9% for the Walzem Creek Watershed, while it caused the average annual baseflow to decrease by 42.9% (51.7 mm) compared to the baseline scenario (X1) (Table 4.10). This may be attributed to the significant reduction in the precipitation pattern and the increase in temperature in TS2 as compared to TS1, where the climate became warmer and drier. Therefore, these likely played an important role in the contribution to the total streamflow for Walzem Creek. Climatic variables, specifically precipitation, largely determined the runoff hydrograph. Precipitation reduction in the second climatic period (TS2) resulted in the significant decline of surface runoff by 20.8 mm (8.2%), and a reduction in evapotranspiration by 2.5%, within the X3 scenario (Table 4.10). These results indicate that impact of climate variability on baseflow and evapotranspiration was larger than the land use alteration scenario; however, both scenarios had opposite impacts on average annual water yield and surface runoff. Overall, the impacts of climate variation were greater than those of land use change.

On a monthly basis, the highest negative impacts of climate change over the monthly average water yield were detected in June, October, and December, with amounts of 19.2, 12.5, and 12.3 mm, respectively, where the average monthly precipitation was significantly greater in TS2 as compared to TS1. On the other hand, monthly water yield increased at the end of summer and the beginning of fall seasons, especially in September; in which it increased by 17.5 mm. It could be inferred that climate variation had a lasting negative effect on water yield (Figure 4.13). Similarly, the climate change scenario (X3) caused a reduction in monthly baseflow in all months except August, September, October, and December, with the highest difference recorded in September (3.1 mm). The increase of baseflow in these months was mainly due to changes in precipitation and temperature patterns from TS1 to TS2. For example, TS2 experienced less precipitation as compared to TS1, while the temperature was greater in TS2 compared to TS1. Hence, baseflow played a role in water contribution to total streamflow when the weather got warmer and drier in the semi-arid watershed (Figure 4.14). The probable climate alteration impacting most of the globe is mainly determined by the combination of temperature increase and either decrease or increase in rainfall intensity, and any particular baseflow response will depend on the direction and magnitude of both precipitation and temperature. For instance, the change in average monthly

precipitation was positive in September, while it was negative in October. Meanwhile, average monthly baseflow showed an increase in both September and October, which might also be explained by the changes in monthly temperature between the two scenarios as it was higher in October than in September.

The streamflow changes under the X3 scenario, which was considered the climate change scenario, were remarkably similar at the UWBDR watersheds to those at the LEC watershed, in which all months exhibited an increase of 12.2–34.5% (Figure 4.15). In addition, the relative change in streamflow percentage in the UWBDR watershed was greater than the change in the LEC watershed, suggesting that streamflow change was more sensitive to climate change than to land use dynamics. Climate change had a similar impact on the average annual water yield in both the UWBDR and the LEC watersheds, in which it increased by 17.9% and 9.9% in the LEC and UWBDR watersheds, respectively. However, negative impacts due to the X3 scenario occurred in Walzem Creek, indicating that urbanization and climate change had opposite impacts in this semi-arid region. On the other hand, the climate change caused the average annual baseflow to increase by 15.2% and 81.6% at the LEC and UWBDR watersheds, respectively. However, it declined by 42.9% at the Walzem Creek Watershed. In addition, the average annual surface runoff exhibited an increase in the LEC Watershed due to the impact of climate change by an amount of 22.7%, but decreased in Walzem Creek by 8.2%. These findings imply that the runoff hydrographs of a catchment are largely impacted by climatic variables, especially precipitation, which in turn affects the percolation of soil water to the groundwater.

4.4.7 Combined Impacts of Both Land Use Change and Climate Variations

To evaluate the combined impacts of land use and climate change, the simulated results under the X4 scenario were compared to the calibrated baseline scenario. The annual mean water yield increased by 11.1% as a response to the X4 scenario at the UWBDR watershed (Table 4.9). These changes, compared to X2 and X3 scenarios, emphasize that the joint effects of land use change and climate variability led to consistent growth in water yield in the UWBDR watershed. Furthermore, the effect of climate variation was larger than that of the land use dynamic on the total water yield. This can be clearly seen by the X3 and X4 scenarios, in which the mean annual precipitation showed an increase of 81.4 mm, resulting in an increase in the mean annual water yield. These changes are similar to the changes reported in the LEC watershed discussed in Chapter

3, resulting from the combined impacts of land use and climate change. In contrast to the LEC watershed, where baseflow decreased, the X4 scenario for the UWBDR watershed led to an increase in the average annual baseflow to 7.1 mm (10.8%) (Table 4.9). This difference might be attributed to the prevalence of negative urbanization impacts for the LEC watershed, in contrast to the significant positive effects of climate variation for the UWBDR watershed.

Similar to the climate scenario, we observed that the average monthly water yield was concentrated in the late fall and early spring in the X4 scenario, totaling 39% of the annual yield. In general, positive changes were detected in all months under different scenarios except for November, January, and February. However, the variation due to the joint effects tended to be higher in all months with a higher precipitation pattern in the second period of time (TS2) than in TS1 (Figure 4.11). For instance, the effect of land use scenario (X2) was greater than those of X3 and X4 in August, as the average monthly rainfall was 127.2 mm in TS1, while it was only 99.8 mm in TS2. Meanwhile, the combined effect of land use change and climate variability and the sole effect of climate change had greater impacts on water yield in July, as the average monthly precipitation was 83.7 in TS1, increasing to 114.8 mm in TS2. Baseflow variations showed increasing trends in warm months from May to September, then decreased from October to April in conjunction with the joint effect of climate variation and land use change (Figure 4.12). The increase in baseflow may be mostly due to an increase in rainfall, and could be explained by fluctuations in both precipitation and temperature between TS1 and TS2. The freeze-thaw processes of the active layer could have changed the soil infiltration capacity and the volume of subsurface water storage, thus impacting baseflow as well (Qin et al., 2017).

Results from the X4 scenario in the Walzem Creek Watershed indicate that the average annual water yield decreased by 25.7%, while the average annual baseflow showed a consistent reduction of 67.9% (Table 4.10). Additionally, the annual evapotranspiration was negatively impacted by the joint effect of climate variation and land use change, decreasing by 4.3%. The decline in evapotranspiration was mainly caused by the reduction in green cover (Table 4.7). Compared to X1, the combined effects of land use change and climate variability under X4 decreased surface runoff by 4.2 mm (1.7%). Therefore, with the concurrent reduction in evapotranspiration, average annual water yield and baseflow had significant decreases under the X4 scenario. These findings indicate that changes of average annual water yield and surface runoff under the joint effects of climate variation and urbanization were smaller than the changes due to

the impacts of the sole impact of climate variation. In other words, the climate alteration had a dominant role, while the land use variation had a counteractive role affecting water yield and runoff. The land use change reduced the negative impacts of climate variation by 3.0% and 6.5% for annual water yield and surface runoff, respectively. However, the joint effect of climate variability and land use change on baseflow was greater than the sole impact of the land use change scenario and climate variation scenario. X4 had the greatest negative impact on evapotranspiration. Thus, when the impacts of individual land use change scenarios and climate alterations occur in the same direction (increase/decrease), the impacts will be intensified when both changes occur at the same time. Of note, the joint effect of climate variation and the urbanization scenario are not a simple summation of each of the individual impacts; however, it represents the interaction of both climate and land use change represented by the SWAT model outputs.

On a monthly basis, the contribution of the joint effects of both climate variability and land use change tended to be similar to the contribution of climate change impacts but with a smaller magnitude for the monthly water yield, with the maximum difference recorded in September (19.0 mm) due to a significant increase in rainfall. Monthly water yield exhibited the greatest reduction in June (18.6), due to the notable decline in precipitation in this month. The impact of land use change played a counteractive role for water yield from the Walzem Creek Watershed (Figure 4.13). Similarly, the greatest average monthly change for baseflow was recorded in September (2.5 mm) as a result of the combined impacts of urbanization and climate variation (Figure 4.14). Generally, the behavior of average monthly baseflow under the combined impact of land use and the climate change scenario was consistent with the changes under the individual impact of climate variation. At a monthly timescale, the streamflow for Walzem Creek Watershed increased only in August, September, and November considering the climate change scenario and the combined scenario of land use and climate variation, with the greatest increase in September of 63.7% (X3) and 71.3% (X4), while it exhibited a reduction in all other months with the greatest decline recorded in June of 35.0% (X3) and 33.8 (X4). Note that streamflow in Walzem Creek showed a minor increase in all months when considering the impacts of land use change scenario (X2), except for July and August that showed a minor reduction of 0.7% and 1.1%, respectively (Figure 4.16). Moreover, the streamflow rate tended to decrease when considering scenarios X3 and X4, except in August, September, and November, due to the increase in precipitation during these months. The impact of the combined effect of land use change and climate variability showed the

same behaviors as the sole impact of climate variability in the Walzem Creek watershed. This situation was well demonstrated by the monthly streamflow variation in the watershed (Figure 4.16), with the greatest streamflow increase estimated in September at 71.3%. Meanwhile, the greatest reduction in monthly streamflow when considering the individual impacts of climate change was estimated in June at 35.0%. These changes were mainly the result of incremental, dynamic precipitation patterns between the two periods, TS1 and TS2. For instance, September experienced the greatest increase in rainfall (40.4 mm), while June showed the greatest reduction in monthly precipitation (45.2 mm) in TS2 as compared to TS1.

Compared to the LEC watershed, in which the urbanization had a prevailing negative effect on baseflow while climate change caused increases in both flows, in the Walzem Creek watershed, both land use change and climate change had an impact on streamflow and baseflow. However, our study showed that the climate change impacts played a more important role than land use dynamics and urban expansion on streamflow and baseflow in this semi-arid region.

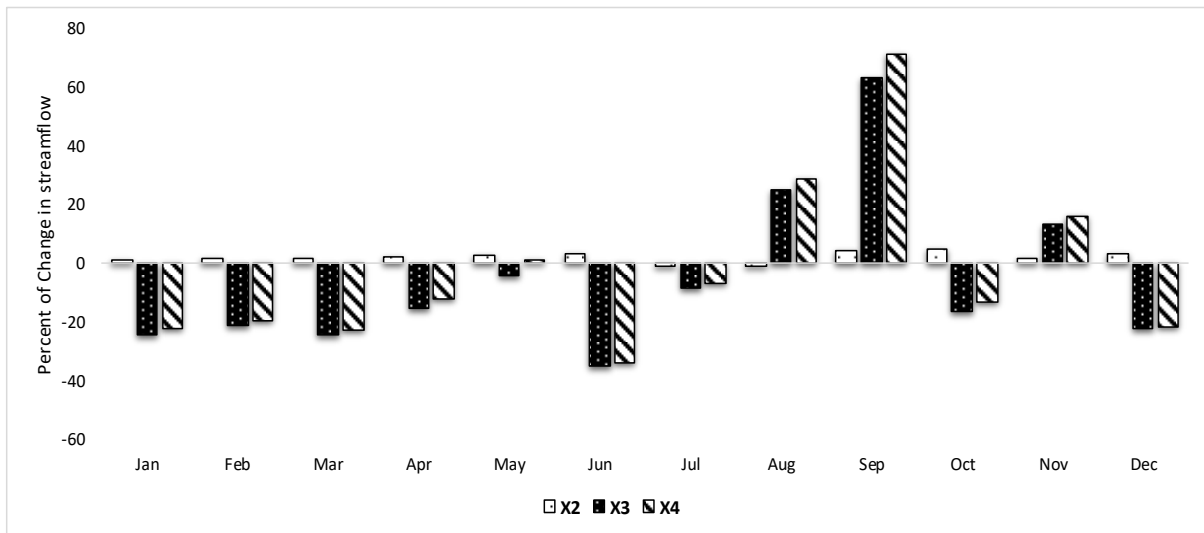


Figure 4.16. Absolute change in mean monthly streamflow for the Walzem Creek watershed under different scenarios.

4.5 Summary and Conclusions

Urbanization and climate change play an important role in altering the spatiotemporal distribution of water resources and hydrologic components. Streamflow and baseflow are two critically important components of hydrology that are essential to sustain water demands by

various sectors, such as agriculture and industry, and are vulnerable to these changes. Therefore, it is of vital significance to understand the behaviors of these components under the separate and combined impacts of climate variation and land use dynamics in different climate regions. In this research, we followed the methodology discussed by in Chapter 3 for computing streamflow and baseflow for diverse watersheds.

Findings of this research indicate that the climate became warmer and wetter for the UWBDR and for the LEC watershed evaluated in Chapter 3, but warmer and drier at the Walzem Creek watershed. The combined effect of these changes showed nonlinear responses to the water balance component. Changes at the UWBDR watershed were remarkably similar to those for the LEC watershed, with the exception that the climate variation was shown to have a greater impact on streamflow, surface runoff, and baseflow, while land use change exerted a relatively small influence on the flow. In other words, in the UWBDR watershed, when the direction of the changes caused by urbanization and climate variation occur in the same direction, the changes of the combined impacts will be intensified. Of note, increasing surface runoff was considered a negative impact as it further strengthened environmental stress by generating more surface erosion and sedimentation. On the other hand, urbanization influenced streamflow positively, while it affected baseflow negatively in the semi-arid Walzem Creek Watershed. However, the climate change had negative impacts on all water components in the area. This might be attributed to the change in rainfall pattern between the two climate periods. The small reduction in mean annual precipitation in the TS2 produced a considerable reduction in runoff. Therefore, the impact of the combined scenario will be amplified when the individual impacts of land use alteration and climate variation are in the same direction (positive/negative). These findings indicate the necessity of evaluating the influences of urbanization and climate alteration separately when assessing the hydrologic effects in urban catchments.

Generally, with the variation in spatiotemporal properties of precipitation, and increasing hazardous events associated with water, such as droughts and floods, stress on water resources will increase and will further encourage the development of mitigation approaches. Based on this research, findings will provide practical suggestions for policy makers on how to sustain water resources more efficiently in relation to its variability as a response to urbanization, land use, and climate change. These changes can be problematic and can incur great costs to establish new infrastructure, especially in undeveloped nations. Therefore, policy makers need to develop

policies to address these types of changes, taking into account the individual influences of human activities and climate variation, for instance, improving infrastructure to be more resilient to human activities, constructing dams following proper regulations on water resources, and limiting the amount of deforestation, which threatens some hydrological components. In addition, outcomes of this study can be used in quantifying the potential impacts of future projected climate change and land use change. Nevertheless, it might be found that the driving factors interact to impact streamflow and baseflow through chain effects, in which one factor is trying to increase/decrease the magnitude of the other. Hence, more studies are crucial to evaluate this potential future impact on the hydrological system, with the emphasis on the interactive effect of environmental change drivers when predicting future change.

While this research showed the separate and combined impacts of human activity and climate alteration using the SWAT model, modelers should be aware that other types of uncertainties associated with the model exist that may result from observed data, the parameterization process, or from the conceptual model itself. One of the potential shortcomings of this study is that the urbanization processes were an integrated part of the watershed, along with climate alteration. Therefore, it was difficult to discern whether the separate effects of human action and climate change were able to be truly simulated and this issue might therefore create a biased condition. Thus, a suggestion to avoid this limitation in future research is to hypothesize an extreme land use/land cover change that is sensitive to the anthropogenic changes instead of a natural system simulated by the model.

CHAPTER 5. IMPACTS OF WATERSHED PHYSICAL PROPERTIES AND LAND-USE ON BASEFLOW IN TEXAS, USA

Abstract

The groundwater component of streamflow is one of the most important components in watershed hydrology because it sustains flow in the stream during dry seasons, moderates seasonal fluctuations in the temperature of the stream, and typically has better quality water compared to surface water. In this study, 140 gauge sites and their associated watershed physical and geological properties were used to develop multiple regression models to predict Baseflow Index (BFI) across Texas, a large state in the US that experiences a diversity of climate conditions and water demands. The measured BFI was derived from USGS daily streamflow data from 1980 to 2017 using the two parameter recursive digital filtering approach of the Web-based Hydrograph Analysis Tool (WHAT). Three scenarios were developed and validated across five study areas (Categories 1 to 5) that were chosen based on categorization of climate conditions, and one model was developed across the whole state. The first two scenarios related BFI to topography, climate and land use. The third scenario used surface geology mapping, soil type and hydrogeology parameters. The models developed for each category showed high performance, low bias and low relative errors to calculate BFI, with R^2 values varying from 0.76 to 0.99, and strong agreement with measured BFI values. The results further showed that there was no specific pattern for BFI variation across Texas, which ranges from 0.17 to 0.71, and could not be accurately captured using a model developed from statewide data. The greatest model accuracy was recorded in Western Texas in Categories 4 and 5, and the lowest model performance occurred in the Category 2 region. Outputs indicated that evapotranspiration attributed to lower model accuracy and that BFIs can be quantified as an integral expression of the fractional areas of each lithology in the basins. Generally, scenarios 1 and 3 within each category showed greater prediction performance than scenario 2. The findings of this study are beneficial for water resources planning and management, as the results can be used to establish water resources plans at local and regional scales in Texas. Additionally, the developed models can be easily applied to other areas that have similar topographic, geologic and climatic conditions. The developed equations reported herein can support further research in groundwater modeling, by presenting independently obtained BFI estimation for ungauged sites.

5.1 Introduction

Identifying the key physical processes that influence watershed hydrology are of vital significance to many fields. This identification is achieved by studying how watersheds with different physical properties are both similar and different in hydrology, enabling broader conclusions about the behavior of similar watersheds. Estimation of some hydrological behavior of different watersheds, based on catchment sizes, can be approached by scaling of different physical properties. Hydrological properties of watersheds, such as streamflow and baseflow, may be estimated using different physical descriptors, including meteorological and physio-graphic parameters, as well as geological and hydrogeological parameters (Bloomfield et al., 2009).

This estimation not only requires physical properties, but also the separation of the total discharge of the watershed into different natural flow components such as surface runoff and low-flow (Haberlandt et al., 2001). Several separation methods have been developed depending on the catchment scale. Estimation of the flow, depending on the need, can range from an average value for a state, to large watersheds, small drainage basins, or smaller project scales (Gebert et al., 2007). For example, in small catchments (one to a few km²) hydrometric techniques and tracer methods can be effective in providing insight into flow generation mechanisms (Bonell, 1999). Hydrograph separation and hydrologic modelling can provide valuable insight for lower mesoscale catchments (100s of km²) (Krysanova et al., 1999). Of note, tracers can also be used to track low flow at larger areas; however, it becomes increasingly difficult to sample larger watersheds (Frisbee et al., 2011). However, with increasing size, a differentiation of discharge into three main flow components may be considered: surface runoff, interflow and baseflow (Becker et al., 1999).

The groundwater component of streamflow is one of the most important components in watershed hydrology, as it sustains flow in the stream during dry seasons, moderates seasonal fluctuations in the temperature and typically has better quality water compared to surface water. Therefore, changes in baseflow play a role in evaluating change in aquatic life of streams. Baseflow is that part of streamflow that is derived from groundwater and other delayed sources such as snowmelt into the stream and is considered one of the most important low-flow components in the hydrological cycle of a watershed in different climatic conditions (Hall, 1968). Baseflow is critical for sustaining flow in rivers and streams and is often assumed to be equal to groundwater recharge (Gebert et al., 2007). The continuation of streamflow during these times of dry seasons is of critical importance to both stream biota and to some recreation based industries

(Neff et al., 2005). In addition, baseflow maintains flow for navigation, water supply, hydroelectric power and recreational uses in reservoirs (Santhi et al., 2008).

Being able to understand and predict what changes will impact this low-flow water component over time is essential to understand the current and future changes to a watershed's hydrology, especially in the face of climate and land use alteration. This understanding helps in developing water management strategies, establishing relationships between aquatic organisms and their environment, estimation of small to medium water supplies, and the management of water salinity. An evaluation of baseflow discharge is also valuable for the calibration and validation of groundwater models that are being used to investigate many water supply problems (Cherkauer, 2004; Gebert et al., 2007). However, baseflow displays spatial and temporal variability and is dependent on a large number of watershed properties, for instance topography, lithology, land use, geomorphology, vegetation, amount of discharge, soil and climatic conditions (Mwakalila et al., 2002), in addition, it is also dependent on the source in which the baseflow was generated. Therefore, improvements in quantification modeling and evaluating the relationships between these properties and baseflow are important to develop a detailed understanding of baseflow generation for specific areas.

Baseflow estimation at various spatial scales has been previously studied (Ahiablame et al., 2013a; Cherkauer, 2004; Gebert et al., 2007; Haberlandt et al., 2001; Longobardi & Villani, 2008), typically by making extensive use of statistical analysis to empirically relate baseflow to catchment characteristics. One such study examined the relationship between baseflow index (BFI) and landscape descriptors, that included a set of qualitative geology-vegetation parameters and dimensionless topographic and climatic indices, for 114 catchments in Australia, but found no trends in plots of baseflow index against any dimensionless topographic parameters within the groups (Lacey & Grayson, 1998). BFI is the long-term ratio of baseflow to overall streamflow and therefore represents the delayed contribution to river flow (Bloomfield et al., 2009). However, a study examining regionalization of flow components to derive the empirical relationship for the estimation of average BFI within large river basins in Germany found that the average BFI was strongly related to topographical, hydrogeological, and precipitation characteristics and less influenced by land use properties of the watersheds (Haberlandt et al., 2001). A study of semi-arid environments in Tanzania investigated the influence of physical catchment properties on baseflow and revealed that the BFI had a strong relationship with both climate and geology. Specifically,

catchments with high rainfall or low evapotranspiration underlain with granites or basalt tended to give high baseflow (Mwakalila et al., 2002). Together, these studies underscore the variability between how physical features affect watershed hydrology when assessed by statistical models.

In another approach, BFI was predicted from the means of different parameters using multiple linear regressions and neural networks within 52 basins in Zimbabwe. This work found that a neural network predicts the BFI with comparable accuracy to multiple regression. However, differences in lithology and land cover type between basins were not significant in explaining the BFI (Mazvimavi et al., 2005). More recently, a regional approach to predict the BFI at ungauged sites in a Mediterranean region was developed using a linear regression model, for which only very poor gaged data were available. The study was able to predict baseflow contribution to streamflow using elevation and permeability index of basins (Longobardi & Villani, 2008). Another approach used linear regression methods to quantify geological controls on BFI within the Thomas Basin in the UK, which suggests that the influence of hydrologic soils on BFI has a geological meaning, in which the presence of different types of rocks results in the formation of different types of soils (Bloomfield et al., 2009).

Many investigators have examined the relationship between landscape descriptors, catchment properties and baseflow/BFI in the USA as well and have helped provide insights into the importance of some components. In a study that examined the influence of a number of geomorphologic parameters on groundwater discharge in Appalachian watersheds in the northeastern part of the US, total length of perennial streams, average basin slope, and drainage density were most closely related to groundwater discharge (Zecharias & Brutsaert, 1988). Additionally, the use of multiple regression analysis and observed geographic and spatial trends in baseflow in the Great Lakes basin suggested that attention must be given to watershed specific properties, such as scale, geology, and surface water, when characterizing baseflow at different locations (Neff et al., 2005). Using the same methodology, these results were supported by the observation that baseflow was naturally influenced by a variety of watershed characteristics in Wisconsin (*i.e.* basin drainage area, soil infiltration rate, and basin storage) (Gebert et al., 2007). Interestingly, relief and percentage of sand were highly correlated with baseflow index, and the amount of baseflow volume can be related to gradient and the amount of effective rainfall (Santhi et al., 2008). In addition, regression models using meteorological, geomorphological and geological variables, were successfully able to predict streamflow, baseflow and storm runoff in

Pennsylvania, Indiana and Wisconsin under different scenarios with an R^2 greater than 0.94 and at reasonable prediction errors, ranging from 0% to 48% (Ahiablame et al., 2013a; Zhang et al., 2013; Zhu & Day, 2009). In general, geology, soil and rock types, geomorphological terrains of different landscapes, topographical relief, subsurface drainage, land use change and climate are some of many factors that control the magnitude of baseflow (Huang et al., 2016). Many of these factors may be altered due to human activities on the landscape, and therefore, it is critical to understand the relationship between catchment physical properties and baseflow.

As mentioned, previous studies indicated that the effects of watershed physical properties on baseflow can be evaluated through relationships between catchment properties and baseflow (Table 5.1). However, this pattern does not appear to accurately represent these properties on regional scales that have different climatic patterns and geologic features (Neff et al., 2005). The relationship between the physical properties and groundwater are poorly understood when it comes to which geologic unit and climate category to consider in quantifying the impacts on baseflow. Even though there is an assumption that the underlying geology influences baseflow, previous studies that estimate baseflow and BFI typically simplify the effect of watershed geology to physical parameters that represent the fractional area of aquifer in a catchment (Bloomfield et al., 2009). To date the relationship between catchment lithology and BFI has not been quantified in a systematic manner.

Therefore, the goal of this study was to develop regression models using study areas in Texas to explore the relationship between BFI, baseflow and catchment properties (including climate and geologic bedrock). Using these relationships, the results are likely to be useful to evaluate baseflow of other watersheds with similar climatic and geologic conditions, potentially beyond the US. For example, in regions where drainage basins lack these kind of data because of poorly developed hydrological networks, these regression models could be applied to predict hydrological components to evaluate water resources (Rodda, 2001). In addition, the need for hydrological data has greatly increased as water resources, which are in some cases scarce, have to be shared among competing uses (Mazvimavi et al., 2005). Therefore, evaluation of baseflow and, in general, hydrological characteristics for water resources planning is a major need globally.

The state of Texas has experienced extensive change in land use over time, and is getting warmer and drier, in particular in western areas. Therefore, the amount of water recharging aquifers and appearing as baseflow has likely changed over the past few decades. Groundwater

has experienced significant declines during the last few decades in some Texas locations (Arciniega & Breña-naranjo, 2016), and water rights demands have increased dramatically due to population growth (Sophocleous & Perkins, 2000). Nevertheless, surface water is usually sustained by groundwater, and in anticipation of the expansion in human use of water and change in climate, there is a growing need to evaluate surface and groundwater as a single resource (Miller et al., 2016; Winter et al. 1998). This requires water resources managers to have better estimates of water supplies for their planning and management, and it is important to know the present contribution of baseflow to total streamflow, to ensure that flow to the stream is sustained and meeting public water demands. These estimates might be done using watershed models, for instance MODFLOW or SWATMOD. However, these models require extensive data and typically need to be calibrated and validated for a specific basin before application. On the other hand, methods for estimating groundwater recharge can be implemented using physical properties of watersheds by developing regression models, as discussed in the literature (Cherkauer & Ansari, 2005; Lorenz & Delin, 2007).

Baseflow is generally calculated from stream flow data using hydrograph separation methods, for instance graphical and analytical methods (McNamara et al., 1997; Szilagyi & Parlange, 1998), recession curve methods, mass balance methods (Hoeg et al., 2000), digital baseflow filter methods (Nathan & McMahon, 1990), and geochemical and isotopic hydrograph separation techniques (Pinder and Jones, 1969; Sklash and Farvolden, 1979). However, most of these methods are limited to estimating baseflow for gauged sites, with the exception of geochemical and isotopic techniques which can be used to estimate a fraction of groundwater without gauge data. With the development of geographic information systems (GIS) and continuously increasing availability of digital data, it is much more feasible today to derive variables representing soil, geology, climate, and geomorphological characteristics of a basin compared to a few decades ago. Therefore, it is now possible to explore relationships between additional basin variables and groundwater recharge in ungauged watersheds, with the possibilities of elucidating more accurate and meaningful models (Zhu & Day, 2009).

The basic philosophy behind using regression and statistical models in estimating baseflow is that regression models relate baseflow and BFI to watershed characteristics. As observed in previous literature, regression models have the advantage of being implemented relatively easily to estimate baseflow with reasonable accuracy (Zhang et al., 2013a). In light of the above

discussion, the main motivation of this study was to evaluate the impact of different climate, lithology and soil types on baseflow and BFI along with other catchment properties. Herein, we report on development of a model that encompasses theoretical and experimental components to estimate baseflow and the effect of different watershed properties on this low-flow to: 1) Estimate the average annual baseflow in watershed tributaries in Texas from gauged sites using hydrograph separation models (recursive digital filter method); 2) Develop lithology-soil groups for Texas to examine the physical relationship between average BFI and lithology/geological control in addition to other descriptive catchment properties, for instance climate, soil and topography; and 3) Develop statewide numerical regression models calibrated to the hydrograph separation results to estimate baseflow for ungauged areas and validate with regional relationships. The results of these research objectives are described in detail below.

Table 5.1. Review of some research evaluating the relationship between watershed properties and baseflow.

Authors	Study areas	Method		Catchments properties
Zecharias & Brutsaert (1988)	Appalachian Plateau, USA	Principle factoring	axis	Area, stream length, elevation, drainage networks
Lacey & Grayson (1998)	Australia	Multiple regression	linear	Drainage area, forest, precipitation stream length, potential ET
Haberlandt et al. (2001)	Germany	Stepwise regression		Topographic index, hydraulic conductivity, slope, precipitation
Mwakalila et al. (2002)	Tanzania	Stepwise multiple regression	and	Channel slope, basin slope, drainage density, geological index, precipitation, potential ET
Mazvimavi et al. (2003)	Zimbabwe	Multiple regression	linear	Slope, wooded grassland, grassland, precipitation
Neff et al. (2005)	Great Lakes	Multiple regression		Surface water proportion, bedrock geology, grain sizes, till
Lorenz & Delin (2007)	Minnesota, USA	Regional regression model		Drainage area, precipitation, growing degree day, specific yield
Gebert et al. (2007)	Wisconsin, USA	Multiple regression		Drainage area, baseflow factor, storage, infiltration rate
Longobardi & Villani (2008)	Italy	Simple multiple regression	and	Permeability index
Santhi et al. (2008)	Conterminous US.	Stepwise regression		Relief, precipitation, potential ET sand percentage
Bloomfield et al. (2009)	United Kingdom	Stepwise regression		Lithology
Zhu & Day (2009)	Pennsylvania, USA	Multiple regression		Drainage area, elevation, precipitation, evapotranspiration
Ahiablame et al. (2013b)	Indiana, USA	Stepwise multiple regression	and	Drainage area, tile drained area, relief, slope, channel slope, bedrock depth, precipitation, ET, land uses, soil groups
Zhang et al. (2013a)	Michigan, USA	Multiple regression	linear	Drainage area, slope, relief, stream length, land covers, precipitation, temperature, ET, transmissivity, water table, surficial geology, soil group

5.2 Materials and Methods

5.2.1 Study area description

Texas is the second largest state, with an area of 691,027 km², and second most populated state in the United States (Hudak, 2000). Found in the south-central US, Texas represents both the wetter eastern and the drier western regions of the country (Zhang & Wurbs, 2018). Climate, geology, topography, hydrology and water management vary dramatically across the state. Geology in Texas ranges from simple-dipping strata structures of the Gulf Coastal Plain, North-Central Texas, and Panhandle, to the complicated geological structure of the Marathon Uplift, the Llano Uplift, and the Big Bend region (Figure 5.1). Mean annual precipitation ranges from 250 mm at El Paso on the Rio Grande in west Texas to 1500 mm in the Sabine River Basin on the eastern border (Figure 5.2). Average temperatures rarely go above 35 °C or below -5 °C (Zhang & Wurbs, 2018). Hydrology is extremely variable, subject to major floods and severe droughts along with seasonal and continuous fluctuations. Figures 5.3 and 5.4 showed the average annual evapotranspiration and runoff in Texas. Agriculture is considered the major industry and the principal land use in Texas.

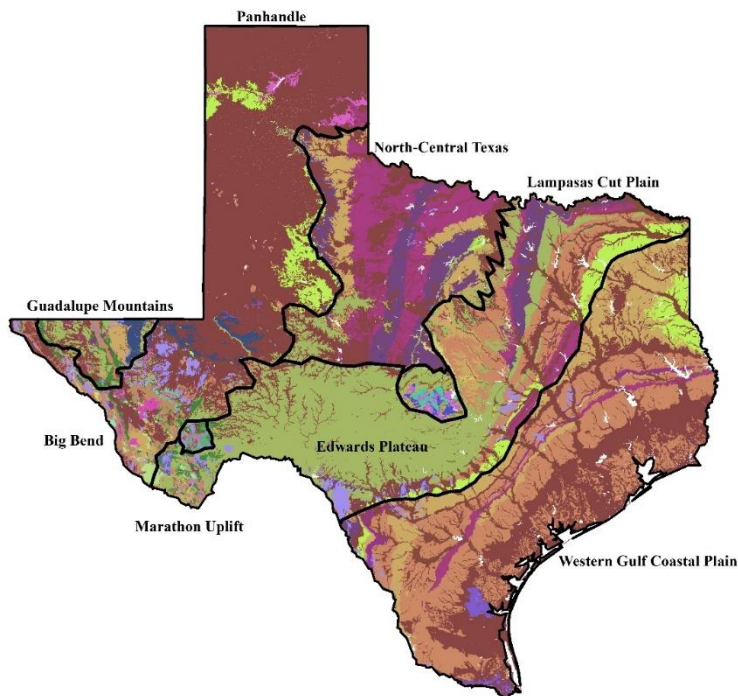


Figure 5.1. Geologic regions of Texas (Texas Water Development Board, 2012).

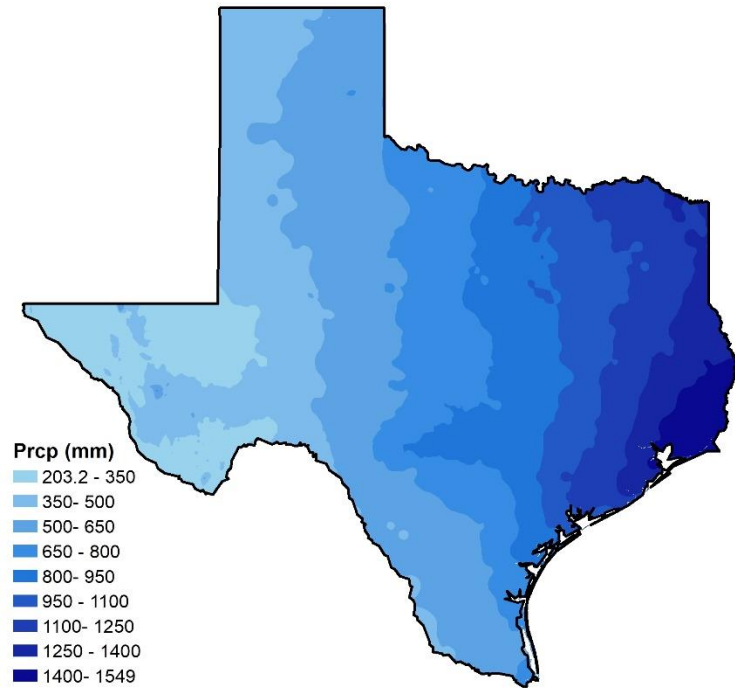


Figure 5.2. Average annual precipitation in Texas (ESRI, 2020).

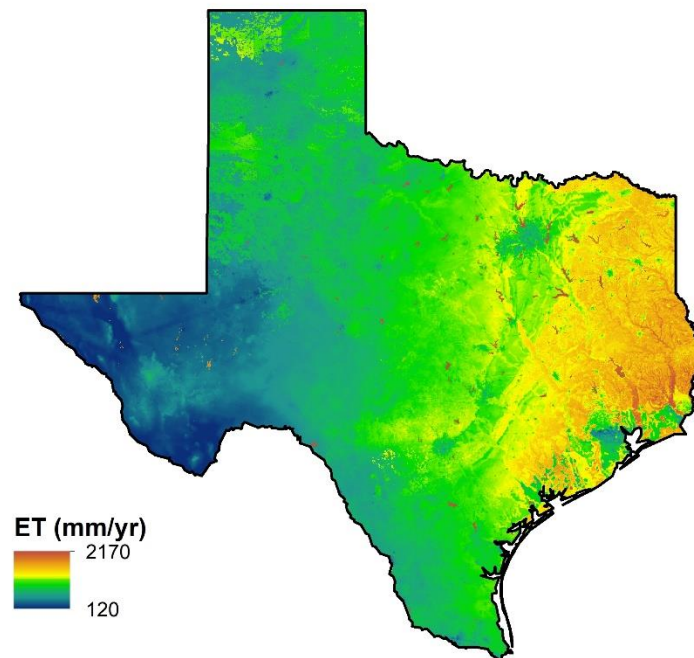


Figure 5.3. Average annual evapotranspiration in Texas (ESRI, 2020).

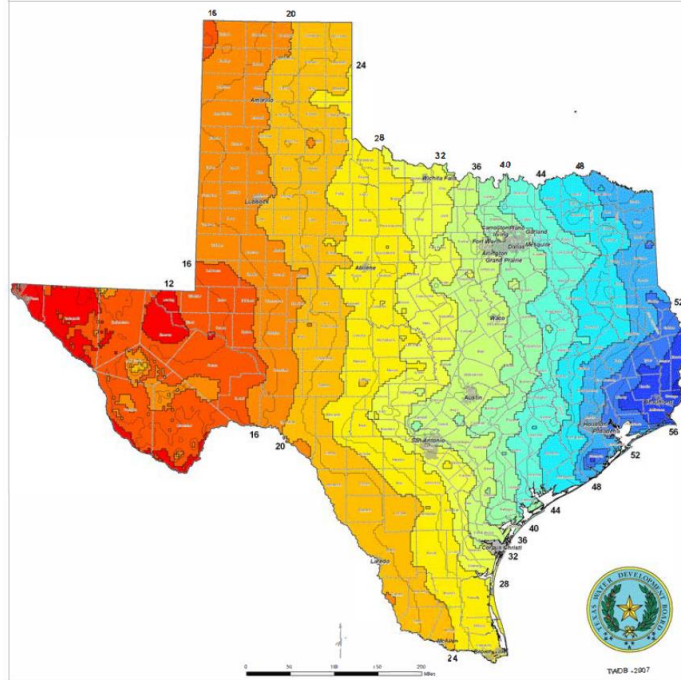


Figure 5.4. Average annual runoff in Texas in thousands of gallons from a typical 2000 ft² area (Texas Water Development Board, 2012).

Groundwater is a major source of water in Texas. Land use change threatens groundwater quality and quantity in Texas, and the amount of water recharging the aquifers and appearing as baseflow has likely changed over the past few decades. Even though groundwater supplies approximately 56% of the statewide water consumed (Strause, 1987), it has experienced significant decline during the last few decades (Arciniega & Breña-naranjo, 2016), while at the same time, water rights demands increased dramatically (Sophocleous & Perkins, 2000). Therefore, with 42% of the supply from surface water and 2% from reuse, it is important to understand the present contribution of baseflow to total streamflow.

Of all the water use in Texas, about 40% is surface water; while the other 60% is groundwater (Texas Water Development Board, 2012). The eastern part of Texas accounts for nearly 80% of residents and 56% of the water consumed each year in Texas; however, the western side contains the other 20% of the state’s population and accounts for 44% of the state’s water consumed (George et al., 2011). In addition, irrigation accounts for 85% of all water demands in west Texas. The eastern humid part of Texas receives plenty of rainfall and contains major industries within

large cities. Surface water used in the east accounts for approximately 85% of the total surface water used in Texas (George et al., 2011). In general, most of the groundwater, 72%, is used for irrigation, and 21% is used for municipal demands. Manufacturing, livestock, mining, and power account for the remaining 7% of groundwater consumed in Texas. Therefore, it is important to continue to research the impacts of physical properties on baseflow in Texas to maintain the viability of the state's natural resources, health and economic development.

As mentioned above, Texas experiences a range of climate and geological conditions. This diversity is essential to the goals of this study, which includes understanding how baseflow is affected by different factors related to climate, soil and bedrock. Additionally, data availability and accuracy are critically important in development and assessment of the regression models and to inform policy decision. Texas has the spatial and temporal datasets needed to achieve the goals of this study and allow us to further test the hypothesis that with inclusion of more variables in the model, the prediction power of the model will be more accurate.

This study was conducted with a group of watersheds distributed throughout the entire state that range in area from 247 to 1499 km². Data selected for this study were obtained from 140 gauging stations that have long-term streamflow records from 1980-2017. Delineated watersheds from the USGS database were selected for this study (Figure 5.5). Of note, in this research, it was assumed that no water is contributed from any neighboring basins and that the surface watershed divides were the same for the groundwater divides.

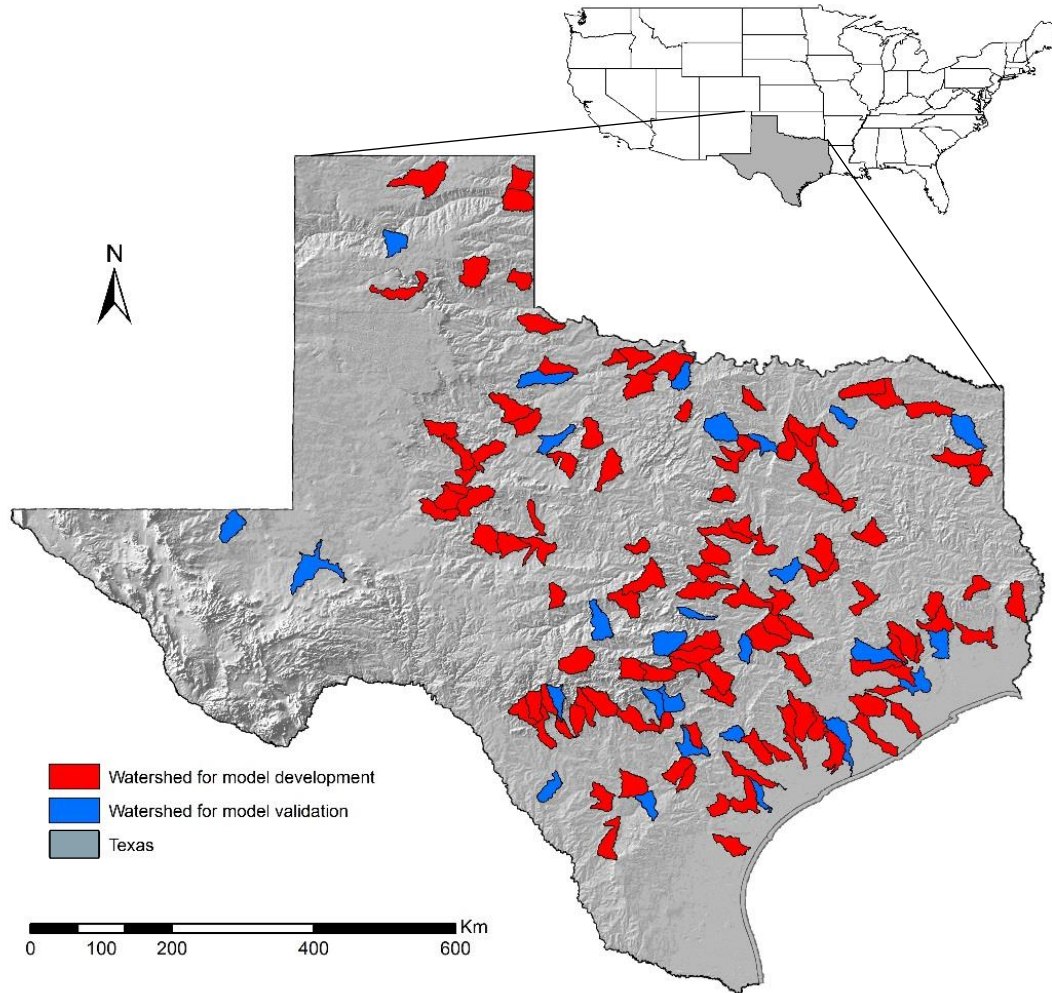


Figure 5.5. Watersheds used for model development and validation in Texas.

5.2.2 Watershed selection

All 1,047 continuous recorded gauged stations were accessed through the USGS database (<https://waterdata.usgs.gov/tx/nwis/sw>). The screening criteria for the gauged stations were as follows: 1) basin for station lies entirely within the Texas border; 2) the station has a continuous streamflow record from 1980 to 2017; 3) at least 90% of the record is available and no missing record in the last 15 years; and 4) diversions structures and regulations such as dams and man-made reservoirs have no impacts on the streamflow on the gauged station to avoid biased results and minimize the influence of flow routing and limit the effects of reservoir release (Santhi et al., 2008). The screening procedure yielded a total of 140 gauged stations across Texas. However, the

western part of the state was poorly represented due to the presence of few perennial streams, data scarcity and missing values.

5.2.3 Baseflow Index Evaluation

Baseflow index (BFI) values were determined by calculating the ratio of long-term baseflow to total stream flow, as this value represents the slow continuous contribution of groundwater to river flow. BFI for a gauging station was calculated from USGS daily streamflow data using the Web-based Hydrograph Analysis Tool (WHAT) (Lim et al., 2005). WHAT provides a fast and consistent baseflow separation technique, with a user-friendly interface that provides an understanding of the behavior of runoff and the contribution of baseflow within streams. WHAT is comprised of three models that the user can select from for baseflow separation: a local minimum method and two digital filter methods, one using a one parameter filter method and the other, known as Eckhardt filtering, using a two-parameter filter method (Eckhardt, 2005). The two parameter filtering method, that consists of a filter parameter and BFI_{max} , was used in this research, as it has previously been validated against several baseflow separation methods (Eckhardt, 2008). The BFI_{max} is the maximum index that the recursive digital filter can model, while the filter parameter defines the rate with time at which the streamflow decreases after recharge and can be computed by recession analysis (Arnold et al., 1995; Eckhardt, 2005). The filter assumes that discharge from the aquifer is linearly proportional to storage and as consequence, there is an exponential decay in the recession. Eckhardt (2005) estimated BFI indices for different hydrological settings by comparing baseflow from conventional separation methods with the digital filter methods. These analyses proposed a value of 0.80 for perennial streams, 0.50 for ephemeral streams, and finally 0.25 for perennial streams with hard rock aquifers. Therefore, in this study, the BFI_{max} was modified according to the geological and hydrogeological properties of different aquifers across Texas. The daily baseflow was computed using the general form of the digital filter method and can be evaluated as follows (Eckhardt, 2005).

$$BF_t = \frac{(1 - BFI_{max}) \times \alpha + b_{t-1} + (1 + \alpha) \times BFI_{max} \times Q_t}{1 - \alpha \times BFI_{max}} \quad (5.1)$$

where BF_t is the baseflow; b_{t-1} at time step $t-1$; α is the filter parameter (0.98), Q_t is the total streamflow at time step t .

5.2.4 Dataset Development

This research established a qualitative physical properties classification scheme to reflect the baseflow rate in terms of BFI. The dataset analyzed in this research was selected using a three-step procedure that represents the physical conditions of the watersheds. Step 1: select variables that represent the physical characteristics of the watersheds that we expect will impact baseflow generation. These variables were selected according to studies that previously characterized hydrogeomorphic, morphometric and geological parameters and found them to be representative of overall watershed properties (Bloomfield et al. 2009; Hale & McDonnell, 2016). Therefore, most of these variables have been found to have empirical relationships to measured baseflow in more than one study (Gebert et al., 2007; Zecharias & Brutsaert, 1988; Zhang et al., 2013a). This procedure yielded 37 variables for the watershed characteristics used for developing the model.

Step 2: categorize these variables in two groups to establish different scenarios for the subsequent procedures based on models that evaluate the empirical relationships between baseflow and the basin physical properties. The first group included variables representing topography, stream characteristics, meteorological conditions and land use of the selected watersheds. This step yielded 19 variables representing the previously mentioned properties. The second group involved considering the variables that represent geomorphology, soil types, lithology and hydrogeological characteristics of the watersheds. This procedure allowed use of 18 variables representing the geological section of this research.

Step 3: establish a well-calibrated regression model, based on different scenarios, to evaluate the relationships between the physical properties of the basins and these variables to make estimates of BFI at ungauged sites. The relationship would be then validated by evaluating the BFI of different basins. This research took into consideration that the selected watersheds' physical properties should be acquired from ready-to-use sources for hydrologists, for instance from geological maps, soil data and national databases.

5.2.4.1 Topographical Variables

A total of 140 watersheds with hydrologic unit code 10 (HUC 10) were selected and acquired from the National Hydrography Dataset (NHD), including the watershed areas and drainage areas of the gauge stations of each watershed. The Digital Elevation Model (DEM) used had a resolution of 10 m by 10 m and was obtained from the Geospatial Data Gateway (GDG). DEMs were used to evaluate topography of the watersheds. The stream power index (SPI), stream density (StrD), total stream length (TStrL), and sediment transport index (STI) of each of the selected watersheds in the study area were evaluated using the DEM. SPI is an index used to evaluate the erosive power of flowing water, while StrD measures how well a basin is drained by channels and is an important indicator of water supply. StrD can be computed by dividing the total stream length by basin area, and it is expected to impact the transformation of precipitation to runoff (Mazvimavi et al., 2003). STI characterizes the process of erosion and deposition of the channels within the basins. In addition, results reported herein used the DEMs to evaluate average slope percent, average elevations and relief, and topographic index to define the topography of the basins. The average slope percent was used as an index for the kinetic energy available for water to move to a watershed's outlet, and accounts for factors such as overland flow to the channels and infiltration (Mwakalila et al., 2002). The topographic index (TI) is a dimensionless index that measures the extent of flow accumulation at the given point of the topographic surface. The TI is directly related to the catchment areas but inversely proportional to the average slope. ArcGIS 10.5 was used for the implementation of SPI, StrD, TStrL and STI. .

5.2.4.2 Hydro-Meteorological and land use data

The sets of data used herein include long-term daily meteorological data from 1980–2017 (precipitation, and minimum/maximum/average air temperature), obtained from the National Climatic Data Center (NCDC). Precipitation and temperatures were acquired from weather stations within or less than 5 km away from each watershed. Evapotranspiration (ET) data were obtained from the National Oceanic and Atmospheric Administration (NOAA). Average annual evapotranspiration rates were weighted from mean values of gridded ET data representing each of the selected watersheds. The evapotranspiration is related to solar energy input, which in turn has an effect of drying out the basins (Lacey & Grayson, 1998).

Hydrological streamflow data were based on observations from 1980 to 2017 at a gauged station within the watersheds. The daily streamflow data, acquired from the USGS National Water Information System (NWIS), were used to separate the baseflow from the direct discharge. Streamflow data were complete with no missing records. Finally, digital land-use data acquired from the National Land Cover Database (NLCD) were used to examine the consequence of different land-use types on BFI of the watersheds. Raster land-use maps from 2016 were used in this research, and the proportion of each land use type was used to characterize main land use in the basins.

5.2.4.3 Soil Types and Lithology

Different lithologies can influence streamflow and baseflow in two ways. The first is that groundwater is stored in the rocks, especially highly fractured ones, and the second impact is on the formation of different soil types. Different lithologies, under the influence of erosion, weathering and plant activities, tend to produce different types and depths of soil which in turn impacts the contribution to stream flow, groundwater and the recharge rate (Mwakalila et al., 2002). Therefore, in this research, area-weighted percentages for hydrologic soil groups, from A to D, were obtained from the Soil Survey Geographic Data (SSURGO) with a resolution ranging from 1:12,000 to 1:63,630. The lithological classification scheme for model development was based on a 1:250,000 digital geologic map of the United States that contains more than 150 different types of surficial materials. A general distribution of different lithologies and surficial materials for each watershed was acquired from the USGS database. A classification system was established to assign the many complex units on source maps into units much more broadly and simply defined. In this study, five surficial-geology classes were defined and the area weighted percent of these classes in each basin were used. These classes included alluvial, coastal, colluvial, eolian and residuals surficial deposits.

5.2.4.4 Hydrogeological variables

A major hydrological challenge was to derive quantitative hydrogeological indices that demonstrate geological impacts on baseflow and runoff. Hydrogeological parameters such as porosity and permeability are often rare and time consuming to acquire. In addition,

hydrogeological characteristics are highly variable in space and differ across different lithologies. Therefore, only four variables were included in this study to represent the hydrogeological parameters for each of the selected watersheds: the available water storage data from 0 to 150 cm, depth to water, transmissivity and hydraulic conductivity. The compilation of these datasets include publicly available published and unpublished data from different resources in Texas, for instance well records at the Texas Water Development Board (TWDB) dataset, files from municipal and industrial groundwater users and water-supply companies, and published and open-file reports of the USGS, TWDB and the Bureau of Economic Geology (BEG). The soil available water storage data were acquired from SSURGO soil data that generally extend 150 cm below the land surface. For this variable, the underlying soil layer was considered to represent the top of the saturated zone, in addition, the texture properties of these deeper layers was assumed to be identical to the material close to the water table (Lorenz & Delin, 2007). These watershed properties, their symbols and units are presented in Table 5.2.

Table 5.2. Variables representing watershed properties for developing regression model.

	Variables	Descriptions	Units
Topography and geomorphology	BFI	Baseflow index	-
	WSA	Watershed areas	km ²
	DA	Basin drainage areas for each stream gauge	km ²
	SPI	Stream power index	-
	STI	Sediment transport index	-
	TStrL	Total stream length	km
	StrD	Stream density	km/km ²
	WSlp	Average watershed slope	%
	Elev	Average watershed elevation	m
	Relv	Average watershed relief	m
TI	Topographic index	-	
Meteorology	PRCP	Annual precipitation	mm
	TMAX	Maximum temperature	°C
	TMIN	Minimum temperature	°C
	TAVG	Average temperature	°C
	ET	Annual Evapotranspiration	mm
Land use	Brn	Barren lands	%
	Clt	Cultivated areas	%
	Dvlp	Developed areas	%
	Frst	Forests	%
	Hrb	Herbaceous cover	%
	Srb	Shrubland	%
	Wtr	Water cover	%
	Wtl	Wetland areas	%
Soil	HydxA, B, C, D	Hydrologic soil group A, B, C and D	%
Lithology	All	Alluvial sediments	%
	Cstl	Coastal zone sediments	%
	Coll	Colluvial sediments	%
	Eol	Eolian sediments	%
	Res	Residual deposits	%
Hydrogeology	WTD	Depth to water	m
	Tr	Transmissivity	m ² /day
	K	Hydrologic conductivity	m/day
	AWS	Available water storage at depth 0-1.5 m	m

5.2.5 Model development

Texas climate varies across the state. Therefore, in order to acquire higher prediction for baseflow, the watersheds in this study were categorized into five divisions according to Texas climatic zones. Smakhtin (2001) suggested that developing distinct regression models for separate regions across the study area would improve the accuracy of baseflow prediction. As stated by the National Data Center, Texas has ten primary climate zones (Figure 5.6). These zones represent areas with similar properties such as temperature, precipitation, humidity, vegetation and seasonal weather changes (Texas Water Development Board, 2012). These zones are listed, from Eastern to Western Texas as follows:

- *East Texas* with sub-tropical humid mixed evergreen-deciduous forestland.
- *Upper Coastal Plain* characterized by sub-tropical humid marine prairies and marshes.
- *North Central* with sub humid mixed savanna and woodland.
- *South Central* zone characterized by sub-tropical sub-humid mixed savanna, woodlands and prairie.
- *Edwards Plateau* characterized by sub-tropical climate and semi-arid savanna and brushland.
- *Southern Plain* also characterized by sub-tropical climate and semi-arid savanna and brushland.
- *Lower Valley* with sub-tropical sub-humid marine.
- *Low Rolling Plains* characterized by sub-tropical steppe and semi-arid savanna.
- *High Plains* with a continental steppe climate and semi-arid savanna.
- *Trans Pecos* that is mainly sub-tropical arid desert.

Based on these classifications and numbers of watersheds within each zone, these zones were divided into five categories to develop multiple distinct models for each of them. Category 1 includes the East Texas and Upper Coastal Plain, Categories 2 and 3 include the North Central and South Central zones, respectively. Edwards Plateau, the Southern Plain and the Lower Valley lie in Category 4. Finally, Category 5 occupies the High Plains, Low Rolling Plains and the Trans Pecos zone (Figure 5.6).

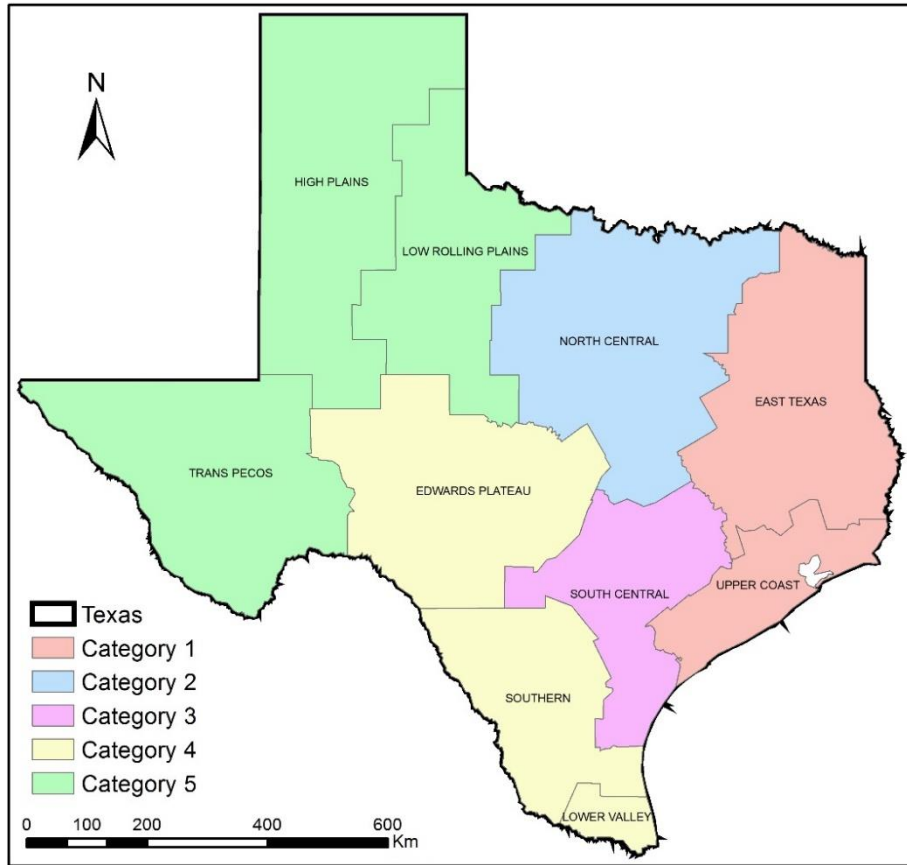


Figure 5.6. Climate zones of Texas and categories used in this study.

The BFI values estimated from the digital filter for the period 1980 to 2017 in 113 watersheds were used to develop the model. The remaining 27 basins were used for model validation and to assess model efficiency for various spatial conditions. These 27 watersheds were randomly selected from each of the previously mentioned categories using bootstrap-resampling. Before model development, watershed variables were logarithm-transformed to meet the normality requirement using the following equation:

$$\log(BFI) = \log(Y_0) + Y_1 \log(X_1) + Y_2 \log(X_2) + Y_3 \log(X_3) + \dots Y_n \log(X_n) \quad (5.2)$$

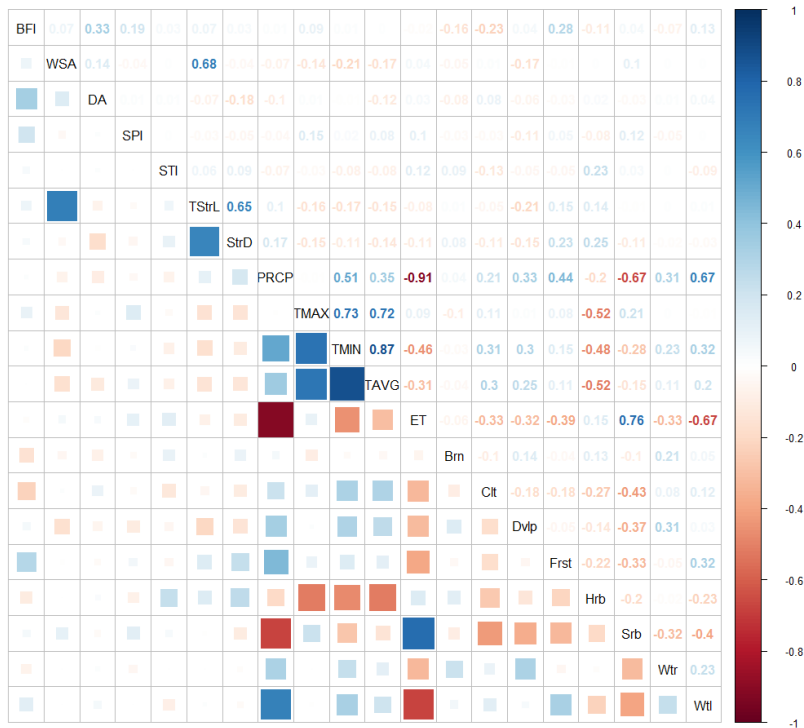
where Y_0 is the regression constant; $X_1, X_2, X_3, \dots, X_n$ are basin physical properties; $Y_1, Y_2, Y_3, \dots, Y_n$ are the regression coefficients, as used before in similar studies (Ahiablame et al., 2013b; Bloomfield et al., 2009; Zhang et al., 2013a; Zhu & Day, 2009). In addition, in this research, preliminary outputs showed that the correlation coefficients (R^2) of the developed regression

model were slightly greater with the use of logarithm-transformed variables than with the use of untransformed variables. The watershed variables were also transformed using the Box-cox transformation (Yue, 1999); however, the logarithm-transformed outputs showed higher R^2 for the regression model.

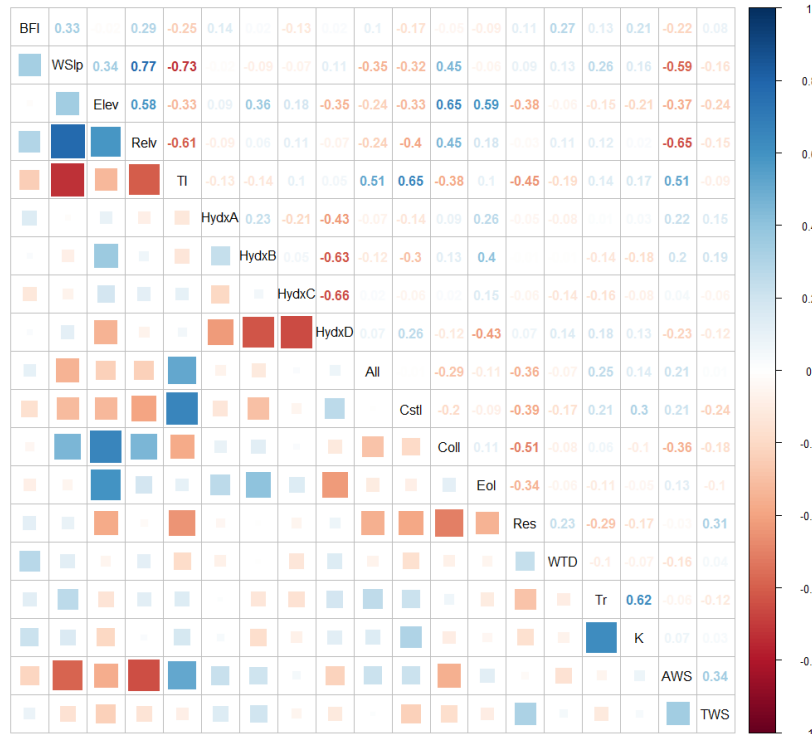
For an ideal model prediction, the correlation should include independent parameters and be physically sensible and statistically significant when producing good BFI estimates. The Auto Correlation Function (ACF) and the Spearman's correlation test were applied to evaluate the independency and the correlation, respectively, between the selected variables. The correlation analysis showed that the transformed variables were independent in this research, but there were some correlations among them. For instance, PRCP and ET were highly correlated. A strong correlation was also found between TAVG and TMIN variables (Figure 5.7).

Based on the computational complexity and number of variables, three scenarios were used to develop the regression models. The first two scenarios used variables that represented areas and stream geomorphologies in addition to meteorological and land use variables (Figure 5.7a). Scanlon et al. (2002) suggested that the geomorphology, land use and meteorological variables should be considered in developing a model for groundwater estimation. The third scenario used topography, hydrogeological, soil, and lithology variables in order to relate BFI to surficial geology in the region (Figure 5.7b). In baseflow research, soil and geology must be considered together since the groundwater flows through both (Lacey & Grayson, 1998). This procedure was important to avoid highly correlated variables in the same scenario that might lead to multicollinearity. Multicollinearity can increase the estimates of coefficient variance and make these estimates sensitive to minor changes in the model, which in turn could negatively affect model stability and quality (Zhu & Day, 2009). Therefore, to avoid multicollinearity and to attain simplicity in the model, scenarios 1 and 2 retained only one parameter from a group of highly correlated parameters in which the correlation coefficient was greater than ± 0.85 . For instance, the correlation between precipitation (PRCP) and evapotranspiration (ET) was -0.91, hence the PRCP was used in scenario 1, while ET was used in scenario 2. The non-highly correlated parameters were all retained for model development and were divided to form three scenarios. The first scenario used variables WSA, DA, SPI, STI, TStrL, StrD, PRCP, TMAX, TMIN, Brn, Clt, Dvlp, Frst, Hrb, Srb, Wtr and Wtl. Scenario 2 retained variables WSA, DA, SPI, STI, TStrL, StrD, ET,

TMAX, TAVG, Brn, Clt, Dvlp, Frst, Hrb, Srb, Wtr and Wtl. Scenario 3 used variables represented in Figure 5.7b.



(a)



(b)

Figure 5.7. Correlation matrix of watershed variables used for BFI prediction in this study. (a) variables representing topography, stream properties, metrology and land use; (b) variables representing geomorphology, soil, lithology and hydrogeology.

After the selection of independent parameters, an initial stepwise multiple regression model was developed using the parameters listed in Figure 5.7. This procedure yielded a large number of regression models; however, the best model was selected based on a combination of explanatory statistical indices and variables, for instance, Akaike Information Criteria (AIC), p -values, correlation coefficient (R^2), and adjusted R^2 . The p -values were used to check the significance of individual parameters. The residuals of the fitted model were also checked for normality. The AIC is used to choose the best predictor subsets in regression models and for comparing non-nested models, which ordinary statistical tests cannot perform. Larger differences in AIC indicate stronger evidence for one model over the other. The R^2 values measure the percentage of parameter variability described by the regression equation.

During stepwise regression modeling, variables were removed when their coefficient at 90% confidence level was not significantly different from zero. However, one of the main goals of this research was to evaluate the optimal regression model for BFI prediction; therefore, all variable combinations were used in developing the model. Of note, this study hypothesized that some variables would be more useful than others in BFI prediction. The stepwise multiple regression analysis identified the best model predictors for BFI. The model that provided a higher correlation coefficient, AIC value, adjusted R^2 , had all variables that were significant and was represented by a minimum number of basin variables, was finally selected for each scenario tested. Finally, an afterwards check for multicollinearity of the developed model was applied using the variance inflation factor (VIF). This step is necessary to measure the degree of collinearity present for each parameter included in the developed model. If the VIF is equal to 1, there is no multicollinearity among parameters; however, a VIF greater than 10 indicates the presence of high multicollinearity that is strong enough to require remedial measures, and therefore, they were omitted from the developed model (Lin, 2008). VIF for an independent factor x_i was calculated as:

$$VF = \frac{1}{1 - R_i^2} \quad (5.3)$$

where R^2 is the coefficient of determination that is acquired when x_i is regressed on all other independent variables in the model (Lin, 2008). In this study, factors that have VIF values more than 5 were removed from the developed model.

A total of 15 best regression models for BFI prediction in the study region were developed, one for each of the three scenarios for the five categories listed above. Multiple linear regression was utilized to develop a model for transferring the filtered BFI at the gauging stations to the prediction of BFI at ungauged stations in the following expression:

$$BFI = Y_0 \times X_1^{Y_1} \times X_2^{Y_2} \times X_3^{Y_3} \times \dots \times X_n^{Y_n} \quad (5.4)$$

Within the inverse logarithmic function, Equation 5.4 is the retransformed version of equation 5.2. Hence, the multiple linear regression models were created based on the transformed parameters. The graphical outputs of these equations were validated using statistical indices to assess the performance of the model. The coefficient of determination (R^2), Nash–Sutcliffe model efficiency (ENS), PBIAS and Relative Error (RE) were used to evaluate the accuracy of the regression outputs (Nash & Sutcliffe, 1970). A regression with lower RE was usually more accurate than one that had a higher RE. The formulas for R^2 and ENS, PBIAS and RE were previously outlined by Gupta et al. (2009) and Nie et al. (2011) and can be calculated as follows:

$$R^2 = \left[\frac{\sum_i [(Y^{obs} - \mu^{obs})(Y^{per} - \mu^{per})]^2}{\sqrt{\sum_i (Y^{obs} - \mu^{obs})^2 \sum_i (Y^{per} - \mu^{per})^2}} \right]^2 \quad (5.5)$$

$$ENS = 1 - \left[\frac{\sum_i (Y^{obs} - Y^{per})^2}{\sum_i (Y^{obs} - \mu^{obs})^2} \right] \quad (5.6)$$

$$PBIAS = \frac{\sum (Y^{obs} - Y^{per})}{\sum Y^{obs}} \times 100 \quad (5.7)$$

$$RE = \frac{Y^{per} - Y^{obs}}{Y^{obs}} \times 100 \quad (5.8)$$

where Y^{obs} is the observed BFI data separated from the digital filter, Y^{per} is the simulated BFI output, μ^{obs} and μ^{per} are the mean of the observed and simulated BFI, respectively. Literature suggests that there is a consensus that the model performance is satisfactory when the values of R^2 and ENS are greater than 0.5 and PBIAS is less than 30% (Engel et al., 2007; Moriasi et al., 2007; Santhi et al., 2001). The RE and the absolute relative error (ARE) will be displayed in boxplots for better interpretation. ARE is the absolute value of the difference between the

measured value and the true value. ARE is different from RE in which ARE measures how large the error is, while the RE measures how large the error is relative to the correct value. After fitting the model, it was also critical to check the residual plots for each of the developed models to avoid the presence of unwanted patterns in the model. The advantage of using stepwise multiple regression modeling in this study lies in the availability of a group of models rather than one model, which in turn helped in generalizing the relationships between basins' properties and BFI; however, this may lead to a group of models that shows similar fits to the dataset (Ahiablame et al., 2013b). The best models were selected as described above. A flow chart depicting procedures used in this study is shown in Figure 5.8.

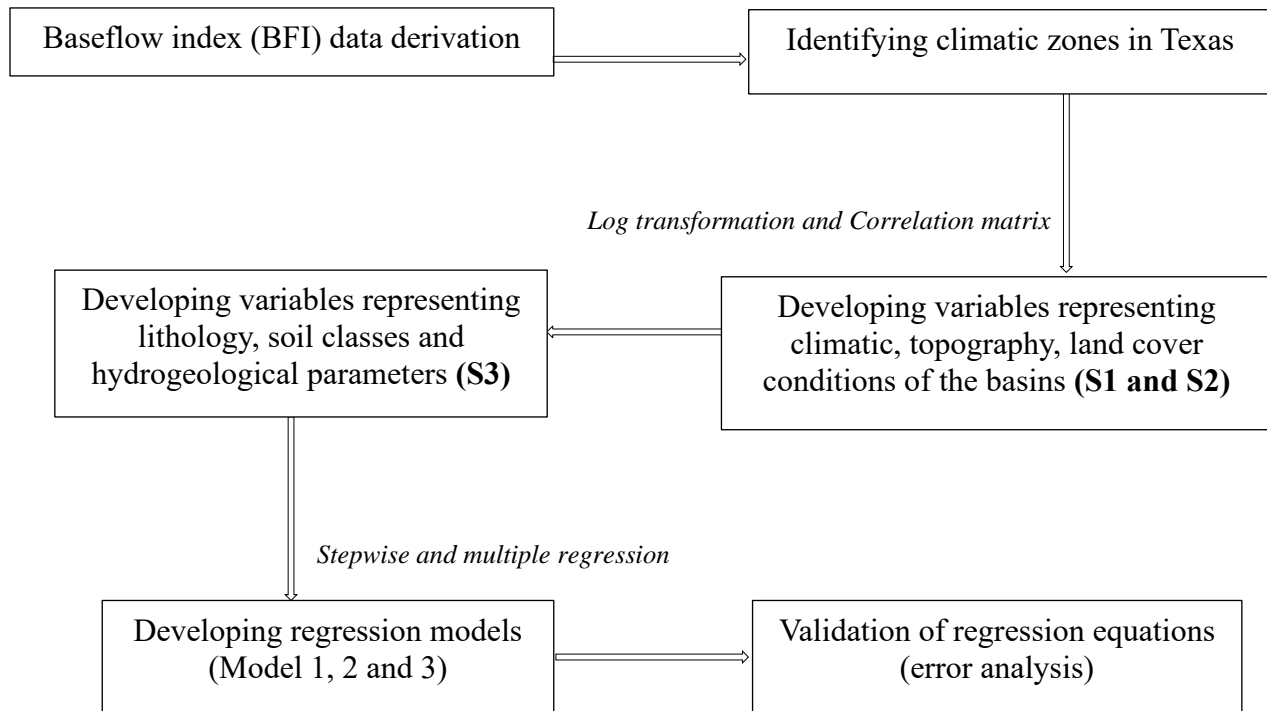


Figure 5.8. Flow charts showing the procedures to develop models examining the relationship between baseflow and watershed properties.

5.3 Results and Discussions

5.3.1 BFI estimation

One aim of this study was to provide an estimate of the contribution of baseflow to total streamflow, using the evaluation of statewide datasets from gauged stations across Texas, US. Baseflow contribution was exhibited using the BFI. A key advantage of using BFI rather than absolute baseflow components was that it provided better comparability across watersheds having different stream densities and total streamflow. In addition, BFI has previously been shown to give smaller variance and better evaluation of the baseflow and direct runoff at the same time (Haberlandt et al., 2001).

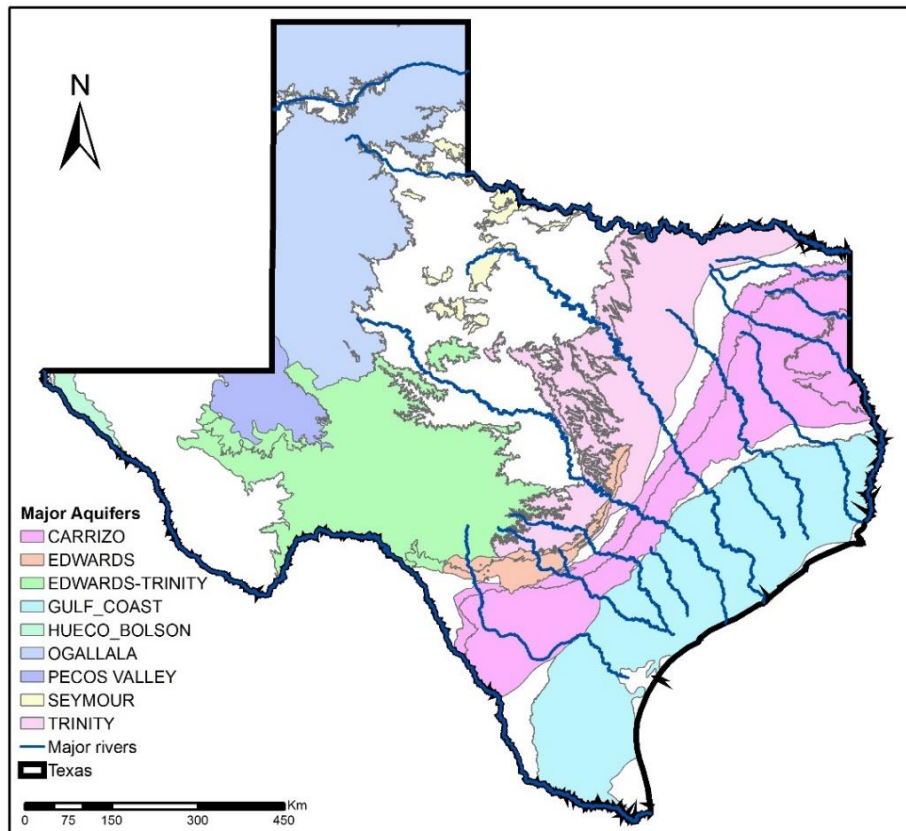


Figure 5.9. Map of major aquifers in Texas (Texas Water Development Board, 2012).

The groundwater contribution to surface water was found to be greatest in East Texas and around major aquifers in Middle Texas. The Edwards aquifer (Figure 5.9), that lies in a fault zone

in central Texas (Category 4), discharged the highest rate of BFI that ranged from 0.20 (Headwaters North Concho Watershed) to 0.70 and had a mean value of 0.52 (Montell Creek Watershed). The differences in BFI between these two watersheds was likely partially attributable to the reduced amount of precipitation received by the Headwaters North Concho Watershed. Springs and seeps (groundwater) in West Texas also contribute locally to significant baseflow to the river system (Category 5); however, the filtered BFI for the period 1980-2017 varied between 0.17 (Upper Palo Duro Creek Watershed) and 0.68 (Oasis Creek Watershed), and had a lower mean value for the BFI than Category 4 with a value of 0.43. The differences in BFI in Category 5 might be due in large part to the Upper Palo Duro Creek Watershed being covered by 86.5% soil type A, unlike many other watersheds in this category, and had a low runoff potential and high infiltration rate.

Across the 38 year time span, the average BFI for Category 1 ranged between 0.29 at the South Bédias Watershed and 0.68 at the Big Creek Watershed. The average BFI was 0.47 in Category 1. The lowest BFI recorded at the South Bédias Watershed might be attributed to the fact that the watershed was covered by 91.4% of low permeable residual materials, developed mostly in metamorphosed sedimentary rocks, that decreased the infiltration rate and groundwater discharge. Similarly to Category 1, the mean BFI for the 27 watersheds in Category 2 was 0.48 with minimum and maximum values of 0.19 (Royse City Watershed) and 0.66 (Village Creek Watershed), respectively. Although the Royse City Watershed had greater precipitation than the Village Creek Watershed, the lower BFI might be caused by the urban coverage and residual sediment, which were greater in the Royse City Watershed. Finally, for Category 3, the average, minimum, and maximum BFI were 0.50, 0.29, and 0.71, respectively. These baseflow outputs were comparable to previously published reports of the TWDB (George et al., 2011).

In general, among the 140 gauged stations selected for model development, BFI values for the whole study area, including the basins used for model validation, ranged between 0.17 to 0.74 with a mean value of 0.48, suggesting that 48% of the long-term streamflow in Texas was coming from shallow subsurface flow and groundwater discharge (Figure 5.6). The lowest BFI value was observed in northwestern Texas, particularly, in the northern Ogallala aquifer that is characterized by clayey soil and relatively small thickness that limits the amount of groundwater recharge to the stream (George et al., 2011). In contrast, the highest BFI was recorded across several regions, including western Texas (Courtney Creek Watershed), as well as central southern Texas

(Headwaters Frio Watershed), particularly, in the Pecos Valley aquifer and Edwards-Trinity (Plateau) aquifer, respectively. Groundwater in the Pecos Valley Aquifer was unconfined. The high BFI for West Texas, the Courtney Creek and Narrow Bow Draw Watersheds, might be attributed to the top of the aquifer, that is exposed at the ground surface over the entire extent of the aquifer, leading to higher groundwater discharge. Springs and seeps in West Texas, where the water table intersects canyons or surface topography, also contribute locally significant baseflow to streams. Another explanation for this might be partial recharge by seepage from ephemeral streams, cross-formational flow, and lower irrigation pumpage rates in the Pecos Valley Aquifer (Meyer et al, 2012; Texas Water Development Board, 2012). The Edwards-Trinity aquifer is mostly under water table or unconfined aquifers that are composed of sand, fractured limestone and dolomite. Natural discharge from the Edwards-Trinity aquifer to surface water occurs mostly from springs along the margins of the aquifer where the water table intersects the ground surface (Bruun et al., 2016). The Edwards is also called the fault zone aquifer, in which the highly fractured limestone outcrop at the surface, allowing large amounts of natural recharge called allogenic recharge, in which the streams cross the permeable formation and go underground, for instance sinkholes that can receive large amounts of recharge and transmit it directly into the aquifer (<https://www.edwardsaquifer.net/intro.html>). Overall, BFI tends to be greater in the eastern side of the state. However, there was no specific pattern for BFI variation across Texas (Figure 5.10). Of note, without explicitly taking basin areas into account, the WHAT model was more likely to overestimate BFI for larger basins. This may be because the algorithms of the model estimate baseflow with substantial smoothing (Lim et al., 2005).

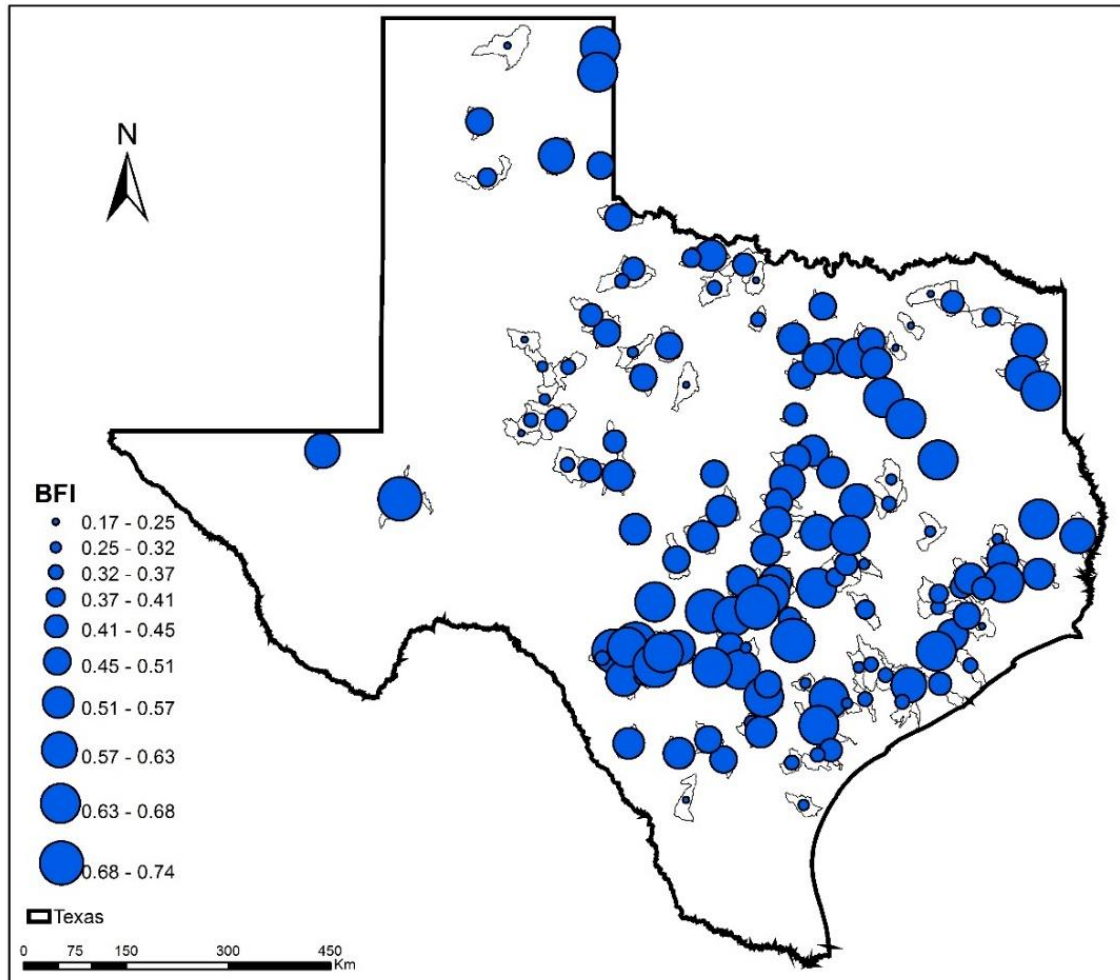


Figure 5.10. BFI at gauged station locations of each selected watershed in this study.

5.3.2 Regression models

5.3.2.1 Category 1

The Category 1 area represents the northern part of the Carrizo aquifer and north and central Gulf Coast aquifers. The Carrizo aquifer is primarily composed of sand locally interbedded with gravel, silt, clay, and lignite. The Gulf coast aquifer lies parallel to the Gulf of Mexico coastline and is primarily composed of discontinuous sand, silt, clay, and gravel beds of Miocene to Holocene age (Figure 5.9). The best low-flow prediction model under the three scenarios, developed in section 5.2.5, involved different variables, but had values of R^2 greater than 0.83 (Table 5.3). Based on an F -test, the best models were significant (p -value < 0.0001) for both

scenarios 1 and 2, and the p-value was less than 0.05 for scenario 3. Significant variables included in scenarios 1 and 2 were similar with the exception that scenario 1 contained the variable PRCP, that was replaced by ET in scenario 2. ET was found to have no impact on BFI prediction in scenario 2 due to the high humidity for the Category 1 region (Figure 5.3). Only the AWS and K variables were significant, at 90% confident level, for BFI prediction in the third scenario. These results suggest that BFI could be modeled using common log transformed meteorological, hydrogeological and topographical parameters with high reliability indicated by the high R² (0.93, 0.83 and 0.95 for scenarios 1, 2 and 3, respectively) and adjusted R² values (0.84, 0.77, and 0.75 for scenarios 1, 2 and 3, respectively) summarized in Table 5.3. Of note, for the same model scenarios, the R² and adjusted R² values were lower than that of the transformed variables.

Table 5.3. Baseflow prediction models developed for the Category 1 area.

Scenario	Model	AIC	R ²	Adj R ²	P-value
S1	$BFI = 5.997 \times WSA^{0.301} \times DA^{0.072**} \times STI^{0.389**}$ $\times TStrL^{0.048} \times PRCP^{2.838*} \times Clt^{0.114*}$ $\times Dvlp^{0.024} \times Wtl^{0.058}$	-67	0.93	0.84	<0.0001
S2	$BFI = -1.081*** \times WSA^{0.296**} \times DA^{0.089***} \times STI^{0.179}$ $\times Clt^{0.139***} \times Devlp^{0.041}$	-60	0.83	0.77	<0.0001
S3	$BFI = -3.801 \times WSlp^{0.817} \times Elev^{0.263} \times TI^{2.376}$ $\times AWS^{0.278} \times All^{0.005} \times Cstl^{0.028}$ $\times K^{0.072}$	-63	0.95	0.75	0.0451

,*, **, and *** stand for statistically significant at 0.1, 0.05, 0.01, and 0.001 probability levels

The evaluation of three model scenarios in the 24 watersheds selected in Category 1 showed that the RE for scenario one varied from -11 to 20%. However, for scenario 2, a larger range, between -20 to 35%, and higher maximum RE were observed. From the model for scenario 3, we showed a lower percentage for the RE, between -16 and 14% (Figure 5.11). The median values for the ARE varied from 5 to 14%, while all scenarios had 3rd interquartile range of less than 9%,

indicating that, with a probability of over 75%, the ARE values were within 9% (Figure 5.12). Model assessment statistics for BFI prediction are summarized in Table 5.4. The R^2 and ENS values between the observed and predicted BFI for model development ranged between 0.82 and 0.93, while the PBIAS varied between -0.3 and -0.7. These findings suggested that model development in scenarios 1 and 3 were slightly better than scenario 2 (Figure 5.13). This observed variance might be attributed to having fewer descriptive parameters in the scenario 2 model. In addition, the presence of the PRCP variable in scenario 1 gave higher prediction accuracy. Precipitation was found to have a significant impact on the amount of groundwater discharge, specifically in humid areas (Aboelnour et al., 2019; Zhu & Day, 2009).

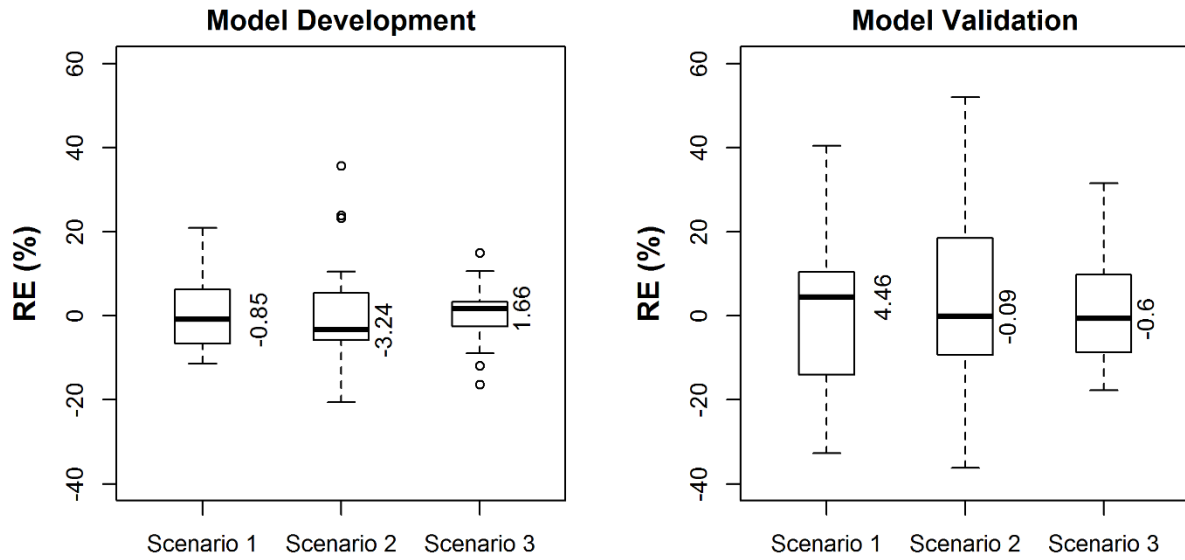


Figure 5.11. Boxplots of RE for BFI prediction model development and validation for the Category 1 region.

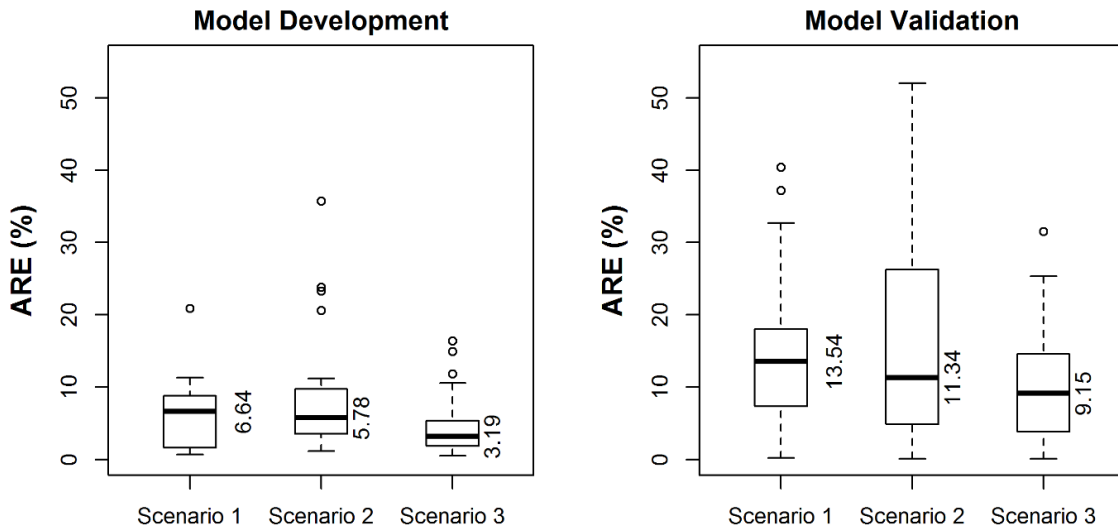


Figure 5.12. Boxplots of ARE for BFI prediction model development and validation for the Category 1 region.

Table 5.4. Values of statistical indicators in model development and validation for BFI prediction in the Category 1 region.

Scenarios	Model development			Model validation		
	R ²	ENS	PBIAS	R ²	ENS	PBIAS
Scenario 1	0.93	0.93	-0.3	0.73	0.72	-1.1
Scenario 2	0.82	0.82	-0.6	0.60	0.57	-1.5
Scenario 3	0.93	0.93	-0.3	0.84	0.84	-0.8

As shown in Figure 5.13, the filtered and predicted BFI showed similar values, indicating some uncertainty in the developed model, as would be expected but with overall agreement of the data. Notably, models for scenarios 1 and 2 showed the highest accuracy. One particular prediction of note that deviates from the filtered BFI was observed in scenario 2 for the Cypress Creek Watershed. The model overestimated the predicted BFI, compared to the filtered BFI value of 0.56; the model predicted BFI was 0.69. This deviation could be in part attributed to the effect on baseflow by the large forest cover (46%) and high topographic index that facilitates baseflow discharge to the stream network within the watershed.

The developed models in the three scenarios were further validated using randomly selected basins from each category during the 1980-2017 study period. Using the model validation watersheds that consist of 27 basins, results provided poorer BFI prediction evaluation metrics than for the development basins with a median RE of 4.46, -0.09 and -0.6% for scenarios 1, 2 and 3, respectively (Figure 5.11). The validation model for the three scenarios had a RE interquartile ranging from -6 and 9%. The median ARE had values of 13.57, 11.34, and 9.15 for scenarios 1, 2 and 3, respectively (Figure 5.12). For the validation dataset, the computed BFI from the filtered USGS streamflow values were reasonably close to the predicted ones. However, the scenario 2 model provided poorer performance than scenarios 1 and 3. This might be attributed to the absence of the PRCP parameter in scenario 2 compared to scenario 1. The evaluation indices R², ENS, and PBIAS for the validation dataset are listed in Table 5.4. In general, the validation dataset resulted in better BFI prediction in scenario 3 with values of 0.84, 0.84 and -0.8 for evaluation indices R², ENS, and PBIAS, respectively.

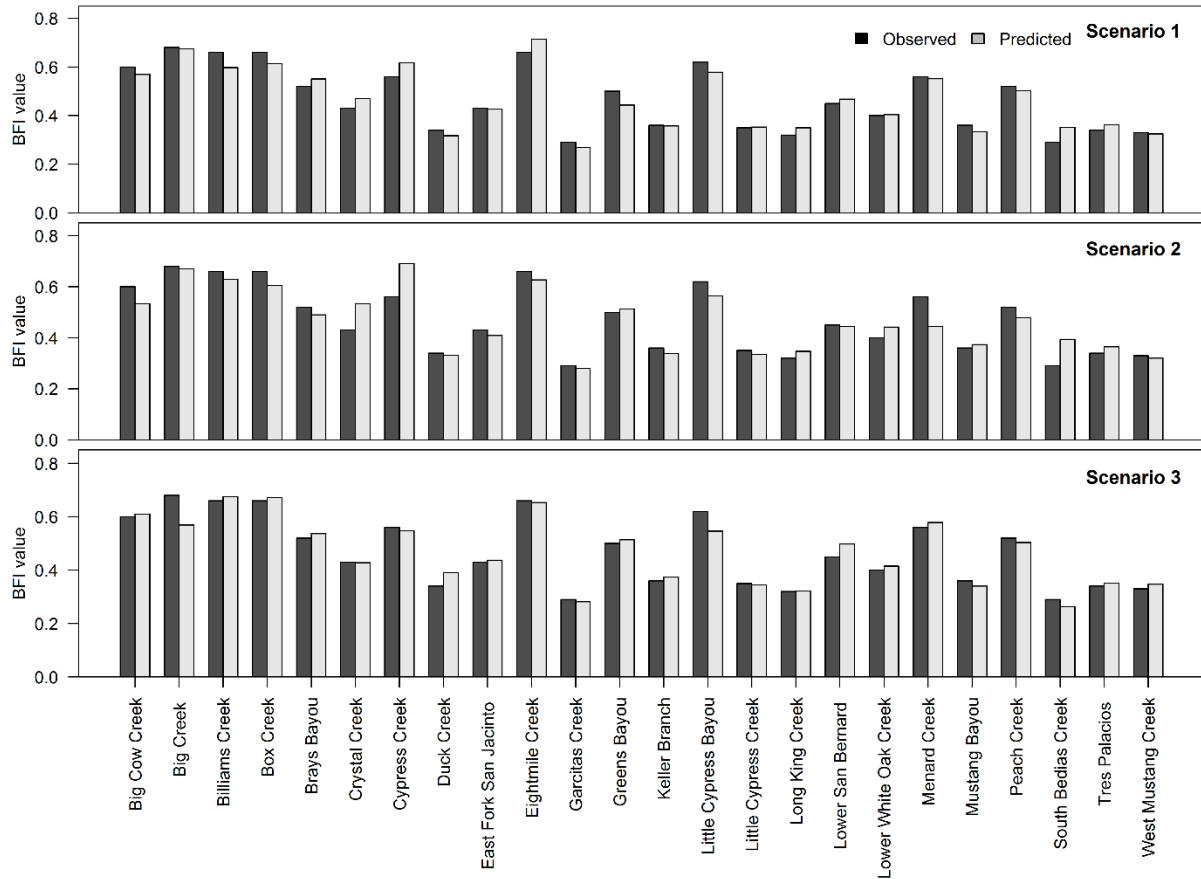


Figure 5.13. Observed (filtered) and predicted BFI measured within the three scenarios in the Category 1 region.

It should be noted that the highest deviations between the filtered and predicted BFI for the validated dataset were observed in the Headwater Frio and Courtney Watersheds in Scenario 2, and Marcelinas Watershed in Scenarios 1 and 2 (Figure 5.14). The model in general tended to underestimate the values in the Marcelinas Watershed. This could be explained by the PRCP variable in which the Marcelinas Watershed had lower annual precipitation compared to other basins included in the validation dataset. Similarly, the Headwater Frio Watershed tends to underestimate BFI prediction in all scenarios because the baseflow in a watershed does not necessarily originate from areas within the border of the watershed, but can migrate from surrounding watersheds as well. The Headwater Frio Watershed lies in the Central Southern Texas and is surrounded by another three watersheds that were included in this study, hence, that might exaggerate the amount of observed baseflow. The Headwater Frio Watershed lies at the southern part of the Balcones fault that enhance the interconnection among the watersheds by fault-

generated fracture system that allow long-distance inter-basin groundwater transfer from higher western topographical areas to the lower, more permeable discharge points towards the east (Woodruff and Abbott, 1986). The Courtney Watershed lies in the western part of Texas and resulted in the highest filtered BFI (0.74). Although the watershed was characterized by low average water storage, the large variability in topography and high conductivity might have enhanced the groundwater flow in the watershed leading to higher prediction of BFI.

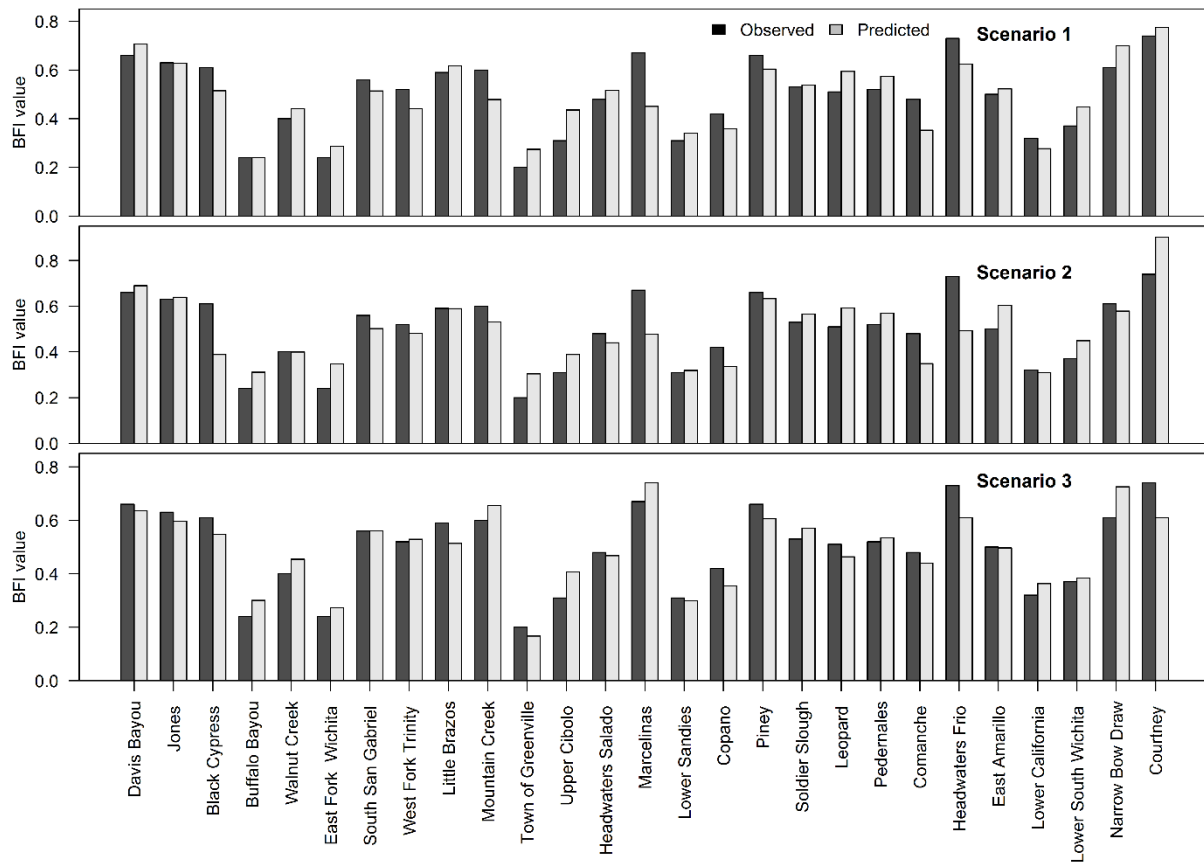


Figure 5.14. Observed (filtered) and predicted BFI for the validation dataset within the three scenarios in the Category 1 region.

5.3.2.2 Category 2

The Category 2 region covers the northern Trinity aquifer in the northeast part of the state (Figure 5.9). The aquifer is composed of several water-bearing formations within the Trinity

Group that consists of limestones, sands, clays, gravels, and conglomerates. The productivity of the aquifer is mainly affected by the thickness and distribution of sandstone. These sandstones were deposited in two different environments resulting in a stratified network of aquifers and aquitards in the Northern Trinity Group that covers the Category 2 region (Bruun et al., 2016).

The regression analysis resulted in the development of two similar models for scenarios 1 and 2, with the exception that scenario 2 involved the variable *Frst* that was not statistically significant at the 0.1 probability level. The watershed properties that affected the BFI in Category 2 included drainage areas, stream power index, maximum temperature, and urban cover for scenarios 1 and 2. These variables were statistically significant at different probability levels. Variables elevation, topographic index, hydrologic soil groups A, B and C, water storage, and alluvial deposits influenced the BFI prediction in scenario 3. Except for *HydxB*, all other parameters were statistically significant. These parameters have previously been utilized for predicting a high precision BFI (Zhang et al., 2013; Zhu & Day, 2009). The fact that the variables *Frst* and *HydxB* are not significant in scenarios 2 and 3, respectively, for BFI prediction, can be explained by the presence of highly significant of urban and *HydxA* parameters in scenarios 2 and 3. Therefore, it makes these variables less important compared to others. The regression models showed that all models developed in the three scenarios had p-values less than 0.0001; however, scenario 3 had higher prediction accuracy with values of -59, 0.89 and 0.79 for AIC, R^2 and adjusted R^2 , respectively (Table 5.5). Although Category 2 represents a humid region, scenarios 1 and 2 lacked precipitation variables in the prediction model and this was likely attributed to the delayed precipitation response, particularly for large watersheds (Ahiablame et al., 2013b). The variables that best predicted BFI in the Category 2 area included elevation and topographic index, in addition to hydrologic soil groups A, B and C. Elevation and topographic index regulate the rate at which soil water moves down a slope, and therefore dictates whether the runoff post event will be directly flushed to the river system or stored in the soil (Price, 2011). As previously mentioned, the impact of hydrological soil groups has a geological impact on BFI prediction. Different soils with differing infiltration capacity were determined by the rock type, which is known to influence groundwater discharge. Different studies have shown that a high correlation between BFI prediction and basin TI, elevation, and percentage of sand in different soil groups exists (Bloomfield et al., 2009; Lacey & Grayson, 1998; Santhi et al., 2008). In addition, average water storage contributed to BFI prediction, in which the *AWS* parameter had an important role in water

redistribution towards the basin outlets (Hector et al., 2015). Additionally, watersheds representing Category 2 had lower stream density and higher forest cover compared to other categories, which may be related to subsurface storage characteristics, with lower stream densities possibly negatively correlated with subsurface water storage capacity. The forest cover has been shown in other studies to increase the infiltration rate and the recharge to subsurface water storage (Price, 2011). Finally, alluvial deposits are closely related to the presence and the extent of baseflow, in which the quantity of groundwater recharge was found to be correlated to topographic positions that have greater cover of alluvial deposits (Schilling, 2009).

Table 5.5. Baseflow prediction models developed for the Category 2 area.

Scenario	Model	AIC	R ²	Adj R ²	P-value
S1	$BFI = -7.463^{**} \times DA^{0.066^{**}} \times SPI^{0.211^{***}} \times TMAX^{4.155^{*}} \times Dvlp^{0.156^{***}}$	-54	0.84	0.74	<0.0001
S2	$BFI = -8.596^{***} \times DA^{0.059^{*}} \times SPI^{0.228^{***}} \times TMAX^{4.978^{**}} \times Dvlp^{0.159^{***}} \times Frst^{-0.070}$	-52	0.76	0.70	<0.0001
S3	$BFI = 4.764^{***} \times Elev^{-0.841^{***}} \times TI^{0.263} \times HydxA^{4.584^{***}} \times HydxB^{0.061} \times HydxC^{0.195^{**}} \times AWS^{-0.879^{**}} \times All^{0.199^{**}}$	-59	0.89	0.79	<0.0001

*, **, and *** stand for statistically significant at 0.1, 0.05, 0.01, and 0.001 probability levels

The three developed models were then applied to the 27 watersheds of Category 2 to compare between the filtered and predicted BFI values. The performance of the three models to predict BFI in Category 2 showed a slightly higher RE compared to Category 1 for the three scenarios. The RE ranges between -26 and 33% for scenario 1 with a median percentage of -1.79%, and varied from -25 to 41% for scenario 2, while it showed the smallest margins that ranged between -21 and 21% for scenario 3 (Figure 5.15). Similarly, the ARE showed relatively higher

percentages compared to Category 1, in which the 3rd interquartile for the three developed models ranged from 11 to 19%, indicating that ARE were below 19% with a probability over 75%. In addition, the median percentages were 10.87, 9.14, and 6.71 for scenarios 1, 2 and 3, respectively (Figure 5.16). These results hold promising outputs for predicting BFI values; however, the model developed for scenario 3 indicated higher accuracy for BFI prediction in the area of Category 2. This can be clearly seen in the outputs listed in Table 5.6. The R^2 and PBIAS values were 0.80, 0.72 and 0.85; and -0.5, -0.9, and -0.2 for scenarios 1, 2 and 3, respectively. Although the model developed in scenario 1 had less representative variables compared to scenario 2, it performed slightly better than scenario 2, indicating that adding variables did not improve the model, and that in this part of the state, the forest cover was not a significant factor affecting the BFI.

Figure 5.17 compares the predicted BFI values with the observed BFI determined by the equations listed in Table 5.5. When the forest land use variable was removed from scenario 2, the bias between the predicted and filtered BFI slightly decreased; however, the model including geological parameters showed the least deviation between the observed and predicted BFI values. The highest deviation was observed in the Lower Little River Watershed in the model developed in scenario 2, in which the predicted BFI was underestimated. This might be related to the higher temperature of the watershed compared to the others included in Category 2. Although the annual ET variable was not significant in scenario 2, the higher temperature played an important part in increasing evapotranspiration and leading to a decrease in infiltration. In addition, only 0.7 and 2.7% of water and wetlands, respectively, cover the Lower Little River Watershed, which would cause a decrease in the amount of water discharged to the subsurface.

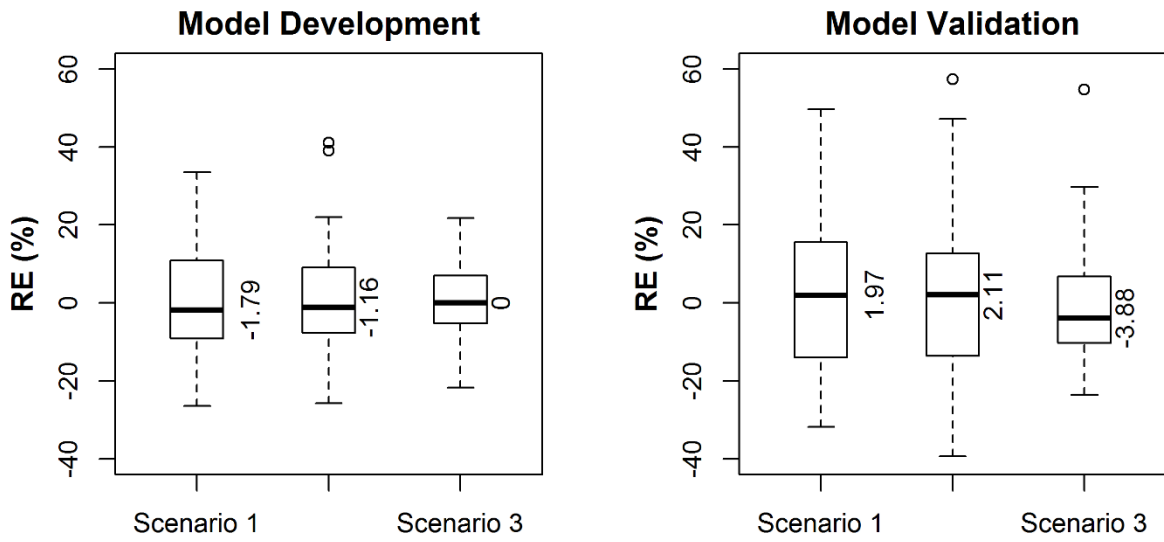


Figure 5.15. Boxplots of RE for BFI prediction model development and validation for the Category 2 region.

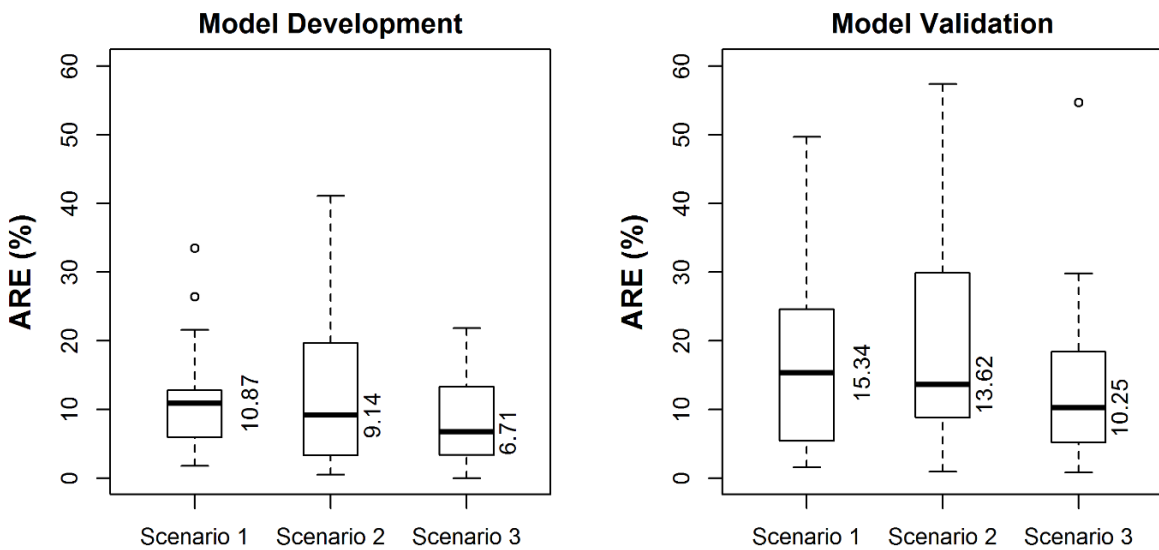


Figure 5.16. Boxplots of ARE for BFI prediction model development and validation for the Category 2 region.

Table 5.6. Values of statistical indicators in model development and validation for BFI prediction in the Category 2 region.

Scenarios	Model development			Model validation		
	R ²	ENS	PBIAS	R ²	ENS	PBIAS
Scenario 1	0.80	0.79	-0.5	0.65	0.64	-1.5
Scenario 2	0.72	0.71	-0.9	0.52	0.50	-2.3
Scenario 3	0.85	0.83	-0.2	0.75	0.75	-1.2

The regression models developed for Category 2 were tested for the period 1980 to 2017 using the 27 basin validation dataset. The performance of the model for validation showed similar trends to the model for the development dataset. Validation watersheds for scenario 2 appeared to have the lowest accuracy, and the RE percentage had a large range from -39 to 57%, while validation for scenario 3 had the narrowest range in the three scenarios (Figure 5.15). Table 5.6 showed the performance of model validation with respect to R², ENS and PBIAS which range from 0.52 to 0.75, 0.50 to 0.75, and -2.3 to -1.2, respectively. While these indices have been used extensively for model performance estimation, it is recommended different indices be used simultaneously to measure the model accuracy. Based on the outputs of these statistics and the percentage of RE, the model showed adequate performance for the validation datasets (Moriassi et al., 2007; Santhi et al., 2001). The consistency in the pattern across the RE and the three indices indicates that the differences between the filtered and predicted BFI for the validation dataset are not attributed to the suitability of the model but may be linked to other reasons such as anthropogenic activities in the region or data quality.

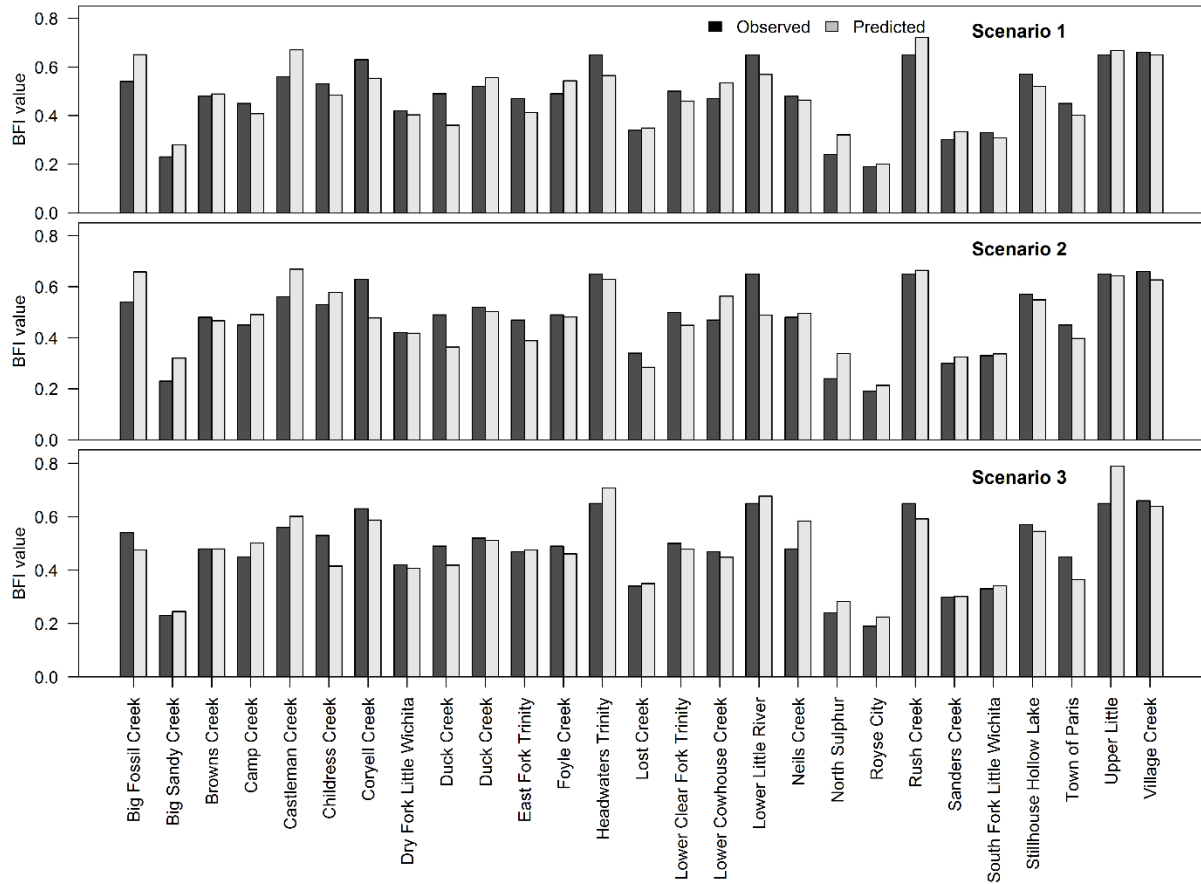


Figure 5.17. Observed (filtered) and predicted BFI measured within the three scenarios in the Category 2 region.

Results for model validation during the 1980 to 2018 period are shown in Figure 5.18. The underestimation for BFI prediction of the Headwaters Frio Watershed might be attributed to factors discussed above in Category 1, while the underestimation of BFI prediction in the Black Cypress Watershed in scenarios 1 and 2 might be related to lower temperature experienced in the watershed compared to others. Generally speaking, the developed models for the three scenarios tended to underestimate the prediction of BFI values in the validation dataset, leading to a slightly negative bias.

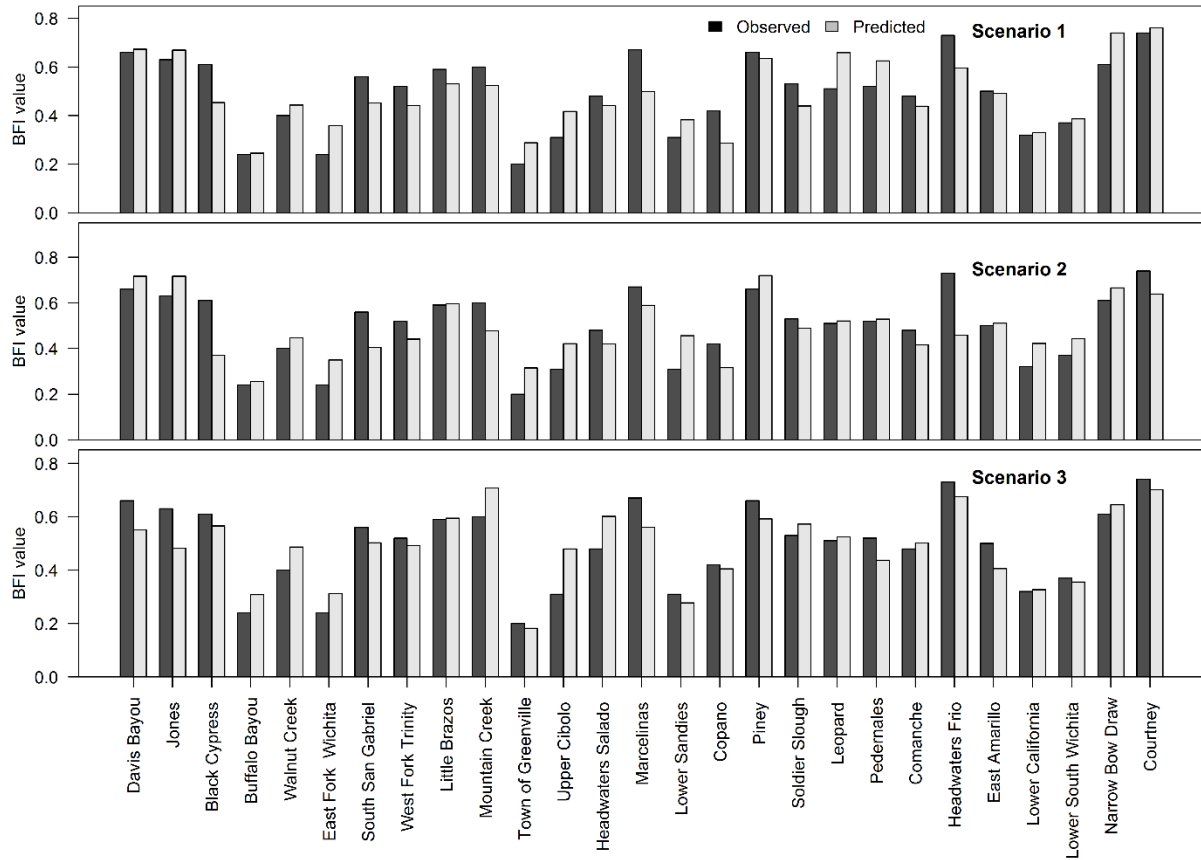


Figure 5.18. Observed (filtered) and predicted BFI for the validation dataset within the three scenarios in the Category 2 region.

5.3.2.3 Category 3

The Category 3 area is characterized by sub-tropical, sub-humid climates in the South Central part of the state that covers the Southern Trinity aquifer, the central parts of Carrizo and the Gulf Coast aquifers. The northern parts of the area are mainly covered by limestone and dolomitic rock types, while the central part is covered by the Middle Eocene Claiborne and Wilcox groups that mainly consist of a vertical sequence of alternating sandstones, siltstones, and claystones of variable thickness of interfering marine and non-marine units. These units can reach up to 800 m in thickness (Davies & Ethridge, 1971). The Central Gulf Coast aquifer consists of Tertiary and Quaternary clastic sediments composed of silt, clay, sand and gravel that dip southeast towards the Gulf of Mexico. The sediments were deposited in a wide array of settings ranging

from non-marine at the up-dip extent of the study area to marine along the coast (Texas Water Development Board, 2003).

The regression equation developed for this category showed that the model could predict BFI with high accuracy in this region (Table 5.7). Among the climate, landscape and geological descriptors, BFI can be predicted using variables DA, SPI, STI, TStrL, PRCP, Wtr and Wtl covers for scenario 1. The model for scenario 1 provided outputs of -61, 0.95, and 0.87 for AIC, R^2 and adjusted R^2 , respectively. Unlike scenario 1, BFI can be predicted by replacing the variables TStrL, PRCP and Wtl with parameters TMAX, ET and Frst cover for scenario 2, with predictive capacity higher than that of scenario 1. These variables are statistically significant at different probability levels for scenario 2; however, DA, Wtr and Wtl were not significant in scenario 1 (Table 5.7). Watershed areas included in Category 3 were characterized by a higher percentage of cultivated and forest cover compared to other Categories, with a percentage of 37 and 25%, respectively. Many studies associate higher watershed forest cover with lower BFI, due to the higher evapotranspiration rates of forests (Sahin & Hall, 1996; Swank et al., 1988), while others indicate increased BFI with higher watershed forest cover due to higher infiltration and recharge of subsurface water storage (Price, 2011; Santhi et al., 2008). Both forest cover and evapotranspiration were included in the model prediction for scenario 2. It can be clearly seen that the ET had a negative correlation with BFI, since ET depletes the water on which baseflow is dependent (Table 5.7).

For scenario 3, BFI can be predicted using the average watershed slopes, basin relief, hydrologic soil group B, water storage, alluvial and colluvial deposits and finally hydrologic conductivity. However, only the alluvial and colluvial lithology are statistically significant at 0.10 and 0.05 probability levels, respectively. Surface topographic properties may express the amount of colluvial deposits available and this likely explains the existence of the variables Relv and Coll in predicting BFI in scenario 3. Colluvial deposits are sedimentary deposits consisting of surface mantle formed at the base of a slope caused by the transportation by gravity and non-channelized flow (Fairbridge, 1968; Millar, 2015). Colluvial deposits have previously been shown to play an important role in shallow reservoirs and play a significant role in explaining the variability in magnitude of groundwater (Schulz et al., 2008). In the Category 3 region, that included 22 basins, only 9 watersheds were found to have colluvial deposits due to the high relief in these watersheds. This relief appears to affect the amount of groundwater discharge. Colluvial deposits that are

significant in scenario 3 may be related to the movement of water, such that the flow from bedrock to colluvium is more likely where the bedrock has layers with strong permeability contrasts that dip out of the slope.

Table 5.7. Baseflow prediction models developed for the Category 3 area.

Scenario	Model	AIC	R ²	Adj R ²	P-value
S1	$BFI = -1.369^{***} \times DA^{0.037} \times SPI^{0.230^{**}}$ $\times STI^{-0.141^*} \times TStrL^{0.182}$ $\times PRCP^{-1.166^{**}} \times Wtr^{0.055} \times Wtl^{0.013}$	-61	0.95	0.87	<0.0001
S2	$BFI = -7.125^{***} \times DA^{0.051} \times SPI^{0.173^{***}} \times STI^{-0.068}$ $\times ET^{-4.126^{***}} \times TMAX^{3.721^*}$ $\times Frst^{-0.110^*} \times Wtr^{0.051^*}$	-81	0.97	0.95	<0.0001
S3	$BFI = -1.076 \times WSlp^{0.239} \times Relv^{0.263} \times HydxB^{0.044}$ $\times AWS^{0.191} \times All^{0.094} \times Coll^{0.108^*}$ $\times K^{0.096}$	-87	0.99	0.94	<0.0001

,*, **, and *** stand for statistically significant at 0.1, 0.05, 0.01, and 0.001 probability levels

The performance of the three models to predict BFI in ungauged stations in Category 3 showed lower RE percentages compared to Categories 1 and 2 for each scenario. The 3rd interquartile RE ranges were less than 5% in all scenarios with a median of -0.69, 0.12, and 0.49 for scenarios 1, 2 and 3, respectively (Figure 5.19). Scenario 3 had the narrowest RE percentages indicating that the model developed using soil and hydrogeological parameters could predict BFI values with the highest accuracy in Category 3. Similarly, the model validation showed a promising RE percentage; however, the highest prediction accuracy in scenario 1 had a median RE percentage of -0.81. The ARE of the models for the development and validation datasets did not differ from the relative prediction errors. Scenario 3 had the narrowest ARE for model development that varied from 0.2 to 8% with a median value of 1.8%. On the other hand, the validation dataset had the narrowest range of ARE with respect to scenario 1, with ranges from

zero to 33% (Figure 5.20). Although the three scenarios had slight differences in the evaluation indices, they predicted the BFI for the development and validation datasets precisely. The R^2 and ENS for the three scenarios varied from 0.94 to 0.98; in addition, the scenario had a low bias percentage of -0.1 (Table 5.8). In general, the results of errors together with the statistical indices suggested that the BFI can be predicted using the model developed with high accuracy. However, the validation dataset had lower performance for the three scenarios. The R^2 , ENS and PBIAS ranged from 0.68 to 0.71, 0.67 to 0.70, and -1.0 to -1.4, respectively (Table 5.8). This variation might be attributed to the change in meteorological patterns across the state since the validation dataset was randomly selected from each of the five categories and may have important features that specifically affect BFI values such as geology or land cover and use. However, the outputs of these statistical indices indicated that the predicted BFI values in the validation dataset were in ‘Very Good’ agreement, according to the Moriasi et al. (2007) criteria.

Table 5.8. Values of statistical indicators in model development and validation for BFI prediction in the Category 3 region.

Scenarios	Model development			Model validation		
	R^2	ENS	PBIAS	R^2	ENS	PBIAS
Scenario 1	0.94	0.94	-0.1	0.71	0.70	-1.0
Scenario 2	0.97	0.97	-0.1	0.68	0.67	-1.4
Scenario 3	0.98	0.98	0.0	0.70	0.69	-1.4

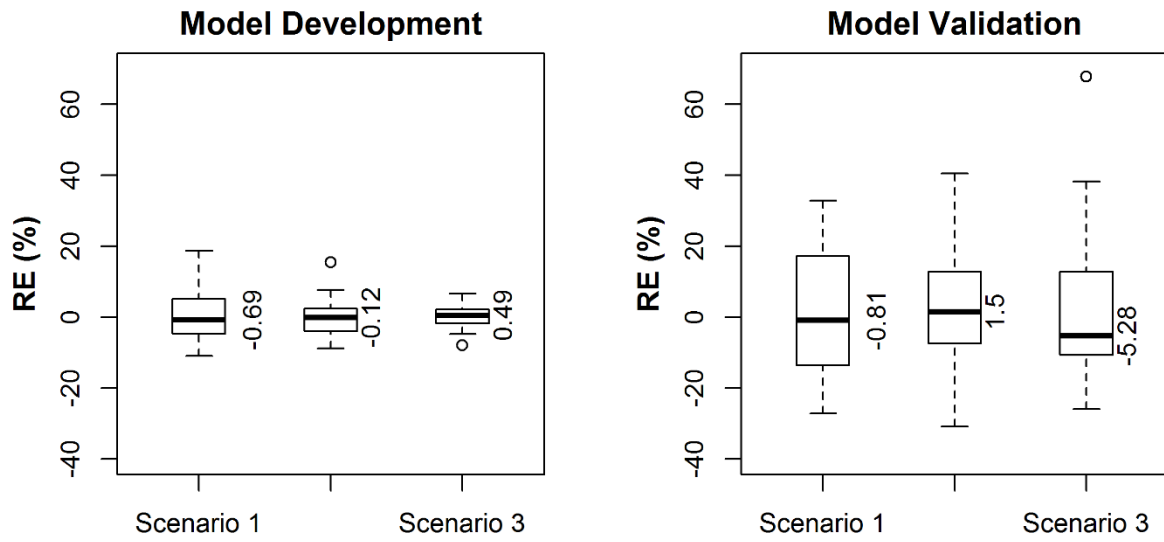


Figure 5.19. Boxplots of RE for BFI prediction model development and validation for the Category 3 region.

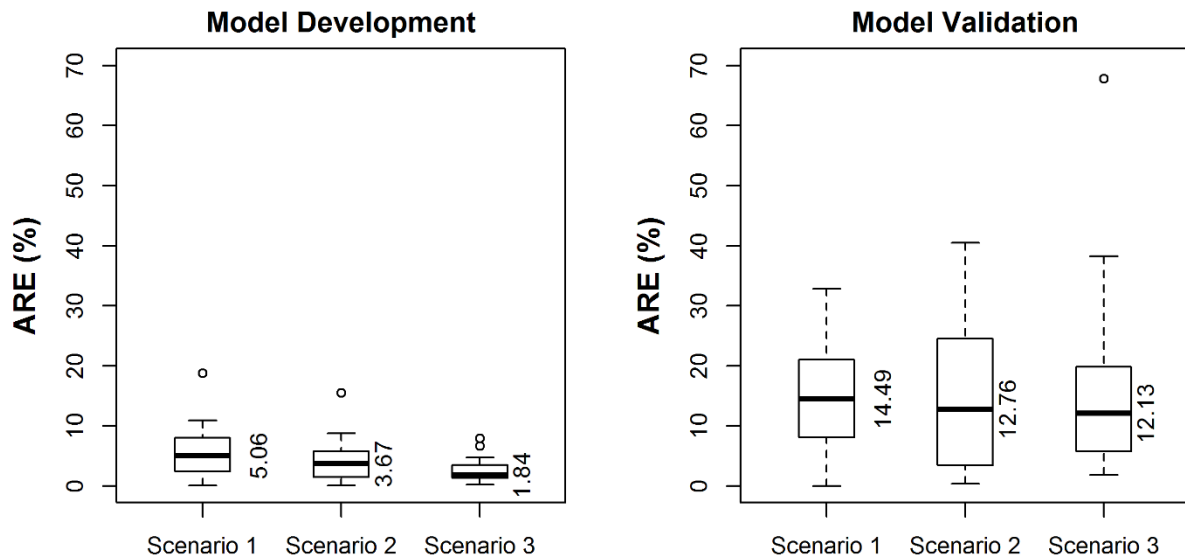


Figure 5.20. Boxplots of ARE for BFI prediction model development and validation for the Category 3 region.

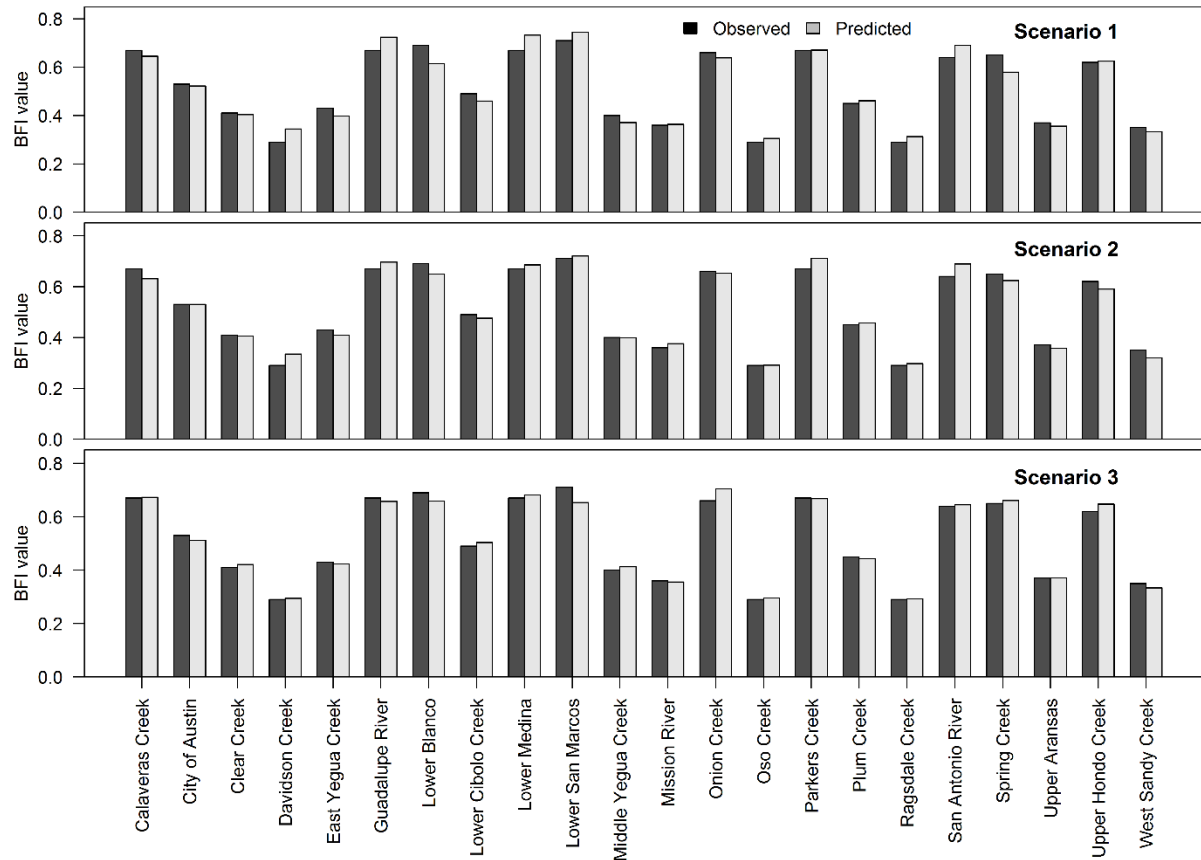


Figure 5.21. Observed (filtered) and predicted BFI measured within the three scenarios in the Category 3 region.

The predicted and observed BFI values filtered using the WHAT model for the three scenarios for the Category 3 region were plotted to visualize similarities and differences (Figures 5.21 and 5.22). The predicted BFI values exhibited the same pattern for the three scenarios with respect to the model development dataset; however, there were some divergences between the simulated and observed BFI values in the validation dataset. For instance the Jones Watershed tended to overestimate BFI in scenario 1. One explanation may be that this difference was related to how the watershed area was subjected to different measurements to prevent flash flood events. The watershed lies directly on the Gulf of Mexico and has been subjected to severe flood events in the past with the last one recorded in 2017. With the inclusion of precipitation variables in scenario 1 and with the high rainfall of the watershed, the model overestimated the predicted BFI.

Overall, for the validation dataset, the lower the filtered BFI value, the lower the divergence between the simulated and observed BFI and the better the performance of model prediction.

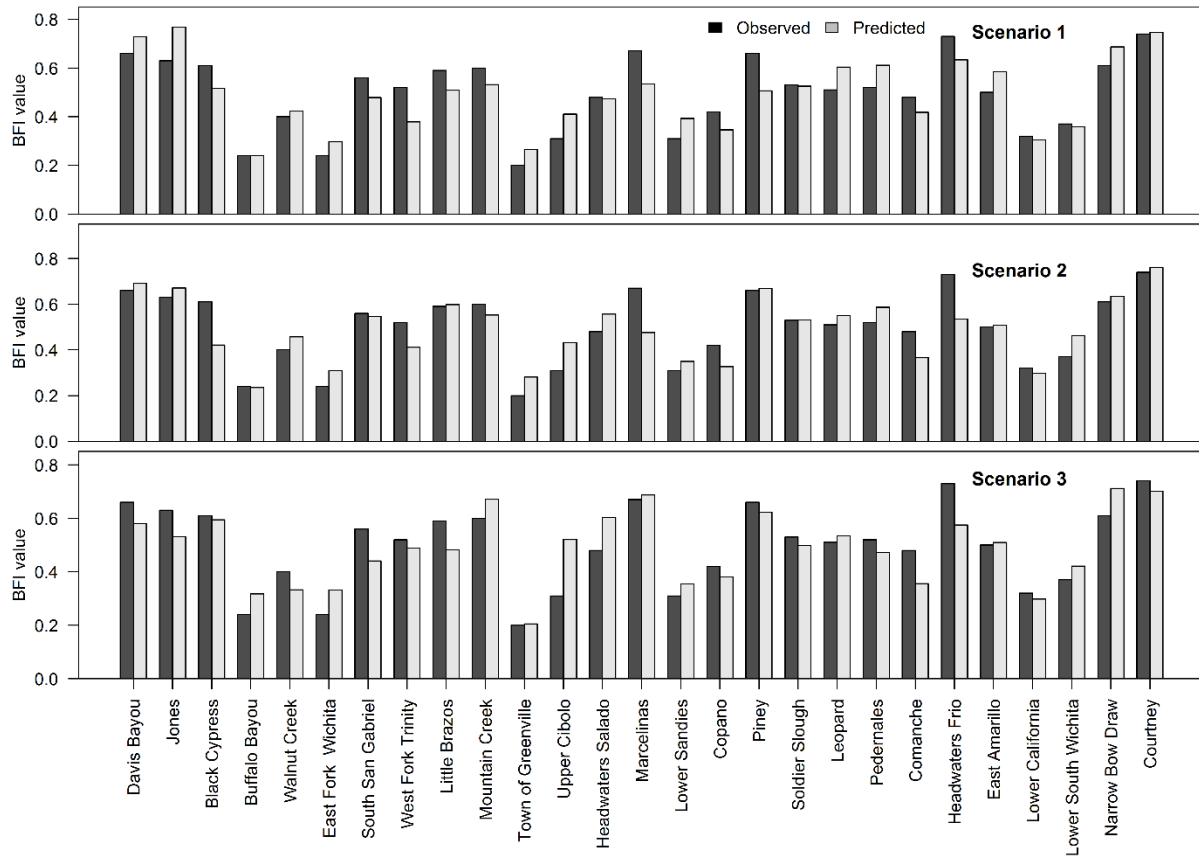


Figure 5.22. Observed (filtered) and predicted BFI for the validation dataset within the three scenarios in the Category 3 region.

5.3.2.4 Category 4

The Category 4 area represents the central and the southern part of the state. It is characterized by sub-tropical and semi-arid climate conditions, with the exception of the southern part called the Lower Valley, which experiences sub-tropical and sub-humid marine climate. The Central region of the area represents the Edward Plateau that contains the Edwards-Trinity Aquifer. The aquifer extends over an area of about 90,500 km² in central-west Texas. The topography of

the Edwards Plateau consists of a flat tableland with stream-cut canyons in the southern and eastern portions of the plateau (Anaya, 2001). The water-bearing units are composed predominantly of limestone and dolomite of the Edwards Group and sands of the Trinity Group. The top of Edwards-Trinity aquifer is mostly unconfined, and sediments rest on top of an uneven erosional surface of folded and faulted Paleozoic to Triassic-age sediment (George et al., 2011). This lower portion of the aquifer is largely confined and being recharged via natural sinkholes, i.e. allogenic recharge (<https://www.edwardsaquifer.net/intro.html>). Towards the central and southern part of the Category 4 region, the area is mainly covered by fluvial-deltaic sediments of the upper Paleocene and lower Eocene Wilcox Group, Carrizo Sand of the Southern Carrizo aquifer (Deeds et al., 2003), and discontinuous silt, clay and sand beds of the Miocene and Holocene ages (Bruun et al., 2016).

The regression equations were developed using three sets of data. Among the potential BFI response predictors for the scenario 1 model, forest, barren lands and wetland areas were the best predictors for BFI (Table 5.9). In addition, stream power and sediment transport indices, precipitation and water cover descriptors were also included in the model; however, they were not significant at a 0.10 probability level. This might be related to the low stream densities in the region, especially towards the west, which in turn reduced the stream power and sediment transport indices. This reduction in stream power index might be attributed to some of the streams in the plateau are sinking streams and never reach an outlet, however, they flow into a fracture zone or sinkholes and turn into allogenic recharge. In addition, there is no pattern in precipitation in the Category 4 area. Precipitation is the highest in late spring and early fall in only the eastern part of the region due to the colliding of cool northern frontal air masses with warm southern air, and from humid air masses coming from the gulf. However, the western part experiences a lower precipitation rate, that occurs due to convectional storm events during late summer (Anaya, 2001).

For the model developed in scenario 2, the variables ET, Clt and Frst were significant in predicting BFI at a 0.05 significance level. This observation was consistent with the attributes of the selected watersheds, representative of areas that were mainly covered by shrublands, forest and cultivated cover with 70, 12, and 10%, respectively. The shrublands had a high correlation with ET, and the cultivated and forest areas had negative impacts on ET (Figure 5.7a). These findings suggest why we observe positive correlation of the Clt and Frst parameters but negative correlation for the ET variable (Table 5.9). Of note, Figure 5.7a represents not only the correlation matrix between variables in the Category 4 watersheds, but also for the 140 selected watersheds across

the state. Based on their recharge and infiltration rate, shrublands may lead to the reduction of evapotranspiration and BFI in the region; however, it was hard to infer the direct relationship without specific information about the types of these land covers. The negative relationship between shrublands and BFI may be the result of covariance with precipitation, since shrublands are typically located in basins with lower precipitation rates.

Table 5.9. Baseflow prediction models developed for the Category 4 area.

Scenario	Model	AIC	R ²	Adj R ²	P-value
S1	$BFI = -0.771 \times SPI^{0.052} \times STI^{0.057}$ $\times PRCP^{0.489} \times Brn^{-0.084*} \times Frst^{0.093*}$ $\times Wtr^{0.057} \times Wtl^{0.1}$	-51	0.95	0.86	<0.01
S2	$BFI = 11.782* \times STI^{0.141} \times ET^{-4.260*} \times TAVG^{-0.1}$ $\times Clt^{0.074*} \times Frst^{0.074*}$	-38	0.86	0.76	<0.001
S3	$BFI = -0.733 \times WSlp^{-0.078}$ $\times AWS^{0.232} \times Coll^{0.110} \times Res^{0.203*}$ $\times K^{0.1}$	-50	0.96	0.82	<0.1

,*, **, and *** stand for statistically significant at 0.1, 0.05, 0.01, and 0.001 probability levels

The watersheds selected in Category 4 were mostly covered by residual and colluvial sediments, 37 and 23%, respectively, supporting the use of these two variables in the model developed for scenario 3. Although the colluvial deposits were not significant at a 0.10 level, the residual deposits were significant at a 0.05 probability level. Average slope, water storage, and hydraulic conductivity were also included in the model, but they were not significant. This could be due to the lack of complex topography, low water storage and conductivity in this area, with an average K of 3 m·day⁻¹ (Barker & Ardis, 1996).

Overall, the model developed for scenario 2 had the lowest BFI prediction accuracy with an R² and adjusted R² values of 0.86 and 0.76, respectively. This was in contrast to the models

developed for scenarios 1 and 3 that showed higher accuracies with R^2 of 0.95 and 0.96 and adjusted R^2 values of 0.86 and 0.82, respectively. These accuracies were reflected in the performance of the models for predicting BFI. Figures 5.23 and 5.24 show the percentages of RE and ARE for both model development and the validation dataset. The median percentages for RE ranged between -4.05 to 0.55% for model development, and varied from -0.54 to 0.59 for the validation dataset. Similarly, the median ARE for the model development were 3.47, 10.12 and 4.53 for scenarios 1, 2 and 3, respectively. Although the ARE reached a maximum of 54 and 73% for scenarios 1 and 2 in the validation dataset, respectively, these margins were considered outliers from the 3rd interquartile, ranging between 15 to 25%. The model predicted BFI with relatively high R^2 values for scenarios 1 and 3 (0.92 and 0.94, respectively), indicating that some meteorological variables were more useful than others (i.e. PRCP is better used as estimator for BFI than ET), and that the continuous coverage of the lithological scheme could be used for predictive purposes pertaining to BFI. The R^2 values and other evaluation statistical indices had lower values for the validation dataset compared to the developed model. The lowest R^2 value was 0.65 for scenario 2, and the highest was recorded in scenario 1 with a value of 0.82 (Table 5.10). Although the correlation coefficient detected in the validation of scenario 2 was lower, the relatively high R^2 and ENS, and low bias of model developments suggests that the BFI can be modeled by utilizing basin lithological, topographic and meteorological variables (Moriasi et al., 2007).

Table 5.10. Values of statistical indicators in model development and validation for BFI prediction in the Category 4 region.

Scenarios	Model development			Model validation		
	R^2	ENS	PBIAS	R^2	ENS	PBIAS
Scenario 1	0.92	0.92	-0.1	0.82	0.82	-0.9
Scenario 2	0.79	0.78	-0.6	0.65	0.68	-1.5
Scenario 3	0.94	0.93	0.0	0.76	0.74	-0.8

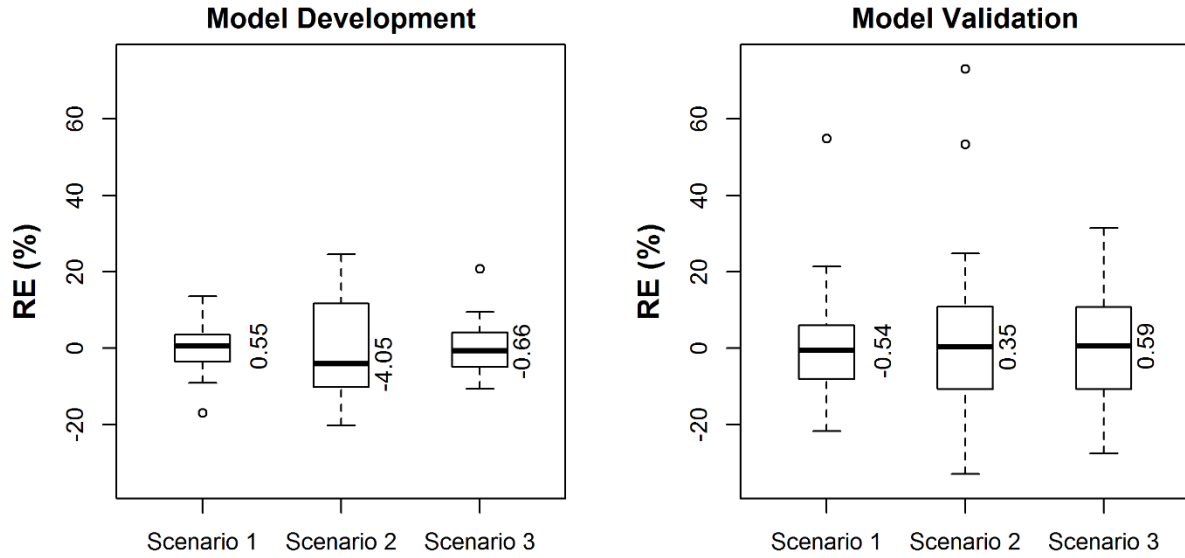


Figure 5.23. Boxplots of RE for BFI prediction model development and validation for the Category 4 region.

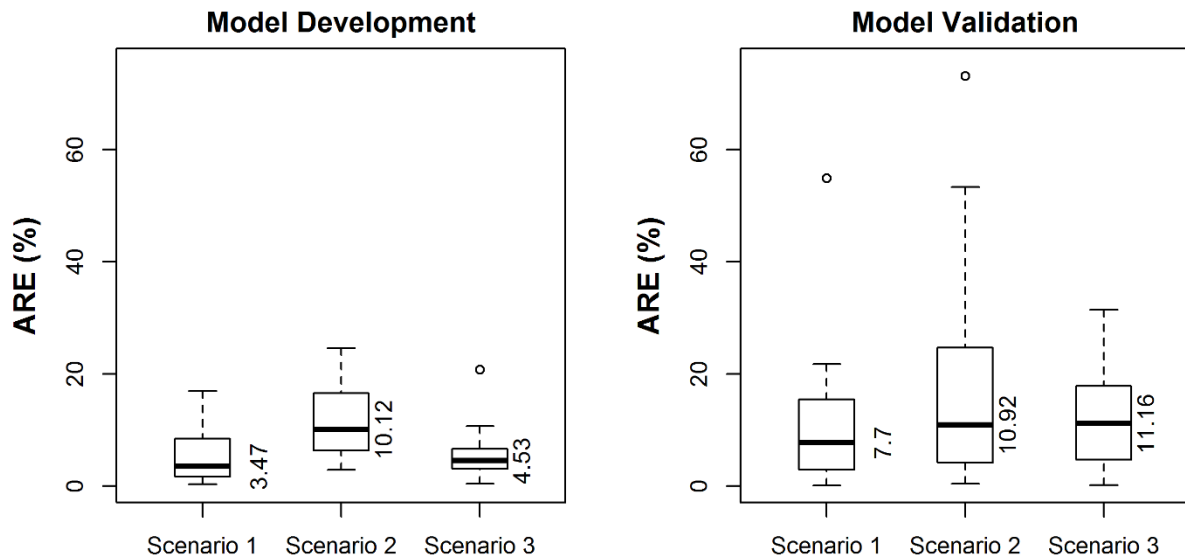


Figure 5.24. Boxplots of ARE for BFI prediction model development and validation for the Category 4 region.

Figures 5.25 and 5.26 compare the simulated BFI to the filtered BFI values using the equation shown in Table 5.9 for the development and validation datasets, respectively. There was low bias in the predictions in all three scenarios, and the developed model equations provide comparable estimates for the BFI. Some predictions were more variable from the measured BFI, such as the overestimation of BFI in the Dry Frio Watershed, and the underestimation of the Lower Sabinal River Watershed in scenario 2. Although the Dry Frio Watershed had the highest forest cover and second highest sediment transport index in the Category 4 region, it was also characterized by higher annual precipitation (924 mm) and lower evapotranspiration (399 mm) rates compared to other watersheds in the region. STI has been shown to be positively correlated to groundwater flow in many regions (Price et al., 2011; Warner et al., 2003). STI relies on water flow to move a load downstream. Water flow is variable, affected not only by the topography, such as slope, but also by the amount of rainfall that will directly affect the water level. The high rainfall observed in the Dry Frio Watershed leads to an initial increase in water level, which is then returned to baseflow over hours or days. Therefore, light or heavy precipitation, in this watershed especially, can impact the amount of water flow and sediment transport. Of note, the impacts of forest and sediment transport index variables exert strong influences on BFI prediction; however, it is uncertain whether these parameters were the main driving forces that controlled baseflow in the region, or if other basin characteristics that more directly influence groundwater discharge and are more strongly influenced by these measurements.

Similarly, the model overestimated the predicted BFI for Montell Creek Watershed in scenario 3 due to the high hydraulic conductivity in the watershed ($12 \text{ m}\cdot\text{day}^{-1}$). Although the watershed is covered by shallow to very shallow gravelly loam and clay, the high conductivity reported was likely caused by the data acquisition. For hydrogeological parameters, data were collected from well reports, and these wells are generally sited at locations with high values of water storage, transmissivity and conductivity. Figure 5.22 showed slight divergence between the estimated and measured BFI in Mountain Creek Watershed. The model overestimated the BFI in scenario 3, in contrast to scenarios 1 and 2 where the values were underestimated. This might be attributed to the high AWS of the watershed in scenario 3, and this is known to generally lead to an increase in the ground water discharge. On the other hand, the underestimated BFI values may be caused by the watershed's low cultivation and forest cover, which has a positive correlation with BFI in the developed model.

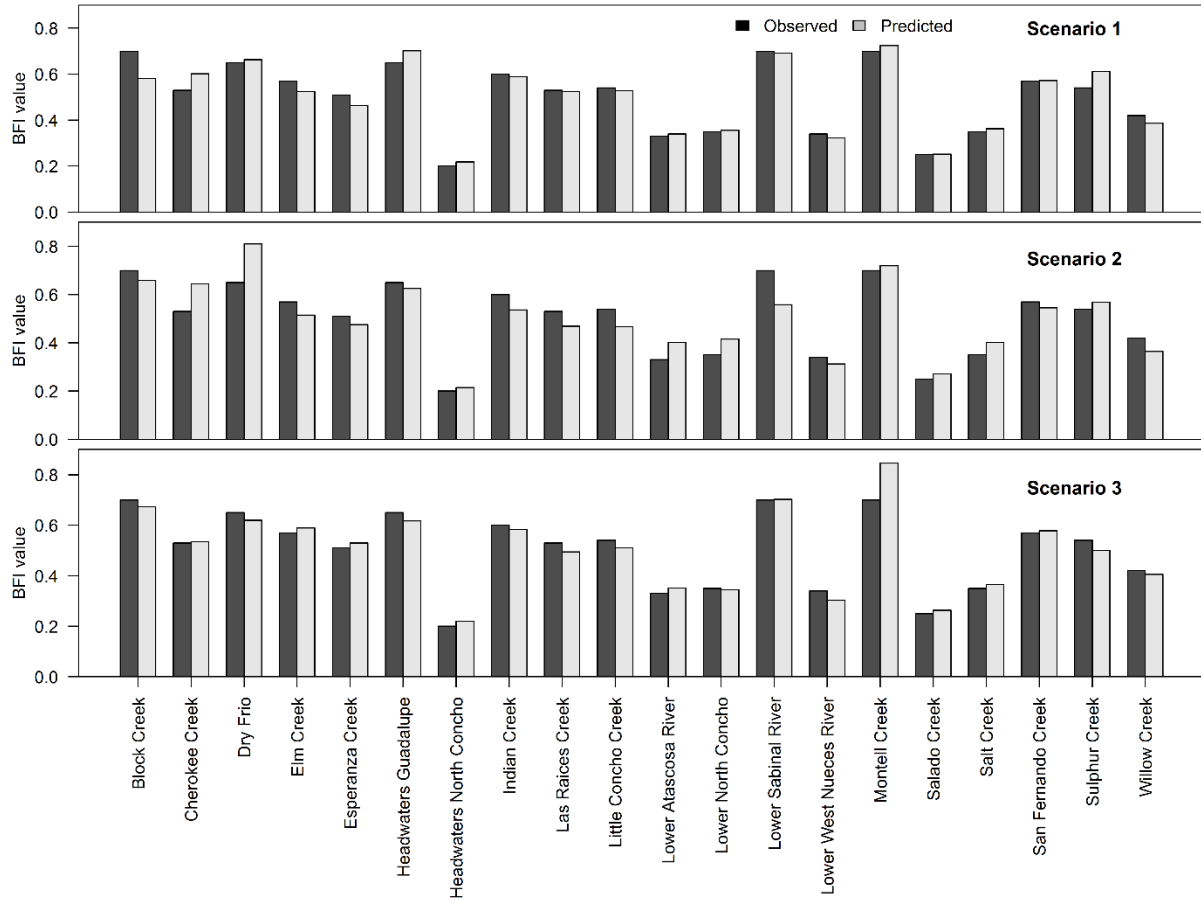


Figure 5.25. Observed (filtered) and predicted BFI measured within the three scenarios in the Category 4 region.

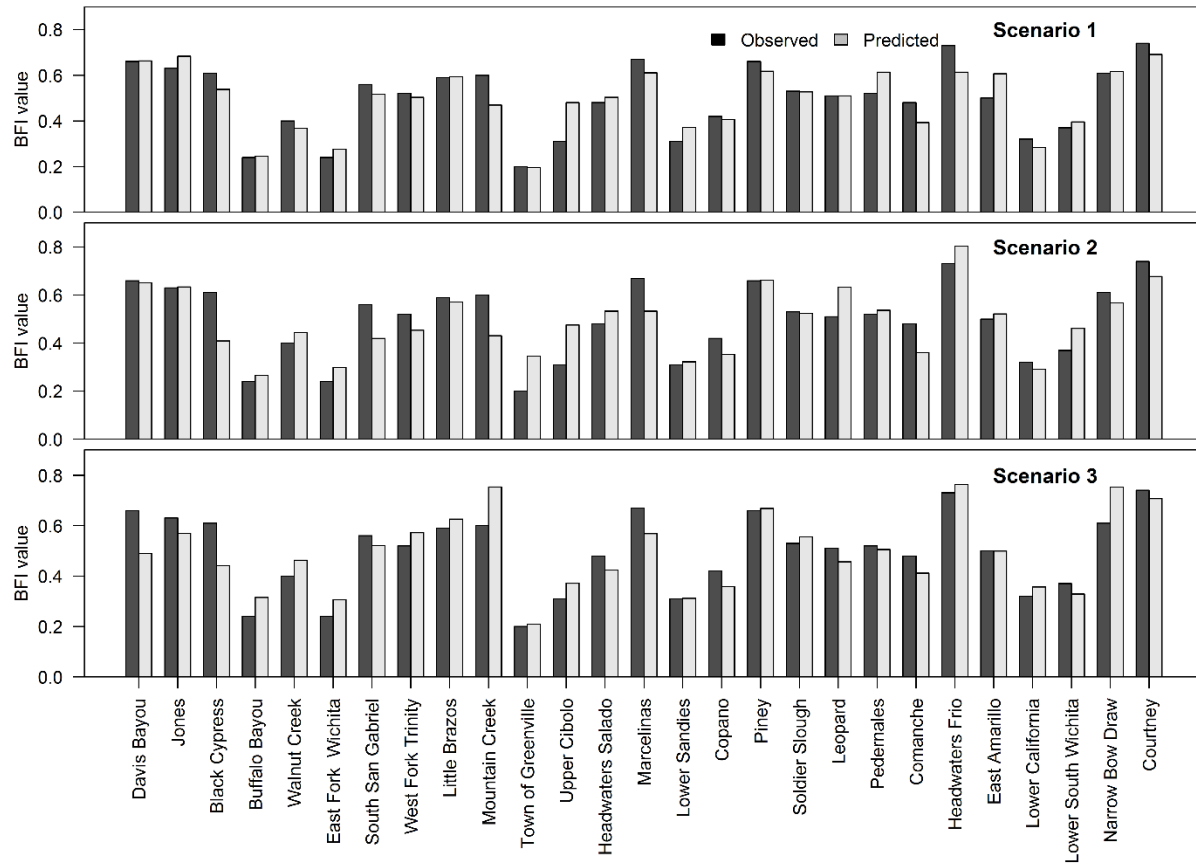


Figure 5.26. Observed (filtered) and predicted BFI for the validation dataset within the three scenarios in the Category 4 region.

5.3.2.5 Category 5

The Category 5 area represents the sub-tropical and semi-arid climates of the Low Rolling and High Plains in North Western Texas, and the dry arid desert of the Trans Pecos Plain in the far western part of the state (Figure 5.6). The region features the Seymour aquifer in Northern Texas, Ogallala aquifer in North Central Texas, and the Pecos Valley aquifer in the west (Figure 5.9). The Seymour Aquifer consists of Quaternary-age, alluvial sediments overlying westerly-dipping Permian-age rocks. The Seymour Aquifer is composed of discontinuous beds of poorly sorted gravel, conglomerate, sand, and silty clay eroded from the High Plains, deposited by eastward moving streams (Duffin & Beynon, 1992; Preston & Bankston, 1978). The Ogallala aquifer consists of sand, gravel, clay, and silt that has a maximum thickness of 800 feet. The selected watersheds for model development and validation mainly lay in the northern part of the

aquifer in the Ogallala formation. The Ogallala Formation was deposited as alluvial outwash from the Rocky Mountains with a coarser grained pebble to boulder size gravel near the mountains, to finer grained sand and gravel with increased distance from the mountains (Gustavson, 1996). The Pecos Valley aquifer consists of alluvial, lacustrine, and eolian deposits of Tertiary and Quaternary age, that can reach up to 450 m in thickness, deposited in the Pecos River Valley. Groundwater in the aquifer is unconfined and the top of the aquifer is exposed at the ground surface over the entire extent of its area (Bruun et al., 2016).

The best low flow regression model developed under the three scenarios in Category 5 showed high R^2 values compared to other categories (0.99, 0.94 and 0.97 for scenarios 1, 2 and 3, respectively). In addition, the developed model for both scenarios 1 and 2 involved similar parameters. The only difference between the model developed in scenarios 1 and 2 was the replacement of PRCP by the ET parameter in scenario 2. However, with this modest change, the factors WSA and Dvlp cover no longer affected the prediction of BFI in scenario 2. Although the precipitation was not statistically significant in scenario 1, the evapotranspiration was significant at a 0.01 probability level. This is likely explained by the areas that lie in the dry western region of the state where the rate of rainfall is significantly lower, with a mean of 500 mm compared to the precipitation of other categories that range from 650 mm in Category 4 up to 1300 mm in Category 1. The precipitation in this category occurs predominantly in April and May, with 115 mm, and July is the driest month with only 45 mm of precipitation. The rainfall in the wet season is mainly due to the convergence of prevailing west and south winds during late spring. On the other hand, some of the watersheds representing the Category 5 area are characterized by highly cultivated areas with a high ET rate (400 mm). Findings in the Category 5 region indicated that the correlation between ET and BFI was negative, and statistically significant at a 0.01 probability level (Table 5.11). In addition, the existence of the ET factor in the model was likely the reason for reduced accuracy of the model developed in scenario 2, as the R^2 reduced from 0.99 to 0.94 from scenario 1 to scenario 2.

Using an *F*-test, the best models were all significant (p -value <0.01) for scenario 1, and the p -value was less than 0.0001 for scenarios 2 and 3. Topographic factors including Relv and TI, hydrologic soil groups A, B and D, alluvial and eolian deposits, and hydrologic conductivity are all significant in the model developed for BFI prediction in scenario 3. Alluvial and eolian deposits in the Trans Pecos Plain and colluvial sediments in the High Plain region are the predominant

lithology groups for watersheds within the Category 5 area. As mentioned previously, these variables are known to be the driving force that controls baseflow (Zhang et al., 2013; Zhu & Day, 2009).

The model developed for BFI prediction in Category 5 was applied on 20 selected watersheds that represent the area. The 1st and 3rd interquartile for RE margins ranged from -5 to only 6% for the three scenarios, with the narrowest RE margin observed in scenario 1 (Figure 5.27). These findings indicate that the percentage of relative errors was between -5 and 6%, with a probability between 25 to 75%. The ARE for the three scenarios also had a narrow percentage range, with a median of 2.76, 6.48 and 4.71% for scenarios 1, 2 and 3, respectively (Figure 5.28). These results show that the regression models developed are accurate for BFI prediction in the western part of Texas using input from topographic, meteorological, lithological and hydrogeological data, and that the model developed for scenario 1 predicts the BFI with the highest accuracy.

Table 5.11. Baseflow prediction models developed for the Category 5 area.

Scenario	Model	AIC	R ²	Adj R ²	P-value
S1	$BFI = 1.097 \times WSA^{0.567} \times SPI^{-0.158}$	-68	0.99	0.93	<0.01
	$\times TStrL^{-0.664*} \times PRCP^{0.443}$ $\times Brn^{-0.071} \times Dvlp^{0.232} \times Frst^{0.158*}$ $\times Wtr^{0.043} \times Wtl^{0.058}$				
S2	$BFI = 14.355* \times SPI^{-0.281**} \times TStrL^{-0.230} \times ET^{-6.185**}$	-45	0.94	0.83	<0.0001
	$\times Brn^{-0.051} \times Frst^{0.108*} \times Wtr^{0.081}$ $\times Wtl^{0.031}$				
S3	$BFI = 1.447 * \times Relv^{-0.180*}$	-53	0.97	0.87	<0.0001
	$\times TI^{-1.266**} \times HydxA^{0.037**}$ $\times HydxB^{-0.060*}$ $\times HydxD^{-0.046*} \times All^{0.050**} \times Eol^{-0.042*}$ $\times K^{0.136*}$				

*, **, and *** stand for statistically significant at 0.1, 0.05, 0.01, and 0.001 probability levels

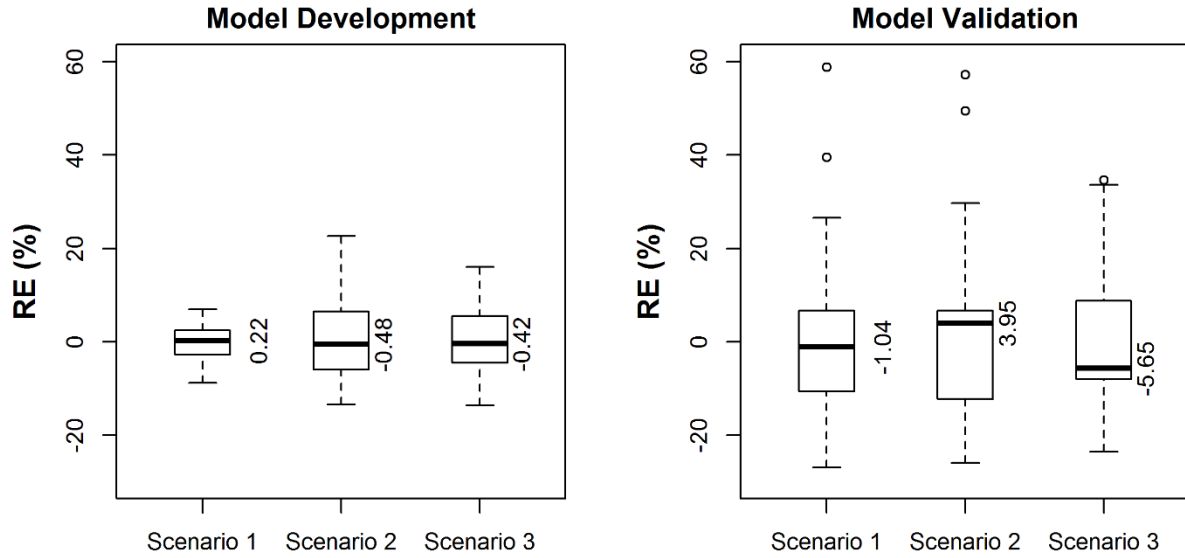


Figure 5.27. Boxplots of RE for BFI prediction model development and validation for the Category 5 region.

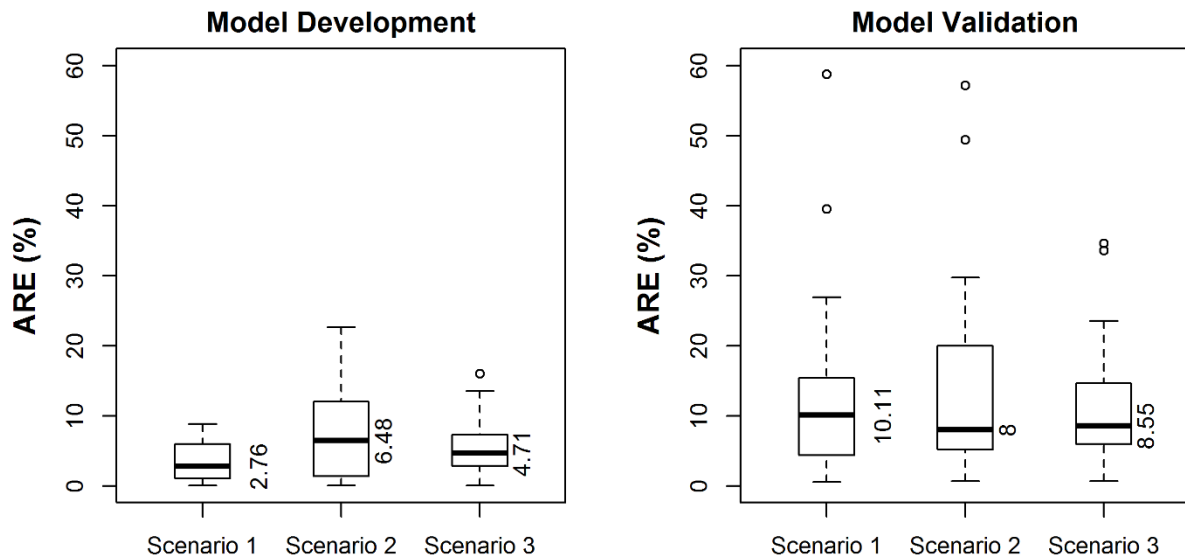


Figure 5.28. Boxplots of ARE for BFI prediction model development and validation for the Category 5 region.

Table 5.12 shows the performance statistics for the developed models used in BFI prediction in Category 5. The R^2 and ENS values between the observed and predicted BFI for model development ranges between 0.91 and 0.98, while PBIAS varied between zero and -0.3. Therefore, it could be concluded that the baseflow has a strong relationship with lithology, soil type and climate in this Category, and that the BFI can be explained as an integrated description of the fractional areas of lithology in the basins. In addition, it can be clearly seen that the predicted BFI values exhibit the same pattern for the three scenarios with respect to the model development dataset in Category 5 (Figure 5.29). The small deviation and extremely low bias between the observed and predicted BFI in Figure 5.29 might be explained by the constant topography of the plains and meteorological conditions in the area.

Table 5.12. Values of statistical indicators in model development and validation for BFI prediction in the Category 5 region.

Scenarios	Model development			Model validation		
	R²	ENS	PBIAS	R²	ENS	PBIAS
Scenario 1	0.98	0.98	0.0	0.75	0.74	-1.1
Scenario 2	0.91	0.91	-0.3	0.73	0.72	-1.2
Scenario 3	0.94	0.94	0.0	0.81	0.81	-0.8

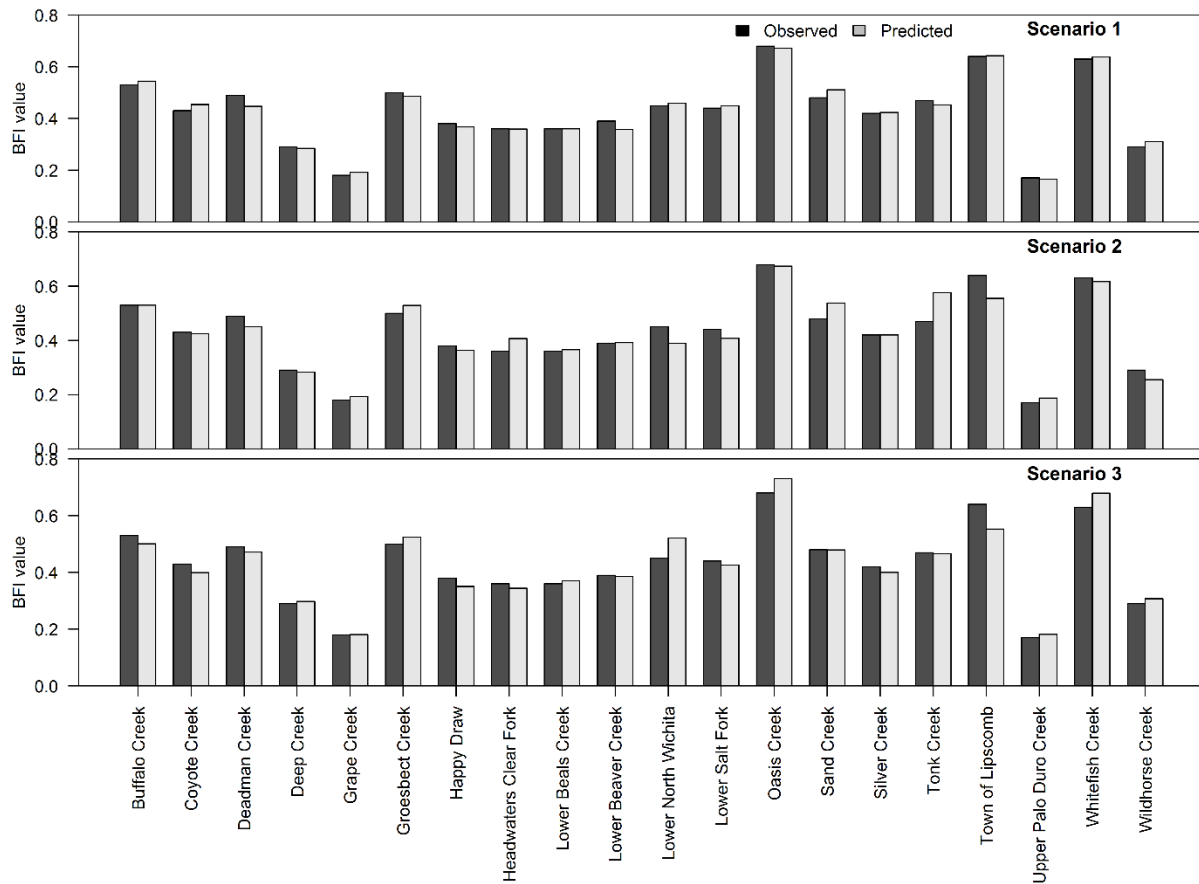


Figure 5.29. Observed (filtered) and predicted BFI measured within the three scenarios in the Category 5 region.

The model validation used datasets from 27 basins, and showed larger margins of RE compared to basins used to model development, with 1st and 3rd quartile range from -12 to 6%, with scenario 2 having the biggest margin. On the other hand, the highest ARE 3rd quartile range for the validation dataset was 20% in scenario 2 (Figures 5.27 and 5.28), indicating that the model developed for scenario 2 had the least accuracy but still can be utilized in predicting BFI values according to the evaluation criteria of Moriasi et al. (2007). The evaluation criteria for the model using the validation datasets is summarized in Table 5.12. The R^2 and ENS values showed a lower performance in the validation process than model development. The lowest R^2 values were recorded in scenario 2 with a value of 0.73, while the highest R^2 value was for scenario 3 (0.81). However, the low bias in the validation dataset indicated that the regression model could be used to predict BFI in areas that have similar climatic, geological and topographic conditions to that of

the Category 5 region. Figure 5.30 shows the comparison of BFI values for the validation dataset derived from streamflow and values evaluated from the equation listed in Table 5.11. A close agreement was observed between the measured and predicted BFI values. Therefore, the developed regression equation can be used to evaluate BFI in similar regions. The higher estimation of baseflow in Jones Creek in scenario 1 might be attributed to the same reasons mentioned in Category 3, that the watershed experiences higher rainfall that had a positive impact on groundwater discharge, that in turn increased the predicted BFI value.

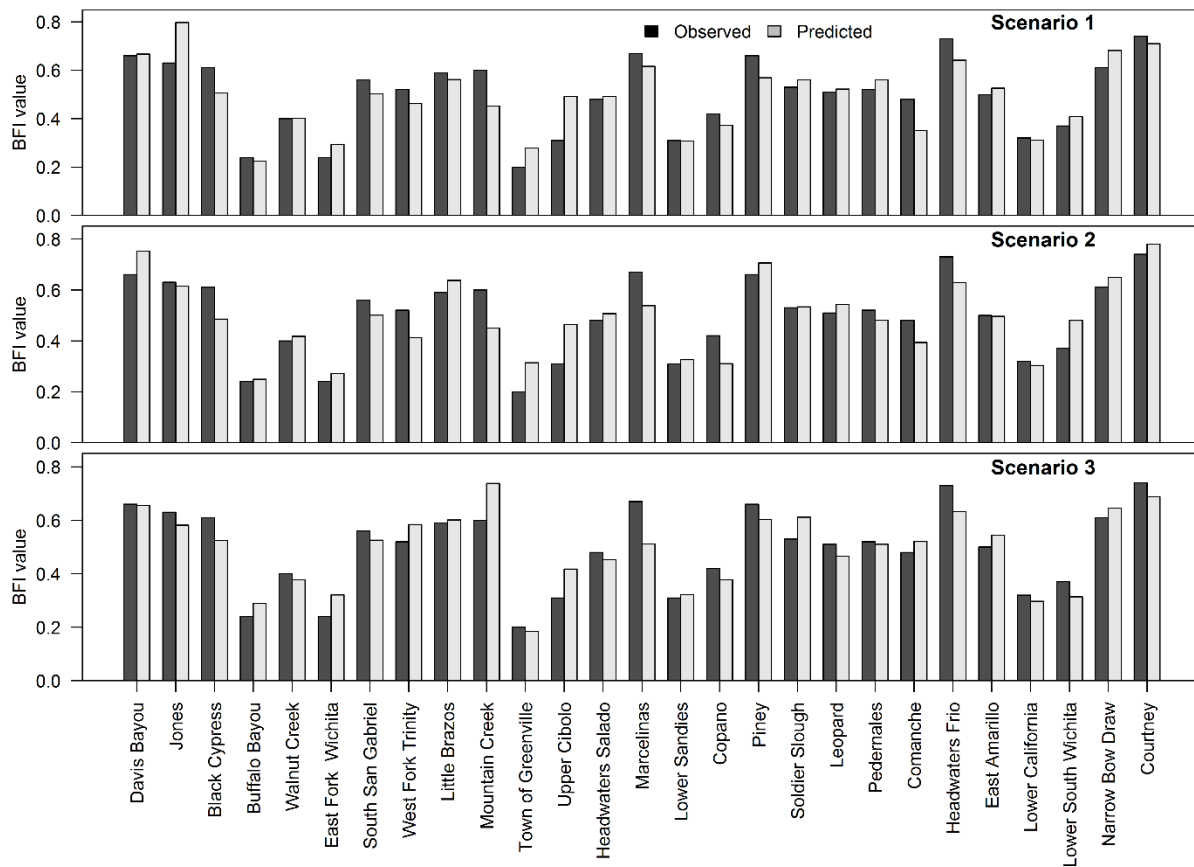


Figure 5.30. Observed (filtered) and predicted BFI for the validation dataset within the three scenarios in the Category 4 region.

Finally, it should be mentioned that, in this research, we tried to develop a model including all the selected watersheds that represent the five categories (113 watersheds); however, outputs of these models were not able to predict baseflow adequately. Table 5.13 summarizes the statistical indices of the best models for the three scenarios. Evaluation criteria for both scenarios 1 and 3 were identical, with R^2 , ENS, and PBIAS values of 0.43, 0.41 and -2.7. Scenario 2 had a lower performance with R^2 , ENS, and PBIAS values of 0.37, 0.36 and -2.9. Regardless of the number of variables included in the model, the lower performance for the statewide models was likely attributed to the variability in climatic and geological conditions and parameters across the state. These findings indicated the benefits of determining appropriate study areas to develop regression models within a larger study region. Although the development of distinct regression equations can be computationally and resource-intensive, specifically over large regions that have several meteorological, geological, and topographic features, the developed models showed an ability to accurately predict the BFI across the state.

Table 5.13. Values of statewide statistical indicators in model development for BFI prediction.

Scenarios	Model development		
	R^2	ENS	PBIAS
Scenario 1	0.43	0.41	-2.7
Scenario 2	0.37	0.36	-2.9
Scenario 3	0.43	0.41	-2.7

5.3.3 Limitations of our Approach

Findings of this research showed that the deviation between the estimated and predictive values were relatively small in all developed and validated models; however, several limitations of this study should be noted and would benefit from further investigation in future studies. First, although the collection of watershed properties representing hydrogeological factors that impact baseflow is a challenging process, as most of these parameters are acquired from areas where data from wells are available. These wells are usually located in areas where the water storage, conductivity and transmissivity are relatively high, and therefore may not be indicative of the

watershed conditions. This might explain why neither depth to water nor transmissivity were involved in any of the developed models of scenario 3, for example. Since the data were derived from pumping test wells, they were considered as point estimates that are constant across the basin. Therefore, it is recommended to apply other representative parameters, for instance, relative elevation topographic surface, in which the floodplain surface was subtracted from the nearest river channel water level elevations, rather than depth to water, and to involve well data throughout the area or by utilizing an area weighted average to acquire values better representing the whole basin. Moreover, other hydrogeological parameters that can be acquired from other groundwater models should be used in developing such models. Additionally, the stepwise model development used in this study has been shown to introduce bias in parameter estimation and some inconsistencies between model selection algorithms (Whittingham et al., 2006). An alternative way that might be used in future studies, especially when using many variables, is principle component analysis (PCA) regression. PCA involves reducing the number of individual models and can be used when the variables are collinear or even highly correlated (Ringnér, 2008).

One of the potential shortcomings of this study is that the baseflow has been estimated from computed filtering methods, and in addition, there is no standard for selecting specific baseflow separation methods for model development and for comparing predicted to filtered values with another separation approach. Since there was no measured baseflow data available to support our decision, it was challenging to select the best baseflow separation technique for the study area. The WHAT filtering technique was selected in this study as it provided fast and consistent baseflow separation with respect to manually separated results. The results of the filtered BFI values might be different if another filtering methods were used or by using the flow duration curve (FDC) method.

Some of the developed models included the impact of slope, basin relief, stream density and different lithology on baseflow. However, knowledge about water storage in different lithology units and their relationship to baseflow is limited, and it remains uncertain if these parameters directly influence groundwater discharge or correlate to other aquifer characteristics that impact groundwater (Price et al., 2011). Thus, there is a critical need for further investigation into the role of subsurface topography on baseflow.

Another limitation of this study is that the soil properties were represented only by the percentages of different HSGs; however, basins may contain various soil types with different

characteristics at different locations based on topography. For example, some soils can be deep and permeable and others can be shallow and impermeable at small depths below the subsurface within the same basins. Unfortunately, there are currently no robust methods to incorporate the effects of all of these varying soil characteristics into the models. In this work, we developed the simplest classification for lithology across the state that is satisfactory for developing the regression model (Bloomfield et al., 2009). However, it is reasonable to identify representative hydrogeological and lithological categories that are continuous and stable across the whole watershed. The proportion of different lithological types in each watershed might not be sensitive enough to measure the impact of lithology on BFI.

Accuracies of model results are also limited to the input of single time point land use data (NLCD 2016). The filtered BFI values were calculated from USGS daily streamflow data from 1980-2017, with the assumption that the land use was constant over this timespan. Therefore, any changes in land use patterns over time have not been specifically addressed by the developed models. An improvement to consider in future studies would be to acquire at least two land use datasets, one from an early time and one current, to obtain a percentage of land cover change of each basin. Lastly, log transformed parameters usually introduce a bias when applied to back transformation that detracts from the accuracy associated prediction as the transform of the error term has been omitted. However, the potential impacts of these biases were minimal due to the low biases acquired from the models.

Taking into account these limitations of our approach, the regression models are suitable in their ability to predict groundwater in Texas and other regions, based on the proposed categories that experience similar topography and climatic conditions. It is challenging to explicitly confirm which of these limitations are more significant than the other. However, the most critical result obtained from this research was to assess whether the developed relationships can provide satisfactory prediction for BFI.

5.4 Summary and Conclusions

Baseflow is defined as the total groundwater discharge to streams that feed water bodies. The evaluation of the baseflow is critical for the appropriate management of these bodies. Regional regression models were developed to predict baseflow indices in the state of Texas. The developed model was based on basin-wide physical, lithological and hydrogeological properties in each

watershed for groundwater discharge estimation across Texas. The baseflow indices were derived from USGS daily streamflow data from 1980 to 2017 using the two parameter recursive digital filtering approach of Web-based Hydrograph Analysis Tool (WHAT). Texas experiences a range of climate and geological conditions. This diversity is essential to the goals of this study, which include understanding how baseflow is affected by different factors related to climate, soil and bedrock. However, to produce accurate models, the watersheds in this study were categorized into five divisions according to Texas climatic zones, as we demonstrated that a state-wide model has low predictive abilities (Table 5.13). The results of models made using these categories indicated that there is no specific pattern for BFI variation across Texas. However, the groundwater contribution to surface water was found to be greatest in east Texas and around major aquifers in middle Texas and in correlation with the variability in precipitation from east to west.

Multiple linear regression models were used to develop three scenarios based on different characteristics affecting baseflow. The first two scenarios used variables that represent areas and stream geomorphologies, in addition to meteorological and land use variables. The third scenario used topography, hydrogeological, soil, and lithology variables. This research used the typical stepwise linear regression approach to correlate independent variables to BFI. The first two scenarios are relatively similar and relate BFI to topography, climate and land use. Surficial geology, soil type and hydrogeology parameters are the primary variables used in building scenario 3 by quantifying the impacts of fractional areas of each lithology on BFI. These regression models were then used to predict BFI for 113 watersheds across the state and tested using another 27 randomly selected basins from within the area of each category. Results of the regression showed the models predicted BFI at ungauged sites with high accuracy. The highest accuracy was recorded in Categories 4 and 5 areas, while the lowest model performance was detected in the Category 2 region. This is likely related to the complexity of topography and the diversity of lithological data acquired in the Category 2 region.

Correlation coefficients (R^2) relating BFI values to basin properties in this research were relatively high, and the percentages of relative errors were relatively low. In general, within each category, scenarios 1 and 3 had higher prediction performance, while scenario 2 was the lowest. Independent variables for ten regression models developed for scenarios 1 and 2 are similar, with differing degrees of significance levels, resulting in predicted BFIs that are similar to the filtered values. The major difference between scenarios 1 and 2 is the use of the factor representing

evapotranspiration, which when applied in the model leads to a lower BFI prediction accuracy. This might be caused by the fact that ET was not categorized as proportional to the percentages of cultivated areas within each basin, but was generalized to represent the whole basin. Independent parameters include precipitations, basin areas, stream power index, sediment transport index; cultivated, forests and developed covers were found to correlate directly to BFI predictions in both scenarios 1 and 2. In agreement with this prediction, it was observed that evapotranspiration was negatively correlated to the BFI values in Categories 3, 4 and 5. ET was found to have no impacts on baseflow in Categories 1 and 2, likely due to the higher humidity of these regions compared to the others, which decreases the amount of evapotranspiration.

For scenario 3, factors including average water storage, hydrologic conductivity, hydrologic soil groups, alluvial, colluvial, and residual lithology are the main explanatory parameters for baseflow. Elevation and topographic index are negatively correlated to groundwater discharge in scenario 3, and eolian deposits have a negative relationship to baseflow prediction only in Category 5 due to the existence of eolian cover in basins included only in this region. Hydrologic soil groups impact the BFI differently, in that the increase in the BFI prediction increases with the increase of percentage of sand in the soil. For instance, hydrologic soil group A was the highest to correlate with BFI prediction in Categories 2 and 5.

This research led to the development of models that are able to predict BFI values that are comparable to those obtained by WHAT, by using categorized areas across the state of Texas, with very high performance. Moreover, these findings show that BFIs are an integral expression of the fractional areas of each lithology in the basins. The regression models have further been tested using validation datasets, and showed a high performance and that the developed models can be adequately used to predict BFI in ungauged regions. Therefore, the developed models can be easily applied in other areas that have similar topographic, geologic and climatic (arid, semi-arid or humid) conditions, where databases for meteorology, hydrogeology and soil types are available.

Some limitations should be taken into account when applying these models to additional study areas and further studies to improve some of the proposed approaches are recommended, as discussed above. However, due to the accessibility and simplicity of independent variables used in scenario 1, it is recommended for use in other regions that have similar characteristics. Findings of these regression models should be beneficial to guide water management strategies and in establishment of water resource plans at local and regional scales. The models developed play a

vital role in planning for an accurate estimation of factors that impact groundwater discharge. In addition, the developed models can support modelers of groundwater by presenting independently obtained BFI estimation in ungauged sites.

CHAPTER 6. CONCLUSIONS AND FUTURE WORK

6.1 Conclusions

Land use conversion and climate variation have generally been considered a local environmental and ecological issue, but these are becoming forces of global importance. Population growth associated with urban expansion is one of the main factors that impacts climate, soil, water quality and quantity. Several studies have shown that land use and climate variation have affected the past and will continue to impact spatial water distribution and availability. Distinguishing the effects of land use change from concurrent climate variability and understanding the water balance are specific challenges for studies on operational management processes. These can be solved by understanding the interactions between the Earth's surface, atmosphere, hydrological components and the dynamics of land use change at various scales that drive them.

The goal of this research was to evaluate the impacts of land use change on surface temperature and the impact of urbanization and climate variation on hydrology in Egypt and USA, respectively, utilizing modeling and statistical techniques. In this dissertation, three main issues or gaps related to the interaction between land use change, surface properties and hydrology, have been identified and addressed through three main objectives to evaluate shortcomings in the current state of land use and climate change science, as applied to the Earth's atmosphere, surface and groundwater resources. Research on these gaps was designed to make recommendations and further understand the dynamics of land use and climate change on different components for future development and develop predictive models for use in areas with limited data.

The first issue relates the change in land use and urbanization to land surface temperature in the Greater Cairo Region (GCR), Egypt. Land use alternation analysis was conducted by utilizing multi-spectral Landsat data of the GCR for 1990, 2003 and 2016, incorporating the integration of both remote sensing and GIS. In addition, these Landsat data were used to estimate land surface temperature (LST) in the GCR. In Egypt, the reduction of vegetation cover, increase of impervious cover, and the morphology of buildings in big cities combines to store heat, lower evaporative cooling and warm the surface air. Therefore, multi-temporal Landsat satellite data were used to monitor the spatial and temporal change of land use and to study the impact of rapid urbanization

on land surface temperature in the GCR in Egypt. The research methodology included image pre-processing and classification, land cover indices derivation, and the evaluation of LST. The study showed the effectiveness of the remote sensing techniques in conjunction with GIS to enable delineation of urban expansion due to the establishment of new settlements and to produce an accurate landscape change map in the study area.

Findings indicated that the most distinct change in land use was related to vegetation cover that drastically decreased by 23.3% from 1990 to 2016. In the same period, significant reduction in barren land by 8.70% occurred. Urban area, due to the construction of new industrial and commercial settlements, showed a considerable increase by 128.3%. The two land covers, barren lands and vegetation, were the main contributors to form new urban areas. Additionally, results showed that mean LST values were higher in barren lands and urban areas than in the surroundings over the entire period. These anomalies were associated with settlements, and industrial and commercial areas, that experienced dense populations. It was believed that the change in LST and climatic response was strongly related to the removal of vegetation cover and their replacement with non-evaporative surfaces. The increase in the magnitude of LST was 2.06 °C in the areas that transformed from vegetation cover to urban and 2.60 °C due to the transformation of barren lands from green areas in the period of study from 1990 to 2016. Statistical analysis showed a strong inverse relationship between LST and Normalized Difference Vegetation Index (NDVI), in contrast to a high positive relationship between LST and Normalized Difference Built-up Index (NDBI). Generally, the study area reveals comparatively higher LST and NDBI, and lower NDVI, over the period of study from 1990-2016. Results demonstrated multi-temporal Landsat images can accurately quantify the change pattern in LULC and LST in the GCR in Egypt.

The second objective evaluated the response of watershed streamflow and baseflow to climate variability and land use change in urban watersheds in the Midwest region of the United States, and compared it with an urban catchment in a semi-arid region. Baseflow is the main component of water balance in many basins, and is regularly evaluated in many watersheds. The study of baseflow can provide further insight into the dynamics of watershed hydrology. Both climate variation and human actions serve as stressors that contribute to putting water resources under severe pressure. Hence, identifying the distinct impacts of changing land use from climate variability and understanding the water balance is considered a particular challenge for studies on operational management of reservoirs and river basins.

This identification can be utilized by the combination of statistical analyses, hydrologic models, and multiple scenarios that were varied in land use and climate change in three watersheds: 1) Little Eagle Creek (LEC), Indiana; 2) Upper West Branch DuPage River Watershed (UWVDR), Illinois; and 3) Walzem Creek Watershed, Texas. These impacts can be identified by utilizing calibrated and validated Soil and Water Assessment (SWAT) models that serve to conceptualize the relationship between climate variation, land-use change, human activities, and their synchronous impacts on watershed hydrology. Additionally, the Sequential Uncertainty Fitting program algorithm (SUFI-2) approach within the SWAT-CUP interface was applied for optimization, calibration, validation and uncertainty analysis of parameters in the model.

Outputs of Chapter 3 emphasized the impacts of climate and land use alteration on hydrology in the LEC watershed. It showed that the SWAT model produced ‘very good’ and ‘good’ results for calibration and validation using observed streamflow and baseflow data. Baseflow was a key component of the total discharge as it accounted for 36.5% of the total flow within the LEC Watershed. By comparing different land use datasets (1992 and 2011), about 30% of the LEC watershed area changed from cultivated to urban areas, while the climate became warmer and wetter. In addition, climate variability had the dominant impact on streamflow, while urban expansion influenced baseflow more significantly than climate change.

For the UWVDR and Walzem Creek watersheds, findings of Chapter 4 indicated that baseflow accounted for almost 55.3% and 33.3% of the annual streamflow in the UWVDR and Walzem Creek watersheds, respectively. Owing to urban expansion, the proportional extent of developed areas increased from 44% to 77% and from 64% to 92% during the study period, in the UWVDR and Walzem Creek watersheds, respectively. Additionally, climate became warmer and wetter for the UWVDR watersheds, but warmer and drier at the Walzem Creek watershed. Changes at the UWVDR watershed were remarkably similar to those for the LEC watershed, with the exception of the climate variation was shown to have the greater impact on streamflow, surface runoff, and baseflow, while land use change exerted a relatively small influence on the flow. In other words, in the UWVDR watershed, when the direction of the changes caused by urbanization and climate variation occur in the same direction, the changes of the combined impacts will be intensified. On the other hand, streamflow increased due to urbanization impacts, while it reduced baseflow in the semi-arid Walzem Creek Watershed. However, the climate change had negative impacts on all water components in the area that might be attributed to the reduction of

precipitation in the catchment. Therefore, the impact of the combined scenario will be amplified when the individual impacts of land use alteration and climate variation are in the same direction (positive/negative).

These findings indicate the necessity of evaluating the influences of urbanization and climate alteration separately when assessing the hydrologic effects in urban catchments. Generally, with the variation in spatiotemporal properties of precipitation, and increasing hazardous events associated with water, such as droughts and floods, stress on water resources will increase and will further encourage the development of mitigation approaches. Based on this research, these findings provide practical suggestions for policy makers on how to sustain water resources more efficiently in relation to its variability as a response to urbanization, land use, and climate change.

The third gap is relating baseflow to watershed physical and lithological properties in Texas by developing numerical regression models. The developed models were used to evaluate the effects of bedrock geology and other catchment properties on baseflow and to estimate average annual baseflow in watershed tributaries. Baseflow displays spatial and temporal variability. Not only do land use variation and climate conditions play a role in controlling baseflow, but also other watershed properties do as well. Baseflow is generally derived from available streamflow data using hydrograph separation methods. Although most of these methods are limited to estimating baseflow in gauged sites, it is now possible to explore relationships between basin variables and groundwater recharge in ungauged watersheds, with possibilities of finding more accurate and meaningful models.

In this study, 140 gauge sites and their physical and geological properties were used to develop multiple regression models to predict baseflow index (BFI) across Texas, a large state in the U.S. that experiences a diversity of climate conditions and water demands. Methodology included measured BFI derived from USGS daily streamflow data from 1980 to 2017, using the two parameter recursive digital filtering approach of Web-based Hydrograph Analysis Tool (WHAT). In addition, three scenarios were developed and validated across five study areas (Categories 1 to 5) that were chosen based on categorization of climate conditions, and one model was developed across the whole state. The first two scenarios are relatively similar and relate BFI to topography, climate and land use. Surficial geology, soil type and hydrogeology parameters are the primary variables used in building the third scenario by quantifying the impacts of fractional

areas of each lithology on BFI. In this study, we used the typical stepwise linear regression approach to correlate the independent variables to BFI.

Results showed that there is no specific pattern for BFI variation across Texas. However, the groundwater contribution to surface water was found to be greatest in East Texas and around major aquifers in Middle Texas, and in correlation with the variability in precipitation from east to west. Results of the regression model showed the models predicted BFI with high accuracy. In Categories 4 and 5 areas, the highest accuracy was recorded, while the lowest model performance was detected in a Category 2 region. This is likely related to the complexity of the topography and the diversity of lithological data acquired in the Category 2 region. In general, within each category, scenarios 1 and 3 had higher prediction performance, while scenario 2 was the lowest. Independent variables for regression models developed for scenarios 1 and 2 are very similar, however, with differing degrees of significance levels. These resulted in predicted BFIs that are very similar to the filtered values. The major difference between scenarios 1 and 2 is the use of the factor representing evapotranspiration, which when applied in the model, leads to lower BFI prediction accuracy. Independent variables that included precipitation, basin area, stream power index, sediment transport index, cultivated, forests, and developed covers were found to correlate directly to BFI predictions in both scenarios 1 and 2. For scenario 3, factors included average water storage, hydrologic conductivity, hydrologic soil groups, alluvial, colluvial, and residual lithology were the main explanatory parameters for baseflow. Hydrologic soil groups impact the BFI differently, in which the BFI prediction increased with the increase of percentage of sand in the soil. For instance, hydrologic soil group A experienced a high correlation with BFI prediction in Categories 2 and 5. In another words, BFIs were found to be an integral expression of the fractional areas of each lithology in the basins. The regression models have further been tested using validation datasets and showed a high performance. This indicates that the developed models can be used to predict BFI in ungauged regions.

The findings from this study can be applied in other areas that have similar topographic, geologic and climatic (arid, semi-arid or humid) conditions, where databases for meteorology, hydrogeology and soil types are available. In addition, the models developed play a vital role in planning for rigorous estimation of factors that impact groundwater discharge as they can support modelers of groundwater by presenting independently obtained BFI estimates at ungauged sites.

Generally speaking, this work made recommendations to understand the dynamics of land use and climate change on different components for future development and apply predictive models in areas with limited data.

6.2 Recommendations and Future Work

Even though the methodologies modified and developed in this dissertation show promise to evaluate the impacts of urbanization and climate variability on surface temperature and hydrology, respectively, this research also indicates that further analysis is needed. Specific recommendations are given in respective chapters of this dissertation and are summarized as follows:

- More multi-date images from the same season for the GCR should be investigated and evaluated to provide more evidence of the thermal behavior on urban areas and for better understanding of the impact of urbanization on LST.
- Generally, satellite images are likely to be affected by cloud cover and other atmospheric effects, in addition to surface roughness, that in turn affect the digital number values. Therefore, it is highly recommended for future work that the integration of remote sensing imageries from different sources with more land surface meteorological data be explored, and more attention on surface roughness be considered for more accurate results.
- Regarding urbanization and vegetation removal in the GCR, it is recommend that additional effort be placed on establishing some measurement that can mitigate the strong effect of increasing LST. For instance, establishing green areas like parks and gardens, and roof top area cultivation with horticultural plants that can alleviate the effect of LST.
- Urbanization was found to be the primary contributor to the change in hydrology in three watersheds in the Midwest and Texas. Thus, watershed managers should give priority to reverse watershed degradation. Agroforestry is advised to increase the vegetation cover, as are practical management and protection techniques for the watersheds.
- Based on the challenges encountered and the outputs obtained in the second objective, results indicated that urbanization processes are an integrated part of the watershed, along with climate alteration. Thus, meteorological station records used in this study reflect data that are the result of the combined impacts of land use alteration and climate variability.

To this end, the number of meteorological stations and the parameters used to calibrate the SWAT model is suggested, if applicable, to be increased.

- Additionally, studies that focus on quantifying the effect of each land use category change on streamflow and baseflow are recommended. These are likely to yield additional useful insights on how climate variability and land use impact hydrological response separately.
- As future research, depending on the availability of continuous data, further development of the water quality model of the three watersheds can be beneficial.
- Additional studies using catchments that exhibit different urbanization and climate regions could provide beneficial comparative results to determine the impacts of these variables on hydrological components.
- Outputs of objective three recognized the interaction between groundwater and watershed physical properties. For improving the developed model, it is possible to utilize denser gauge networks. It is also recommended, for future studies, to involve well data throughout the area or by utilizing an area weighted average to acquire values better representing the whole basin, and additionally to apply other techniques to develop the regression models, for instance, principle component analysis.
- The filtered BFI values were calculated from USGS daily streamflow data from 1980-2017, with the assumption that the land use was constant over this timespan. An improvement to consider for future studies would be to acquire at least two land use datasets. One from an early time point and one current, to obtain a percentage of land cover change of each basin.
- For water resources management and planning, the developed regression models can be utilized in water quality models to extend the capabilities of those models for evaluation of the advantages of best management practice on streamflow, baseflow, and direct discharge at different scales.
- The developed models can be automated in the future to be used as web tools by incorporating different datasets. The web-based model could be enhanced with the addition of GIS capabilities in order to estimate baseflow index in other regions that have similar characteristics and climatic conditions.

REFERENCES

- Abbaspour, K. C. (2015). *SWAT-CUP: SWAT Calibration and Uncertainty Programs*. Swiss Federal Institute of Aquatic Science and Technology, Eawag, Duebendorf, Switzerland. (Vol. 130). <https://doi.org/10.1007/s00402-009-1032-4>
- Abbaspour, K. C., Rouholahnejad, E., Vaghefi, S., Srinivasan, R., Yang, H., & Kløve, B. (2015). A continental-scale hydrology and water quality model for Europe: Calibration and uncertainty of a high-resolution large-scale SWAT model. *Journal of Hydrology*, *524*, 733–752. <https://doi.org/10.1016/j.jhydrol.2015.03.027>
- Abdi, R., & Yasi, M. (2015). Evaluation of environmental flow requirements using eco-hydrologic-hydraulic methods in perennial rivers. *Water Science and Technology*, *72*(3), 354–363. <https://doi.org/10.2166/wst.2015.200>
- Abdulaziz, A. M., Hurtado, J., J. M., & Al-Douri, R. (2009). Application of multitemporal Landsat data to monitor land cover changes in the Eastern Nile Delta region, Egypt. *International Journal of Remote Sensing*, *30*(11), 2977–2996. <https://doi.org/10.1080/01431160802558675>
- Aboelnour, M., & Engel, B. A. (2018a). Application of remote sensing techniques and geographic information systems to analyze land surface temperature in response to land use/land cover change in Greater Cairo Region, Egypt. *Journal of Geographic Information System*, *10*(1), 57–88. <https://doi.org/10.4236/jgis.2018.101003>
- Aboelnour, M., & Engel, B. A. (2018b). Responses of streamflow and baseflow hydrology to climate variability and land use dynamics in an urban watershed. In *AGU Fall Meeting Abstracts*.
- Aboelnour, M., Engel, B. A., & Gitau, M. W. (2019). Hydrologic response in an urban watershed as affected by climate and land-use change. *Water (Switzerland)*, *11*(8), 1603.
- Aboelnour, M., Gitau, M. W., & Engel, B. A. (2020). A comparison of streamflow and baseflow responses to land-use change and the variation in climate parameters using SWAT. *Water (Switzerland)*, *12*, 191. <https://doi.org/doi:10.3390/w12010191>
- Adger, W. N., Arnell, N. W., & Tompkins, E. L. (2005). Successful adaptation to climate change across scales. *Global Environmental Change*, *15*(2), 77–86. <https://doi.org/10.1016/j.gloenvcha.2004.12.005>
- Ahiablame, L. ., Engel, B. A., & Chaubey, I. (2013a). Effectiveness of low impact development practices in two urbanized watersheds: Retrofitting with rain barrel/cistern and porous pavement. *Journal of Environmental Management*, *119*, 151–161. <https://doi.org/10.1016/j.jenvman.2013.01.019>

- Ahiablame, L., Chaubey, I., Engel, B., Cherkauer, K., & Merwade, V. (2013b). Estimation of annual baseflow at ungauged sites in Indiana USA. *Journal of Hydrology*, 476, 13–27. <https://doi.org/10.1016/j.jhydrol.2012.10.002>
- Ahmed, B. (2011). *Urban Land Cover Change Detection Analysis and Modelling Spatio-Temporal Growth Dynamics Using Remote Sensing and GIS Techniques: a Case Study of Dhaka , Bangladesh*. <https://doi.org/10.13140/2.1.1413.5364>
- Ahmed, B., Kamruzzaman, M., Zhu, X., Rahman, M. S., & Choi, K. (2013). Simulating Land Cover Changes and Their Impacts on Land Surface Temperature in Dhaka, Bangladesh. *Remote Sensing*, 5(11), 5969–5998. <https://doi.org/10.3390/rs5115969>
- Al-Bakri, J. T., Dauqqah, M., & Brewer, T. (2013). Application of remote sensing and gis for modeling and assessment of land use/cover change in Amman/Jordan. *Journal of Geographic Information System*, 5, 509–519. <https://doi.org/10.4236/jgis.2013.55048>
- Alhawiti, R. H., & Mitsova, D. (2016). Using Landsat-8 data to explore the correlation between urban heat island and urban land uses. *International Journal of Research in Engineering and Technology*, 5(3), 457–466.
- Alley, M., Healy, W., Labaugh, W., & Reilly, E. (2002). Flow and storage in groundwater systems. *Science*, 296(June), 1985–1990. <https://doi.org/10.1126/science.1067123>
- Almeida, R. A., Pereira, S. B., & Pinto, D. B. F. (2018). Calibration and validation of the SWAT hydrological model for the Mucuri River Basin, 4430, 55–63.
- Anache, J. A. A., Wendland, E. C., Oliveira, P. T. S., Flanagan, D. C., & Nearing, M. A. (2017). Runoff and soil erosion plot-scale studies under natural rainfall: A meta-analysis of the Brazilian experience. *Catena*, 152, 29–39. <https://doi.org/10.1016/j.catena.2017.01.003>
- Anaya, R. (2001). An overview of the Edwards-Trinity aquifer system, central-west Texas. *US Geological Survey Professional Paper*, 100–119. Retrieved from http://www.ncbi.nlm.nih.gov/entrez/query.fcgi?db=pubmed&cmd=Retrieve&dopt=AbstractPlus&list_uids=14516406265419041665related:YuOUZaidMkJ%5Cnpapers2://publication/uuid/3F288ED2-BA72-436E-AD20-9ADADA538E31
- Arciniega, S., & Breña-naranjo, J. A. (2016). Baseflow recession analysis across the Eagle Ford shale play (Texas , USA). *EGU General Assembly*, (April).
- Arnold, J. G., Moriasi, D. N., Gassman, P. W, Abbaspour, K. C., White, M. J., Srinivasan, R., ... Jha, M. K. (2012). SWAT: Model use, calibration, and validation. *Transactions of the ASABE*, 55(4), 1491–1508. <https://doi.org/10.13031/2013.42256>
- Arnold, J. G., Srinivasan, R., Muttiah, R. S., & Williams, J. R. (1998). Large area hydrologic modeling and assesment Part I: Model development. *JAWRA Journal of the American Water Resources Association*, 34(1), 73–89. <https://doi.org/10.1111/j.1752-1688.1998.tb05961.x>

- Arnold, J. R., Allen, P. ., Muttiah, R. ., & Bernhardt, G. (1995). Automated baseflow separation and recession analysis techniques. *Ground*, 33, 1010–1018.
- Barker, R. A., & Ardis, A. F. (1996). Hydrogeologic framework of the Edwards-Trinity aquifer system, west-central Texas. *US Geological Survey Professional Paper*, (1421 B).
- Barsi, J. A., Barker, J. L., & Schott, J. R. (2003). An Atmospheric Correction Parameter Calculator for a single thermal band earth-sensing instrument. *IEEE International Geoscience and Remote Sensing Symposium 2003*, 5, 3014–3016. <https://doi.org/10.1109/IGARSS.2003.1294665>
- Barsi, J. A., Schott, J. R., Palluconi, F. D., & Hook, S. J. (2005). Validation of a web-based atmospheric correction tool for single thermal band instruments. In *International Society for Optics and Photonics* (Vol. 5882, pp. 136–142). <https://doi.org/10.1117/12.619990>
- Bauer, M. E., Burk, T. E., Ek, A. R., Coppin, P. R., Lime, S. D., Walsh, T. A., ... Heinzen, D. F. (1994). Satellite inventory of Minnesota forest resources. *Photogrammetric Engineering and Remote Sensing.*, 60(3), 287–298.
- Bayarjargal, Y., Karnieli, A., Bayasgalan, M., Khudulmur, S., Gandush, C., & Tucker, C. J. (2006). A comparative study of NOAA – AVHRR derived drought indices using change vector analysis. *Remote Sensing of Environment*, 105(1), 9–22. <https://doi.org/10.1016/j.rse.2006.06.003>
- Becker, A., Güntner, A., & Katzenmaier, D. (1999). Required integrated approach to understand runoff generation and flow-path dynamics in catchments. *Integrated Methods in Catchment Hydrology - Tracers, Remote Sensing and New Ydrometric Techniques. IAHS-AISH Publication*, 258(258), 3–9. Retrieved from <http://cat.inist.fr/?aModele=afficheN&cpsidt=1827972>
- Beven, K. (2006). A manifesto for the equifinality thesis. *Journal of Hydrology*, 320(1–2), 18–36. <https://doi.org/10.1016/j.jhydrol.2005.07.007>
- Bhaduri, B., Harbor, J., Engel, B., & Grove, M. (2000). Assessing watershed-scale, long-term hydrologic impacts of land-use change using a GIS-NPS model. *Environmental Management*, 26(6), 643–658. <https://doi.org/10.1007/s002670010122>
- Bhagyanagar, R., Kawal, B. M., Dwarakish, G. S., & Surathkal, S. (2012). Land use / land cover change and urban expansion during 1983–2008 in the coastal area of Dakshina Kannada district, South India. *Journal of Applied Remote Sensing*, 6, 063576–1. <https://doi.org/10.1117/1.JRS.6.063576>
- Bhaskar, A. S., Beesley, L., Burns, M. J., Fletcher, T. D., Hamel, P., & Oldham, C. E. (2016). Will it rise or will it fall ? Managing the complex effects of urbanization on baseflow, 35(February 2015), 293–310. <https://doi.org/10.1086/685084>.

- Bloomfield, J. P., Allen, D. J., & Griffiths, K. J. (2009). Examining geological controls on baseflow index (BFI) using regression analysis: An illustration from the Thames Basin, UK. *Journal of Hydrology*, 373(1–2), 164–176. <https://doi.org/10.1016/j.jhydrol.2009.04.025>
- Bonell, M. (1999). Selected challenges in runoff generation research in forests from the hillslope to headwater drainage basin scale. *JAWRA Journal of the American Water Resources Association*, 34(4), 765–785. <https://doi.org/10.1111/j.1752-1688.1998.tb01514.x>
- Bridget R. Scanlon, Richard W. Healy, & Peter G. Cook. (2002). Choosing appropriate techniques for quantifying groundwater recharge. *Hydrogeology Journal*, 10, 18–39. <https://doi.org/10.1007/s10040-0010176-2>
- Bruun, B., Jackson, K., Lake, P., & Walker, J. (2016). *Texas Aquifers Study (Groundwater Quantity, Quality, Flow, and Contributions to Surface Water)*.
- Burke, C. B., West, E., Street, W. M., Charles, S., & Burke, C. B. (2006). *West Branch Dupage River Watershed Plan* (Vol. 60174).
- Butt, A., Shabbir, R., Ahmad, S. S., & Aziz, N. (2015). Land use change mapping and analysis using Remote Sensing and GIS: A case study of Simly watershed, Islamabad, Pakistan. *The Egyptian Journal of Remote Sensing and Space Science*, 18(2), 251–259. <https://doi.org/10.1016/j.ejrs.2015.07.003>
- CAPMAS. (2017). Greater Cairo Region Population. Retrieved July 20, 2005, from <http://www.capmas.gov.eg/>
- Castilla, G., & Hay, G. J. (2007). Uncertainties in land use data. *Hydrology and Earth System Sciences*, 11(6), 1857–1868. <https://doi.org/10.5194/hess-11-1857-2007>
- Chander, G., & Markham, B. (2003). Revised Landsat-5 TM radiometric calibration procedures and postcalibration dynamic ranges. *IEEE Transactions on Geoscience and Remote Sensing*, 41(11), 2674–2677. <https://doi.org/10.1109/TGRS.2003.818464>
- Charles, D. (2007). Assessing regional land-use/cover influences on New Jersey Pinelands streamflow through hydrograph analysis. *Hydrological Processes*, 21, 185–197. <https://doi.org/10.1002/hyp>
- Chavez, P. S., Berlin, G. L., & Sowers, L. B. (1982). Statistical method for selecting Landsat MSS ratios. *Journal of Applied Photographic Engineering*, 8(1), 23–30.
- Chen, J., Theller, L., Gitau, M. W., Engel, B. A., & Harbor, J. M. (2017). Urbanization impacts on surface runoff of the contiguous United States. *Journal of Environmental Management*, 187, 470–481. <https://doi.org/10.1016/j.jenvman.2016.11.017>
- Cherkauer, D. S. (2004). Quantifying ground water recharge at multiple scales using PRMS and GIS. *Ground Water*, 42(1), 97–110.

- Cherkauer, D. S., & Ansari, S. A. (2005). Estimating ground water recharge from topography, hydrogeology, and land cover. *Ground Water*, 43(1), 102–112. <https://doi.org/10.1007/s13398-014-0173-7.2>
- Choi, J., Engel, B. a, Muthukrishnan, S., & Harbor, J. (2003). GIS Based Long Term Hydrologic Impact Evaluation for Watershed Urbanization. *Journal Of The American Water Resources Association*, 2051, 623–635.
- Clean River Program San Antonio River Basin. (2017). *Watershed Characterizations for the Upper San Antonio River, Salado Creek and Upper Cibolo Creek Watersheds*. Retrieved from <https://www.sara-tx.org/wp-content/uploads/2017/05/2017-BCR-web.pdf>
- Cohen, W. B., Fiorella, M., Gray, J., Helmer, E., & Anderson, K. (1998). An efficient and accurate method for mapping forest clearcuts in the Pacific Northwest using Landsat Imagery. *Photogrammetric Engineering & Remote Sensing*, 64(4), 293–300.
- Congalton, R. G. (1991). A review of assessing the accuracy of classifications of remotely sensed data. *Remote Sensing of Environment*, 37(1), 35–46. [https://doi.org/10.1016/0034-4257\(91\)90048-B](https://doi.org/10.1016/0034-4257(91)90048-B)
- Davies, D. K., & Ethridge, F. G. (1971). Claiborne group of central Texas: record of Middle Eocene marine and coastal plain deposition. *AAPG Bulletin*, 55. <https://doi.org/10.1306/819a3d54-16c5-11d7-8645000102c1865d>
- Deeds, N., Kelley, V., Fryar, D., Jones, T., Whallon, A. J., & Dean, K. E. (2003). *Groundwater Availability Model for the Southern Carrizo-Wilcox Aquifer*.
- Dey, P., & Mishra, A. (2017). Separating the impacts of climate change and human activities on streamflow: A review of methodologies and critical assumptions. *Journal of Hydrology*, 548, 278–290. <https://doi.org/10.1016/j.jhydrol.2017.03.014>
- DigitalGlobe. (n.d.). ImageFinder. Retrieved from <https://browse.digitalglobe.com/imagefinder/main.jsp?>
- Doyle, M. W., Harbor, J. M., Rich, C. F., & Spacie, A. B. (2000). Examining the effects of urbanization on streams using indicators of geomorphic stability. *Physical Geography*, 21(2), 37–41. <https://doi.org/10.1080/02723646.2000.10642704>
- Drury, B., Rosi-Marshall, E., & Kelly, J. J. (2013). Wastewater treatment effluent reduces the abundance and diversity of benthic bacterial communities in urban and suburban rivers. *Applied and Environmental Microbiology*, 79(6), 1897–1905. <https://doi.org/10.1128/AEM.03527-12>
- Duan, W., Chen, Y., Zou, S., & Nover, D. (2019a). Managing the water-climate- food nexus for sustainable development in Turkmenistan. *Journal of Cleaner Production*, 220, 212–224. <https://doi.org/10.1016/j.jclepro.2019.02.040>

- Duan, W., Hanasaki, N., Shiogama, H., Chen, Y., Zou, S., Nover, D., ... Wang, Y. (2019b). Evaluation and future projection of Chinese precipitation extremes using large ensemble high-resolution climate simulations. *Journal of Climate*, 32(8), 2169–2183. <https://doi.org/10.1175/JCLI-D-18-0465.1>
- Duan, W., He, B., Nover, D., Fan, J., Yang, G., Chen, W., ... Liu, C. (2016). Floods and associated socioeconomic damages in China over the last century. *Natural Hazards*, 82(1), 401–413. <https://doi.org/10.1007/s11069-016-2207-2>
- Duan, W., He, B., Takara, K., Luo, P., Nover, D., & Hu, M. (2017). Impacts of climate change on the hydro-climatology of the upper Ishikari river basin, Japan. *Environmental Earth Sciences*, 76(14), 1–16. <https://doi.org/10.1007/s12665-017-6805-4>
- Duffin, G. L., & Beynon, B. E. (1992). *Evaluation of Water Resources in Parts of the Rolling Prairie Region of North-Central Texas*. Retrieved from http://www.twdb.texas.gov/publications/reports/numbered_reports/doc/R337/R337.pdf?d=10878.995
- Eckhardt, K. (2005). How to construct recursive digital filters for baseflow separation. *Hydrological Processes*, 19(2), 507–515. <https://doi.org/10.1002/hyp.5675>
- Eckhardt, K. (2008). A comparison of baseflow indices, which were calculated with seven different baseflow separation methods. *Journal of Hydrology*, 352(1–2), 168–173. <https://doi.org/10.1016/j.jhydrol.2008.01.005>
- El-batran, M., & Arandel, C. (1998). A shelter of their own: informal settlement expansion in Greater Cairo and government responses. *Environment and Urbanization*, 10(1), 217–232.
- Engel, B., Storm, D., White, M., Arnold, J., & Arabi, M. (2007). A hydrologic/water quality model application protocol. *Journal of the American Water Resources Association*, 43(5), 1223–1226. <https://doi.org/10.1111/j.1752-1688.2007.00105.x>
- Esam, I., Abdalla, F., & Erich, N. (2012). Land use and land cover changes of West Tahta Region, Sohag Governorate, Upper Egypt. *Journal of Geographic Information System*, 4, 483–493. <https://doi.org/10.4236/jgis.2012.46053>
- ESRI 2020. ArcGIS Desktop: Release 10. Redlands, CA: Environmental Systems Research Institute.
- Fairbridge R.W. (1968) Colluvium. In: Geomorphology. Encyclopedia of Earth Science. Springer, Berlin, Heidelberg
- Faridatul, M. I. (2017). Spatiotemporal effects of land use and river morphological change on the microclimate of Rajshahi Metropolitan Area. *Journal of Geographic Information System*, 9, 466–481. <https://doi.org/10.4236/jgis.2017.94029>

- Feyereisen, G. W., Strickland, T. C., Bosch, D. D., & Sullivan, D. G. (2007). Evaluation of SWAT manual calibration and input parameter sensitivity in the Little River Watershed. *Transactions of the American Society of Agricultural and Biological Engineers*, 50(2002), 843–856. <https://doi.org/10.13031/2013.23149>
- Ficklin, D. L., Robeson, S. M., & Knouft, J. H. (2016). Impacts of recent climate change on trends in baseflow and stormflow in United States watersheds. *Geophysical Research Letters*, 43(10), 5079–5088. <https://doi.org/10.1002/2016GL069121>
- Fohrer, N., Haverkamp, S., Eckhardt, K., & Frede, H.-G. (2001). Hydrologic response to land use changes on the catchment scale. *Pergamon Phys. Chem. Earth (B)*, 26(7), 577–582. [https://doi.org/10.1016/S1464-1909\(01\)00052-1](https://doi.org/10.1016/S1464-1909(01)00052-1)
- Foley, J. A., Barford, C., Coe, M. T., Gibbs, H. K., Helkowski, J. H., Holloway, T., ... Snyder, P. K. (2005). Global consequences of land use. *Science*, 309(5734), 570–574.
- Frans, C., Istanbuluoglu, E., Mishra, V., Munoz-Arriola, F., & Lettenmaier, D. P. (2013). Are climatic or land cover changes the dominant cause of runoff trends in the Upper Mississippi River Basin? *Geophysical Research Letters*, 40(6), 1104–1110. <https://doi.org/10.1002/grl.50262>
- Frisbee, M. D., Phillips, F. M., Campbell, A. R., Liu, F., & Sanchez, S. A. (2011). Streamflow generation in a large, alpine watershed in the southern Rocky Mountains of Colorado: Is streamflow generation simply the aggregation of hillslope runoff responses?. *Water Resources Research*, 47(6). W06512, doi:10.1029/2010WR009391
- Gao, J., & Liu, Y. (2010). Determination of land degradation causes in Tongyu County, Northeast China via land cover change detection. *International Journal of Applied Earth Observation and Geoinformation*, 12(1), 9–16. <https://doi.org/10.1016/j.jag.2009.08.003>
- Gebert, W. A., Radloff, M. J., Considine, E. J., & Kennedy, J. L. (2007). Use of streamflow data to estimate base flowground-water recharge for Wisconsin. *Journal of the American Water Resources Association*, 43(1), 220–236. <https://doi.org/10.1111/j.1752-1688.2007.00018.x>
- George, P. G., Mace, R. E., & Petrossian, R. (2011). Aquifers of Texas. *Texas Water Development Board*, 380(July), 1–182.
- Ghazal, K. A., Leta, O. T., El-Kadi, A. I., & Dulai, H. (2019). Assessment of wetland restoration and climate change impacts on water balance components of the Heeia coastalwetland in Hawaii. *Hydrology*, 6(2), 37. <https://doi.org/10.3390/hydrology6020037>
- Giannini, M. B., Belfiore, O. R., Parente, C., & Santamaria, R. (2015). Land surface temperature from Landsat 5 TM images: comparison of different methods using airborne thermal data. *Journal of Engineering Science and Technology Review*, 8(3), 83–90.

- Gilmore, M. S., Wilson, E. H., Barrett, N., Civco, D. L., Prisloe, S., Hurd, J. D., & Chadwick, C. (2008). Integrating multi-temporal spectral and structural information to map wetland vegetation in a lower Connecticut River tidal marsh. *Remote Sensing of Environment*, *112*(11), 4048–4060. <https://doi.org/10.1016/j.rse.2008.05.020>
- Gitau, M., & Bailey, N. (2012). Multi-layer assessment of land use and related changes for decision support in a coastal zone watershed. *Land*, *1*(1), 5–31. <https://doi.org/10.3390/land1010005>
- Gitau, M. W., & Chaubey, I. (2010). Regionalization of SWAT model parameters for use in ungauged watersheds. *Water*, *2*(4), 849–871. <https://doi.org/10.3390/w2040849>
- Grove, M., Harbor, J., Engel, B., & Muthukrishnan, S. (2001). Impacts of urbanization on surface hydrology, Little Eagle Creek, Indiana, and analysis of LTHIA model sensitivity to data resolution. *Physical Geography*, *22*(2), 135–153. <https://doi.org/10.1080/02723646.2001.10642734>
- Guo, J., Zhang, Z., Zhou, J., Wang, S., & Strauss, P. (2014). Decoupling streamflow responses to climate variability and land use/cover changes in a watershed in northern China. *Journal of the American Water Resources Association*, *50*(6), 1425–1438. <https://doi.org/10.1111/jawr.12197>
- Gupta, H. V., Kling, H., Yilmaz, K. K., & Martinez, G. F. (2009). Decomposition of the mean squared error and NSE performance criteria: Implications for improving hydrological modelling. *Journal of Hydrology*, *377*, 80–91. <https://doi.org/10.1016/j.jhydrol.2009.08.003>
- Gustavson, T. C. (1996). *Fluvial and eolian depositional systems, paleosols, and paleoclimate of the upper Cenozoic Ogallala and Blackwater Draw formations, southern High Plains, Texas and New Mexico* (Vol. 239). Bureau of Economic Geology, The University of Texas at Austin.
- Gwet, K. (2002). Kappa statistic is not satisfactory for assessing the extent of agreement between raters. *Statistical Methods For Inter-Rater Reliability Assessmen*, *1*(6), 1–6. Retrieved from http://www.agreestat.com/research_papers/kappa_statistic_is_not_satisfactory.pdf
- Haberlandt, U., Klöcking, B., Krysanova, V., & Becker, A. (2001). Regionalisation of the base flow index from dynamically simulated flow components - A case study in the Elbe River Basin. *Journal of Hydrology*, *248*(1–4), 35–53. [https://doi.org/10.1016/S0022-1694\(01\)00391-2](https://doi.org/10.1016/S0022-1694(01)00391-2)
- Hale, V. C., & McDonnell, J. J. (2016). Effect of bedrock permeability on stream base flow mean transit time scaling relations: 1. A multiscale catchment intercomparison. *Water Resources Research*, *52*, 1358–1374. <https://doi.org/10.1002/2015WR017660>.Effect
- Hall, F. R. (1968). Base-flow recessions—A review. *Water resources research*, *4*(5), 973–983.
- Hamed, K. H., & Rao, R. A. (1998). A modified Mann-Kendall trend test for autocorrelated data. *Journal of Hydrology*, *204*(1–4), 182–196. [https://doi.org/10.1016/S0022-1694\(97\)00125-X](https://doi.org/10.1016/S0022-1694(97)00125-X)

- Hector, B., Seguis, L., Hinderer, J., Cohard, J.-M., Wubda, M., Descloitres, M., ... Boy, J.-P. (2015). Water storage changes as a marker for base flow generation processes in a tropical humid basement catchment (Benin): Insights from hybrid gravimetry. *Water Resour. Res.*, *51*, 8331–8361. <https://doi.org/10.1002/2014WR015773>. Received
- Hejazi, M. I., & Markus, M. (2009). Impacts of urbanization and climate variability on floods in northeastern Illinois. *Journal of Hydrologic Engineering*, *14*(6), 606–616. [https://doi.org/10.1061/\(ASCE\)HE.1943-5584.0000020](https://doi.org/10.1061/(ASCE)HE.1943-5584.0000020)
- Hirsch, R. M., Slack, J. R., & Smith, R. A. (1982). Techniques of trend analysis for monthly water quality data. *Water Resources Research*, *18*(1), 107–121. <https://doi.org/10.1029/WR018i001p00107>
- Hoeg, S., Uhlenbrook, S., & Leibundgut, C. (2000). Hydrograph separation in a mountainous catchment — combining hydrochemical and isotopic tracers. *Hydrological Processes*, *14*(September 1998), 1199–1216. [https://doi.org/10.1002/\(SICI\)1099-1085\(200005\)14:7<1199::AID-HYP35>3.0.CO;2-K](https://doi.org/10.1002/(SICI)1099-1085(200005)14:7<1199::AID-HYP35>3.0.CO;2-K)
- Huang, X. D., Shi, Z. H., Fang, N. F., & Li, X. (2016). Influences of land use change on baseflow in mountainous watersheds. *Forests*, *7*(1), 1–15. <https://doi.org/10.3390/f7010016>
- Hudak, P. F. (2000). Regional trends in nitrate content of Texas groundwater. *Journal of Hydrology*, *228*(1–2), 37–47. [https://doi.org/10.1016/S0022-1694\(99\)00206-1](https://doi.org/10.1016/S0022-1694(99)00206-1)
- Huyen, N. T., Tu, L. H., Liem, N. D., Tram, V. N. Q., Minh, D. N., & Loi, N. K. (2016). Assessing impacts of land use and climate change on soil and water resources in the Srepok Watershed, Central Highland of Vietnam. *Discussion Paper Series-Southeast Asian Regional Center for Graduate Study and Research in Agriculture (SEARCA)*, 2016–2. <https://doi.org/10.13140/RG.2.2.28700.08326>
- Jang, W. S., Engel, B., & Ryu, J. (2018). Efficient flow calibration method for accurate estimation of baseflow using a watershed scale hydrological model (SWAT). *Ecological Engineering*, *125*(May), 50–67. <https://doi.org/10.1016/j.ecoleng.2018.10.007>
- Javed Mallick, Y. K., & Bharath, B.D. (2008). Estimation of land surface temperature over Delhi using Landsat-7 ETM+. *J. Ind. Geophys. Union*, *12*(3), 131–140.
- Jiménez-Muñoz, J. C., & Sobrino, J. A. (2004). Land surface temperature retrieval from LANDSAT TM 5. *Remote Sensing of Environment*, *90*(4), 434–440. <https://doi.org/10.1016/j.rse.2004.02.003>
- Jin, H., Zhu, Q., Zhao, X., & Zhang, Y. (2016). Simulation and prediction of climate variability and assessment of the response of water resources in a typical watershed in china. *Water (Switzerland)*, *8*(11), 490. <https://doi.org/10.3390/w8110490>

- Jothityangkoon, C., Sivapalan, M., & Farmer, D. L. (2001). Process controls of water balance variability in a large semi-arid catchment: Downward approach to hydrological model development. *Journal of Hydrology*, 254(1–4), 174–198. [https://doi.org/10.1016/S0022-1694\(01\)00496-6](https://doi.org/10.1016/S0022-1694(01)00496-6)
- Jung, Y., Shin, Y., Won, N. Il, & Lim, K. J. (2016). Web-based BFlow system for the assessment of streamflow characteristics at national level. *Water (Switzerland)*, 8(9), 384. <https://doi.org/10.3390/w8090384>
- Kafi, K. M., Shafri, H. Z. M., & Shariff, A. B. M. (2014). An analysis of LULC change detection using remotely sensed data; A Case study of Bauchi City. *IOP Conference Series: Earth and Environmental Science*, 20, 12056. <https://doi.org/10.1088/1755-1315/20/1/012056>
- Kendall, M. G. (1975). Rank correlation methods. 4th Edition, Charles Griffin, London. Griffin.
- Khoder, M. I. (2009). Diurnal, seasonal and weekdays–weekends variations of ground level ozone concentrations in an urban area in greater Cairo. *Environmental Monitoring and Assessment*, 149(1), 349–362. <https://doi.org/10.1007/s10661-008-0208-7>
- Khoi, D. N., & Thom, V. T. (2015). Impacts of climate variability and land-use change on hydrology in the period 1981–2009 in the central highlands of vietnam. *Global Nest Journal*, 17(4), 870–881.
- Kibria, K., Ahiablame, L., Hay, C., & Djira, G. (2016). Streamflow trends and responses to climate variability and land cover change in South Dakota. *Hydrology*, 3(1), 2. <https://doi.org/10.3390/hydrology3010002>
- Kim, J., Choi, J., Choi, C., & Park, S. (2013). Impacts of changes in climate and land use/land cover under IPCC RCP scenarios on streamflow in the Hoeya River Basin, Korea. *Science of the Total Environment*, 452–453, 181–195. <https://doi.org/10.1016/j.scitotenv.2013.02.005>
- Kimuku, C. W., & Ngigi, M. (2017). Study of urban heat island trends to aid in urban planning in Nakuru County-Kenya. *Journal of Geographic Information System*, 9, 309–325. <https://doi.org/10.4236/jgis.2017.93019>
- King, R. S., Scoggins, M., & Porras, A. (2016). Stream biodiversity is disproportionately lost to urbanization when flow permanence declines: Evidence from southwestern North America. *Freshwater Science*, 35(1), 340–352. <https://doi.org/10.1086/684943>
- Kottek, M., Grieser, J., Beck, C., Rudolf, B., & Rubel, F. (2006). World map of the Köppen-Geiger climate classification updated. *Meteorologische Zeitschrift*, 15(3), 259–263. <https://doi.org/10.1127/0941-2948/2006/0130>
- Krysanova, V., Bronstert, A., & Müller-Wohlfeil, D. (1999). Modelling river discharge for large drainage basins: From lumped to distributed approach. *Hydrological Sciences Journal*, 44(2), 313–331. <https://doi.org/10.1109/ISGTEurope.2017.8260241>

- Kumar, S., Merwade, V., Kam, J., & Thurner, K. (2009). Streamflow trends in Indiana: Effects of long term persistence, precipitation and subsurface drains. *Journal of Hydrology*, 374(1–2), 171–183. <https://doi.org/10.1016/j.jhydrol.2009.06.012>
- Lacey, G. C., & Grayson, R. B. (1998). Relating baseflow to catchment properties in south-eastern Australia. *Journal of Hydrology*, 204, 231–250.
- Lazzari Franco, A. C., & Bonumá, N. B. (2017). Multi-variable SWAT model calibration with remotely sensed evapotranspiration and observed flow. *Revista Brasileira de Recursos Hídricos - Brazilian Journal of Water Resources*, 22(35), ISSN 2318-0331. <https://doi.org/http://dx.doi.org/10.1590/2318-0331.011716090> Multi-variable
- Lee, J., Kim, J., Jang, W. S., Lim, K. J., & Engel, B. A. (2018). Assessment of baseflow estimates considering recession characteristics in SWAT. *Water (Switzerland)*, 10(4), 371. <https://doi.org/10.3390/w10040371>
- Legesse, D., Vallet-Coulomb, C., & Gasse, F. (2003). Hydrological response of a catchment to climate and land use changes in Tropical Africa: Case study south central Ethiopia. *Journal of Hydrology*, 275(1–2), 67–85. [https://doi.org/10.1016/S0022-1694\(03\)00019-2](https://doi.org/10.1016/S0022-1694(03)00019-2)
- Lerner, D. N. (2002). Identifying and quantifying urban recharge: A review. *Hydrogeology Journal*, 10(1), 143–152. <https://doi.org/10.1007/s10040-001-0177-1>
- Li, L., Tan, Y., Ying, S., Yu, Z., Li, Z., & Lan, H. (2014). Impact of land cover and population density on land surface temperature: case study in Wuhan, China. *Journal of Applied Remote Sensing*, 8, 1–19. <https://doi.org/10.1117/1.JRS.8.084993>
- Li, Z., Liu, W. zhao, Zhang, X. chang, & Zheng, F. li. (2009). Impacts of land use change and climate variability on hydrology in an agricultural catchment on the Loess Plateau of China. *Journal of Hydrology*, 377(1–2), 35–42. <https://doi.org/10.1016/j.jhydrol.2009.08.007>
- Lillesand, T. M., Kiefer, R. W., & Chipman, J. W. (2004). *Remote Sensing and Image Interpretation. Chap.7 “Digital Image Processing”* (5th Eds., Vol. 53). Wiley & Sons, New York. <https://doi.org/10.1017/CBO9781107415324.004>
- Lim, K. J., Engel, B. A., Muthukrishnan, S., & Harbor, J. (2006). Effects of initial abstraction and urbanization on estimated runoff using CN technology. *Journal of the American Water Resources Association*, 42(3), 629–643. <https://doi.org/10.1111/j.1752-1688.2006.tb04481.x>
- Lim, K. J., Engel, B. A., Tang, Z., & Choi, J. (2005). Automated Web GIS based Hydrographs Analysis Tool, WHAT. *Journal of the American Water Resources Association*, 1397, 1407–1416.
- Lim, K. J., Engel, B. A., Tang, Z., Muthukrishnan, S., Choi, J., & Kim, K. (2006). Effects of calibration on L-THIA GIS runoff and pollutant estimation. *Journal of Environmental Management*, 78(1), 35–43. <https://doi.org/10.1016/j.jenvman.2005.03.014>

- Lin, F. J. (2008). Solving multicollinearity in the process of fitting regression model using the nested estimate procedure. *Quality & Quantity*, 42(3), 417-426. <https://doi.org/10.1007/s11135-006-9055-1>
- Liu, G., He, Z., Luan, Z., & Qi, S. (2018). Intercomparison of a lumped model and a distributed model for streamflow simulation in the Naoli River Watershed, Northeast China. *Water (Switzerland)*, 10(8). <https://doi.org/10.3390/w10081004>
- Liu, L., & Zhang, Y. (2011). Urban heat island analysis using the Landsat TM data and ASTER Data: A case study in Hong Kong. *Remote Sensing*, 3(7), 1535–1552. <https://doi.org/10.3390/rs3071535>
- Longobardi, A., & Villani, P. (2008). Baseflow index regionalization analysis in a mediterranean area and data scarcity context: Role of the catchment permeability index. *Journal of Hydrology*, 355(1–4), 63–75. <https://doi.org/10.1016/j.jhydrol.2008.03.011>
- Lorenz, D. L., & Delin, G. N. (2007). A regression model to estimate regional ground water recharge. *Ground Water*, 45(2), 196–208. <https://doi.org/10.1111/j.1745-6584.2006.00273.x>
- Lu, Z., Zou, S., Xiao, H., Zheng, C., Yin, Z., & Wang, W. (2015). Comprehensive hydrologic calibration of SWAT and water balance analysis in mountainous watersheds in northwest China. *Physics and Chemistry of the Earth*, 79–82, 76–85. <https://doi.org/10.1016/j.pce.2014.11.003>
- Luo, Y., Arnold, J., Allen, P., & Chen, X. (2012). Baseflow simulation using SWAT model in an inland river basin in Tianshan Mountains, Northwest China. *Hydrology and Earth System Sciences*, 16(4), 1259–1267. <https://doi.org/10.5194/hess-16-1259-2012>
- Markham, B. L., & Barker, J. L. (1985). Spectral characterization of the LANDSAT Thematic Mapper sensors. *International Journal of Remote Sensing*, 6(5), 697–716. <https://doi.org/10.1080/01431168508948492>
- Martinez-Martinez, E., Nejadhashemi, A. P., Woznicki, S. A., & Love, B. J. (2014). Modeling the hydrological significance of wetland restoration scenarios. *Journal of Environmental Management*, 133, 121–134. <https://doi.org/10.1016/j.jenvman.2013.11.046>
- Mazvimavi, D., Meijerink, A. M. J., Savenije, H. H. G., & Stein, A. (2005). Prediction of flow characteristics using multiple regression and neural networks: A case study in Zimbabwe. *Physics and Chemistry of the Earth*, 30(11–16 SPEC. ISS.), 639–647. <https://doi.org/10.1016/j.pce.2005.08.003>
- Mazvimavi, D., Stein, A., Meijerink, A. M. J., & Savenije, H. H. G. (2003). Estimation of flow characteristics of ungauged catchments: a case study in Zimbabwe. *ITC Dissertation PhD thesis Wageningen University and Research Centre; Summaries in Dutch and English*. Retrieved from http://www.itc.nl/library/Papers_2003/phd_theses/mazvimavi.pdf

- McIntyre, N., Ballard, C., Bruen, M., Bulygina, N., Buytaert, W., Cluckie, I., ... Wheeler, H. (2014). Modelling the hydrological impacts of rural land use change. *Hydrology Research*, 45(6), 737–754. <https://doi.org/10.2166/nh.2013.145>
- McNamara, J., Kane, D. L., & Hinzman, L. D. (1997). Hydrograph separation in an Arctic watershed using mixing model and graphical techniques. *Water Resources Research*, 33(7), 1707–1719.
- Megahed, Y., Cabral, P., Silva, J., & Caetano, M. (2015). Land cover mapping analysis and urban growth modelling using remote sensing techniques in Greater Cairo Region—Egypt. *ISPRS International Journal of Geo-Information*, 4(3), 1750–1769. <https://doi.org/10.3390/ijgi4031750>
- Mehan, S., Neupane, R. P., & Kumar, S. (2017). Coupling of SUFI 2 and SWAT for improving the simulation of streamflow in an agricultural watershed of South Dakota. *Hydrology: Current Research*, 8(3). <https://doi.org/10.4172/2157-7587.1000280>
- Meyer, S. C. (2005). Analysis of base flow trends in urban streams, Northeastern Illinois, USA. *Hydrogeology Journal*, 13(5–6), 871–885. <https://doi.org/10.1007/s10040-004-0383-8>
- Meyer, J. E., Wise, M. R., & Kalaswad, S. (2012). *Pecos Valley aquifer, west Texas: structure and brackish groundwater*. Texas Water Development Board.
- Millar S.W.S. (2015) Colluvial Deposit. In: Hargitai H., Kereszturi Á. (eds) Encyclopedia of Planetary Landforms. Springer, New York, NY
- Miller, M., Buto, S., David, S., & Rumsey, C. (2016). The importance of base flow in sustaining surface water flow in the Upper Colorado River Basin Matthew. *American Geophysical Union*, 1–16. <https://doi.org/10.1002/2015WR017963>.Received
- Moriasi, D. N., Arnold, J. G., Van Liew, M. W., Bingner, R. L., Harmel, R. D., & Veith, T. L. (2007). Model evaluation guidelines for systematic quantification of accuracy in watershed simulations. *Transactions of the ASABE*, 50(3), 885–900. <https://doi.org/10.13031/2013.23153>
- Moriasi, D. N., Gitau, M. W., Pai, N., & Daggupati, P. (2015). Hydrologic and water quality models: performance measures and evaluation criteria. *Transactions of the ASABE*, 58(6), 1763–1785. <https://doi.org/10.13031/trans.58.10715>
- Moriasi, D. N., Gowda, P. H., Arnold, J. G., Mulla, D. J., Ale, S., Steiner, J. L., & Tomer, M. D. (2013). Evaluation of the Hooghoudt and Kirkham tile drain equations in the Soil and Water Assessment Tool to simulate tile flow and Nitrate-Nitrogen. *Journal of Environment Quality*, 42(6), 1699. <https://doi.org/10.2134/jeq2013.01.0018>
- Mwakalila, S., Feyen, J., & Wyseure, G. (2002). The influence of physical catchment properties on baseflow in semi-arid environments. *Journal of Arid Environments*, 52(2), 245–258. <https://doi.org/10.1006/jare.2001.0947>

- Nash, J. E., & Sutcliffe, J. V. (1970). River flow forecasting through conceptual models part I - A discussion of principles. *Journal of Hydrology*, 10(3), 282–290. [https://doi.org/10.1016/0022-1694\(70\)90255-6](https://doi.org/10.1016/0022-1694(70)90255-6)
- Nathan, R. J., & McMahon, T. A. (1990). Evaluation of automated techniques for base flow and recession analyses. *Water Resources Research*, 26(7), 1465–1473. <https://doi.org/10.1029/WR026i007p01465>
- Neff, B. P., Day, S. M., Piggott, A. R., & Fuller, L. M. (2005). Base flow in the Great Lakes basin. *U.S. Geological Survey Scientific Investigations Report*, (2005–5217), 32. <https://doi.org/10.3133/sir20055217>
- Neitsch, S. ., Arnold, J. ., Kiniry, J. ., & Williams, J. . (2009). Soil and Water Assessment Tool Theoretical Documentation - Version 2009, Technical Report no 406, 618. <https://doi.org/10.1016/j.scitotenv.2015.11.063>
- Neitsch, S. ., Arnold, J. ., Kiniry, J. ., & Williams, J. . (2011). Soil & Water Assessment Tool Theoretical Documentation Version 2009. *Texas Water Resources Institute*, 1–647. <https://doi.org/10.1016/j.scitotenv.2015.11.063>
- Neitsch, S. L., Arnold, J. G., Kiniry, J. R., Srinivasan, R., & Williams, J. R. (2002). Soil and Water Assessment Tool User’s Manual. *TWRI Report TR-192*, 412.
- Neitsch, S. L., Arnold, J. G., Kiniry, J. R., & Williams., J. R. (2005). Soil and Water Assessment Tool User’s Manual Version 2005. *Diffuse Pollution Conference Dublin*, 494.
- Nie, W., Yuan, Y., Kepner, W., Nash, M. S., Jackson, M., & Erickson, C. (2011). Assessing impacts of landuse and landcover changes on hydrology for the upper San Pedro watershed. *Journal of Hydrology*, 407(1–4), 105–114. <https://doi.org/10.1016/j.jhydrol.2011.07.012>
- Novotny, E. V., & Stefan, H. G. (2007). Stream flow in Minnesota: Indicator of climate change. *Journal of Hydrology*, 334(3–4), 319–333. <https://doi.org/10.1016/j.jhydrol.2006.10.011>
- Ogashawara, I., & Bastos, V. (2012). A quantitative approach for analyzing the relationship between urban heat islands and land cover. *Remote Sensing*, 4(12), 3596–3618. <https://doi.org/10.3390/rs4113596>
- Omer, A., Wang, W., Basheer, A. K., & Yong, B. (2017). Integrated assessment of the impacts of climate variability and anthropogenic activities on river runoff: a case study in the Hutuo River Basin, China. *Hydrology Research*, 48(2), 416–430. <https://doi.org/10.2166/nh.2016.229>
- Omran, E. S. E. (2012). Detection of land-use and surface temperature change at different resolutions. *Journal of Geographic Information System*, 4(3), 189–203. <https://doi.org/10.4236/jgis.2012.43024>
- OpenStreetMap. (n.d.). Road Networks. Retrieved from <https://www.openstreetmap.org/#map=12/30.0550/31.2376>

- Owen, T. W., Carlson, T. N., & Gillies, R. R. (1998). An assessment of satellite remotely-sensed land cover parameters in quantitatively describing the climatic effect of urbanization. *International Journal of Remote Sensing*, 19(9), 1663–1681. <https://doi.org/10.1080/014311698215171>
- Ozesmi, S. L., & Bauer, M. E. (2002). Satellite remote sensing of wetlands. *Wetlands Ecology and Management*, 10(5), 381–402. <https://doi.org/10.1023/A:1020908432489>
- Pal, S., & Ziaul, S. (2016). Detection of land use and land cover change and land surface temperature in English Bazar urban centre. *The Egyptian Journal of Remote Sensing and Space Science*, 20(1), 125–145. <https://doi.org/10.1016/j.ejrs.2016.11.003>
- Park, J. . Y., Park, M. J., Joh, H. K., Shin, H. J., Kwon, H. J., Srinivasan, R., & Kim, S. J. (2011). Assessment of MIROC 3.2 HiRes Climate and CLUE-s land use change impacts on watershed hydrology Using SWAT. *Transactions of the ASABE*, 54(5), 1713–1724. <https://doi.org/10.13031/2013.39842>
- Pinder, G. F., & Jones, J. F. (1969). Determination of the ground-water component of peak discharge from the chemistry of total runoff. *Water Resources Research*, 5(2), 438-445. <https://doi.org/10.1029/WR005i002p00438>
- Preston, R. D., & Bankston, W. O. (1978). Occurance and quality of ground water in the vicinity of Brownsville, Texas. *Texas Department of Water Resources*, 1–100.
- Price, K. (2011). Effects of watershed topography, soils, land use, and climate on baseflow hydrology in humid regions: A review. *Progress in Physical Geography*, 35(4), 465–492. <https://doi.org/10.1177/0309133311402714>
- Price, K., Jackson, C. R., Parker, A. J., Reitan, T., Dowd, J., & Cyterski, M. (2011). Effects of watershed land use and geomorphology on stream low flows during severe drought conditions in the southern Blue Ridge Mountains, Georgia and North Carolina, United States. *Water Resources Research*, 47(2). <https://doi.org/10.1029/2010WR009340>
- Qaid, A. M., & Basavarajappa, H. T. (2008). Application of optimum index factor technique to Lansat-7 Data for geological mapping of North East of Hajjah, Yemen. *American-Eurasian Journal Scientific Research*, 3(1), 84–91. <https://doi.org/10.1007/s10661-012-2631-z>
- Qin, J., Ding, Y., Han, T., & Liu, Y. (2017). Identification of the factors influencing the baseflow in the permafrost region of the northeastern qinghai-tibet plateau. *Water (Switzerland)*, 9(9), 666. <https://doi.org/10.3390/w9090666>
- Rahman, M. T. (2016). Land use and land cover changes and urban sprawl in Riyadh, Saudi Arabia: An analysis using Multi-Temporal Landsat data and Shannon’s Entropy Index. *ISPRS - International Archives of the Photogrammetry, Remote Sensing and Spatial Information Sciences*, XLI-B8, 1017–1021. <https://doi.org/10.5194/isprs-archives-XLI-B8-1017-2016>
- Rao, P. K. (1972). Remote sensing of urban heat islands from an environmental satellite. *Bulletin of the American Meteorological Society*, 53, 647–648.

- Rasul, A., Balzter, H., Smith, C., Remedios, J., Adamu, B., Sobrino, J. A., ... Weng, Q. (2017). A Review on remote sensing of urban heat and cool islands. *Land*, 6(2), 38–47. <https://doi.org/10.3390/land6020038>
- Rawat, J. S., & Kumar, M. (2015). Monitoring land use / cover change using remote sensing and GIS techniques : A case study of Hawalbagh block, district Almora, Uttarakhand, India. *The Egyptian Journal of Remote Sensing and Space Sciences*, 18(1), 77–84. <https://doi.org/10.1016/j.ejrs.2015.02.002>
- Ridd, M. K., & Liu, J. (1998). A Comparison of four algorithms for change detection in an urban environment. *Remote Sensing of Environment*, 63(2), 95–100. [https://doi.org/10.1016/S0034-4257\(97\)00112-0](https://doi.org/10.1016/S0034-4257(97)00112-0)
- Ringnér, M. (2008). What is principal component analysis? *Nature Biotechnology*, 26(3), 303–304. <https://doi.org/10.1038/nbt0308-303>
- Rodda, J. (2001). Water under pressure. *Hydrological Sciences Journal*, 46(6), 841–853. <https://doi.org/10.1103/PhysRevLett.84.2429>
- Rusli, N., Majid, M. R., Yusop, Z., Tan, M. L., Hashim, S., & Bohari, S. N. (2017). Integrating manual calibration and auto-calibration of SWAT model in Muar Watershed, Johor. *2016 7th IEEE Control and System Graduate Research Colloquium, ICSGRC 2016 - Proceeding*, (August), 197–202. <https://doi.org/10.1109/ICSGRC.2016.7813327>
- Sahana, M., Ahmed, R., & Sajjad, H. (2016). Analyzing land surface temperature distribution in response to land use/land cover change using split window algorithm and spectral radiance model in Sundarban Biosphere Reserve, India. *Modeling Earth Systems and Environment*, 2(2), 81. <https://doi.org/10.1007/s40808-016-0135-5>
- Sahin, V., & Hall, M. J. (1996). The effects of afforestation and deforestation on water yields. *Journal of Hydrology*, 178, 293–309. <https://doi.org/10.1109/IGARSS.2005.1525425>
- Santhi, C., Allen, P. M., Muttiah, R. S., Arnold, J. G., & Tuppada, P. (2008). Regional estimation of base flow for the conterminous United States by hydrologic landscape regions. *Journal of Hydrology*, 351(1–2), 139–153. <https://doi.org/10.1016/j.jhydrol.2007.12.018>
- Santhi, C., Arnold, J. G., Williams, J. R., Dugas, W. A., Srinivasan, R., & Hauck, L. M. (2001). Validation of the SWAT model on a large river basin with point and nonpoint sources. *Journal of the American Water Resources Association*, 37(5), 1169–1188. <https://doi.org/10.1111/j.1752-1688.2001.tb03630.x>
- Scanlon, B. R., Healy, R. W., & Cook, P. G. (2002). Choosing appropriate techniques for quantifying groundwater recharge. *Hydrogeology journal*, 10(1), 18–39. <https://doi.org/10.1007/s10040-0010176-2>
- Schilling, K. E. (2009). Investigating local variation in groundwater recharge along a topographic gradient, Walnut Creek, Iowa, USA. *Hydrogeology Journal*, 17(2), 397–407. <https://doi.org/10.1007/s10040-008-0347-5>

- Schilling, K. E., Jha, M. K., Zhang, Y.-K., Gassman, P. W., & Wolter, C. F. (2008). Impact of land use and land cover change on the water balance of a large agricultural watershed: Historical effects and future directions. *Water Resources Research*, 44(7), 1–12. <https://doi.org/10.1029/2007WR006644>
- Schulz, W. H., Lidke, D. J., & Godt, J. W. (2008). Modeling the spatial distribution of landslide-prone colluvium and shallow groundwater on hillslopes of Seattle, WA. *Earth Surface Processes and Landforms*, 33, 123–141. <https://doi.org/10.1002/esp>
- Sekaluvu, L., Zhang, L., & Gitau, M. (2018). Evaluation of constraints to water quality improvements in the Western Lake Erie Basin. *Journal of Environmental Management*, 205, 85–98. <https://doi.org/10.1016/j.jenvman.2017.09.063>
- Sen, P. K. (1968). Estimates of the regression coefficient based on Kendall's Tau. *Journal of the American Statistical Association*, 63(324), 1379–1389. <https://doi.org/10.1080/01621459.1968.10480934>
- Setegn, S. G., Srinivasan, R., & Dargahi, B. (2008). Hydrological modelling in the Lake Tana Basin, Ethiopia using SWAT model. *The Open Hydrology Journal*, 2(1), 49–62. <https://doi.org/10.2174/1874378100802010049>
- Shahin, M. (1990). Impacts of urbanization of the Greater Cairo Area on the groundwater in the underlying aquifer. In *Hydrological Processes and Water Management in Urban Areas*. (pp. 243–249).
- Sheikhi, A., Kanniah, K. D., & Ho, C. H. (2015). Effect of land cover and green space on land surface temperature of a fast growing economic region in Malaysia. *Proceedings of SPIE*, 9644(964413), 1–8. <https://doi.org/10.1117/12.2194796>
- Shi, P., Ma, X., Hou, Y., Li, Q., Zhang, Z., Qu, S., ... Fang, X. (2013). Effects of land-use and climate change on hydrological processes in the upstream of Huai River, China. *Water Resources Management*, 27(5), 1263–1278. <https://doi.org/10.1007/s11269-012-0237-4>
- Sklash, M. G., & Farvolden, R. N. (1979). The role of groundwater in storm runoff. In *Developments in water science* (Vol. 12, pp. 45-65). Elsevier.
- Smakhtin, V. . (2001). Low flow hydrology: a review. *Journal of Hydrology*, 240, 147–186. [https://doi.org/10.1016/S0022-1694\(00\)00340-1](https://doi.org/10.1016/S0022-1694(00)00340-1)
- Solly, W. B., Pierce, R. R., & Perlman, H. . (1998). Estimated use of water in the United States in 1995. In *U.S. Geological Survey Circular 1200*. Retrieved from <https://water.usgs.gov/edu/characteristics.html>
- Sophocleous, M., & Perkins, S. P. (2000). Methodology and application of combined watershed and ground-water models in Kansas. *Journal of Hydrology*, 236(3–4), 185–201. [https://doi.org/10.1016/S0022-1694\(00\)00293-6](https://doi.org/10.1016/S0022-1694(00)00293-6)

- Strause, J. L. (1987). Texas ground-water quality. *United States Geological Survey Open-File Report*, 87(754), 1–12.
- Sun, D., & Kafatos, M. (2007). Note on the NDVI-LST relationship and the use of temperature-related drought indices over North America. *Geophysical Research Letters*, 34(September), 1–4. <https://doi.org/10.1029/2007GL031485>
- Swank, W. T., Swift, L. W., & Douglass, J. E. (1988). Streamflow changes associated with forest cutting, species conversions, and natural disturbances. In W. T. Swank & D. A. Crossley (Eds.), *Forest Hydrology and Ecology at Coweeta* (pp. 297–312). New York, NY: Springer New York. https://doi.org/10.1007/978-1-4612-3732-7_22
- Szilagyi, J., & Parlange, M. B. (1998). Baseflow separation based on analytical solutions of the Boussinesq equation. *Journal of Hydrology*, 204(1–4), 251–260. [https://doi.org/10.1016/S0022-1694\(97\)00132-7](https://doi.org/10.1016/S0022-1694(97)00132-7)
- Tan, M. L., Ibrahim, A. L., Yusop, Z., Duan, Z., & Ling, L. (2015). Impacts of land-use and climate variability on hydrological components in the Johor River basin, Malaysia. *Hydrological Sciences Journal*, 60(5), 1–17. <https://doi.org/10.1080/02626667.2014.967246>
- Tang, Z., Engel, B. A., Lim, K. J., Pijanowski, B. C., & Harbor, J. (2005). Minimizing the impact of urbanization on long term runoff. *Journal of the American Water Resources Association*, 41(6), 1347–1359. <https://doi.org/10.1111/j.1752-1688.2005.tb03804.x>
- Tao, X. e., Chen, H., Xu, C. yu, Hou, Y. kun, & Jie, M. xuan. (2015). Analysis and prediction of reference evapotranspiration with climate change in Xiangjiang River Basin, China. *Water Science and Engineering*, 8(4), 273–281. <https://doi.org/10.1016/j.wse.2015.11.002>
- Tesemma, Z. K., Mohamed, Y. A., & Steenhuis, T. S. (2010). Trends in rainfall and runoff in the Blue Nile Basin: 1964-2003. *Hydrological Processes*, 24(25), 3747–3758. <https://doi.org/10.1002/hyp.7893>
- Texas Water Development Board. (2003). *Groundwater Availability of the Central Gulf Coast Aquifer: Numerical Simulations to 2050 Central Gulf Coast, Texas*.
- Texas Water Development Board. (2012). Chapter 4 Climate of Texas. *Water For Texas 2012 State Water Plan*, 145–155. Retrieved from <https://www.mendeley.com/viewer/?fileId=0ec0c4ff-06ba-832f-0042-1a4fa3e46231&documentId=0abfb413-0a9d-3fa4-8c83-87957a3263c7>
- Thirel, G., Andréassian, V., Perrin, C., Audouy, J. N., Berthet, L., Edwards, P., ... Vaze, J. (2015). Hydrology under change: an evaluation protocol to investigate how hydrological models deal with changing catchments. *Hydrological Sciences Journal*, 60(7–8), 1184–1199. <https://doi.org/10.1080/02626667.2014.967248>
- Tobin, K. J., & Bennett, M. E. (2009). Using SWAT to model streamflow in two river basins with ground and satellite precipitation data. *Journal of the American Water Resources Association*, 45(1), 253–271. <https://doi.org/10.1111/j.1752-1688.2008.00276.x>

- Tong, S. T. Y., Sun, Y., Ranatunga, T., He, J., & Yang, Y. J. (2012). Predicting plausible impacts of sets of climate and land use change scenarios on water resources. *Applied Geography*, 32(2), 477–489. <https://doi.org/10.1016/j.apgeog.2011.06.014>
- Tran, D. X., Pla, F., Latorre-Carmona, P., Myint, S. W., Caetano, M., & Kieu, H. V. (2017). Characterizing the relationship between land use land cover change and land surface temperature. *ISPRS Journal of Photogrammetry and Remote Sensing*, 124, 119–132. <https://doi.org/10.1016/j.isprsjprs.2017.01.001>
- Tu, J. (2009). Combined impact of climate and land use changes on streamflow and water quality in eastern Massachusetts, USA. *Journal of Hydrology*, 379(3–4), 268–283. <https://doi.org/10.1016/j.jhydrol.2009.10.009>
- U.S. Geological Survey. (n.d.). EarthExplorer. Retrieved from <https://earthexplorer.usgs.gov/>
- Van Liew, M. W., Arnold, J. G., & Bosch, D. D. (2005). Problem and Potential of Autocalibrating a Hydrologic Model. *Transactions of the ASABE*, 48(3), 1025–1040.
- Van Liew, M. W., Veith, T. L., Bosch, D. D., & Arnold, J. G. (2007). Suitability of SWAT for the conservation effects assessment project: Comparison on USDA Agricultural Research Service Watersheds. *Journal of Hydrologic Engineering*, 12(2), 173–189. [https://doi.org/10.1061/\(ASCE\)1084-0699\(2007\)12:2\(173\)](https://doi.org/10.1061/(ASCE)1084-0699(2007)12:2(173))
- Veith, T. L., Van Liew, M. W., Bosch, D. D., & Arnold, J. G. (2010). Parameter sensitivity and uncertainty in SWAT: A comparison across five USDA-ARS Watersheds. *Transactions of the ASABE*, 53, 1477–1486. <https://doi.org/10.13031/2013.34906>
- Viera, A. J., & Garrett, J. M. (2005). Understanding Interobserver Agreement: The Kappa Statistic. *Family Medicine*, 37(5), 360–363. <https://doi.org/Vol. 37, No. 5>
- VIS, I. (2009). ENVI Atmospheric Correction Module: QUAC and FLAASH user's guide. *Module Version 4*. Retrieved from <http://scholar.google.com/scholar?hl=en&btnG=Search&q=intitle:ENVI+Atmospheric+Correction+Module:+QUAC+and+FLAASH+user's+guide#0>
- Wallace, C. W., Flanagan, D. C., & Engel, B. A. (2018). Evaluating the effects of watershed size on SWAT calibration. *Water (Switzerland)*, 10(7), 1–27. <https://doi.org/10.3390/w10070898>
- Wang, W., Shao, Q., Yang, T., Peng, S., Xing, W., Sun, F., & Luo, Y. (2013). Quantitative assessment of the impact of climate variability and human activities on runoff changes: A case study in four catchments of the Haihe River basin, China. *Hydrological Processes*, 27(8), 1158–1174. <https://doi.org/10.1002/hyp.9299>
- Wang, X., Engel, B., Yuan, X., & Yuan, P. (2018). Variation analysis of streamflows from 1956 to 2016 along the Yellow River, China. *Water (Switzerland)*, 10(1231), 1–20. <https://doi.org/10.3390/w10091231>

- Warner, G. S., García-Martinó, A. R., Scatena, F. N., & Civco, D. L. (2003). Watershed characterization by GIS for low flow prediction. *GIS for Water Resources and Watershed Management*, 101–107.
- Welde, K., & Gebremariam, B. (2017). Effect of land use land cover dynamics on hydrological response of watershed: Case study of Tekeze Dam watershed, northern Ethiopia. *International Soil and Water Conservation Research*, 5(1), 1–16. <https://doi.org/10.1016/j.iswcr.2017.03.002>
- Weng, Q., Lu, D., & Schubring, J. (2004). Estimation of land surface temperature-vegetation abundance relationship for urban heat island studies. *Remote Sensing of Environment*, 89(4), 467–483. <https://doi.org/10.1016/j.rse.2003.11.005>
- Whittingham, M. J., Stephens, P. A., Bradbury, R. B., & Freckleton, R. P. (2006). Why do we still use stepwise modelling in ecology and behaviour? *Journal of Animal Ecology*, 75(5), 1182–1189. <https://doi.org/10.1111/j.1365-2656.2006.01141.x>
- Wilson, E. H., Sader, S. A., Hoffhine, E., & Sader, S. A. (2002). Detection of forest harvest type using multiple dates of Landsat TM imagery Detection of forest harvest type using multiple dates. *Remote Sensing of Environment*, 80(June 2002), 385–396. [https://doi.org/10.1016/S0034-4257\(01\)00318-2](https://doi.org/10.1016/S0034-4257(01)00318-2)
- Wilson, J., Clay, M., Martin, E., Stuckey, D., & Vedder-Risch, K. (2003). Evaluating environmental influences of zoning in urban ecosystems with remote sensing. *Remote Sensing of Environment*, 86(3), 303–321. [https://doi.org/10.1016/S0034-4257\(03\)00084-1](https://doi.org/10.1016/S0034-4257(03)00084-1)
- Winter, T. C., Harvey, J. W., Franke, O. L., & Alley, W. M. (1998). US Geological Survey Circular 1139. *Ground Water and Surface Water: A Single Resource*, 50.
- Woodruff Jr, C. M., & Abbott, P. L. (1986). Stream piracy and evolution of the Edwards Aquifer along the Balcones Escarpment, central Texas. *The Balcones escarpment-geology, hydrology, ecology and social development in central Texas: Geological Society of America*, 77-90.
- Xiong, Y., Huang, S., Chen, F., Ye, H., Wang, C., & Zhu, C. (2012). The Impacts of Rapid Urbanization on the Thermal Environment: A Remote Sensing Study of Guangzhou, South China. *Remote Sensing*, 4(7), 2033–2056. <https://doi.org/10.3390/rs4072033>
- Xu, X., Scanlon, B. R., Schilling, K., & Sun, A. (2013). Relative importance of climate and land surface changes on hydrologic changes in the US Midwest since the 1930s: Implications for biofuel production. *Journal of Hydrology*, 497, 110–120. <https://doi.org/10.1016/j.jhydrol.2013.05.041>
- Yan, T., Bai, J., Lee Zhi Yi, A., & Shen, Z. (2018). SWAT-simulated streamflow responses to climate variability and human activities in the Miyun Reservoir basin by considering streamflow components. *Sustainability (Switzerland)*, 10(4). <https://doi.org/10.3390/su10040941>

- Yang, X. (2002). Satellite monitoring of urban spatial growth in the Atlanta Metropolitan Area. *Photogrammetric Engineering and Remote Sensing*, 68(7), 725–734.
- Younesazadeh, S., Amiri, N., & Pilesjo, P. (2015). The effect of land use on land surface temperature in the Netherlands. *The International Archives of Photogrammetry, Remote Sensing and Spatial Information Sciences* 40(1), 745.
- Yuan, E., Nie, W., & Sanders, E. (2015). Problems and prospects of SWAT model application on an arid/semi-arid watershed in Arizona. *SEDHYD 2014 Joint Conference*.
- Yuan, F., Sawaya, K. E., Loeffelholz, B. C., & Bauer, M. E. (2005). Land cover classification and change analysis of the Twin Cities (Minnesota) Metropolitan Area by multitemporal Landsat remote sensing. *Remote Sensing of Environment*, 98, 317–328. <https://doi.org/10.1016/j.rse.2005.08.006>
- Yue, S. (1999). Applying bivariate normal distribution to flood frequency analysis. *Water international*, 24(3), 248-254. <https://doi.org/10.1080/02508069908692168>
- Zaki, R., Zaki, A., & Ahmed, S. (2011). Land use and land cover changes in arid region: the case new urbanized zone, Northeast Cairo, Egypt. *Journal of Geographic Information System*, 3(3), 173–194. <https://doi.org/10.4236/jgis.2011.33015>
- Zanter, K. (2016). Landsat 8 (L8) Data Users Handbook. *LSDS-1574 Version 2*, 1–106.
- Zecharias, Y. B., & Brutsaert, W. (1988). The influence of basin morphology on groundwater outflow. *Water Resources Research*, 24(10), 1645–1650. <https://doi.org/10.1029/WR024i010p01645>
- Zha, Y., Gao, J., & Ni, S. (2003). Use of normalized difference built-up index in automatically mapping urban areas from TM imagery. *International Journal of Remote Sensing*, 24(3), 583–594. <https://doi.org/10.1080/01431160304987>
- Zhang, D., Liu, X., Liu, C., & Bai, P. (2013b). Responses of runoff to climatic variation and human activities in the Fenhe River, China. *Stochastic Environmental Research and Risk Assessment*, 27(6), 1293–1301. <https://doi.org/10.1007/s00477-012-0665-y>
- Zhang, L., Karthikeyan, R., Bai, Z., & Srinivasan, R. (2017). Analysis of streamflow responses to climate variability and land use change in the Loess Plateau region of China. *Catena*, 154, 1–11. <https://doi.org/10.1016/j.catena.2017.02.012>
- Zhang, L., Nan, Z., Xu, Y., & Li, S. (2016). Hydrological impacts of land use change and climate variability in the headwater region of the Heihe River Basin, northwest China. *PLoS ONE*, 11(6), 1–25. <https://doi.org/10.1371/journal.pone.0158394>
- Zhang, L., Nan, Z., Yu, W., & Ge, Y. (2015). Modeling land-use and land-cover change and hydrological responses under consistent climate change scenarios in the Heihe River Basin, China. *Water Resources Management*, 29(13), 4701–4717. <https://doi.org/10.1007/s11269-015-1085-9>

- Zhang, X., Srinivasan, R., Arnold, J., Izaurre, R. C., & Bosch, D. (2011). Simultaneous calibration of surface flow and baseflow simulations: A revisit of the SWAT model calibration framework. *Hydrological Processes*, 25(14), 2313–2320. <https://doi.org/10.1002/hyp.8058>
- Zhang, Y., Ahiablame, L., Engel, B., & Liu, J. (2013a). Regression modeling of baseflow and baseflow index for Michigan USA. *Water (Switzerland)*, 5(4), 1797–1815. <https://doi.org/10.3390/w5041797>
- Zhang, Y., Engel, B., Ahiablame, L., & Liu, J. (2015). Impacts of climate change on mean annual water balance for watersheds in Michigan, USA. *Water (Switzerland)*, 7, 3565–3578. <https://doi.org/10.3390/w7073565>
- Zhang, Y. K., & Schilling, K. E. (2006). Increasing streamflow and baseflow in Mississippi River since the 1940 s: Effect of land use change. *Journal of Hydrology*, 324(1–4), 412–422. <https://doi.org/10.1016/j.jhydrol.2005.09.033>
- Zhang, Y., & Wurbs, R. (2018). Long-term changes in river system hydrology in Texas. *Proceedings of the International Association of Hydrological Sciences*, 379(2006), 255–261. <https://doi.org/10.5194/piahs-379-255-2018>
- Zhao, A., Zhu, X., Liu, X., Pan, Y., & Zuo, D. (2015). Impacts of land use change and climate variability on green and blue water resources in the Weihe River Basin of northwest China. *Catena*, 137, 318–327. <https://doi.org/10.1016/j.catena.2015.09.018>
- Zheng, H., Zhang, L., Zhu, R., Liu, C., Sato, Y., & Fukushima, Y. (2009). Responses of streamflow to climate and land surface change in the headwaters of the Yellow River Basin. *Water Resources Research*, 45(7), 1–9. <https://doi.org/10.1029/2007WR006665>
- Zhu, Y., & Day, R. L. (2009). Regression modeling of streamflow, baseflow, and runoff using geographic information systems. *Journal of Environmental Management*, 90(2), 946–953. <https://doi.org/10.1016/j.jenvman.2008.02.011>
- Zou, S., Jilili, A., Duan, W., De Maeyer, P., & Van de Voorde, T. (2019). Human and natural impacts on the water resources in the Syr Darya River Basin, Central Asia. *Sustainability (Switzerland)*, 11(11). <https://doi.org/10.3390/su11113084>
- Zuo, D., Xu, Z., Yao, W., Jin, S., Xiao, P., & Ran, D. (2016). Assessing the effects of changes in land use and climate on runoff and sediment yields from a watershed in the Loess Plateau of China. *Science of the Total Environment*, 544, 238–250. <https://doi.org/10.1016/j.scitotenv.2015.11.060>

VITA

PROFESSIONAL SUMMARY (*Years of Experience: 10 years*)

- **Hydrologic modeler;** trained in modeling of surface and subsurface flow processes and interactions for prediction of physical principles and interrelationships with land use alteration and climate change.
- **Geo-detection and information technology;** trained in analysis, visualization and interpretation of environmental and land use changes using Remote Sensing and Geographic Information Systems.
- **Strong background in geology;** in-depth knowledge of geological structures, soil and rock types.
- **Strong oral and written communication skills;** ability to identify complex problems and review related information to develop and evaluate options and implement solutions.

EDUCATION

- **Ph.D:** Agriculture and Biological Engineering, 2015-Present
Purdue University • West Lafayette, IN, USA
- **Master of Science:** Earth Science and Resources, 2010-2013
China University of Geosciences • Beijing, China
- **Bachelor of Science:** Geology with honors, 2009
Suez Canal University • Ismailia, Egypt

CAREER OBJECTIVE

It is my ambition to apply my analytical and modeling expertise to an academic career in which I have the opportunity to develop detailed environmental studies and identify recommended solutions to problems related to economics, environment, urbanization, natural resources and homeland security. I strongly desire to continue to not only apply my knowledge of hydrology, modeling, statistics and GIS approaches, but to also develop new analytical techniques or applications to facilitate lasting, impactful solutions to environmental/economic problems in agriculture and potentially other sectors.

PUBLICATIONS

- ⁵*In preparation:* **Aboelnour, M., et. al.** Working title: Impacts of Watershed Physical Properties and Land-Use on Baseflow at Regional Scales.
- ⁴**Aboelnour, M.,** Gitau, M. W., & Engel, B. A. (2020). “A Comparison of Streamflow and Baseflow Responses to Land-Use Change and the Variation in Climate Parameters using SWAT. *Water*.
- ³**Aboelnour, M.,** Gitau, M. W., & Engel, B. A. (2019). Hydrologic Response in an Urban Watershed as Affected by Climate and Land-Use Change. *Water*, 11(8), 1603.
- ²**Aboelnour, M.,** & Engel, B. A. (2018). Application of remote sensing techniques and geographic information systems to analyze land surface temperature in response to land use/land cover change in greater Cairo region, Egypt. *Journal of Geographic Information System*, 10(1).
- ¹Li, C., Chen, D., Chen, J., Chen, X., Yang, X., & **Aboelnour, M. A.** (2015). Correlations between the North China Craton and the Indian Shield: Constraints from regional metallogeny. *Geoscience Frontiers*, 6(6), 861-873.

AWARDS AND HONORS

- **PRF Research Fellowship:** One-year Assistantship, 2019 • Purdue Research Foundation
- **College of Engineering Graduate School Scholarship:** Awardee, 2018 • Purdue University
- **The Frederick N. Andrews Environmental Grant:** Awardee, 2018 • Purdue University
- **Purdue Graduate Student Government Travel Award:** Awardee, 2018 • Purdue University
- **The Egyptian Governmental Scholarship:** Full Ph.D. mission, 2014 • Purdue University
- **China Scholarship Council: Master’s degree,** 2010 • China University of Geosciences, Beijing

SELECTED CONFERENCE PRESENTATIONS

- “Urban Watershed Responses to Climate Variability and Land Use Dynamics.” *ABE Symposium.* West Lafayette, IN. 2019.
- “Responses of Streamflow and Baseflow Hydrology to Climate Variability and Land Use Dynamics in an Urban Watershed.” *American Geophysical Union.* Washington D. C. 2018.
- “Impacts of Climate Variability and Land Use Change on Streamflow and Baseflow in an Urban Watershed.” *Indiana Water Resources Association.* Bloomington, IN. 2018.
- “Analysis of the Impact of Land Use/Land Cover Change on Land Surface Temperature Using Remote Sensing: A Case Study in Greater Cairo Region, Egypt.” *American Assoc. of ABE.* Spokane, WA. 2017.
- *Outstanding Poster Award:* “Statistical Correlation between NDVI and Land Surface Temperature Using Geo-Spatial Techniques in Greater Cairo Region, Egypt.” *Indiana Water Resources Association.* Marshal, IN. 2017.
- “Geologic Mapping Using MASTER Multispectral Data Analysis: A Case Study in Cuprite Area, Nevada, USA.” *ABE Meeting.* West Lafayette, IN. 2017.
- “Monitoring Geothermal Areas Using Satellite-based Thermal Infrared: A Case Study in the Gulf of Suez, Egypt.” *Ecological Sci & Engineering Conf.* West Lafayette, IN. 2016.

TEACHING ASSISTANTSHIPS

Spring 2019	Introduction to survey (200-level class, Purdue University)
Spring 2015	Geographic Information System (GIS) (300-level class, Suez Canal University)
	Hydrogeology (200-level class, Suez Canal University)
Fall 2015	Structural Geology (300-level class, Suez Canal University)
Spring 2014	Physical Geology- for non-majors (100-level class, Suez Canal University)
Fall 2014	Engineering Geology- for non-majors (200-level class, Suez Canal University)
Fall 2012	Remote Sensing and Image Processing (Grad level, China Univ. of Geosciences)
Spring 2010	Optical mineralogy (200-level class, Suez Canal University)
Spring 2009	Crystallography (200-level class, Suez Canal University)
	Geology of Egypt (400-level class, Suez Canal University)
	Optical mineralogy (200-level class, Suez Canal University)
Fall 2009	Introduction to General Geology (100-level class, Suez Canal University)

LEADERSHIP AND SERVICE

2020-Present	Agriculture Water Management , Reviewer
2020-Present	Environmental Science and Pollution Research , Reviewer
2018-Present	American Geophysical Union , Member
2017-Present	Agricultural and Biological Engineering Graduate Committee , Representative
2017-Present	Egyptian Student Assoc in North America , Treasurer (<i>Funded \$40,000</i>)
2017-Present	American Society of Agricultural and Biological Engineers
2017-2018	Egyptian Student Association at Purdue University , Vice President
2016-2018	Graduate Student Organization , Treasurer (<i>Funded \$15,000</i>)
2016-2018	Annual Graduate Ag. and Bio. Eng. Research Symposium , Coordinator
2013-Present	The Egyptian Society for Environmental Sciences , Member
2010-2013	American Association of Petroleum Geologists , Representative

MENTORING EXPERIENCE:

I have mentored three Master’s students in the development of hydrogeological models and guided thesis presentations, emphasizing excellence in communication, data management and interpretation.